Dual Loop Rider Control
of a Dynamic Motorcycle Riding Simulator

Vom Fachbereich Maschinenbau an der

Technischen Universität Darmstadt

zur Erlangung des Grades eines

Doktor-Ingenieurs (Dr.-Ing.)

genehmigte

Dissertation

vorgelegt von

Raphael Amadeus Maria Pleß M.Sc.

aus Herrenberg

Berichterstatter: Prof. Dr. rer. nat. Hermann Winner

Mitberichterstatter: Prof. Dr.-Ing. Günther Prokop

Acknowledgements

Table of Content

List of Abbreviations

Abbreviation	Description
ABS	Anti-Lock Braking System
AEB	Autonomous Emergency Braking
BRT	BikeRealTime (VI-grade Software)
CAN	Controler Area Network
CDF	Cumulative Distribution Function
CoG	Center of Gravity
CoSy	Coordinate System
DESMORI	*Development Services for Motorcycle Riding Interactions* (Project Name)
DLRC	Dual Loop Rider Control
DMRS	Dynamic Motorcycle Riding Simulator
DoF	Degrees of Freedom
DS / RS	Driving / Riding Simulators
HMD	Head Mounted Display
IMU	Inertial Measurement Unit
LCM	Lane Change Maneuver
LCRI	Lane Change Roll Index
LTI	Lean Turn Index
MAEB	Motorcycle Autonomous Emergency Brake
MSC	Motorcycle Stability Control
MSC	Minimal Scenario
PM	Performance Measure
PSD	Power Spectral Density
RAS	Riding Assistance Systems
RSC	Reality-Simulation-Converter
SRC	Simulation-Reality-Converter
SSC	Steady State Cornering
SCP	Simulation Computer Processing
SDD	Sensory Display Device
SFG	Sensory Feedback Generator
STI	Steer Turn Index
UTM	U-Turn Maneuver

List of Symbols and Indices

Symbol	Unit	Description
a	m/s²	acceleration
c	N/m, N/rad	stiffness (translational or rotational)
d	Ns/m, Ns/rad	damping
F	N	force
f	Hz	frequency
G	1	gain (e.g. loop gain or PT_2-gain)
g	9.81 m/s²	gravity constant
h	m	height
KP	1	proportional control gain
KI	1	integral control gain
KD	1	differential control gain
l	m	length (e.g. bar length)
M	Nm	moment / torque
m	kg	mass
P	W	power
r	m	radius (e.g. radius of a circle)
R	m	radius (e.g. radius of a curve)
sr	m	scrub radius (lateral lever arm from tire contact point towards steering axis)
T	Nm	torque
t	s	time
v	m/s	velocity
x, y, z	m	coordinate position
α	rad	slip angle
$\beta_{1,2,3}$	kgm², kgm, kgm	Mockup & body parameters
γ	rad	camber angle
δ	rad	wheel steer angle
ϵ	rad	angular deviation
κ	1/m	curvature
ρ	m	radius of gyration
Θ	kgm²	moment of inertia
ϑ	rad	pitch angle
τ	rad	steering head angle
ψ	rad	yaw angle
φ	rad	roll angle
ω	rad/s	angular frequency

List of Symbols and Indices

Index	Description
act	actuation
avg	average
c	contour
CG	center of gravity
brt	BikeRealTime (indicating values used / calculated in the virtual motorcycle model)
design	Design parameter of a scenario
dist	disturbance
entry	segment of the lane change maneuver that constrains the starting lane
exit	segment of the lane change maneuver that constrains the exiting lane
hb	handlebar
HEX	hexapod / Stewart Platform
kin	kinematic
lim	limit
max	maximum
mcy	motorcycle
mean	mean
mid	segment of the lane change maneuver, where the lateral movement happens
min	minimum
mock	mockup (indicating values measured / applied on the simulator mockup)
ofl	offline (indicating that a model is controlled by a virtual rider)
onl	online (indicating that a real rider is using the simulator / controlling the virtual model)
P	platform
p-p	peak to peak
pre	segment before entering the lane change maneuver
post	segment after exiting the lane change maneuver
ref	reference
rid	rider
rot	rotation
s	side
set	set value (achieving this value is controlled e.g. by a cruise control)
sim	simulation
target	target value (achieving this value is controlled by a human)
trans	translation
x	in x-direction (i.e. vehicle longitudinal direction)
y	in y-direction (i.e. vehicle lateral direction)
z	in z-direction (i.e. vehicle vertical direction)
ω	centrifugal
0	zero-configuration (i.e. rider without hip movement or body lean angle)

List of Figures and Tables

Kurzzusammenfassung

Im Motorradsektor haben Fahrsimulatoren verglichen mit der Automobilbranche nur eine geringe Bedeutung, da ihr Einsatzbereich bislang stark eingeschränkt ist. Nach Stand der Technik ist es bspw. Motorradfahrenden oftmals nicht möglich, einen dynamischen Motorradfahrsimulator mit realgetreuem Fahrdynamikmodell und Bewegungsdarstellung bereits im Erstkontakt intuitiv zu kontrollieren. Für die unzureichende Darstellungsqualität dynamischer Motorradfahrsimulatoren zeigen sich vier Faktoren hauptverantwortlich:

- Die Instabilität von Einspurfahrzeugen bei Niedriggeschwindigkeit,
- Die Lenkungsdarstellung mit stark geschwindigkeitsabhängigem Verhalten,
- Die Bewegungsdarstellung (hohe Dynamik, Rollwinkel, Umweltkontakt),
- Der besondere Fahrereinfluss auf die Fahrdynamik (inkl. Fahrerbewegungen).

Insbesondere der letztgenannte Faktor stellt eine Besonderheit von Motorrädern und Motorradfahrsimulatoren im Vergleich mit anderen Fahrzeugsimulatoren dar, da Motorräder signifikant durch die Bewegungen des Aufsassen in ihrer Dynamik beeinflusst werden. Dennoch fand bislang kaum eine Berücksichtigung von Fahrerbewegungen auf dynamischen Motorradfahrsimulatoren statt.

In der vorliegenden Arbeit wird ein Motorradfahrsimulator konzipiert, entwickelt und in Betrieb genommen. Dabei steht insbesondere die Anbindung eines realen Aufsassen an ein virtuelles Motorrad im Vordergrund. Auf Basis eines kommerziellen Fahrdynamikmodells wird eine Simulator-Architektur entworfen, die es ermöglicht, das virtuelle Motorrad nicht nur, wie bislang üblich, durch Lenkeingaben zu steuern, sondern auch durch Fahrerbewegungen. Letzteres erfolgt durch die Erfassung des fahrerinduzierten Rollmoments. Dies ermöglicht eine ganzheitliche Betrachtung der zwischen Fahrer und Fahrzeug bestehenden Koppelkräfte auf dem dynamischen Motorradfahrsimulator.

Zur Beurteilung des Systems werden Bewertungskriterien und Studienkonzepte entwickelt. In Experten- und Probandenstudien werden die Einflüsse der Bewegungserfassung auf das Fahrverhalten untersucht. Es wird gezeigt, dass die Bewegungserfassung realitätsnahe Steuereingaben ermöglicht und einen positiven Effekt auf die Stabilisierung in verschiedenen Geschwindigkeitsbereichen hat. Die Rückführung des fahrerinduzierten Rollmoments als Eingang in das virtuelle Fahrdynamikmodell hilft Probanden auf dem Simulator, das virtuelle Motorrad intuitiver zu steuern. Fahrzeugzustände in der Kurvenfahrt werden erwartungskonform beeinflusst. Darüber hinaus deuten erste Ergebnisse auf eine Erleichterung des Erstkontakts mit dem Simulator für naive Probanden hin. Die erreichten Verbesserungen hinsichtlich der Fahrbarkeit des Simulators reichen jedoch nicht aus, die zuvor genannten Herausforderungen so weit zu kompensieren, dass eine vollständig intuitive Interaktion mit dem Simulator im gesamten Dynamikbereich erreicht wird.

Summary

Compared to the automotive industry, the use of simulators in the motorcycle domain is negligible as for their lack of usability and accessibility. According to the state-of-the-art, it is e.g. not possible for motorcyclists to intuitively control a high-fidelity dynamic motorcycle riding simulator when getting in contact with it for the first time. There are four main reasons for the insufficient simulation quality of dynamic motorcycle riding simulators:

- The instability of single-track vehicles at low speed,

- The steering force-feedback with highly velocity-dependent behavior,

- Motion-simulation (high dynamics, roll angle, direct contact to the environment),

- The specific influence of the rider to vehicle dynamics (incl. rider motion).

The last bullet point is peculiar for motorcycles and dynamic motorcycle riding simulators in comparison with other vehicle simulators, as motorcycles are significantly affected in their dynamics by the rider's body motion. However, up until today, almost no special emphasis has been put on the consideration of rider motion on dynamic motorcycle riding simulators.

In this thesis, a motorcycle riding simulator is designed, constructed and put into operation. The focus here is attaching a real rider to a virtual motorcycle. Based on a commercially available multi-body-simulation model, a simulator architecture is designed, that allows to control the virtual motorcycle not only by steering, but by rider leaning as well. This is realized by determining the so-called rider induced roll torque, that allows a holistic measurement of the apparent coupling forces between rider and simulator mockup.

Performance measures and study concepts are developed that allow to rate the system. In expert and participant studies, the influence of the system on the riding behavior of the simulator is investigated. It is shown that the rider motion determination allows realistic control inputs and has a positive effect on the stabilization at various velocities. The feedback of the rider induced roll torque to the virtual dynamics model allows study participants to control the virtual motorcycle more intuitively. The vehicle states during cornering are affected as expected from real riding. First results indicate that it becomes easier for naïve study participants to access the simulator in first-contact scenarios. The achieved improvements regarding the rideability of the simulator however do not suffice to overcome the abovementioned challenges to a degree that allows for a completely intuitive interaction with the simulator throughout the whole dynamic range.

1 Introduction and Aim

A driving simulator (DS) will only ever be a technological construction, aiming to represent a real system's behavior and will always intrinsically behave differently than the real system. A simulator used to answer a certain research and development question allows for those differences as long as they are not significantly influencing decisive factors of a certain study. The same is true for motorcycle riding simulators (MRS), which search their way to be included in the motorcycle development process as car simulators have successfully done in the recent decades.

1.1 Motivation

Today, cheap and simple static MRS like the Honda Riding Trainer (Figure 1.1 left) are used e.g. for training purposes, where the focus is to learn about traffic rules, hazard perception and basic controls of the vehicle (i.e. positions of throttle, clutch, brake, etc.). While such simulators can behave vastly different than real motorcycles in terms of vehicle dynamics, steering feedback and riding effort, they prove to be applicable for their respective use case.[1]

Figure 1.1: Honda Riding Trainer[2] as an example for simplified MRS for training purposes and hazard perception (left); IFSTTAR Motorcycle Riding Simulator[3] as an exemplary solution for MRS in the research and development domain (right)

---

[1] Vidotto, G. et al.: Improve Hazard Perception (2008).

[2] HME: Honda Riding Trainer (2005).

[3] Arioui, H. et al.: Mechatronics of a Motorcycle Simulator (2010), p. 815.

However, such simulators evidently fail to be applicable for studies with special focus on the dynamic vehicle behavior and rider interaction, as e.g. studies investigating active riding assistance systems (RAS). In the motorcycle industry, there is an increasing trend towards the virtualization of the development processes. It is crucial in the virtual development process, to make the virtual systems tangible to developers, but also managers and customers even before mechanical prototypes exist. This results in a great demand for high fidelity MRS that nowadays only exist in a few universities and companies (e.g. Figure 1.1 right).

Until today all of them are unable to sufficiently reproduce a realistic, dynamic riding experience. Thus, a regular use even of high fidelity MRS is yet limited to specific studies of e.g. rider hazard perception or human machine interface (HMI) designs, in which rider perception and behavior rather than system dynamics are the decisive factor, see e.g. Huth[4].

As shown by Guth[5], a dynamic motorcycle riding simulator (DMRS) is supposed to provide "mental correlation" with real riding (i.e. provoking equal behavioral patterns). In conclusion, the action-effect associations a motorcyclist acquired in real life riding must be made applicable on a simulator as well. This includes not just steering but leaning actions.

Towards dynamic applications of MRS

The system dynamics of a motorcycle are highly dependent to the rider dynamics due to the similar masses of rider and motorcycle[6]. In the development of modern RAS like BOSCH's Motorcycle Stability Control (MSC)[7] and assistance systems like their sliding mitigation system[8] presented in 2018 (both systems are depicted in Figure 1.2), the rider's influence in terms of both body dynamics and steering and leaning control (re-)actions are not negligible.
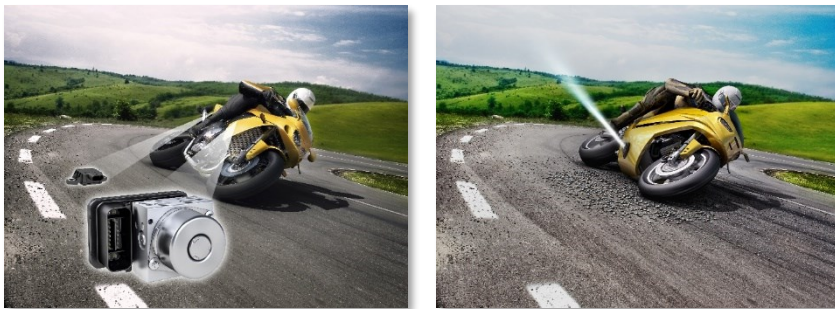
Figure 1.2: MSC with IMU and ABS Module[9] (left); Sliding Mitigation System[10] (right)

---

[4] Huth, V. et al.: Comparison of Warning Concepts (2012).

[5] Guth, S.: Diss., Absicherungsmethode von Anzeigekonzepten mittels Motorradfahrsimulator.

[6] a rider can easily cumulate 30…50% of the system mass

[7] Matschl, G. et al.: Motorcycle Stability Control (2014).

[8] Klews, M. et al.: Preventing lateral sliding in curves (2018).

[9] BOSCH: Motorcycle Stability Control.

[10] BOSCH: Sliding Mitigation.

At any time, a rider can unintentionally destabilize the motorcycle through wrong controlling inputs e.g. as a reaction to overwhelming system behavior. In this case, the abovementioned action-effect associations, contain not only e.g. visual or auditory stimuli, but also to the rider's perception of vehicle stability, sensed through e.g. proprioceptive cues, steering and rolling dynamics. Thus, it is recommendable to provide riders of motorcycle simulators with dynamic cues, if the study aims for the evaluation of such RAS.

As Will recaps: "*While visualization plays a particularly important role, further improvements* [to presence] *could be achieved by adding more consistent sensory stimuli to the virtual environment.*" [11] This thesis investigates a holistic approach to implement haptic, vestibular and proprioceptive stimuli on a DMRS. As these dynamic cues are influenced by the rider's actions directly, such stimuli are considered highly important: "*Sensory stimuli resulting from one's own actions are perceptually attenuated compared to identical but externally produced stimuli. This may enable the organism to discriminate between self-produced events and externally produced events […]*"[12]. Despite this strong and direct connection between the rider's typical body's actions and vehicle dynamics, all motorcycle simulators known to the author at the date of printing of this document lack of proper consideration of both rider motion control (i.e. leaning input) and feedback (i.e. proprioceptive rider body actuation). So far, only vehicle internal states (e.g. steering angle) have been considered in DMRS, but no rider dynamic states (e.g. rider lean, body stiffness).

The rider's motion influence on the vehicle dynamics increases with decreasing vehicle speeds, as self-stabilizing effects diminish. Without correct steering and leaning inputs, the motorcycle cannot ride slowly. Todays, MRS use artificial stabilization like virtual springs, to prevent capsizing at low speeds, leading to an unnatural riding feeling. The abovementioned implementation of motion control and feedback systems on a DMRS is suspected to improve controllability when riding the simulator at low speeds.

1.2 Scientific Goal of The Thesis

This work analyzes if and how a DMRS can benefit from a rider-motion-based control system in various stationary, transient or dynamic riding scenarios. In the further course, this approach will be called **dual loop rider control (DLRC)**, as it does not only take steering, but leaning into account for controlling the virtual motorcycle. It promises to solve the drawback of state-of-the-art DMRS regarding the coupling between rider and vehicle. While these are presenting the vehicle dynamics to the rider rather in terms of open loop control (the mockup motorcycle will act independently from the rider's body responses, but only dependent from the vehicle dynamics), this novel approach tries to close this loop.

---

[11] Will, S.: Diss., Presence Model for Driving Simulators, Page: IX.

[12] Weller, L. et al.: Was it me? (2017), p. 241.

1.3 Methodology and Structure of the Thesis

The methodology of this thesis is shown in Figure 1.3 and follows a top-down approach: The first step investigating the usability of rider motion control systems on DMRS is to design and build a respective simulator. Requirements for such a design derive from the analysis of vehicle dynamics and rider behavior.

The design process results in the *DESMORI*[13] simulator that is equipped with DLRC capabilities, as it measures the rider induced roll torque that acts on the motorcycle chassis.

In order to investigate if DLRC can improve the fidelity of DMRS, performance measures have to be defined. Based on measures known from literature and real-life testing, a set of riding maneuvers and performance measures are developed that allow to compare and rate the fidelity of the DESMORI simulator.

The performance of the DLRC system is then evaluated by means of an expert study and a naïve rider study. The first one allows to investigate the potential of the system, while the second one investigates if standard motorcyclists that are by no means trained on a simulator can utilize this potential and benefit from DLRC.
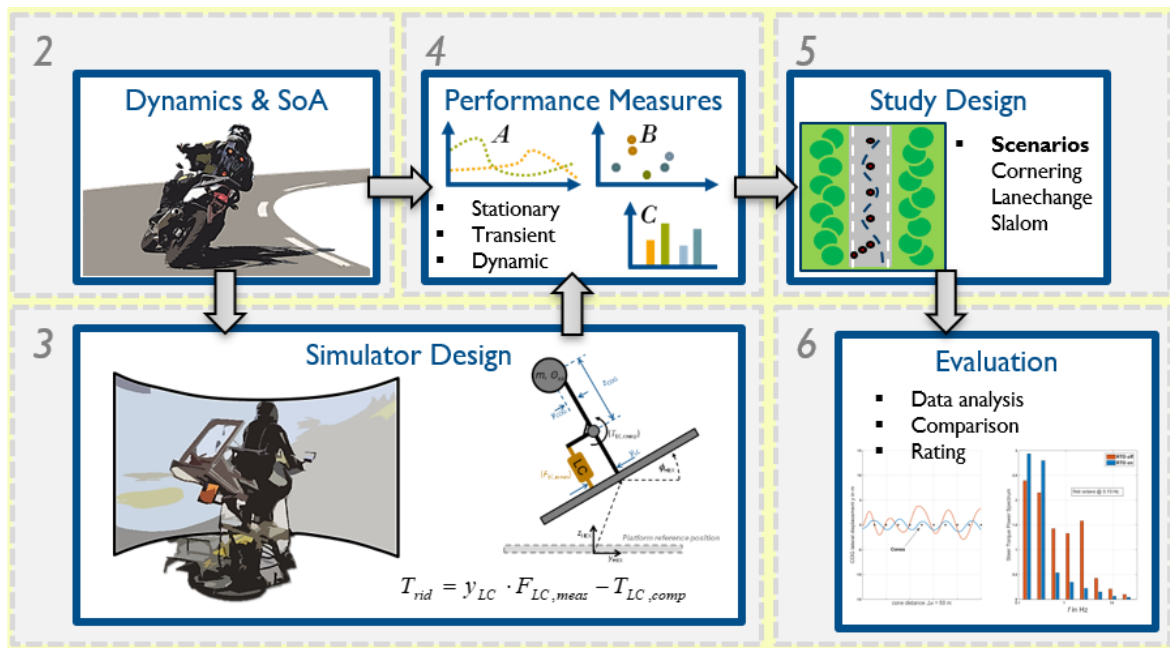
Figure 1.3: Overview of the applied methodology and corresponding chapter numbers. The detailed dynamics and SoA-analysis provide input for the simulator design and performance measures. Studies are designed based on the performance measures and finally tested in chapter 6.

---

[13] DESMORI – Development Services for Motorcycle Rider Interaction, nationally funded research cooperation 2014-2016. Namesake for the Simulator that was designed during that cooperation.

The present work consists of six chapters, following the abovementioned methodology:

2. Motorcycle and Simulator Fundamentals

At the beginning of this chapter, basics and definitions necessary for the understanding of this thesis are given, including motorcycle and tire dynamics (section 2.1 and 2.2), motorcycle rider behavior and controls (section 2.3) as well as simulators (section 2.4 and 2.5). Lastly, open research questions resulting from the state-of-the-art are formulated and working hypotheses are defined (section 2.6).

3. Simulator Design and Rider Coupling

This chapter provides a comprehensive development documentation of the complete DESMORI simulator that is used in this thesis as evaluation tool. This includes the general mechatronic architecture of the simulator (section 3.1.1 and 3.1.2), the used steering actuators and controls (section 3.1.4), as well as the multi cueing system (section 3.1.5). Then, a detailed discussion on the implementation of DLRC on the DESMORI simulator is given (section3.2). The chapter ends with a short discussion on the simulator's applicability by referring to several conducted studies (section 3.3)

4. Performance Measures

In order to generate reliable qualitative and quantitative ratings of DLRC simulation, this chapter introduces performance measures and scales, that were developed for the purpose of this thesis. These are derived from real life testing and adapted to the specific requirements of simulator assessment. Measures for the assessment of stationary (section 4.1), transient (section 4.2) and dynamic maneuvers (section 4.3) are described, as well as measures to rate the low speed boundary (section 4.4). Lastly, the mental model accordance is discussed (section 4.5) and an overview about the measures selected for testing is given (section 4.6).

5. Study Design

With the performance measures (chapter 4) defined, this chapter discusses, how to collect the relevant data with reliable studies. It results in a two-part study: Firstly, an expert study aims to highlight effects that result from the newly introduced system in stationary, transient and dynamic maneuvers (sections 5.1). Then, a study is developed that shall test for beneficial effects of DLRC for untrained simulator riders (section 5.2).

6. Results

This chapter describes the data acquisition and evaluation process in detail. The results for the previously selected performance measures are presented.

7. Conclusion and Outlook

This chapter summarizes the thesis, considering the previously gained results. The hypotheses presented in section 2.6 are evaluated and further details regarding the usability of rider motion control systems as well as possible optimizations are discussed.

1.4 Delimitation of the Topic

The development and application of a dynamic motorcycle riding simulator unites many topics and research questions. Each of these topics – from vehicle dynamics, over the design of mechatronic systems to rider psychology – branches out into subtopics – from tire modeling and steer-roll-coupling over platform kinematics and motion controllers to human perception and error models. Every such subtopic provides its own peculiarities and affects the overall simulator behavior and fidelity to some extent. For the course of this thesis, it is obvious, that not all of them can be discussed in full detail.

The next chapter will provide a brief overview on several of these topics, and whenever necessary for the evaluation and discussion of results, specific details are provided. But in general, the following delimitations apply:

- The focus of this thesis lies on dynamic motorcycle riding simulators, i.e. the overall **architecture**, application and fidelity. This specifically excludes detailed work and improvements on parts of the vehicle model, their parametrization and validation. Such work is subject to motorcycle manufacturers and software providers of the dynamic models.

- The focus of this thesis lies on rating **simulators**, not motorcycles. This specifically excludes investigations of different vehicle configurations, ergonomics and other parameters. Such investigations are subject to current development projects, but not to this research.

- The focus of this thesis lies on adding a control cue to the simulator, that is sensitive to **rider motion**. This specifically excludes detailed work and improvements on steering controllers for motorcycle riding simulators. These are subject to many recent and ongoing research activities throughout the motorcycle simulator community.

- The focus of this thesis lies on **lateral dynamics** induced by rider motion. The in-plane dynamics of the motorcycle as well as drivetrain configurations and their effect on cornering and handling properties are irrelevant here, as are the rider's effects of longitudinal weight shifting.

- The focus of this thesis lies on the **DESMORI** simulator in its default configuration. No variations of the hardware setup (e.g. the visual system or motion platform) are investigated for the course of this thesis. However, there is no immediate reason why the results of this research should not be generalizable for other DMRS as well.

2 Motorcycle and Simulator Fundamentals

This chapter provides information on the technological background, necessary for the understanding of this document. For the ease of reading, this document will talk about "motorcycles". But, the provided information is in general true for any kind of single-track vehicle like scooters and bicycles or even some tilting three-wheeled or four-wheeled vehicles.

After the fundamentals of motorcycle dynamics are presented (section 2.1), special emphasis is put on motorcycle stability and handling (section 2.2) as well as motorcycle control and rider models (section 2.3). Afterwards, the first step towards simulators is done by presenting their fundamentals and controls respectively (section 2.4).

2.1 Motorcycle and Tire Dynamics

Motorcycles are intrinsically instable and will tilt over ("capsize"), if not stabilized by the rider or certain dynamic effects. Also, the rider adds significant amounts of mass and inertia, elastically coupled, to the motorcycle. Thus, the rider is an immanent part of the vehicle system. Nevertheless, many aspects of the relevant vehicle dynamics can be explained with the motorcycle's open loop dynamics, i.e. neglecting the rider, as described in the following. The influences of the rider are in the focus of section 2.3.

2.1.1 Motorcycle Geometry

A simple model, capable of describing essential motorcycle dynamics consists of four rigid bodies, the front and rear assembly as well as front and rear wheels and is depicted in Figure 2.1 aside of the motorcycle's coordinate system (CoSy) nomenclature. Three revolute joints connect the front to the rear assembly and each wheel to the respective assembly.
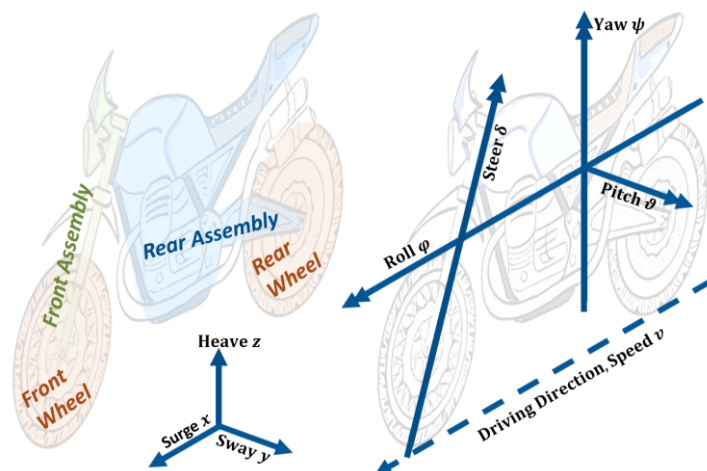
Figure 2.1: Motorcycle degrees of freedom. Left: Motorcycle subsystems and translational degrees of freedom. Right: Rotational degrees of freedom of the motorcycle

This combination of four rigid bodies with three revolute joints and translational wheel-ground constraints creates three remaining degrees of freedom (DoF) of a motorcycle that can be associated with three principal motions

- Forward motion of the motorcycle (represented by the rear wheel rotation)
- Roll motion around the tire contact point line
- Steering rotation

A rider can vary these three DoF according to their individual skill and style, leading to various corresponding trajectories. The position of the motorcycle w.r.t an earth CoSy is then described through its translations and rotations along the longitudinal axis (surge x / roll φ), lateral axis (sway y / pitch ϑ) and vertical axis (heave z / yaw ψ). Three coordinate systems are typically used to describe the vehicle's motion:

1. **Levelled CoSy**
   Horizontal projection of the motorcycle body CoSy into the global x-y-plane. Usually located in the rear tire contact point. See (x_w, y_w, z_w) in Figure 2.2.
2. **Motorcycle body CoSy**
   Fixed to the motorcycle main frame. Usually located in the swingarm pivot point or CoG. See (x_m, y_m, z_m) in Figure 2.2.
3. **Steering CoSy**
   Fixed to the steering system with its z-axis pointing upwards, aligned to the steering axis. See (x_{st}, y_{st}, z_{st}) in Figure 2.2.
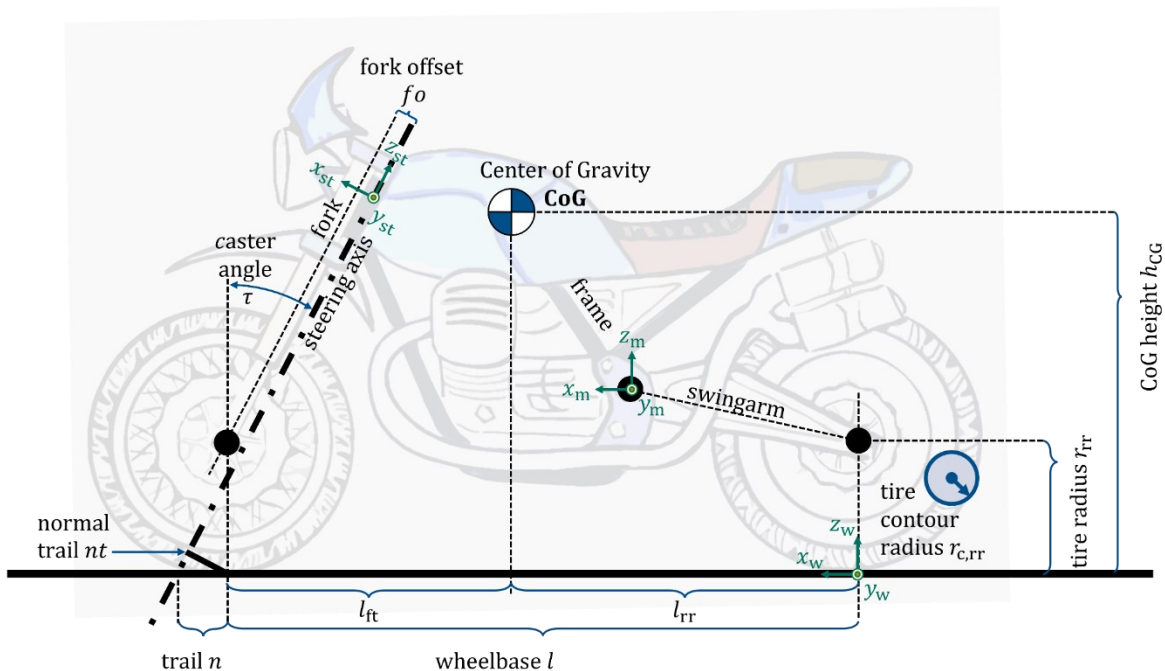
Figure 2.2: Geometric parameters of a standard motorcycle. The three relevant coordinate systems are highlighted in green. The CoG position is vastly influenced e.g. by luggage.

Specific coordinate systems for each relevant model or system (vehicle dynamics model, simulator mockup, etc.) will be described in the respective subchapters.

On contemporary production motorcycles, a variety of different suspension concepts is utilized. However, this thesis does only consider the standard chassis consisting of a telescopic fork as front suspension, while having a standard swingarm as rear suspension. While changes to this configuration may result in changing handling qualities, they do not change the basic dynamic properties or even riders' control strategies of the motorcycle. Independent of the suspension design, several basic geometric parameters exist on a motorcycle that will define its handling properties[14] and can be found in Figure 2.2:

- **Wheelbase l**
  The wheelbase of a motorcycle will vary depending on the bike's purpose. Small, agile vehicles will begin from 1200 mm, while large touring bikes may reach values above 1600 mm. Larger wheelbases provide an increased directional stability, which on the other hand might as well be described as a decrease in handling performance or higher efforts to steer the motorcycle.

- **Trail n**
  The trail has a big influence on vehicle stability, as it generates a self-aligning torque at velocities $v > 0$. As it acts like a lever between the tire contact point and the steering axis, thrust and side forces "push" the steering towards the steady state equilibrium. Its values range from 75 mm in competition motorcycles to more than 120 mm in touring bikes. As for the wheelbase, large values tend to increase the motorcycles stability, trading off agility and ease of handling. Negative values generate a destabilizing effect due to a self-amplification of the steering angle. The orthogonal distance of the steering axis to the rear tire contact point can be referred to as normal rear trail.

- **Caster angle τ**
  The caster angle of a motorcycle lies around 20°-25° for street or sport motorcycles and may increase to over 30° for touring bikes. It has an influence on the fork's bending properties when decelerating (critical at very low caster angles) and can influence oscillations of the front assembly (wobble) as steering angles at high caster angles reduce the potential energy of the system by lowering the motorcycle's CoG.

- **CoG position**
  The longitudinal and vertical position of the CoG will define the motorcycle's tendency to tilt over, when large accelerations are applied. A low CoG will improve acceleration and braking performance and make the motorcycle easy to maneuver at low speeds but cannot always be realized due to packaging reasons. As described later, the position of the total system's CoG is vastly influenced by the rider and must not be considered constant.

---

[14] Cossalter, V.: Motorcycle Dynamics (2006).

2.1.2 Motorcycle Cornering

This section describes the lateral dynamic behavior of a motorcycle. Longitudinal dynamics are not in the focus of this thesis, as only standard maneuvering at rather low dynamics is performed (no lifting wheels). Thus, no special emphasis is needed in this regard.

Steady State Cornering (SSC)

When riding at a constant velocity v on a circular trajectory with constant radius R, a motorcycle on infinitesimally thin tires reaches an equilibrium that is defined by the theoretical roll angle φ_{th} which is only dependent to the centrifugal acceleration a_ω, see equation (2.1):

$$\tan \varphi_{\text{th}} = \frac{a_\omega}{g} = \frac{\omega^2 \cdot R}{g} = \frac{v^2}{R \cdot g} \tag{2.1}$$

However, as the tire contour radius r_{c} increases, so does the tire scrub radius sr, which is the lateral lever arm from the tire contact point towards the steering axis. As the tire contact point moves towards the inside of the curve, the theoretical roll angle is decreased, i.e. the motorcycle roll angle φ must be further increased by an amount of φ' if the theoretical roll angle is to be kept constant[14].

$$\varphi = \varphi_{\text{th}} + \varphi' \tag{2.2}$$

$$\sin \varphi' = \frac{r_{\text{c}}}{h_{\text{CG}} - r_{\text{c}}} \cdot \sin \varphi_{\text{th}} \tag{2.3}$$

While equation (2.3) is only true for the CoG being located in the middle plane of the motorcycle, the rider can vary the lateral position of the total CoG by shifting their body mass sideways, thus affecting φ' as visualized in Figure 2.3. If the CoG's lateral shift towards the curve center turns bigger than the tire scrub radius $sr = (\overline{AC} \perp B)$, φ' becomes negative, i.e. decreasing the motorcycle roll angle while keeping φ_{th} at constant.
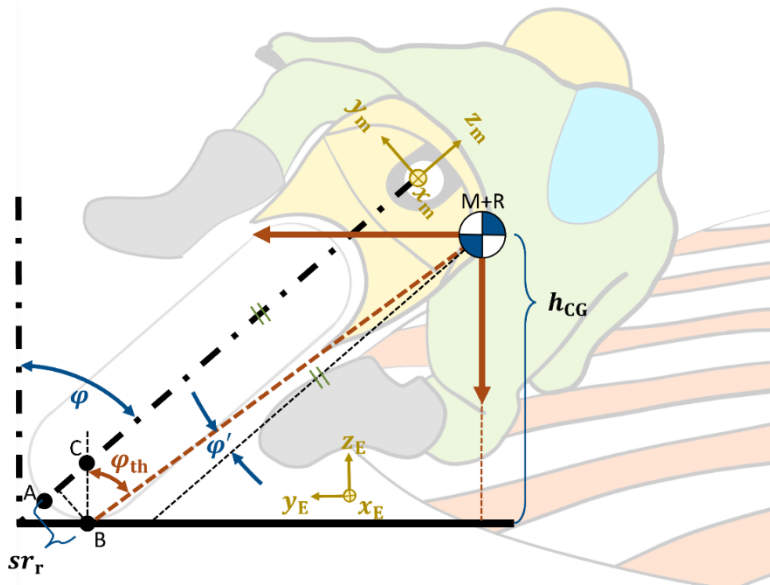
Figure 2.3: Roll angles in steady state cornering with a rider performing "Lean-In". Tire contact point with the road moving from A to B whilst cornering, resulting in additional roll angle φ'

2.1.3   Tire Road Interaction

In the course of this thesis, exceeding the maximum force transfer potential between tire and road is not in the focus. Nevertheless, the fundamentals of tire road interaction will help understanding certain dynamic properties of the motorcycle.

One of the simplest descriptions of the maximum transferrable longitudinal and lateral tire forces is used in Kamm's friction circle:

$$\sqrt{F_x^2 + F_y^2} \leq \mu_0 \cdot F_z \,, \tag{2.4}$$

Where the maximal friction coefficient between the road and the tire is μ_0 and $F_{x/y/z}$ represent the longitudinal, lateral and normal forces at their contact point. Considering a constant vertical load and dividing by the mass, this formula can be restated using the longitudinal and lateral accelerations in the levelled CoSy, a_x and a_y respectively:

$$\sqrt{a_x^2 + a_y^2} \leq \mu_0 \cdot g \,, \tag{2.5}$$

This shows that a certain lateral acceleration – and therefore roll angle and curvature – can only be reached while the friction limits are not yet exceeded by longitudinal accelerations and vice versa. However, considering a friction coefficient of $\mu_0 = 1$ (a fairly low value for modern tires and good road conditions), a motorcycle at a roll angle of $\varphi_{\text{th}} = 35°$ (a fairly high value for too many motorcyclists, corresponding to a lateral acceleration of $a_y \approx 7\frac{m}{s^2}$) is according to equation (2.5) capable of accelerating or decelerating with the same amount $a_x \lesssim \pm 7\frac{m}{s^2}$, which again is a fairly high value that some untrained riders would not even approach in straight running.

These considerations provide the limit forces that a tire can transmit. As stated before, the focus of this thesis lies in the lateral dynamics and therefore, the side forces that consume a part of the maximum force potential shall be described more deeply in the following.

The side forces F_s are generated by adding the camber and sideslip lateral forces[15]:

$$F_s = F_{s,\gamma} + F_{s,\alpha} \approx k_\gamma \cdot \gamma + k_\alpha \cdot \alpha \tag{2.6}$$

With γ being the camber angle, which at the rear wheel can be directly attributed to the motorcycle roll angle φ in good approximation. The sideslip angle α is defined as the levelled projection of the difference angle between the tire symmetry plane and its direction of travel and thus strongly connected to the steering angle. The coefficients $k_{\gamma/\alpha}$ are the camber and sideslip stiffness respectively, that are used to describe the linear behavior of the side forces at low angles.

---

[15] Cossalter, V.: Motorcycle Dynamics (2006), p. 51.

Figure 2.4 shows typical values of the two side force components. In steady state cornering scenarios, the camber side force dominates the side force due to sideslip, the latter one being used to modulate the overall side force balance through the input of (very) small steering angles. Generally, the side forces due to camber of the tire are enough to generate the needed centripetal forces in a turn. In certain scenarios they might even exceed the side force demand so that opposing sideslip angles (steering outside the curve) are needed to reach equilibrium. As the sideslip forces increase rapidly with even small angles, motorcycle dynamics are very sensitive to them, explaining their importance for rider control.
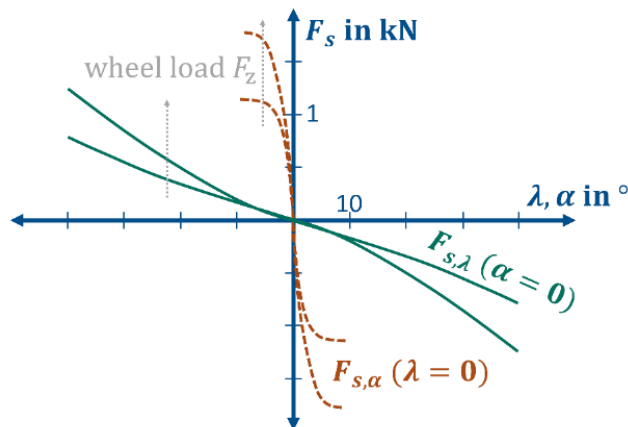
Figure 2.4: Exemplary values for camber and sideslip forces of a motorcycle tire for different wheel loads. Sideslip forces (dashed, red line) demand much less angle than camber forces (green)

2.1.4 Motorcycle Steering

The steering of a motorcycle is considered its main control input and at the same time is one of the most important feedback cues for the rider. As shown above, the steering angle, that is closely related with the side slip angle, provides high side forces at low angle excitations, exceeding the force potential due to camber. When a steering angle is applied, side forces are generated in the tire due to friction, allowing for manipulation of the vehicle states, i.e. roll and yaw angles and rates.

Depending on the geometrical properties of the front assembly as well as the dynamic state of the motorcycle, the forces and torques acting on the tire-road-contact point and the steering head sum up to a steering torque that can be perceived and reacted to by the rider. As the steering system is important both as input and feedback cue and has small time constants, it also is of highest importance in simulator design and controls.

Several superimposing components have an aligning or misaligning effect to the steering as depicted in Figure 2.5. In steady state cornering, the misaligning torques (inwards the turn) typically exceed the aligning torques so that the rider has to "push" against the inner handlebar to maintain a constant steering angle.
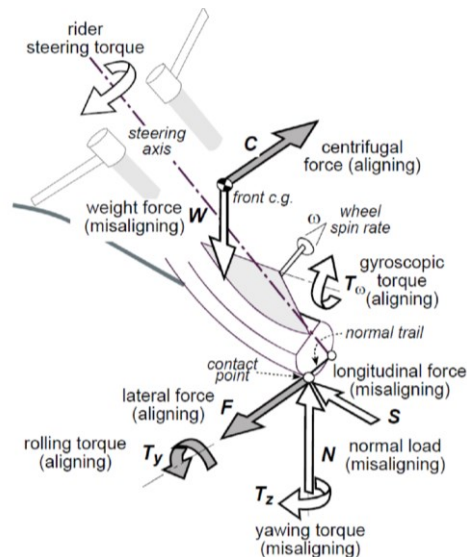
Figure 2.5: Influences on steering torque demand[16]. In contrast to the nomenclature of this thesis, the "normal trail" is here defined as perpendicular connection between tire contact point and steering axis. (see the scrub radius sr and normal trail nt definitions in Figure 2.2 and Figure 2.3.)

As the motorcycle is subject to significant roll angles in curves, it is not possible to just assume the Ackermann angle for a motorcycle. The combination of motorcycle steer and roll motion is depicted in Figure 2.6 and shows the steering angle δ of the handlebar, i.e. the angle between the front and rear assembly and the motorcycle roll angle φ between the rear assembly and the ground plane.
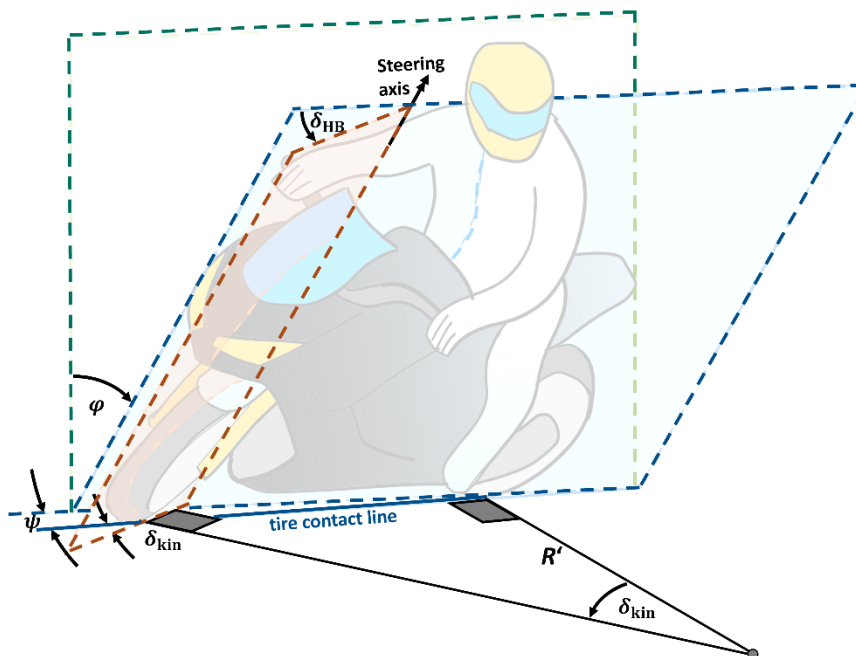
Figure 2.6: Motorcycle cornering. The resulting effective steering angle depends on both steering of the handlebar and the motorcycle roll angle.

---

[16] Cossalter, V.: Motorcycle Dynamics (2006), p. 134.

The kinematic steering angle δ_{kin} represents the intersection of δ with the road plane $z = 0$ With the steering head angle τ and motorcycle pitch angle ϑ, it results to[17]

$$\delta_{\text{kin}} = \arctan\left(\frac{\sin\delta\cos(\tau+\vartheta)}{\cos\varphi\cos\delta-\sin\varphi\sin\delta\sin(\tau+\vartheta)}\right). \tag{2.7}$$

With l denoting the wheelbase of the motorcycle, the curvature κ of the trajectory under no-slip condition yields:

$$\kappa = \tan(\delta_{\text{kin}})/l \tag{2.8}$$

As the roll angle increases, the steering angle demand decreases. At the same time, the steering motion does not only increase side forces due to the sideslip angles alone.

Additionally, because of the steering head angle τ an additional camber $\Delta\gamma$ is generated:

$$\Delta\gamma = \delta_{\text{kin}} \cdot \tan\tau \tag{2.9}$$

This increases the generated side forces furthermore and is one part of the explanation for the small steering angle demands of motorcycles at high velocities.

Gyroscopic effect

Further influence on the steering and vehicle dynamics results from the gyroscopic effect. As an inertia I_{xx} rotates around an axis $\vec{x}$ with an angular velocity ω_x, it is subject to gyroscopic stabilization. Therefore, as the inertia gets disturbed around an axis $\vec{y}$ at an angular velocity ω_y, it experiences a stabilizing torque acting orthogonally to the disturbance:

$$T_{\text{gyr},z} = I_{xx} \cdot \omega_x \cdot \omega_y \tag{2.10}$$

Multiple components generate gyroscopic effects when entering a turn with a motorcycle. At first, the front wheel will generate a roll torque as a response to steering "disturbances" and vice versa. Furthermore, all rotating masses of the motorcycle's drivetrain are subject to yaw rates when cornering. This generates additional roll torques that act towards the outside of the turn for components rotating "forwards" as the wheels. The gyroscopic torque induced by steering acts in the same direction as the roll torque induced by the centrifugal forces that result from the same steering motion. (i.e. steering to the left generates a roll to the right due to both gyroscopic and centrifugal effect). Therefore, rotating the steering to the left when running straight will induce a right corner and vice versa. This effect is often referred to as "counter-steering"[18] and is immanent to any tilting single-track vehicle.

---

[17] Cossalter, V.: Motorcycle Dynamics (2006), p. 26.

[18] Cossalter, V. et al.: Steady turning of motorcycles (2007).

2.2 Stability and Handling of Motorcycles

Several quality and performance measures for motorcycles are known from literature. They are typically grouped into the three classes. listed and described below in accordance with Cossalter[19] and Kooijman and Schwab[20].

- ▪ **Stability**
  The quality of a motorcycle that governs the tendency to maintain in or return to an equilibrium condition in response to outside disturbances.
- ▪ **Maneuverability**
  The quality of a motorcycle that governs the ability to execute complicated maneuvers considering an optimal control.
- ▪ **Handling**
  The quality of a motorcycle that governs the ease and precision with which a rider can perform the correct controls required in support of a certain maneuver.

Following the abovementioned definition, the *maneuverability* of a motorcycle relates to optimal control and purely depends on vehicle parameters. For the course of this thesis, such purely vehicle related properties are not in the focus, as described in section 1.4 and only stability and handling will be further discussed, as both depend highly on the rider as well.

2.2.1   Motorcycle Instabilities

System theory defines stability as a system's property to return back to its equilibrium condition after being subject to a disturbance. As depicted in Figure 2.7, an equilibrium may be stable or instable. While the lower ball in the stable area will always return to the midpoint, the upper ball will fall of the elliptic surface and not return, once a disturbance is applied.

Equilibrium condition:
$$\frac{d}{dt}x = f(x), f(x_{eq}) = 0$$

Stability condition:
$$|x(t) - x_{eq}| \leq \epsilon$$
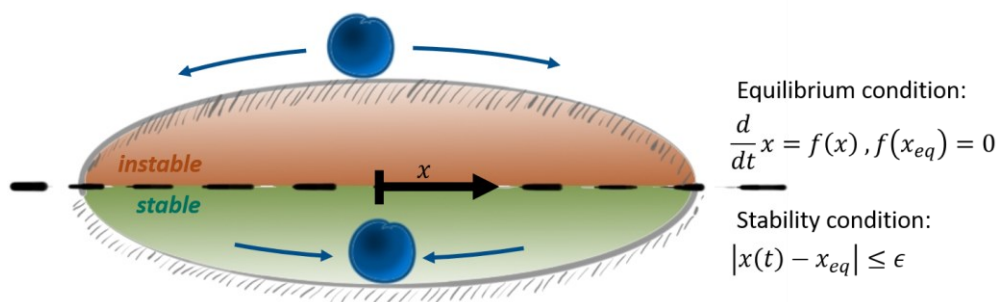
Figure 2.7: Stable and Instable Equilibrium. The instable equilibrium (top ball) is not able to return to the equilibrium after a disturbance.

---

[19] Cossalter, V.: Motorcycle Dynamics (2006), p. 283.

[20] Kooijman, J. D.; Schwab, A. L.: A Review on Handling Aspects in Bicycle and Motorcycle Control (2011).

In control theory, the stability of a system can be determined through analysis of its (complex) eigenvalues λ. A system is stable if it only has eigenvalues with negative real parts. Each eigenvalue is connected to separate mode of instability. The following three modes are most relevant in motorcycle dynamics:

Capsize – a non-oscillating mode, where the motorcycle tilts over to the side

Wobble – an oscillating mode of the steering system

Weave – an oscillating mode of steering and frame around multiple axes

For details on each mode and dynamic properties, please refer to standard motorcycle dynamic literature of e.g. Tanelli[21], Stoffregen[22] or Cossalter[14].This thesis is concentrating on standard riding scenarios. Thus, the realistic simulation of wobble and weave modes in terms of motion simulation, rider behavior and body influence are not in the focus but should be investigated in future research. The capsize mode however is of huge interest, as the simulator rider must always ensure to stabilize this mode to be able to ride at all.

2.2.2 Directional Stability

The directional stability is the quality of a vehicle that describes its tendency to naturally maintain its equilibrium against external distortions (e.g. wind, body shake, road roughness). It contrasts with *handling* or *maneuverability*, as the system cannot distinguish between external distortions and external control inputs. Thus, a motorcycle with high directional stability will not only be robust against external distortions but also need higher efforts to maneuver it through quick turns on twisty roads. Cossalter quantifies the directional stability as the angular deviation ϵ from a rectilinear trajectory[19]

$$\epsilon = \arctan \frac{v_y}{v_x} \tag{2.11}$$

The directional stability is influenced by various factors, including the inertial and geometric properties of the motorcycle and tire as well as the forward speed and gyroscopic effects.

2.2.3 Motorcycle Handling

In literature, various maneuvers with various measures are used to quantify the handling of a motorcycle. Kooijman and Schwab[20] give an overview on handling and control aspects.

---

[21] Tanelli, M. et al.: Modelling, Simulation and Control of Two-Wheeled Vehicles (2014).

[22] Stoffregen, J.: Motorradtechnik (2012).

Cossalter provides information on handling tests for motorcycles[14] and motorcycle simulators[23,24]. If not stated otherwise, the following descriptions are based on these four sources.

2.2.3.1 Handling Indexes

One of the first scales, developed to rating handling qualities of a vehicle, is the purely subjective Cooper and Harper scale for aircrafts[25] published in 1969 and depicted in Figure 2.8.

Since then, handling aspects have been investigated for multiple means of transportation with the goal of objectifying handling properties based on measurable data. In the motorcycle domain, several characteristic values are established to rate handling. Typically, they all attribute better handling to needing smaller input actions (mostly steer torque) to achieve higher output actions (e.g. lateral acceleration). Following this base approach, different ratios of input and output sizes are used for different test maneuvers. For steady state cornering (SSC), average values are used, while e.g. a U-turn maneuver (UTM) calls for the evaluation of maximum values and a lane change maneuver (LCM) for the use of peak-to-peak values.
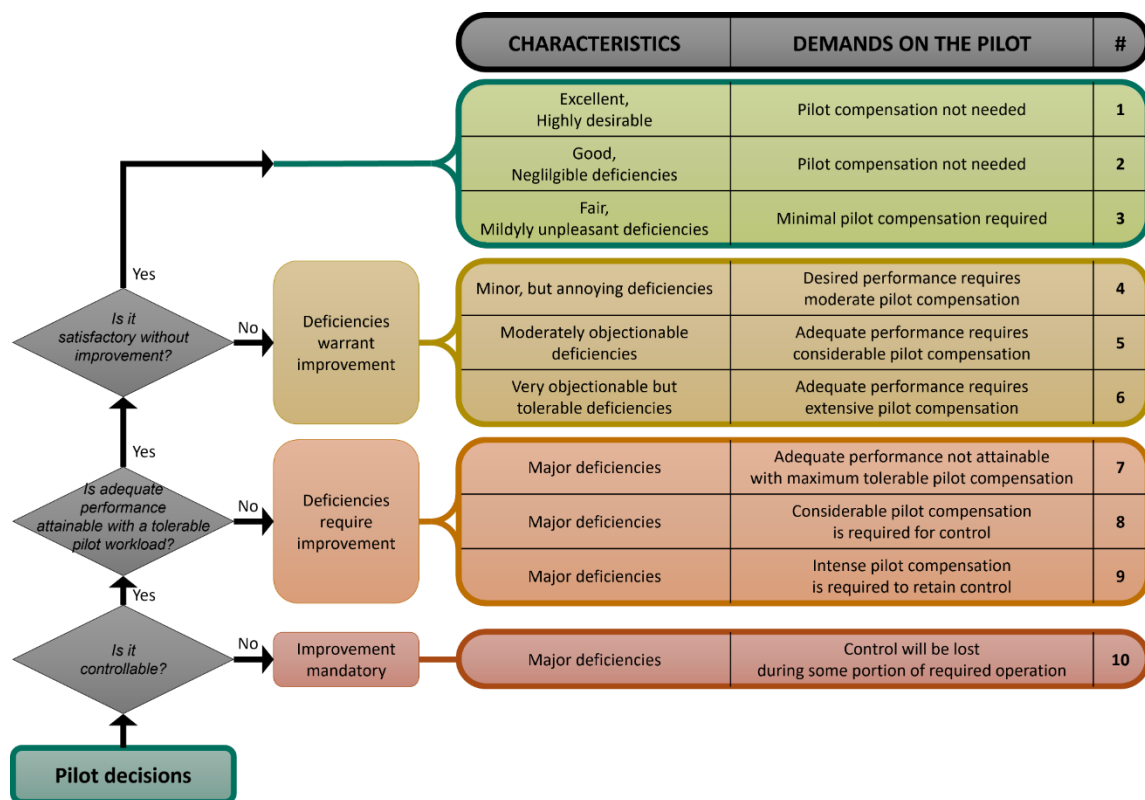
Figure 2.8: The Cooper-Harper handling qualities rating scale. (Own representation after [25])

---

[23] Cossalter, V. et al.: Objective and subjective evaluation of an advanced motorcycle riding simulator (2010).

[24] Cossalter, V.; Sadauckas, J.: Elaboration and quantitative assessment of manoeuvrability (2006).

[25] Cooper, G.; Harper, R.: The Use of Pilot Rating in the Evaluation of Aircraft Handling Qualities (1969).

In Table 2.1 on page 19, the known indexes from literature are listed. Most indexes concentrate only on steering inputs, while e.g. Cheli et al.[26] will also consider rider motion inputs in the derived indexes. Bartolozzi[27] finds similarities in handling indexes from cars and motorcycles. The *Roll Index* and *Acceleration Index* are corresponding, as the roll angle is directly linked to the motorcycle's velocity and curvature of the trajectory ($v^2 \kappa = g \tan \varphi_{\text{th}}$ in steady state). They both emphasize on the physical ease to control the vehicle, as low operating torques at the handlebar are evaluated. The influence of a moving rider is only considered indirectly, as e.g. the rider's lean towards the curve will reduce the steering torque demand. Cheli et al.[26] have documented this behavior by measuring the *Steering Mechanical Equivalent Impedance:* For an "inactive" rider (i.e. maintaining center position with no lean motion), "harder" (sic) steering is experienced at higher speeds compared to the rider being "active". However, at certain combinations of rider lean and velocity, the steering torque would change sign, leading to an unstable capsize mode, which – according to Cheli – "certainly makes driving more difficult"[26]. Furthermore, Cheli introduces the two *Driver Control Indexes* that relate either the rider lean angle or lateral displacement to the vehicle yaw rate. It is concluded that riders of different experience utilize different amounts of leaning and hip displacement. A movement of the hip towards the inside of the curve whilst keeping the torso rather vertically with respect to the road is considered "professional" by the authors. The same behavior is also observed by Bocciolone[28] who shows experimental data of unspecified riders but doesn't further discuss his findings. No optimum value for these indexes is discussed. While the observed values differ vastly in sign and amplitude for each study participant, it can be seen, that the absolute values of the indexes will always decrease with speed. This indicates the decreasing effect of rider motion at higher velocities which is expected due to increasing self-stabilizing effects.

The *Koch Index* puts the peak handlebar torque $T_{\text{hb,max}}$ during a U-turn in relation to the peak motorcycle roll rate $\dot{\varphi}_{\text{max}}$ and is scaled by the vehicle's velocity. As before, no direct evaluation of rider motion is possible. But – again – a rider leaning inwards the turn will have a reducing effect on the steer torque demand. Also, the needed motorcycle roll rate will decrease in sequence of such an input, as the same theoretical roll angle is achieved with less motorcycle roll. Furthermore, less motorcycle roll will reduce the lateral displacement of the tire-road contact point, again leading to a decrease of steer torque demand.

The *Lane Change Roll Index* is defined as the relation between steering torque and roll rate, scaled by the velocity. While the *Koch Index* uses maximum values, the Lane Change Roll index uses the peak-to-peak values $T_{\text{hb,p-p}}$ and $\dot{\varphi}_{\text{p-p}}$ instead. Bartolozzi[27] uses the yaw rate as output size, rather than the roll angle, as this allows to compare handling quantities of motorcycles and cars. This approach is used to implement a simplified car model to a low

---

[26] Federico Cheli et al.: Driver's movements influence on the lateral dynamic of a sport motorbike.

[27] Bartolozzi, M. et al.: Similarities in steering control between cars and motorcycles (2022).

[28] Bocciolone, M. et al.: Experimental Identification of Kinematic Coupled Effects (2007).

budget motorcycle simulator. Bartolozzi finds similarities between the steering behavior of a motorcycle with that of an understeering car.

Table 2.1: Handling indexes used in literature

Name	*Calculation*	*Maneuver*	*Sources*
Roll Index	$T_{\text{hb,avg}}/\varphi_{\text{th,avg}}$	SSC	[29,30,31,32]
Acceleration Index	$T_{\text{hb,avg}}/(v_{\text{avg}}^2 \cdot \kappa_{\text{avg}})$	SSC	[29,31,32]
Steering Mechanical Equivalent Impedance	$T_{\text{hb,avg}}/\delta_{\text{avg}}$	SSC	[31,33]
Driver Control Index$_p$	$\varphi_{\text{rid,avg}}/\dot{\psi}_{\text{avg}}$	SSC	[31]
Driver Control Index$_y$	$y_{\text{rid,avg}}/\dot{\psi}_{\text{avg}}$	SSC	[31]
Koch Index	$T_{\text{hb,max}}/(v_{\text{avg}} \cdot \dot{\varphi}_{\text{max}})$	UTM	[29,30,32]
Lane Change Roll Index	$T_{\text{hb,p-p}}/(v_{\text{avg}} \cdot \dot{\varphi}_{\text{p-p}})$	LCM	[29,30,32]
Lane Change Yaw Index	$T_{\text{hb,p-p}}/\dot{\psi}_{\text{p-p}}$	LCM	[30]

It becomes obvious, that most of the abovementioned indexes purely concentrate on the steer torque as rider input. As rider motion can reduce the steering torque demand, it is indirectly connected to the indexes. However, it would be short sighted to argue that using lean-in (therefore decreasing steer torque) would generally cause a better handling of any motorcycle. Obviously, the indexes can only provide relative ratings about the rider's control efforts (in terms of strength) with specific vehicle configurations in specific riding scenarios and are not suitable for differentiation between different control inputs.

2.2.3.2 Lane Change Delays

As the lane change describes a rather transient maneuver, it is interesting to look at time series of certain values rather than just mean or maximum values as before. Different vehicle behavior between maneuvers with moving and non-moving riders is discussed by Cheli[26]. Therefore, he determines the delay $\Delta s_{\varphi,T_\delta}$ between the peak steer torque and peak roll angle for five characteristic points during a double lane change maneuver. They are depicted in the exemplary curves in Figure 2.9.

---

[29] Cossalter, V.: Motorcycle Dynamics (2006), pp. 314–326.

[30] Cossalter, V.; Sadauckas, J.: Elaboration and quantitative assessment of manoeuvrability (2006).

[31] Federico Cheli et al.: Driver's movements influence on the lateral dynamic of a sport motorbike.

[32] Kooijman, J. D.; Schwab, A. L.: A Review on Handling Aspects in Bicycle and Motorcycle Control (2011).

[33] Bartolozzi, M. et al.: Similarities in steering control between cars and motorcycles (2022).
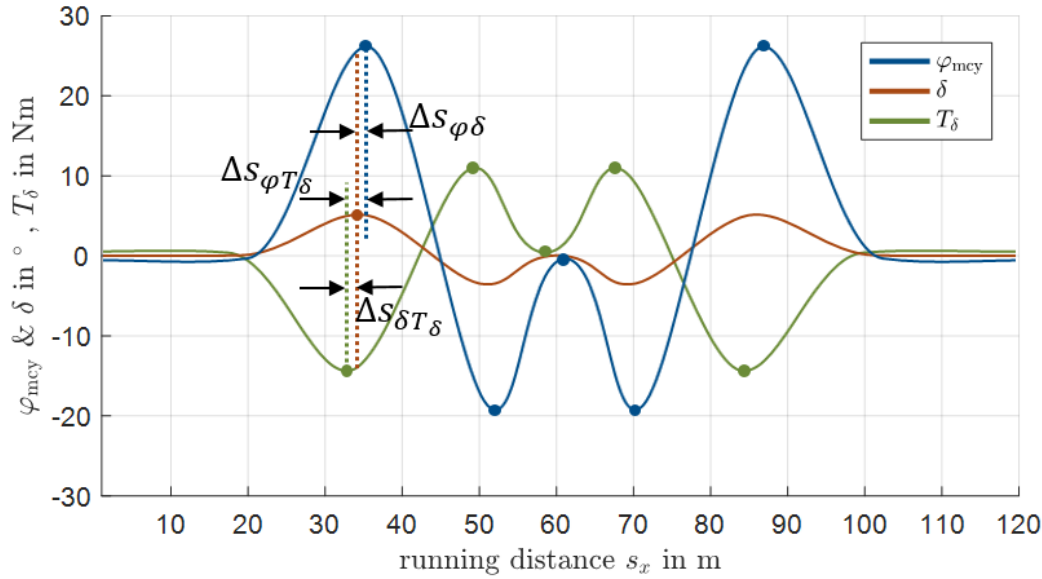
Figure 2.9: Simplified representation of double lane change maneuver. In this example, firstly the peak steer torque (green) is applied. Then, the steer angle peak (red) is reached followed by the roll peak. Own figure based on Cheli[34]

The results presented by Cheli[34] show, that the advance of the steer torque peak to the roll angle peak increases with velocity and that it is typically larger for a rider maintaining a neutral position than a rider that is utilizing lean-in. The steer angle peak typically happens with a short delay with respect to the roll angle peak, with increasing delay, if the rider utilizes lean-in, as depicted in Figure 2.10. Cheli[34] relates this behavior with experience or skill of the study participants while acknowledging that every rider will behave very individually. To the author's knowledge there exists no generally accepted definition or rating for a rider's skill. Until today different behavioral patterns become observable in various studies, but an optimal rider behavior in terms of rider lean has not yet been defined.
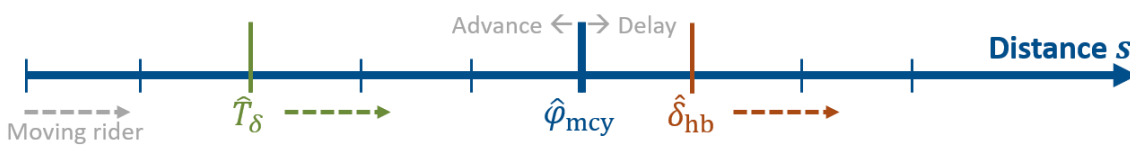
Figure 2.10: Advance of steer torque peak (green) and delay of steering angle peak (red) w.r.t. roll motion peak (blue). The steering peaks supposedly happen later when the rider utilizes lean-in[34].

According to Cossalter[29], "expert riders carry out the double lane change maneuver with a high initial *out-tracking* and use their body inclination to remain vertical or even to generate an additional input with respect to steering torque." Without specifying his reasoning, Cossalter emphasizes the importance of the "phase between yaw velocity and steering torque" as a "quantity more highly perceived by the rider when carrying out such a maneuver" [29].

---

[34] Federico Cheli et al.: Driver's movements influence on the lateral dynamic of a sport motorbike.

2.2.3.3 Handling in Slalom

A slalom maneuver is defined by setting two of the three slalom parameters velocity, frequency, or cone distance.

$$f_{\text{slalom}} = \frac{v}{2 \cdot d_{\text{cone}}} \tag{2.12}$$

A typical cone distance for slow motorcycle slalom (e.g. used for examinations in driving schools) is 7 m. Multiples of that value (14 m, 21 m) can be found in several motorcycle related publications[35,36,37] and will be used here as well. Figure 2.11 shows the connection of these values. A frequency above about 1 Hz is considered as uncontrollable.
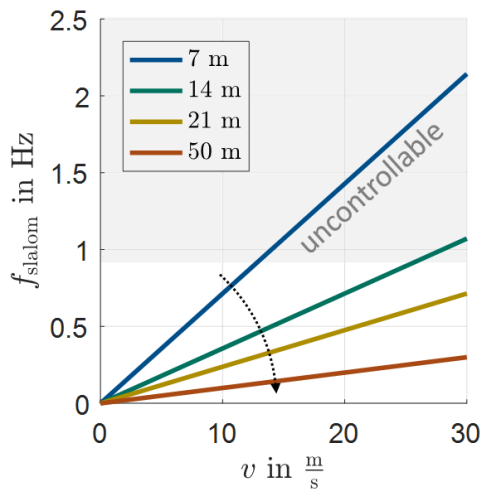
Figure 2.11: Slalom frequencies depending on the set cone distance and velocity. High frequencies will eventually become uncontrollable due to rider and/or vehicle limitations.

Cossalter[38] performed comparisons of slalom maneuvers between real road testing and simulator testing. Therefore, the mean values of several quantities were compared: Slalom frequency f_{slalom} , peak values of roll rate and yaw rate, steer angle and torque $\hat{\varphi}_{\text{mcy}}, \hat{\psi}_{\text{mcy}}, \hat{\delta}$ and $\hat{T}_{\delta}$, as well as each phase, and the ratios $\hat{\varphi}_{\text{mcy}}/\hat{T}_{\text{hb}}$ and $\hat{\varphi}_{\text{mcy}}/\hat{\psi}_{\text{mcy}}$. In the cited study, "the agreement between simulator and experimental road tests is [rated] good for all maneuvers"[38]. However, the authors fail to provide a scale to rate the values as "good" or "bad". Some large deviations – especially concerning the phase delays of some signals – remain undiscussed.

---

[35] Cossalter, V.: Motorcycle Dynamics (2006), p. 320.

[36] Biral, F. et al.: Experimental Study of Motorcycle Transfer Functions for Evaluating Handling (2003).

[37] Cossalter, V.; Doria, A.: Analysis of Motorcycle Slalom Manoeuvres Using the Mozzi Axis Concept (2004).

[38] Cossalter, V. et al.: Development of a motorcycle riding simulator (2011), p. 11.

The **transfer functions** of motorcycles in slalom maneuvers have been investigated experimentally by Biral[39]. Three transfer functions were of special interest and exemplary plots are depicted in Figure 2.12:

$$G_{\varphi,T_\delta}(s) = \frac{\hat{\varphi}(s)}{\hat{T}_\delta(s)}, \qquad G_{\dot{\psi},\delta}(s) = \frac{\hat{\dot{\psi}}(s)}{\hat{\delta}_{hb}(s)}, \qquad G_{\dot{\varphi},\dot{\psi}}(s) = \frac{\hat{\dot{\varphi}}(s)}{\hat{\dot{\psi}}(s)} \qquad (2.13)$$
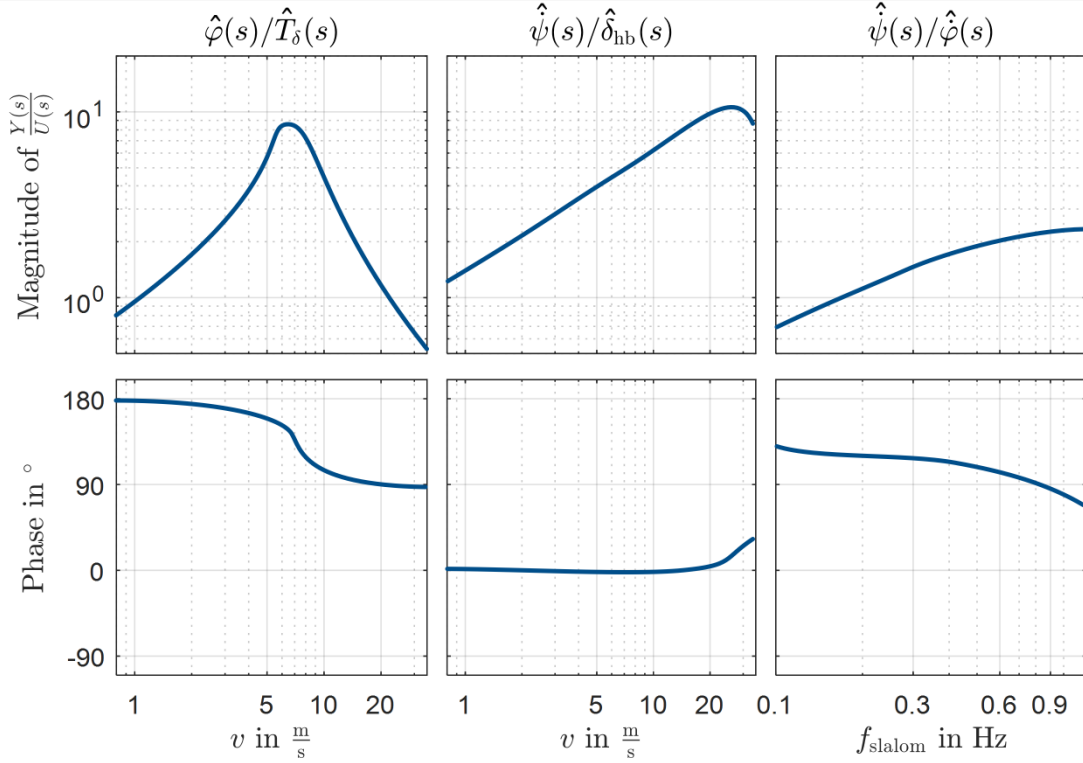
Figure 2.12: Exemplary Bode plots of slalom transfer functions according to Biral[39]. The magnitudes and phase shifts depend on the cone distance and vehicle parameters.

High magnitudes of the **steer torque to roll angle** transfer function (left equation (2.13)) are related to low necessary steer torque values and therefore better handling (as the physical workload decreases). There exists a single magnitude maximum at a characteristic speed, where the least torque input is necessary to perform the slalom maneuver. The phase lead starts above 180° for low velocities and reaches 90° at high velocities, the transition happens around the characteristic speed.

The **steer angle to yaw rate** transfer function (mid equation (2.13)) shows an almost linear behavior with phase delays being close to zero, which is exactly true with pure kinematic rolling (i.e. no sideslip). Considering the same trajectory (i.e. same curvature), a faster vehicle must utilize higher roll angles. Therefore, the **yaw rate to roll rate** transfer function (right equation (2.13)) increases in magnitude with rising speeds. If sideslip is neglected, the phase lead would ideally be at 90° with the maximum yaw rate at the location of the cones

---

[39] Biral, F. et al.: Experimental Study of Motorcycle Transfer Functions for Evaluating Handling (2003).

and the maximum roll rate in between two cones. However, Biral's experimental results show values between 90°-120°.

In Figure 2.12 note, that velocity and frequency are proportional by a factor of $1/(2 \cdot d_{\text{cone}})$ and each plot is only true for one defined cone distance. However, the abscissae of the plots have been chosen to be representative for the respective transfer function. For example, the steer torque to roll angle transfer function G_{φ, T_δ} on the left side of the plot shows the maximum magnitude at a speed around 6 to 8 m/s. This maximum is independent from the slalom frequency which would be either 0.5 Hz, 0.25 Hz or 0.167 Hz for slaloms of cone distances with 7 m, 14 m or 21 m respectively. Accordingly, in the roll rate to yaw rate transfer function on the right side of the plot, the maximum magnitude will always be around 1 Hz, which would happen at different velocities for different slalom cone distances.

2.2.3.4 Mozzi Axis

The previous sub-sections show, how little rider motion is taken into consideration when rating the handling qualities of a motorcycle. Only a few publications are known to the author of this document that investigate rider (motion) behavior, and only some of them investigate the maneuvering capabilities of rider motion. One concept that is capable of discussing the rider motion's effect on vehicle dynamics was introduced by Cossalter et al.[40,41] and utilizes the so-called *Mozzi axis*. It is based upon the idea, that a rigid body's motion is in every instant represented by a rotation about and translation along this axis.

To calculate the Mozzi axis' location and orientation, firstly the pitching motion of the motorcycle is considered negligible. The velocity components $_w v_{x,y,z}$ of any point connected to this body at a distance x_p, y_p, z_p described in the levelled CoSy $(x_{\text{w}}, y_{\text{w}}, z_{\text{w}})$ known from Figure 2.2., can be calculated as

$$\begin{bmatrix} v_x \\ v_y \\ v_z \end{bmatrix} = \begin{bmatrix} V_x \\ V_y \\ V_z \end{bmatrix} + \begin{bmatrix} 0 & -\dot{\psi} & 0 \\ \dot{\psi} & 0 & -\dot{\varphi} \\ 0 & \dot{\varphi} & 0 \end{bmatrix} \cdot \begin{bmatrix} x_p \\ y_p \\ z_p \end{bmatrix} \tag{2.14}$$

With $V_{x,y,z}$ being the components of the velocity of the origin of the levelled CoSy. On the Mozzi Axis, the cross product of angular and linear velocity will become zero:

$$\begin{bmatrix} 0 & -\dot{\psi} & 0 \\ \dot{\psi} & 0 & -\dot{\varphi} \\ 0 & \dot{\varphi} & 0 \end{bmatrix} \left\{ \begin{bmatrix} V_x \\ V_y \\ 0 \end{bmatrix} + \begin{bmatrix} 0 & -\dot{\psi} & 0 \\ \dot{\psi} & 0 & -\dot{\varphi} \\ 0 & \dot{\varphi} & 0 \end{bmatrix} \cdot \begin{bmatrix} x_{Mz} \\ y_{Mz} \\ z_{Mz} \end{bmatrix} \right\} = \begin{bmatrix} 0 \\ 0 \\ 0 \end{bmatrix} \tag{2.15}$$

The point of intersection of the Mozzi axis with the road, expressed in the levelled CoSy is calculated by solving for x_{Mz} and y_{Mz} with $z_{Mz} = 0$ and yields to

---

[40] Cossalter, V.; Doria, A.: Analysis of Motorcycle Slalom Manoeuvres Using the Mozzi Axis Concept (2004).

[41] Cossalter, V.; Doria, A.: Instantaneous Screw Axis of two-wheeled vehicles (2006).

$$_w x_{\text{Mz}} = \frac{-\,_w v_y}{\dot{\psi}} \tag{2.16}$$

$$_w y_{\text{Mz}} = \frac{\dot{\psi} \cdot {_w v_x}}{\dot{\psi}^2 + \dot{\varphi}^2} \tag{2.17}$$

The inclination ς_{Mz} of the Mozzi axis yields to the Mozzi angle

$$\varsigma_{\text{Mz}} = \arctan\frac{\dot{\psi}}{\dot{\varphi}} \tag{2.18}$$

For standard maneuvers way below dynamic limits of the tire, the sideslip angle at the rear wheel can be considered small. Therefore, the longitudinal position $_w x_{\text{Mz}} \approx 0$ and

$$_w y_{\text{Mz}} \approx \frac{\dot{\psi} \cdot v}{\dot{\psi}^2 + \dot{\varphi}^2} \tag{2.19}$$

Figure 2.13 shows a schematic representation of the Mozzi trace.
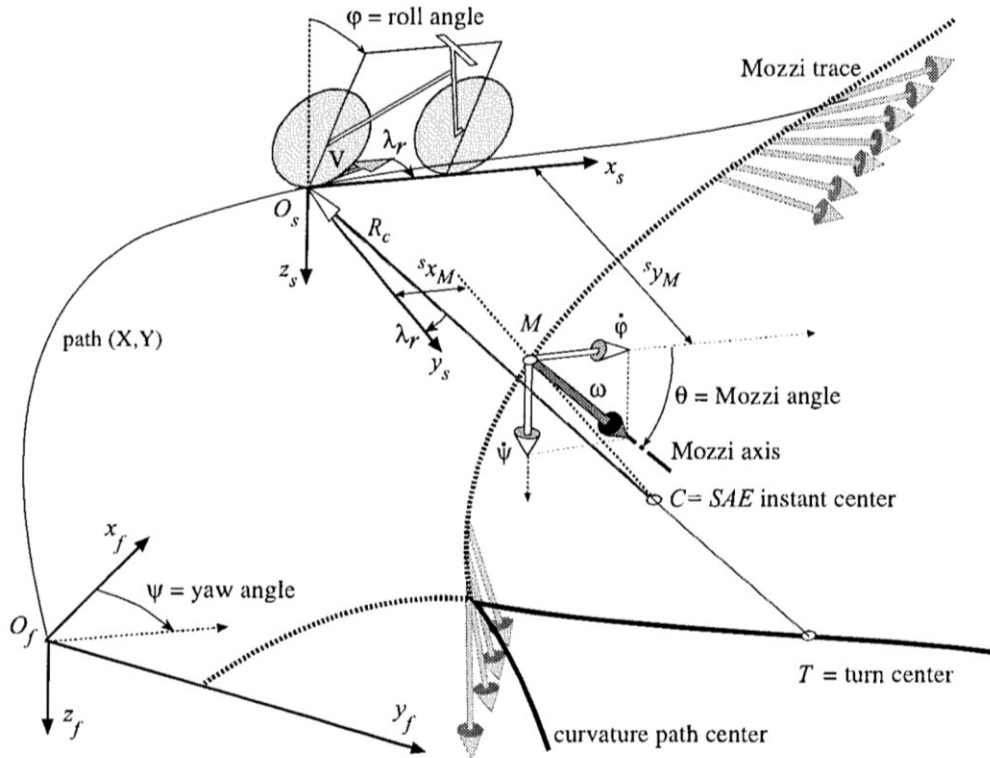
Figure 2.13: Representation of the Mozzi Trace (c.f. Cossalter[40]) The Mozzi trace (dotted line) connects the intersection of the Mozzi axis with the ground plane at every time step.

Two more relevant points are depicted there: The center of rotation C of the levelled CoSy represents the point in the $x_w y_w$-plane that has no horizontal velocity in the earth CoSy $(x_{\text{E}}, y_{\text{E}}, z_{\text{E}})$ and can be calculated from equation (2.16) and (2.17) by assuming $\dot{\varphi} = 0$.

The turn center T of the rear wheel's trajectory depends on its planar velocities, yaw rate and time derivative of rear sideslip angle $\dot{\gamma}_r$. It can be calculated by equations (2.20) and (2.21)

$$_w x_{\mathrm{T}} = \frac{-{}_w v_y}{\dot{\psi} - \dot{\gamma}_{\mathrm{r}}} \qquad (2.20)$$

$$_w y_{\mathrm{T}} = \frac{{}_w v_x}{\dot{\psi} - \dot{\gamma}_{\mathrm{r}}} \qquad (2.21)$$

It can be seen, that the trace of the trajectory turn center only depends on the yaw rate, while the Mozzi trace is furthermore influenced by the vehicle's roll rate. Therefore, a changing rider motion behavior will become observable in the trace and inclination of the Mozzi axis, while this is not the case for the trace of the trajectory's turn center.

Figure 2.14 show results of a simulation study by Cossalter and Doria[40]. In the left picture, the roll and yaw rate for a slalom maneuver are plotted as well as the Mozzi angle. This angle becomes 0 or 180° if the yaw rate is zero (the Mozzi axis lying in the road plane), and $\pm 90°$ if the roll rate is zero (the Mozzi axis perpendicular to the road plane). The right plot shows the traces of the trajectory, its turn center and the Mozzi trace. While the first two stay the same, the latter will change depending on the roll rate. If the magnitude of the roll rate is decreased (as it would happen for a rider utilizing lean-in), the Mozzi trace becomes more and more linear and loses its wave form, as seen in Figure 2.14.
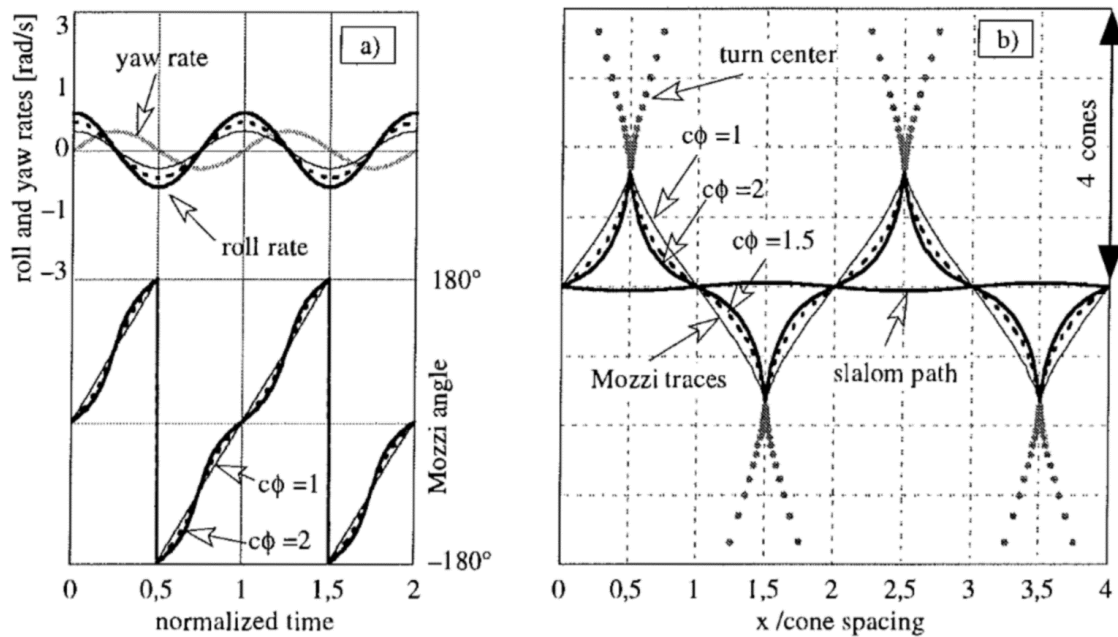
Figure 2.14: Mozzi angle and trace for different roll rate magnitudes, (c.f. Cossalter[40]). The Mozzi angle (bottom left plot) and Mozzi trace (right plot) tend to become piecewise linear when the magnitude of the roll rate to yaw rate transfer function $c\phi = 1$, i.e. the roll rate is as slow as the yaw rate.

Only two publications are known to the author of this document, discussing the habits of the Mozzi axis. While both proclaim an applicability to derive information on rider motion behavior, no specific results were shown and discussed in that regard.

2.2.3.5 Other Performance Ratings in Literature

The overview on bicycle and motorcycle handling and control aspects from Kooijman and Schwab[42] lists further performance measures. Typically, they involve the rating of a minimum time to perform a certain maneuver or the maximum velocity where the maneuver is performed successfully. For all straight and slalom maneuvers, boundary crossings of a defined riding path are suggested as further performance rating.

For bicycling, a further experiment has been suggested by Mortimer et al.[43], where the rider is asked to perform a slow 90° turn. The minimum possible radius is then evaluated to measure the "control" (sic) capabilities. Such a maneuver can easily be adopted for the motorcycle use and is especially reasonable when investigating urban scenarios where the rider e.g. must turn right at an intersection. However, the author would argue that such a maneuver is rather investigating the rider skill but the vehicle handling.

2.3 Motorcycle Rider Control

As the saying "it is like riding a bicycle" implies, once the control behavior is learned, it is hard to unlearn it. However, this behavior doesn't really have to be understood to be applied correctly. A child riding a bicycle will not be able to understand and discuss the abovementioned dynamic properties but will be able to ride a bicycle, nonetheless. Even professional motorcyclists are not always aware of the correct dynamics but are still most capable of controlling the motorcycle in a fast and safe way.

In the YouTube channel "Smarter Every Day", the popular scientist Destin Sandlin produced a video about learning to ride a bicycle with an inverted steering system (i.e. handlebar steering angle to the right leads to the front wheel steering to the left)[44]. After gathering experience with a similar bicycle by himself, the author of this thesis fully supports his findings: Even a deep knowledge and understanding of the vehicle dynamics and the needed control actions as well as experience with manifold differently behaving bicycles will not enable a rider to stabilize the "backwards steering bicycle". While they might know how to behave, it is crucially demanding to "overwrite" the manifested behavioral patterns that have been learned and applied in the past years and decades. Once, the newly needed patterns are available for the rider, it might as well happen that the old ones cannot be accessed anymore, i.e. needing to re-learn riding a standard bicycle.

---

[42] Kooijman, J. D.; Schwab, A. L.: A Review on Handling Aspects in Bicycle and Motorcycle Control (2011).

[43] Mortimer, R. G. et al.: The relationship of bicycle manoeuvrability to handlebar configuration (1976).

[44] Sandlin, D.: Beckwards Brain Bicycle (2015).

These findings follow the concept of neuro plasticity, first described by Hebb[45]. It describes, how the brain can continuously vary the connections of its neural network to optimize for specific tasks. However, once a certain optimization (e.g. for bicycle control) has been developed and reinforced over a long period, these patterns are hard to adjust or reconfigure.

As a human identifies a system as a bicycle or motorcycle, they will instantly access the behavioral patterns connected to this system. Thus, as a simulation gains fidelity, its controls must increasingly suffice the rider's expectations and ideally provoke the rider's unconscious control behavior by accessing the action-action patterns acquired in real life. If however the rider doesn't identify the simulation as a motorcycle, they will start to learn the controls of a new, previously unknown system. As the rider might not have the right understanding of vehicle dynamics, they might however utilize wrong control actions. This can be seen with new study participants on the simulator that will utilize "positive steering" instead of "counter steering" as they consciously concentrate on "making it right" without understanding what "right" really means. This misperception and misunderstanding of a motorcycle's (or bicycle's) steering behavior possibly results from the vehicles responsiveness to rider motion. As a rider leans towards a curve, both frame and steering will follow in the same direction. The rider will then "positive steer" to stop the roll motion. "Counter-steering" is therefore often not consciously perceived by the rider. This effect can however not exist on a DMRS that only uses steering as an input and therefore will not tilt into a curve without a (counter-) steering input.

2.3.1 Rider Behavior Models

The previous sections show the importance of rider perception and behavior regarding vehicle control of a motorcycle. This section is thus concentrating on the general modeling of rider behavior with respect to vehicle guidance and control. This background knowledge is relevant to understand possible slips or mistakes, a rider of a DMRS might perform.

A widely spread approach to describe rider-vehicle interaction is the combination of Rasmussen's three level model of human behavior and Donges' three level hierarchy of the driving task as depicted in Figure 2.15. It shows, how a transport mission (i.e. the task of getting from A to B) is separated into three hierarchically clustered levels with different resolution in terms of preview or duration.

---

[45] Hebb, D. O.: Organization of Behavior (1949).
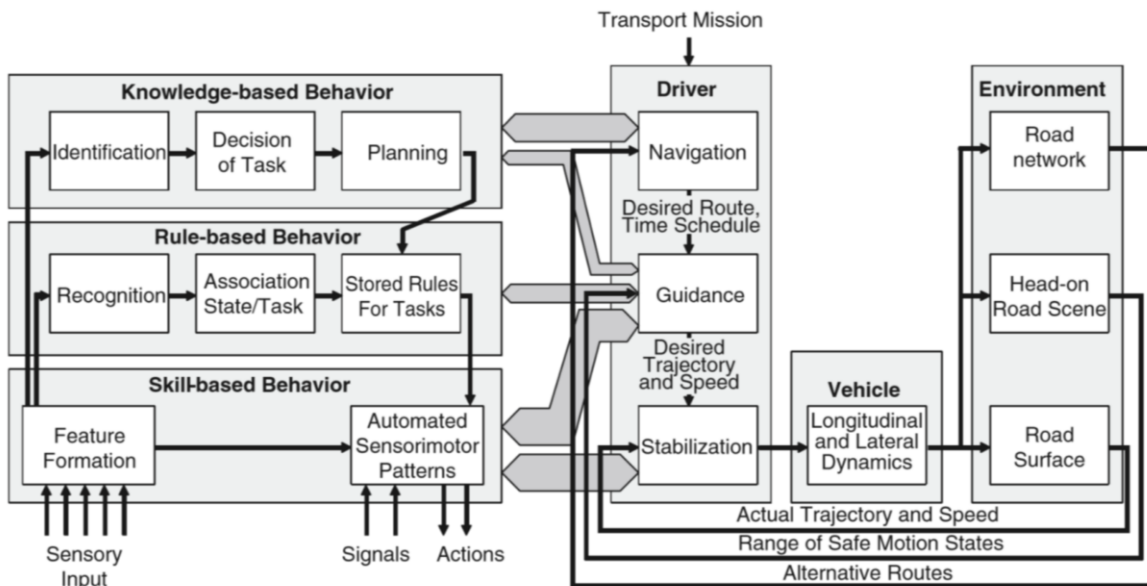
Figure 2.15: Three level model of human behavior and three level hierarchy of the driving task according to Donges[46]

The upmost layer considers the navigation task. There, a rider must plan as certain route across a given road network, mainly using knowledge-based behavior. At any point in time and with no temporal criticality he may decide one way or another. The next, more granular level relates to vehicle guidance. There, depending on specific road geometry and environmental scenario, the rider must choose to go straight or initiate a turn with a desired speed. This level cannot only be served by knowledge-based behavior, as e.g. the environmental conditions and other traffic participants cannot be anticipated but must be recognized and reacted to. These reactions mostly rely on rule-based behavior. IF there is a slow car ahead, THEN perform an overtaking maneuver. IF overtaking, THEN accelerate and turn the steering wheel left/right.

The highest demand in terms of timing comes from the stabilization level. Quick adjustments to the control inputs might be necessary to stabilize the vehicle in highly dynamic scenarios. Therefore, as there might not be enough time to think about and evaluate different possible reactions, the rider cannot rely on knowledge- or even rule-based behavior but must utilize skill-based behavior. In cars, the stabilization task becomes less demanding day by day. They are mostly used within their dynamic potential (i.e. not exceeding tire limits) and even if this potential is exceeded, various assistance systems nowadays support the driver to keep the vehicle stable at all times. On the contrary, a motorcycle is per se an instable vehicle and the stabilization task must be fulfilled at any time, demanding a certain workload from the rider.

According to Donges[46], a rider will apply skill-based behavior to perform the stabilization task. The skill-based mode is the least conscious mode and consists of smooth executions of

---

[46] Donges, E.: Driver Behavior Models (2016), p. 20.

highly practiced actions[47]. On the other side of the spectrum is the knowledge-based mode that supposedly happens in a completely conscious manner.

Applying this scheme to riding a motorcycle or DMRS implies, that the successful stabilization of the (virtual) motorcycle (and therefore riding at all) necessitates unconscious actions performed by the rider through the skill-based mode that includes two main functions:

- Receive information from sensory inputs to provide features for relevant planning or acting functions
- Perform control actions based on automated sensorimotor patterns

The first function is important for all subsequent modes (rule, skill-based) as well, as they rely on the feature formation that is attributed to the skill-based behavior. Furthermore, the actions resulting from skill-based behavior supposedly follow automated patterns. This highlights the importance of correct feedback cues on the simulator, without which no reliable features can be formed, possibly resulting in the automated actuation of wrongly selected control patterns. Norman[48] refers to such errors as "slips" instead of "mistakes" as the intention is correct, but a failure occurs anyway. A simulator performs well if it minimizes the occurring number of slips resulting from improper input sensing and rider feedback.
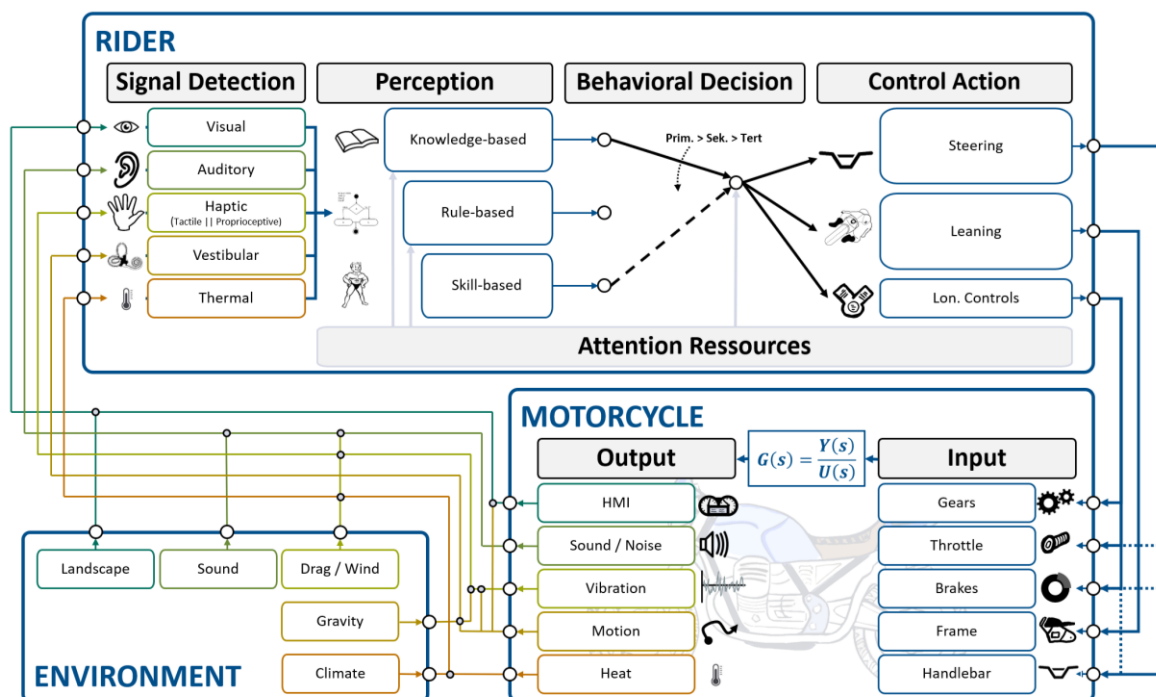
Figure 2.16: Applying the skill, rule, knowledge-based approach to controlling a motorcycle, highlighting the signal flow between rider, motorcycle and environment. Own image based on Guth[49]

---

[47] Embrey David: Understanding Human Behavior and Error (2005).

[48] Norman, D. A.: Design rules based on analyses of human error (1983).

[49] Guth, S.: Diss., Absicherungsmethode von Anzeigekonzepten mittels Motorradfahrsimulator, p. 26.

Figure 2.16 shows the signals and quantities usable by the rider to perceive information and perform actions on the motorcycle as well as the rider's internal decision process. The motorcycle uses the rider's inputs to throttle, brakes, transmission, frame and handlebar to perform a maneuver, resulting in a specific output. This output can be decomposed into the vehicle motion, vibration, sound and noise, information from HMI systems or temperature. Furthermore, external cues from the environment exist: gravity, wind/drag, sound, climate, or the perception of the landscape. All these cues will be detected by the rider through their visual, auditory, haptic, vestibular and thermal sensory cues, closing the loop between rider, vehicle and environment.

When looking at Figure 2.16, it becomes obvious that single outputs from the motorcycle or environment can be experienced by the rider through multiple sensory cues. E.g. a longitudinal motion generates visual cues, as the landscape passes by, auditory cues due to engine and wind noise, haptic cues that might be tactile (vibration of the handlebars or saddle) or proprioceptive (muscle tension to counter drag) and thermal, as the engine or exhausts produce heat.

While these cues are often assimilated unconsciously, the human can direct their attention specifically on certain cues. Each visual, auditory, haptic, vestibular or thermal cue is combined to one holistic perception (i.e. an understanding of the actual scene). Depending on this perception riders can call for the different behavior modes discussed above. If they for example perceive a well-known and trained scene (e.g. a car entering a priority road from the side) they will rely on skill to perform an avoidance maneuver. If, however, they are unfamiliar and untrained in such a scenario, they must rely on the rule-mode and decide about the next steps. Depending on the rider's abilities and the importance of the performed action (primary driving task, or secondary/tertiary tasks) they will decide for a certain behavior and perform a certain control action which – in case of a motorcycle – will either be a steering input, leaning motion, or an input to the longitudinal controls like throttle or brakes. Utilizing the knowledge-based behavior has the prerequisite however, that one really must *know*, or rather *understand*, how to behave. Unfortunately, this becomes an issue with most bicyclists and motorcyclists, who are unaware of their behavior in everyday riding, as discussed previously.

2.3.2 The Relevance of Rider Motion

A model to analyze the effect of rider lean has been presented by Aström et al.[50] The linearized model includes a rider point mass and a motorcycle body with inertial tensor (especially $\Theta_{xz} \neq 0$). It is controlled via rider's steering torque T_δ and rider lean angle φ_{rid}. The model's equation, adjusted to the nomenclature used here, is as follows:

---

[50] Aström, K. et al.: Bicycle Dynamics And Control (2005).

$$\Theta_{xx}\ddot{\varphi}_{\text{mcy}} + \Theta_{xz}\frac{v \cdot k_2(v)}{l}\dot{\varphi}_{\text{mcy}} + \left(\frac{mv^2 \cdot h_{\text{CG}} \cdot k_2(v)}{l} - mgh_{\text{CG}}\right)\varphi_{\text{mcy}}$$
$$= \Theta_{xz}\frac{v \cdot k_1(v)}{l}\dot{T}_\delta + \frac{mv^2 \cdot k_1(v)}{l}T_\delta - m_{\text{rid}}h_{\text{rid}}^2\ddot{\varphi}_{\text{rid}} + m_{\text{rid}}gh_{\text{rid}}\varphi_{\text{rid}} \tag{2.22}$$

The coefficients $k_i(v)$ result from the static torque balance of the front fork. They follow the shape of a hyperbolic cosecant function that is offset along the velocity axis by an amount that depends on geometric properties (mainly wheelbase and steering head angle). The system described in equation (2.22) is stable for sufficiently large $k_2(v)$. The coefficients are depicted in Figure A.1 in Appendix A.3. Assuming riding without hands (i.e. $\dot{T}_\delta = T_\delta = 0$) and performing a Laplace transformation yields the transfer function

$$G_{\text{lean}}(s) = \frac{\varphi_{\text{mcy}}(s)}{\varphi_{\text{rid}}(s)} = \frac{-m_{\text{rid}}h_{\text{rid}}^2s^2 + m_{\text{rid}}gh_{\text{rid}}}{\Theta_{xx}s^2 + \Theta_{xz}s\frac{v \cdot k_2(v)}{l} + \left(\frac{mv^2 \cdot h_{\text{CG}} \cdot k_2(v)}{l} - mgh\right)} \tag{2.23}$$

While this second order transfer function is a result from many simplifications, it is nevertheless capable of showing the vehicle behavior following to a rider's leaning action. The motorcycle will generate a roll angle in the opposite direction to the rider's lean angle at first, as shown in Figure 2.17.
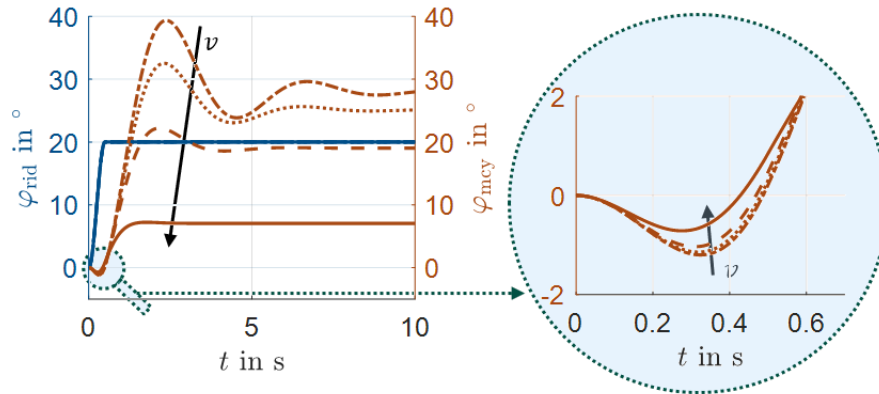
Figure 2.17: Response of the Lean-to-Roll Transfer Function for different vehicle speeds. The rider lean excitation (blue) initially results in an opposing motorcycle roll response, before heading in the same direction. Roll amplitudes decrease with increasing velocity. (Own timeseries visualization based on the transfer function derived from Aström[50])

The excitation in this plot is a rider lean angle following a cosine function from zero to 20° within 0.5 seconds:

$$\varphi_{\text{rid}} = 10°\left(1 - \cos\frac{\pi t}{0.5\text{ s}}\right); 0 \le t \le 0.5\text{ s} \tag{2.24}$$

This signal has been chosen instead of the typically used step function for the more realistic, continuous character of the excitation.

Looking at the transfer function (2.23) it is clear, that the rider can use quick lean accelerations in the opposite direction of the curve to increase the motorcycles roll acceleration and therefore generate side forces more quickly. A rider accelerating relatively to the frame will

always influence the motorcycle's roll angle and therefore the camber side force at both tires opposite to their own direction of leaning. This initial side force towards the opposite side of rider leaning will initiate a roll motion towards the direction of leaning, as the tire contact line undergoes the system CoG (c.f. section 2.3). For increasing velocities, this behavior becomes ever less obvious and only attentive and sensitive riders will experience this opposing movement.

While the capsize mode of the used motorcycle is stable and the rider motion is small, the system will enter a new equilibrium, even with the rider body constantly displaced from the symmetry plane as shown in Figure 2.17. If however the capsize mode is unstable, the rider must at some point lean back towards the outside of the curve to prevent the motorcycle from tipping over. The changing roll angle will inevitably result in a changing curvature, as long as no steering input is used.

Until today, there are many discussions about the exact control strategies riders will use on their motorcycles. This includes all kinds of combinations of steering, leaning, pressure on the foot pegs and pushing the knee against the tank.

The latter two methods alone are ineffective for controlling a motorcycle, as any force, the rider applies at one point of the motorcycle frame will generate a reaction force that has to be supported somewhere else on the motorcycle frame. Thus, e.g. pressure on the foot pegs will only become effective when it results in a relative shift of the rider CoG with respect to the motorcycle CoG, when it increases the body tension leading to a changing impedance, or when the reaction force is supported against the handlebar leading to a steering input.

The steering input on the contrary is the most effective for maneuvering along a given trajectory. As shown in Figure 2.4, very small changes in the steering angle – and therefore sideslip angle – will cause big changes in the tire's side forces. This leads to an instant change of the roll angle equilibrium and therefore to a change of trajectory.

The effect of rider motion to the lateral dynamics on the contrary is smaller and less direct. Two principles of rider motion control can be stated:

- A static lateral offset of the rider will result in a roll motion and/or affect the steady state equilibrium of the motorcycle
- A dynamic lateral motion of the rider generates support forces that push/pull on the motorcycle, thereby dynamically affecting e.g. the camber angle.

Considerable investigations on the rider's motion's influence on vehicle dynamics start in the late 70's. Fu et al.[51], is referred to as the first investigation of riding without hands both theoretically and experimentally. However, they conclude that the problem considering rider's movements is too complex to solve. In the late 80's, e.g. Yokomori et al.[52] and

---

[51] Fu et al.: Stability Analysis of Uncontrolled Motion Single-track vehicles (1978).,after [52]

[52] Yokomori, M.; Yamaguchi, S.: The Rider's Motion Control of Stability (1999).

Katayama et al.[53] were able to further investigate rider's motion with more complex models (e.g. including detailed tire characteristics) and measurement equipment.

The latter publication describes a device for measurements of the rider's body movements that uses a motorcycle fixed support frame and a combination of joints, rods and potentiometers to measure the lateral movement of the rider's back as well as all three rotations relative to the motorcycle frame. It is concluded, that "The rider controls the motorcycle mainly by means of the steering torque. […] The lower body is controlled in order to assist the major control by the steering torque. […] The upper body is controlled to keep nearly upright for the sake of the rider's comfort.". According to the authors, the simulation results represent well the results from experiments with 12 riders running at fixed speed of 60 km/h.

The investigation shows multiple imperfections that are characteristic to the research of rider motion influence in this and many other studies until today (among others, see[52,54,55,56]). These are as follows:

- **Measurement method:**
  While it is obvious, that forces between rider and motorcycle are the cause of dynamic changes, those cannot easily be measured. A holistic measurement of rider-vehicle interaction would necessitate multi-axial sensing at every contact point between rider and motorcycle. It is yet feasible to apply strain gauges e.g. to the ends of the handlebar and the foot pegs[57]. Measuring forces and torques transmitted through the saddle is tedious but manageable with specially manufactured saddle fixtures[58]. Measuring the pressure between legs and motorcycle fairing was until today only performed with smaller demands for precision[59]. Therefore, most investigations rely on measuring distances or angles of certain reference points and assuming point masses.

- **Model simplifications:**
  The assumption of point masses moving strictly along one or two degrees of freedom is necessary to reduce the system complexity to a manageable level. All-body models are known from literature, that utilize 20 degrees of freedom and are actuated by 36 muscles[60]. However, such complex models have not yet been applied in combination

---

[53] Katayama, T. et al.: Control Behaviour of Motorcycle Riders (1988).

[54] Yokomori, M. et al.: Rider's Operation of a Motorcycle Running Straight at Low Speed (1992).

[55] Bocciolone, M. et al.: Experimental Identification of Kinematic Coupled Effects (2007).

[56] Federico Cheli et al.: Driver's movements influence on the lateral dynamic of a sport motorbike.

[57] Evertse, M.: Master Thesis, Rider Analysis using a fully instrumented motorcycle (2010).

[58] Bandow, F. et al.: Bestimmung der Fahrersitzposition im Fahrversuch (2004).

[59] Staffetius, T.; Beitelschmidt, M.: Fahrstilerkennung durch Detektion der Sitzposition.

[60] Walter, J. R. et al.: A control architecture for synthesising biological movement (2021).

with motorcycle multi body simulations for the purpose of analyzing motorcycle controls and handling.

- **Rider behavior assumptions:**
  There are many ways to maneuver through a given trajectory. Depending on rider style, type of motorcycle, etc. different rider motion patterns will be utilized. But most publications concentrate on one control strategy they define as "the right" one and lack of critical discussions on other strategies. Katayama[53] states, that "the upper body is controlled to keep nearly upright for the sake of rider's comfort". This might be a valid assumption on the behavior of some riders. Others might however lean their upper bodies inside the curve instead and consider it as inferior riding if a rider always maintains the upper body upright.

- **Dynamic range:**
  Due to different dynamic behavior of single-track vehicles across different velocity ranges, it is obvious, that the rider's control behavior is not always the same. Therefore, motion control strategies will not only differ between riders, but even during a single course. Depending on the velocity, curvature, preview distance, friction or other environmental parameters, a rider might use different motion strategies.

- **Causation and correlation:**
  Depending on the used working hypotheses and measurement equipment, one might find a strong correlation e.g. between pressure on the foot pegs and roll rate. Following the widespread assumption, that pressure on the foot pegs can be used to steer the vehicle, such a correlation may easily be misunderstood for causation. As stated above, not pressure, but relative motion will ultimately affect the lateral dynamics.

Keeping in mind these imperfections of many studies on rider motion, there are a few outcomes to agree upon:

- The steering input is dominant compared to leaning inputs throughout the full velocity range of the motorcycle. It suffices for the control of the typically used simulation models in typically relevant riding scenarios
- The rider motion has a measurable and perceptible influence on the vehicle dynamics. It will cause changes in steer torque throughout differently dynamic riding scenarios. It suffices for the control of certain riding scenarios but will inevitably fail as singular control input at high speeds or whenever high yaw rates are needed.

A few publications that take interest in the rider mass as integral part to the system dynamics of a motorcycle come from the research group of Professor Cossalter at the University of Padua, Italy. Cossalter[61] shows, how a rider's body will influence the vehicle dynamics in straight running by means of simulations. The oscillating body mass/ impedance acts like a steering damper when the rider grips the handlebars. This improves stability for wobble mode but decreases stability in high-speed weave. The coupling between rider body and

---

[61] Cossalter V. et al.: The effect of rider's passive steering impedance on motorcycle stability (2010)

motorcycle frame is not further investigated in the context of this thesis. It is however the focus of Doria[62], who shows, how the roll oscillations of a mockup motorcycle will provoke repeatable frequency response functions in the rider's upper body. The measurements are compared against four modelling approaches with 1-DoF (rider lean angle), 2-DoF (+lateral shift), 3-DoF (+lateral bend of the upper torso) or 5-DoF (+elbow bend) respectively, as depicted in Figure 2.18.
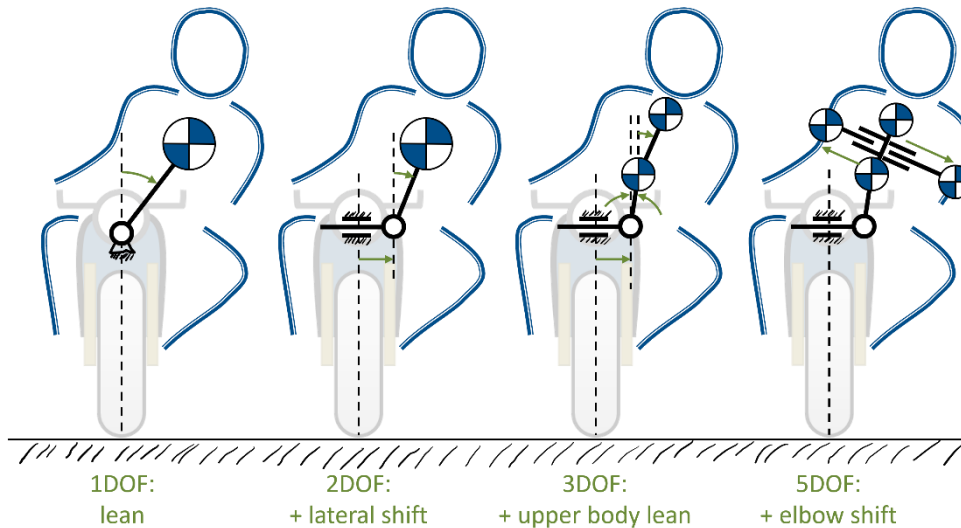
Figure 2.18: Rider lean models with different number of degrees of freedom, after Doria[62]

Tests have been performed in "normal conditions" and "with increased grasping force" on a simplified frame in a purely passive environment, i.e. no riding scenario was presented and no rider inputs were used to manipulate the mockup. The study shows, that even the 1-DoF model is sufficiently representing the dynamics below 4 Hz, while the 2-DoF model shows satisfactory results in the frequency response functions up to 10 Hz. Improvements of the higher tier models become only visible in the steering system and result in impractically high parametrization efforts.

2.4 Driving and Riding Simulators

Vehicle Simulators are widely spread across both research and development departments worldwide. This subchapter will show noteworthy simulators and concepts and discuss the challenges of designing a new dynamic motorcycle riding simulator.

---

[62] Doria, A. et al.: The response of the rider's body to roll oscillations

2.4.1 General Aspects of Simulator Design

While the present work focuses on a single cue within DMRS, an introduction to the nexus of driving and riding simulators is given in the next sections.

A simulator is a machine that resembles the properties and behavior of a given real system. Therefore, it generates cues that are perceivable by the driver/ rider through the different sensory cues of the human (visual, auditory, haptic, proprioceptive, vestibular, olfactory) and measures human inputs that affect the (virtual) system states. The quality demands for each provided control and feedback cue depend on the use case and validity demands of the study.

An overview over the functional elements that are needed to build a simulator is given by Allen et al.[63]. The *simulation computer processing* (SCP) shown left in Figure 2.19 contains virtual components of the simulator (e.g. the virtual environment and vehicle dynamics model) without which no simulation would be possible. Both vehicle and environment are supposed to be modelled according to physical constraints. However, also empirical or phenomenological models can be applied in some use cases. Data base processing merges the vehicle and environment information to a holistic set of states that is provided to the rider.
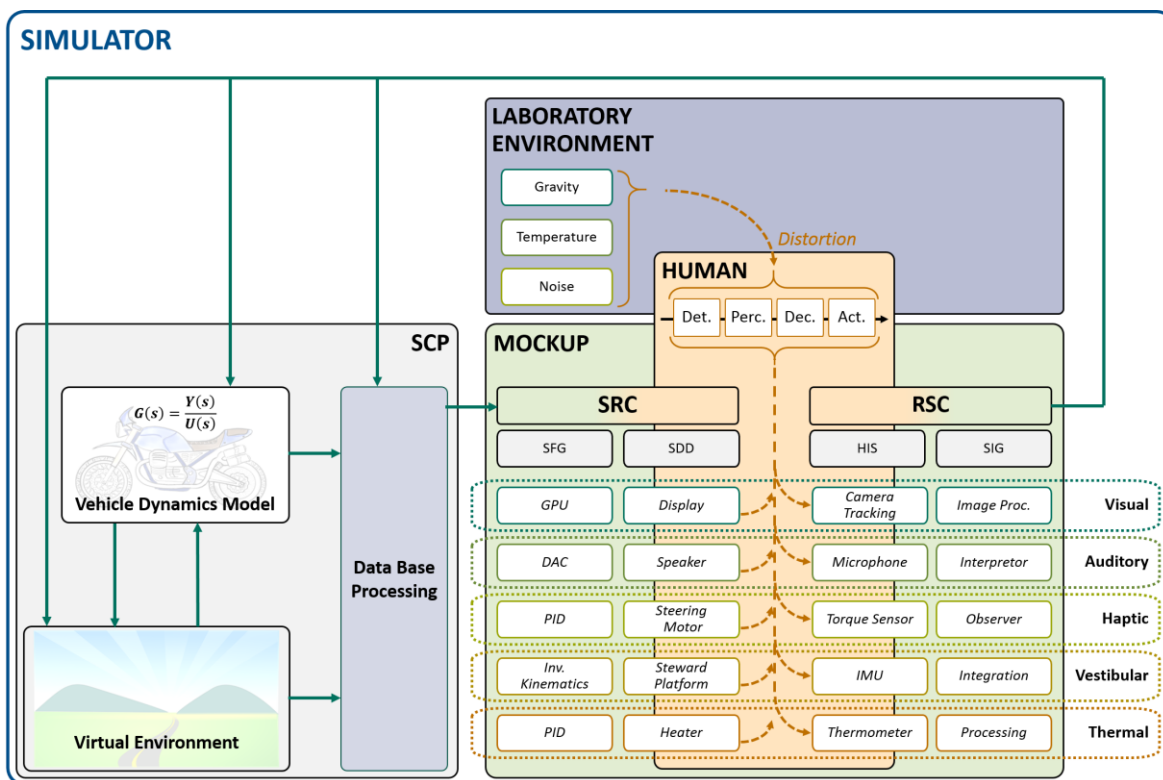
Figure 2.19: Functional Elements of DS (diagram based on Allen et al.[63], but extended by a laboratory environment as a potential disturbance to the human behavior model.)

Therefore, the simulated quantities are converted into feedback cues (c.f. Allen et al. [63]: *Sensory Feedback Generation* (SFG)) and provided to the user by means of actuators,

---

[63] Allen, R. et al.: A Short History of Driving Simulation (2011).

loudspeakers, displays or projections, etc. (c.f. Allen et al. [63]: *Sensory Display Devices* (SDD)). SFG and SDD are here grouped as *Simulation-Reality-Converters* (SRC).

The measured rider inputs (*Human Input Sensing* (HIS)) are converted into quantities that are usable by the vehicle dynamic model or virtual environment ((*Simulation Input Generation* (SIG), e.g. measuring rider angle with respect to the mockup by means of an angular potentiometer and estimate the head position within the virtual environment). HIS and SIG are here grouped as *Reality-Simulation-Converter* (RSC)

According to Allen, the human receives the displayed cues ideally within a cabin to exclude external stimuli. To the author's knowledge, there exists no motorcycle simulator using a cabin at the date of printing this document. Therefore, Figure 2.19 shows the Laboratory environment as a possible source of distraction and other disturbances to the rider that can decrease the perceived quality of the simulator.

2.4.2 Involvement, Immersion and Presence

With simulators it is not possible to completely exclude the reality, neither regarding the environment, nor regarding the system. The human will always interact with a real interface that is digitally connected to a virtual subsystem. They will not see a virtual environment, but pixels on a screen and they will not grip a virtual handlebar, but its real representation. In psychology, three concepts are known to describe the fidelity of a simulation and its interfaces from a human centered point of view.

Presence describes the sensation of experiencing a virtual environment or situation. According to Witmer and Singer this necessitates two factors[64]: Involvement and Immersion. With high presence, the human will consider themself an interactive part of the virtual environment or scenario instead of an external controller of a system. Thereby it allows the human to act successfully in the virtual environment[65].

Involvement describes a psychological state that results from concentrating attention to a set of stimuli. E.g. focusing on reading a book with full attention can produce high involvement. However, it depends on the individual importance or value that human assign to the stimuli and is influenced by the correlation of each stimulus of a set. E.g. steering a virtual car with a keyboard can involve a kid very much, while steering a virtual car with a steering wheel but receiving no or false lateral accelerations can distract the driver, although the steering wheel alone provides higher fidelity than the arrow keys on a keyboard.

Immersion is the technical precondition for presence and can be seen as the quality of the used RSC and SRC. It is obvious, that a high resolution of projection systems owns a higher potential to create a realistic environment than low resolution systems and that a continuous

---

[64] Witmer, B. G.; Singer, M. J.: Measuring Presence in Virtual Environments (1998).

[65] Will, S.: Diss., Presence Model for Driving Simulators.

steering input performs better than discrete steering with the arrow keys of a keyboard. A high immersion provides the feeling to be able to interact with the virtual environment and receive correct and timely feedback to any given action. To increase immersion, it is beneficial to isolate the human from real cues and provide purely simulated cues. A high-resolution head mounted display (HMD) providing 360° surround view will thus provide higher immersion than e.g. a cylindrical screen with limited height and wrapping angle. Increasing the immersion of RSC and SRC is typically cost intensive for their higher resolution, precision and computing power.

When the human participant of a simulation experiences errors of the virtually provided scenario their involvement and immersion might suffer up to a degree, where they loses presence. This is *called break in presence* (BIP)[66]. BIPs can e.g. happen, if cues from the real environment cannot be integrated into the virtual environment.

Witmer and Singer[67] hypothesize that the factors listed in Table 2.2 contribute to presence:

Table 2.2: Factors contributing to a sensing of presence, after Witmer and Singer[67] Targeted DLRC effects are highlighted in blue

Control Factors	Sensory Factors	Distraction Factors	Realism Factors
Degree of control	Sensory modality	Isolation	Scene realism
Immediacy of control	Environmental richness	Selective attention	Information consistent with objective world
Anticipation of events	Multimodal presentation	Interface awareness	Meaningfulness of experience
Mode of control	Consistency of multimodal information		Separation anxiety/ disorientation
Physical environment modifiability	Degree of movement perception Active search		

---

[66] Slater, M.; Steed, A.: A Virtual Presence Counter (2000).

[67] Witmer, B. G.; Singer, M. J.: Measuring Presence in Virtual Environments (1998), p. 229.

The DLRC system discussed in this thesis aims to contribute especially to the control factors and sensory factors. According to the highlighted elements of Table 2.2 it should

- provide the rider with more control over the vehicle,
- cause immediate vehicle responses to rider motions,
- cause responses that are anticipated by the rider of a motorcycle,
- allow to interact in a natural manner,
- provide a more holistic rider vehicle coupling, not just by steering,
- allow for a direct and effortless interpretation of (and interaction with) the virtual environment.

2.4.3 Motorcycle Motion Simulation

Aiming for a highly immersive simulation, it is important to provide the correct cues that enable the user to experiencing the motion of the virtual vehicle relative to the virtual environment. While in literature the term "motion cueing[68]" is often used for vestibular information only, this thesis will often speak about "multi cueing" instead. This implies, that the perception of motion is a result not only of vestibular information but can be supported or even substituted by e.g. haptic information. This is for example achieved by using a longitudinal steering head displacement[69], or pressurized air cushions and active seat belts[70].

Such measures become necessary, as the available motion space is typically rather limited, except for e.g. on wheeled mobile driving simulators as presented by Betz[71]. Performing a horizontal acceleration of 0.5 g for a duration of just 2 s requires 10 m of translational motion. Typical acceleration maneuvers would however take more time and might even reach to values higher than 0.5 g.

One way to circumvent this issue on a simulator is to scale the provided accelerations. However, not all studies allow for reduced motion amplitudes. A second way is the abovementioned utilization of haptic cues. Thirdly, the so-called *tilt coordination* (TC) is commonly used. A platform tilted at an angle of 30° will reduce the perceived gravity in the rider frame (g' in Figure 2.20, left) by just 0.13 g but therefore generate a perceived horizontal acceleration of 0.5 g (a_x' in Figure 2.20, left).[72]

---

[68] Baarspul: Motion cues of flight simulation, 1986, according to Betz

[69] Arioui, H. et al.: Mechatronics of a Motorcycle Simulator (2010).

[70] VI-grade: Compact Simulator.

[71] Betz, A.: Diss., Feasibility Analysis of Wheeled Mobile Driving Simulators (2013).

[72] Reid, L.; Nahon, M.: Flight simulation motion-base drive algorithms (1985).
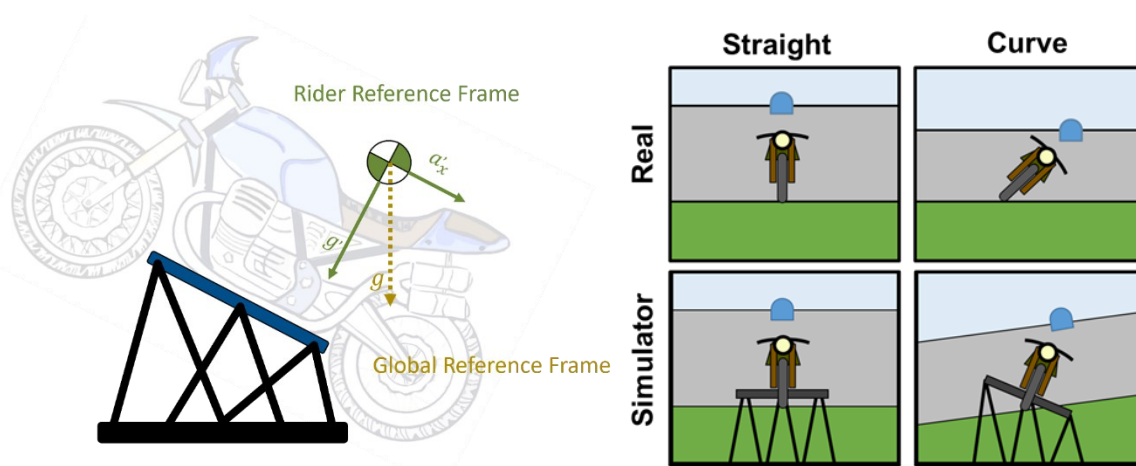
Figure 2.20: Effects of platform tilting motions to motion simulation. Left: Tilt-coordination used to simulate longitudinal accelerations. Right: Combination of platform and image roll angles to mimic the real motorcycle's roll angle.

Such accelerations provided through tilt coordination can be held for unlimited time and do not increase the platform's demand for horizontal motion. However, the dynamics of the tilting motion must be beneath the perception limits of the human to prevent false cues. The tilting amplitude is limited by the visual system if the projection is not platform fixed.

On a first glance, it would seem reasonable to simulate a motorcycle's roll angle through tilting the motion platform. This is not really an option however, if the platform doesn't provide a corresponding centrifugal force that pushes the rider into the saddle as in real life cornering scenarios. At a certain platform roll angle, a simulator rider would rather fall off the mockup instead of being pushed into the saddle, due to the lack of this horizontal force component (see section 2.1). Motorcycle roll angles are thus rather simulated by a combination of platform tilting and rotation of the projection view, as depicted right in Figure 2.20. Guth[73] performs a comparison of different motion cueing concepts, showing that despite constant platform roll angles being somewhat unreasonable (as they impose the abovementioned effect of tilt coordination in a lateral direction), they improve subjective ratings when performing maneuvers on a DMRS. The provided platform roll rates will furthermore influence the perceived steering torque and total agility of the simulator.

Lastly, so called washout filters are used to provide the user with acceleration perceptions. A washoutfilter scales accelerations and feeds them into the platform controller through a high-pass filter. Therefore, the platform will always tend to return to its center position. As stated by Barbagli[74], a motorcycle simulator is typically designed to reproduce a wider range of dynamics and is not just optimized for one specific use case. He concludes, that this leads, in general, to poorer performances of the washout filter.

---

[73] Guth, S. et al.: Motion cueing algorithm to reproduce motorcycle dynamics (2015).

[74] Barbagli, F. et al.: Washout filter design for a motorcycle simulator (2001).

2.4.4 Force Feedback Systems for Steering Simulation

So-called force-feedback (FFB) systems are used in a manifold of technical applications. They are used to generate a bilateral haptic interface to either a virtual object or – adding even another actuation in the signal path – a remote object. Typical applications outside the vehicle simulation domain are e.g. robots in collaborative manufacturing processes, enabling safe interaction between robot and human as well as medical robots enabling tele-operated medical procedures. Force feedback systems in the car simulation domain have shown rapid improvements over the past years. Motorcycle FFB systems however pose different demands to the controllers e.g. due to vastly changing dynamical properties at different velocities.

There exist different classifications of haptic control schemes[75]. In this document, a classification is used that emphasizes the two manipulators acting in series – the device and the operator:

- **Impedance Control**
  The actuator is considered to act as a mechanical impedance, while the human operator acts as a mechanical admittance. This describes the manipulator as a body that is subject to a motion excitation imposed by the operator and is resisting this excitation with a certain force. The human on the contrary is subject to this contact force moves the manipulator to the desired position. This approach does not necessitate a force measurement but will benefit from such in terms of controller stability.

- **Admittance Control**
  The actuator is considered to act as a mechanical admittance, while the human operator acts as a mechanical impedance. Opposed to the abovementioned method, the manipulator is controlled to move in certain direction, when it is subject to a contact force. Obviously, it is therefore mandatory to measure this force, which is not seldom a mechanical challenge on its own.

The decision to use one control concept over the other depends on the mechanical properties of the manipulator, the operator, as well as the virtual object that is being simulated.

A system controlled by impedance control benefits from low(est possible) inertia. As this property is typically limited to a certain minimum, an open loop force control is usually only applied, when the system has very low natural dynamics. The system dynamics can be improved by measuring the contact force and implementing a closed loop controller. However, the large necessary controller gains will eventually reduce system stability. Most commercially available haptic devices (i.e. gaming wheels and joysticks) use impedance control, as it may work without expensive force sensors. Admittance controlled devices on the contrary are suited for higher system dynamics as well as hard nonlinearities and are said to provide a somewhat more 'natural feeling'. Due to peculiar characteristics of the underlying controllers, simple admittance-controlled devices can show rather big phase lags. There exist

---

[75] Ueberle, M.: Diss., Design, Control, and Evaluation of Kinesthetic Haptic Interfaces (2006).

different implementations of impedance- and admittance controllers as well as methods to combine the benefits of both methods e.g. by means of hybrid solutions.

The question for the best way to design a steering system for a motorcycle simulator is yet unanswered. There exist only few publications deliberately focusing on this niche topic.[76,77] However, it can be found, that the rider's steering torque is generally used as input to the vehicle dynamics models and the steering columns of known motorcycle simulators usually contain torque sensors. Therefore, it is assumed, that a variant of admittance control is typically applied. The steering implementation on motorcycle riding simulators is still an active research field. In the future, steering controllers might benefit from improvements in control theory and utilize combinations of impedance and admittance controllers that adjust to the changing impedance of the steering system at different velocities.

2.5 State-of-the-Art Motorcycle Simulators

This section gives an overview of motorcycle simulators that are mainly used in research and development. Aside from some highly sophisticated simulators, there exist more cost-efficient solutions that are rather used e.g. for entertainment and gaming reasons, but also for training purposes, as the first example shows. If not stated otherwise, the information provided in this section originates from Nehoua et al.[78], Young et al.[79] as well as Will[80].

2.5.1 Honda Riding Trainer

One of the simplest, most widely spread motorcycle simulators until today is manufactured by Honda (Figure 2.21, mid picture). It is used by driving schools in Japan, where it is mandatory to perform a certain number of driving lessons on a simulator to familiarize with the motorcycle's controls and typical hazard scenarios. The main development objective of this simulator was to reach out to a broad number of users, thus it had to be manufactured at a very low cost. After designing two dynamic simulator prototypes with four or three DoF respectively, Honda finally settled for a static simulator. A linear model was implemented that provided neither instabilities nor counter-steering. It was supposed that this – physically speaking *wrong* – strategy improves the rideability of the virtual motorcycle, as the simulator user doesn't experience centrifugal forces and behaves like driving a car.

---

[76] Nehaoua, L. et al.: How to Estimate Robustly the Rider's Action (2013).

[77] Nehaoua, L. et al.: Rider Steer Torque Estimation for Motorcycle Riding Simulator (2010).

[78] Nehaoua, L. et al.: Review on Motorcycle Simulators.

[79] Stedmon, A. W. et al.: Motorcycle Simulator Solutions for Rider Research (2017).

[80] Will, S.: Diss., Presence Model for Driving Simulators.

Similar models have been manufactured e.g. by Kawasaki or the Foerst GmbH[81].

Figure 2.21: History of Motorcycle Simulators: l.t.r.: Honda First (4DoF) and Second (3DoF) Prototype, Honda Rider Trainer (Steering only), Kawasaki Motorcycle Simulator with HMD, Foerst Motorcycle Simulator with kinematic unstable mount.

2.5.2 Serial Kinematic Platform Simulators

Most of the motorcycle simulators that have been built in the current millennium are based on serial kinematic platforms (i.e. actuating each DoF separately with one end effector fixed to another) and are used in research institutes across Europe. While parallel kinematic platforms provide several advantages, as shown below, they are usually too budget intensive for small motorcycle research groups.
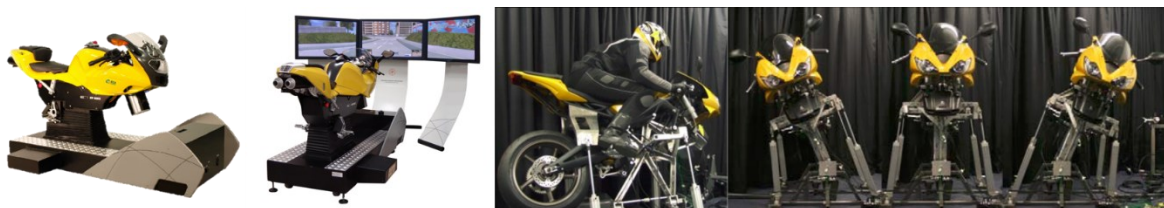
Figure 2.22: Serial-Kinematic Platform Simulators: left: EF-Bike, ECA Group, right: MotorcycleSim, University of Nottingham

Simple representations of such simulators are the *MotorcycleSim*[82] at the University of Nottingham, UK and the *EF-Bike* from ECA Group. They implement roll-motion or both roll- and pitch-motion respectively and are depicted in Figure 2.22. Neither one uses haptic or proprioceptive cues or considers rider motion as an input but only steering. Visuals are presented through either monitors or projection screens of rather small size. Both Université Gustave Eiffel (former IFSTTAR former INRETS) in France and the Hellenic Institute of Transport (CERTH-HIT) use a 4DoF Simulator with corresponding technology as shown left in Figure 2.23. Aside of steer, roll and pitch motion it is utilizing yaw motions with the goal of reproducing rear wheel skidding scenarios (but no front wheel skidding). The visual presentation is again either done by three 42 Inch TFT-screens or three projections respectively. The sound is presented via a 5.1 surround system and steering motion via an electric motor. So far, the simulator represents the "best practice" of motorcycle simulation.

---

[81] Foerst, R.: Foerst Fahrsimulatoren Firmenhistorie (2011).

[82] Stedmon, A. W. et al.: MotorcycleSim (2011).

However, one very special and unique cue is utilized at the simulator: To generate the impression of longitudinal acceleration or deceleration, a linear actuator can adjust the **distance between seat and handlebar**. This motion represents the perception of pulling the handlebar away when accelerating or pushing against the handlebar while braking. While this variation of distance is obviously no realistic input, it is nevertheless generating a proprioceptive cue associated with accelerations. This shows, how innovative approaches to multi cueing can solve limitations of dynamic platforms, at least to some degree. However, limitations are set by e.g. perception limits of the rider when the ergonomics of the mockup change too drastically. Also, such a concept can only be used with one specific, generic mockup but no changeable customer motorcycle. The used motorcycle parts come from a 125 cc Yamaha road bike. The influence of the perceived ergonomics to riding behavior on a simulator has not been an issue of past research. However, it is assumed that e.g. the tank and seat contour influence the mockup roll angles that are comfortably achievable without struggling due to the lack of centrifugal forces (see section 2.4.3), and that a small bike is anticipated to behave more agile than a big touring bike, as well in simulators.
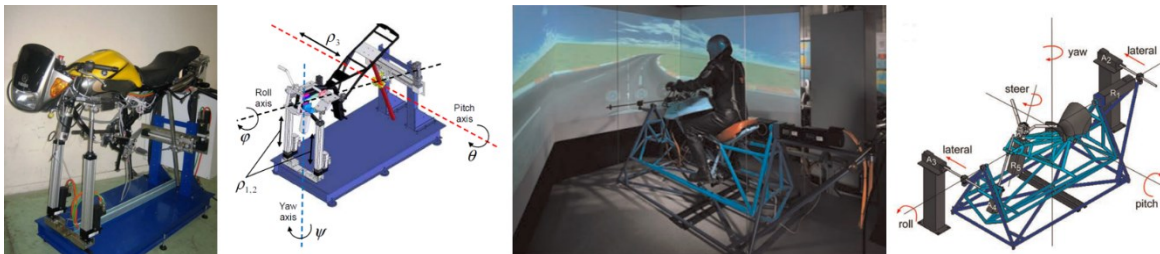
Figure 2.23: Research Simulators: left: IFSTTAR[83], right: DIMEG Simulator, UniPd[84]

The right side of Figure 2.23 shows the DIMEG Simulator at the University Of Padova, Italy, that was developed by the research group of Prof. Vittore Cossalter. The DIMEG Simulator allows 5DoF including all three rotational motions of the frame, steer angle and – unique at this point of the document – lateral displacement. It consists of a support frame that is fixed hanging on four steel cables to carry the static weight of the simulator. Two spindle drives at the front and rear generate the lateral and yaw motion of the support frame. Inside of the support frame, the mockup frame rotates around a longitudinal axis that is lying close to the CoG of the mockup, driven by an electric motor. The mockup frame then carries the steering actuator. Due to the possibility of lateral displacements, both roll axis and yaw axis of the simulator are virtually moveable. E.g. superposing a rightwards roll actuation of the mockup frame with a lateral motion to the right of the support frame lowers the virtual roll axis. In real riding scenarios, the height depends on the roll rate and lateral velocity of the vehicle. It lies at ground level for $v = 0$ and at CoG height for $\mu = 0$.

The motion platform is located in front of three projection screens ($h \times w = 1.5 \text{ m} \times 2.0 \text{ m}$ each) that provide a 180° horizontal field of view. As for the aforementioned simulators, a

[83] Nehaoua, L. et al.: Design and Modeling of a New Motorcycle Riding Simulator.

[84] Cossalter, V. et al.: Development of a motorcycle riding simulator (2011).

5.1 surround sound system is used. The dynamic model is based on the equations presented in [85] and compiled from Fortran code.

According to Cossalter[84], the simulator is equipped with a vertical load **measurement at the foot pegs** and indirect estimation of body leaning. With this, it is possible to utilize pressure on each foot to provoke a roll motion of the virtual motorcycle. From a mechanical context it is known that a rider pushing thier feet on the foot pegs is not able to generate free torques on the motorcycle frame (see section 2.3.2). However, from a behavioral point of view, it can be argued, that even professional riders claim to utilize pressure on the foot pegs to control their bike[86]. The chosen input shows to be effective for certain study participants and allows for manipulation of the motorcycle's lateral dynamics. However, this manipulation is also strictly limited to this specific input cue. A leaning motion of the rider or other kind of weight shifting will not influence the vehicle dynamics if no change in foot load is measured.

2.5.3 Parallel Kinematic Platform Simulators

The more recent motorcycle simulators known to the author of this document are almost all based on Stewart Platforms, also known – and in this document referred to – as *Hexapods*. These parallel manipulators allow for the control of all six DoF, each three translations along as rotations around the coordinate axes. As all six DoF can be combined independently, it is able to configure the instantaneous center of rotation precisely to almost any position in space. Therefore, the positions of the three (virtual) rotation axes can be chosen freely, providing much more variability for the motion cueing algorithm. This can prevent false movements due to couplings of single DoF of serial kinematic platforms. Typically, a hexapod is very cost-intensive and the needed investment is not bearable for small companies and institutes. However, hexapods prove to be the choice when it comes to vehicle simulation for not only motorcycles, but also cars or airplanes. Figure 2.24 depicts the short history of hexapod-based bike simulators since the year 2000. There, a motorcycle simulator was developed by a team at Tokyo University[87], trying to overcome the shortcomings of the previously shown Honda simulator prototypes. The system uses a head mounted display (HMD) with head tracking for visualization. No further information was found on this simulator.

The same concept (hexapod + HMD) is present on the scooter simulator developed in the European project MOTORIST[88] or the most recent motorcycle simulator that was built by the Dutch simulator company Cruden[89].

---

[85] Cossalter, V.; Lot, R.: A Motorcycle Multi-Body Model for real time simulations (2002).

[86] Adams, B.: Pressuring the Pegs (2014).

[87] Chiyoda, S. et al.: Development of a Motorcycle Simulator Using Parallel Manipulator (2000).

[88] Celiberti, F. et al.: MOTORIST Simulator (2016).

[89] Westerhof, B. E.: Evaluation of the Cruden Motorcycle Simulator (2018).
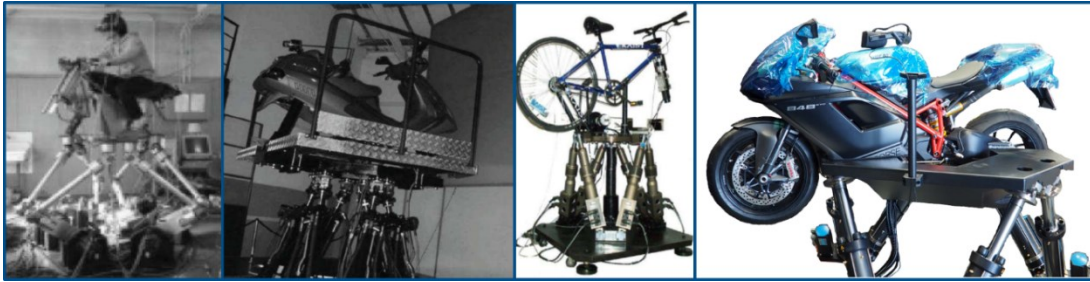
Figure 2.24: Hexapod Based Simulators. L.t.r.: Tokyo University, Japan; PERCRO & Piaggio, Italy; Korean Advanced Institute of Sciences and Technologies; Cruden, Netherlands[89].

As HMDs until today don't necessarily reach sufficient image resolutions or update rates, some simulators will opt for a projection screen instead, like the PERCRO[90] or BMW Motorrad[91] Simulator and the DESMORI simulator which is content of this thesis and will be discussed in detail below. Attempts have also been made to use hexapods for bicycle simulators, as seen in the second right picture of Figure 2.24. Of the abovementioned simulators, only the Cruden and BMW Motorrad simulators provide optical rider tracking mechanisms to utilize rider motion as an input, while the KAIST bicycle Simulator measures the load on each leg of the hexapod to estimate the rider moment[92]. Westerhof[89] concludes, that using the optical tracking device had no significant influence on the performance or quality of the simulator. However, he sees issues with the selected test maneuvers that didn't necessitate any leaning motion and questions the precision of the used sensor setup. He also reports that most participants were mentioning that they could usually steer their own motorcycle more by using body motion.

No other of the comparative simulator publications cited above puts special emphasis on the rider motion input. As Nehaoua et al.[93] concentrate on the mechatronic configurations and Stedmon et al.[94] as well as Will [95] concentrate on study applications and human factors, it seems, that the consideration of rider motion is of only minor importance. Also, the specific publications of each simulator development group will only call rider motion in side notes and rather put emphasis on other control, perception, or cueing problems instead.

The most recent (published) dissertation regarding high fidelity motorcycle simulators comes from Grottoli[96]. There, a dynamic scooter riding simulator is designed with the goal to perform well at low speeds. The simulator utilizes a multi body simulation model that is

---

[90] Ferrazzin, D. et al.: THE MORIS MOTORCYCLE SIMULATOR: AN OVERVIEW (2001).

[91] Guth, S.: Diss., Absicherungsmethode von Anzeigekonzepten mittels Motorradfahrsimulator.

[92] Shin, J.-C.; Lee, C.-W.: Rider's Net Moment Estimation (2004).

[93] Nehaoua, L. et al.: Review on Motorcycle Simulators.

[94] Stedmon, A. W. et al.: Motorcycle Simulator Solutions for Rider Research (2017).

[95] Will, S.: Diss., Presence Model for Driving Simulators.

[96] Grottoli, M.: Development and evaluation of a motorcycle riding simulator (2021).a) p. 93 seq.

artificially stabilized via a horizontal force acting on the vehicle CoG at low velocities. The steer torque that controls the virtual motorcycle is calculated by a controller that takes the user's steer angle input and from that calculates a target roll angle assuming steady state conditions of a simplified point mass model. This indicates, that the simulator rider is rather decoupled from the actual steering dynamics and must rather point the steering in the direction they desires to ride. Furthermore, Grottoli reports a lag in the motorcycle's lateral dynamics resulting from the lateral controller. The relevance of rider motion is shortly mentioned, but it is not used as an input to the simulator. After experiencing sickness issues with most of his study participants, Grottoli changes from a HMD visualization to a 17" platform mounted screen and turns off the motion controller of the Hexapod in order to let at least some riders successfully perform a cornering maneuver in two thirds of the repetitions of the experiment[96a)].

Many issues of this and comparable studies could possibly be reduced by extensive training of the participants, thereby reducing simulator sickness effects resulting from visualization and motion perception. Alternatively, assistance systems and model simplifications are used to enable the rider to perform a certain maneuver. Regardless of the exact simulator setup and false cues, by gaining experience, the rider will more and more ride a simulator, instead of a motorcycle. Getting used to the perceptions and dynamic behavior will quickly manifest in new control strategies of the rider and soon enough, they will be able to successfully maneuver through a given scenario. While this might not negatively affect the study results and still provide relative validity (e.g. when comparing HMI-A vs. HMI-B), it is always the goal to provide a simulator rider with the most realistic riding experience possible.

2.5.4 Conclusions From the State of the Art

The previous section has provided an oversight about the current state of the art of motorcycle simulators. It can be summarized, that – especially compared to flight- and car simulators, there are still many unharvested potentials in the development of motorcycle simulators. They face special challenges mainly due to the peculiarities in vehicle dynamics, motion cueing and human factors:

- **Vehicle Dynamics:** Motorcycle instability, balancing operation, tire modelling
- **Motion Cueing:** representation of roll angles, lacking centrifugal forces, force feedback controllers, exposure to wind and other environmental influences, typically high dynamics (accelerating and braking)
- **Human factors:** biased expectations based on individual experiences, misperceptions preventing to access motorcycle-specific behavior patterns

Of the presented DMRS, one might subjectively provide the best visualization, another might provide a subjectively better platform motion behavior and the third one a better steering. However, the whole thing is more than just the sum of its parts. A motorcycle simulator will therefore not automatically perform better, as it is adopting the MCA of another ("better") simulator, as this might badly interfere with the steering or the visual system. Therefore,

during the development and setup of the DESMORI motorcycle riding simulator that is described in the following chapter, it was not possible to just select the best working components from each existing simulator that suffices the state of the art.

2.6 Open Research Questions

The previous sections have shown some of the peculiarities of motorcycle dynamics, rider behavior and simulator design that affect the points that have to be considered in order to provide riders of a DMRS with a highly realistic experience. All state-of-the-art DMRS struggle to some extend to providing their users with a highly realistic feel caused by several system immanent limitations including:

- Lack of centrifugal accelerations on all (reasonable) motion platforms
- Simulating an instable system with a stable platform
- Limited representation of realistic cues e.g. wind load
- Potentially limited field of view (except with HMD)

As such limitations cause riders to understand the provided system rather as a computerized driving simulation tool than as a real motorcycle, they often show vast behavioral differences to real riding. The biggest of which is incorrect steering behavior that rather resembles the steering behavior of a stable two track vehicle (i.e. steer 20° to the right, to drive a right corner). Several (especially static) motorcycle riding simulators will encounter this for example by implementing a "positive-steering controller".

This thesis follows another approach. Instead of simplifying the vehicle model, adjusting the steering controller and preventing instabilities by introducing artificial stabilization controllers, a solution is searched for, that eliminates the factors that make the rider act wrongly in the first place. Therefore, the riders must intuitively – or even unconsciously[97] – understand the simulator as a real motorcycle and be able to access the action-effect patterns they acquired in real life riding. It is assumed, that introducing the rider motion as a usable input cue on a DMRS will help riders to intuitively understand the simulated vehicle as a motorcycle and therefore access control strategies and riding patterns known from real riding. This should in return help to increase the presence on the simulator, as several of the factors contributing to a sense of presence shown in Table 2.2 are positively affected.

As stated in section 1.2, this approach is be called **dual loop rider control (DLRC)**, as it does not only take steering, but leaning into account for controlling the virtual motorcycle. The goal of implementing DLRC leads to a set of research questions:

---

[97] See the discussion on skill based behavior in section 2.3.1

- How can the effect that rider motion has on a motorcycle be measured on a DMRS?
- Which quantity should preferably be used as an input to the vehicle dynamics model?
- Which dynamic effects known from real riding can be replicated using this technology, that weren't possible to replicate on state-of-the-art DMRS before?
- Does the introduction of a rider motion input on a DMRS help normal riders accessing the simulator?
- How well does the system perform? How can the quality of the technology be rated?

To the author's knowledge, a comprehensive analysis with respect to the feasibility of DLRC has not been carried out within the scope of any research project. Based on the stated research questions, the following hypotheses are derived, that are investigated in this thesis.

H_1: DLRC capabilities increase the fidelity of lateral dynamic behavior on motorcycle simulators, as they enable riders to employ control strategies known from real riding.

A DMRS equipped with a properly designed DLRC module will benefit the rider in four ways compared to the same simulator with disabled DLRC capabilities:

H_{Wa}: It will provide an additional controllable input allowing simulator riders to intentionally change vehicle states.

H_{Wb}: It will show more realistic vehicle responses in lateral dynamic maneuvers.

H_{Wc}: It will ease access to the simulator to naïve riders.

H_{Wd}: It will reduce the simulator's achievable low speed boundary through stabilizing effects induced by rider impedance and motion.

To test these hypotheses, it is at first necessary to design and build a simulator capable of using DLRC. The following chapter will therefore concentrate on the DESMORI simulator, introducing a DLRC that measures the rider induced roll torque.

Reliable performance measures (PM) and scales are required, that are ideally known from real riding tests and are applicable for the assessment of DMRS (Chapter 4). Given the current state of the art of DMRS, the aim of this thesis is not to test the simulator against absolute performance levels of a specific, real motorcycle. The performance ratings must rather allow an overall rating that qualifies the simulator as any plausible motorcycle type. Then, studies must be defined, that allow to test for the developed performance measures and to rate the newly introduced technology (Chapter 5). These studies must then be performed and evaluated (Chapter 6). Lastly, based on the study results, the abovementioned hypotheses must be evaluated (Chapter 7).

3 Simulator Design and Rider Coupling

The following sections describe the development of the DESMORI simulator by quickly introducing its main components, before concentrating on the rider motion determination.
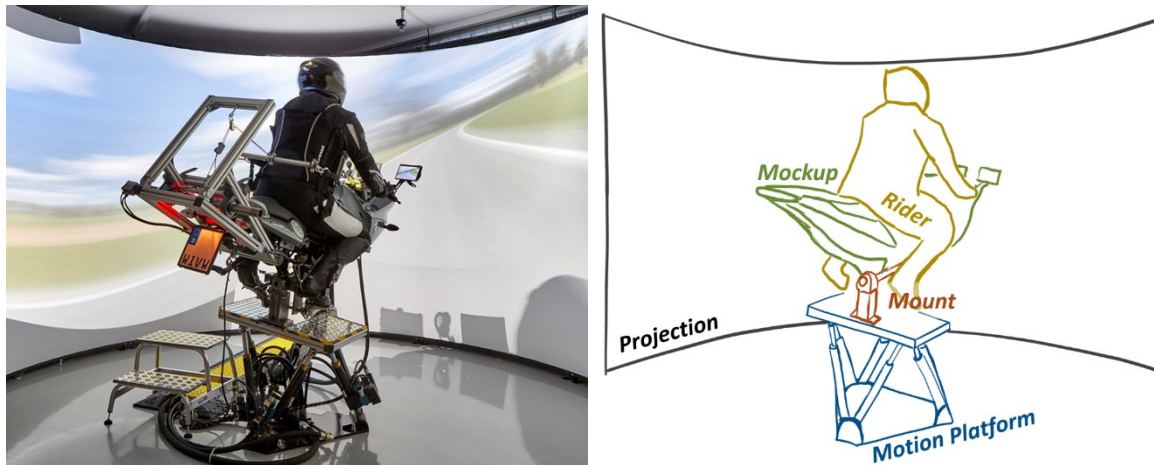
Figure 3.1: The DESMORI motorcycle riding simulator The sketch on the right highlights the main components of the simulator except for the rope-towing-mechanism.

3.1 Introducing the DESMORI Simulator

The dynamic motorcycle riding simulator that is subject in this study (see Figure 3.1) was developed in the publicly funded project DESMORI[13] as a tool to enable simulator based human factors research for motorcycles at the Würzburg Institute for Traffic Sciences GmbH (WIVW). The desired use cases of the simulator included

- verification of end user acceptance of newly developed HMI concepts
- rating of ergonomic aspects of newly developed HMI concepts
- measuring the rider's effort and distraction when using such HMI
- frontloading of HMI development processes to prevent the dependency on expensive vehicle prototypes
- investigation of different motorcycle models in a controlled and equal environment

Given the actual trends in the development of rider assistance and warning systems, such HMI are especially relevant in urban scenarios, which – at the same time – are rather difficult to simulate. The relevant velocity range is rather low, thus reducing the stabilizing effects of the motorcycle. The lack of stability leads to more roll dynamics as well as higher rider motion influence (see section 2.3), thus putting higher demands on the motion simulation. Also, the acceleration potential of a motorcycle is rather high especially in lower gears. This necessitates to put special efforts into providing longitudinal dynamic cues to the rider by means of vestibular and proprioceptive excitation. The system development was constrained by the availability of a specific motorcycle, motion platform and simulation environment.

3.1.1 General Mockup Overview

The DESMORI simulator is based on a hydraulic Hexapod (blue in Figure 3.1, right) with a payload of 325 kg that is capable of linear velocities up to 0.25 m/s and rotational velocities up to 30 °/s and accelerating in the horizontal plane with up to 8 m/s², vertically with up to 10 m/s² and rotationally with 200 °/s². While these parameters result from availability of the hardware rather than a deliberate selection process, they match the dynamics observed in real life riding quite well[98]. The manufacturer provides a motion cueing algorithm that is designed for cars however. Therefore, an own motion cueing algorithm is designed later.

The **Hexapod** is placed in the center of a **cylindrical projection** screen with a diameter of 4.5 m, a height of 2.8 m and a horizontal field of view of 220° (black in Figure 3.1, right). Provided that the study participant is wearing a helmet with a usual visor size, the lab environment around the projection is easily faded out, as long as the head rotation is kept to a reasonable limit. A **wooden floor** (not depicted here) is installed between the motion platform and the screen that emulates the height of the road surface when the hexapod is lifted to its default position. This allows simulator riders to find a correct reference of the road when turning their heads away from the projection screen. Both cylindrical screen and parts of the wooden floor are used as projection surfaces for a total of four Full-HD **projectors**. In addition to the front projection, two 7" TFT monitors are simulating the **rear mirror** view. The simulation sound comes from **headphones**, installed into the helmet, instead of external loudspeakers in order to keep the noise level to a reasonable limit in surrounding offices and laboratories. The motion platform carries the frame, fairing and controls of a **BMW F800S**. (green in Figure 3.1, right) The drivetrain, front- and rear-suspension have been dismounted to keep the weight of the mockup including the rider below the payload of the motion platform. The **mount** of the mockup includes the DLRC system that is the focus of this thesis. The brakes are sensed by pressure sensors, clutch and throttle values come from potentiometers. The **gearbox** simply detects UP and DOWN trigger signals to switch between gears, with the neutral position resulting from a downshift from second gear. The **steering** is simulated by a synchronous servo motor with an attached strain wave gear by Harmonic Drive[99] (see Figure 3.4, in section 3.1.4). The output of the transmission shaft is flanged to a **torque sensor**, which is then mounted to the lower fork crown of the motorcycle (see). An additional feedback cue is provided by the so-called *g-vest*. This is an airbag vest which is being pulled forth and back by a rope towing mechanism to stimulate proprioceptive cues of low frequent, high amplitude longitudinal accelerations and wind forces (see Figure 3.6, in section 3.1.5). All components are integrated into a simulation environment provided by SILAB ®, that allows to interface between the several hardware and software modules.

---

[98] Scherer, F. et al.: Schräglagenangst (2021).

[99] Harmonic Drive AG: Harmonic Drive Mechatronik.

Alternative solutions for some submodules were discussed during the development but discarded due to the lack of quality (e.g. mixed-reality head up display) or cost (e.g. rails or turn tables) or practicality (e.g. wind simulation). Their discussion is however not relevant for the course of this thesis.

3.1.2 Virtual System Architecture

SILAB ® is a simulation environment developed by WIVW since 1998. It provides a real-time-framework that allows for a synchronized communication between different *Data Processing Units* (DPU). A DPU is a functional element that could contain any type of hard- or software module, i.e. the environment simulation, sound simulation, a communication interface to a DirectX device, a MATLAB/Simulink Model, Python Code, or a CAN Interface. Any DPU will have input and output ports that may be connected to each other to generate a complete simulation network. Such a system may contain DPUs running at various update rates, implemented on various networked PCs or microcontrollers.

Figure 3.2: SILAB virtual scenario in a crowded, urban environment

One core element of the DESMORI simulator is the vehicle dynamics model. It is built in the simulation software BikeRealTime (BRT) from VI-grade which is based on MSC Adams multibody simulation[100] and is widely used among motorcycle OEMs. The BRT model is then integrated into a co-simulation[101] with MATLAB/Simulink. This allows to easily implement additional vehicle systems (e.g. ABS, traction control) or controllers (e.g. roll torque determination) to the dynamic system. The co-simulation model of BRT and MATLAB/Simulink is self-sufficient and can be used for offline simulations as well. The term **"offline"** therein implies "not controlled by a human rider", while **"online"** refers to a simulation that is performed on the simulator with a rider controlling it.

---

[100] VI-grade: VI-BikeRealTime.

[101] A co-simulation combines different simulation tools and solvers, allowing to build interacting models.

To enable the online simulation of the co-simulation model, it is compiled as runnable C-code that is included as a DPU into the SILAB environment. All I-/O- ports of each DPU can be connected to any other sub-system within the SILAB environment. Figure 3.3 provides an overview of the most relevant components of the overall simulator architecture. For better readability however, some components (e.g. audio DPU, traffic simulation DPU, HMI DPU, etc.) are not depicted, as is the distribution of the subsystems to different host PCs.
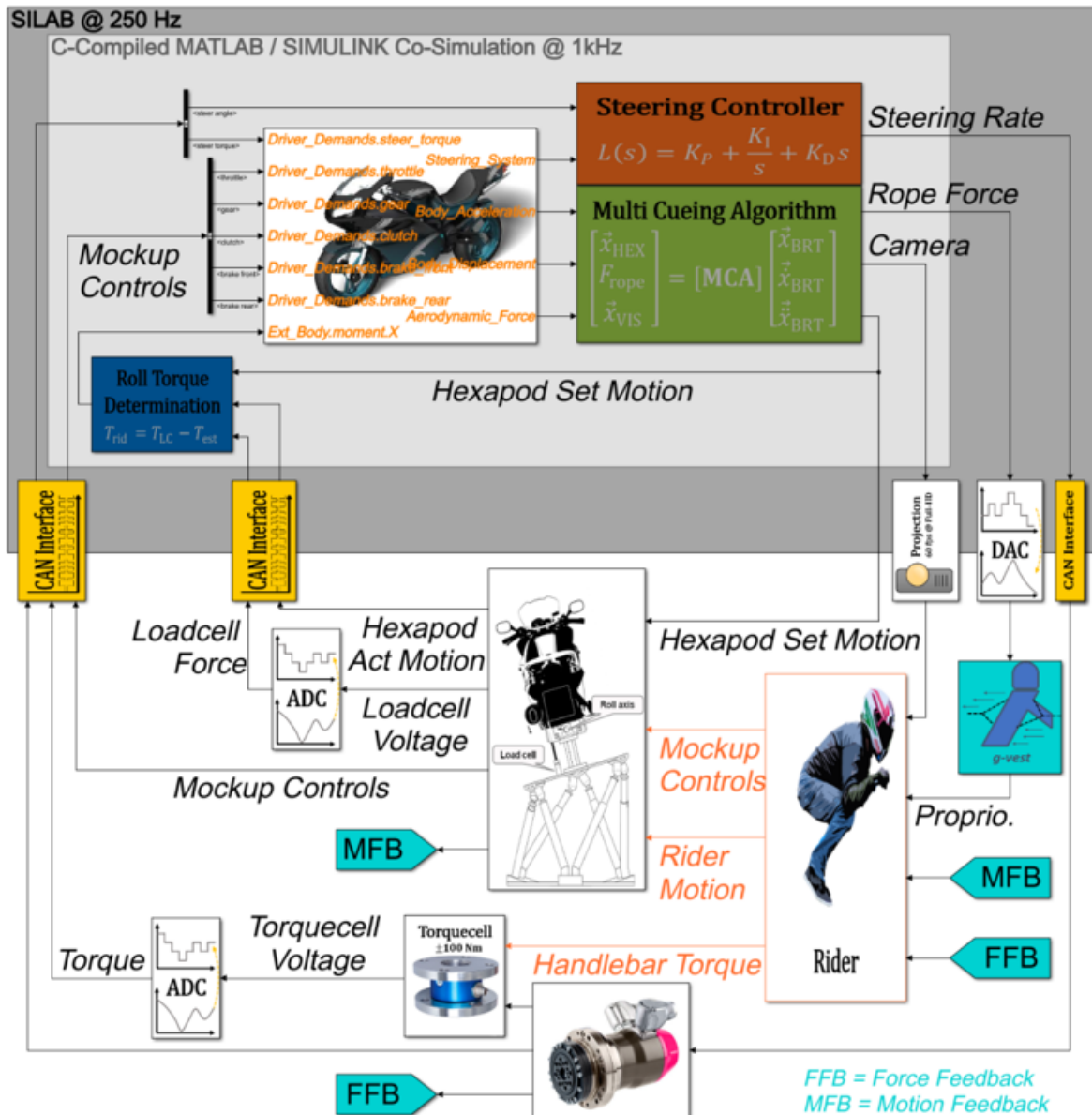
Figure 3.3: Overview of Relevant Components of the DESMORI Simulator Architecture

The light gray area in Figure 3.3 represents the DPU containing the co-simulation model. It communicates states and setpoints to other DPUs (e.g. engine sound) that are members of the SILAB environment (dark gray). A communication to external hardware, sensors and actuators is possible e.g. through a CAN-BUS DPU (yellow). The steering torquecell (see section 3.1.4) and leaning loadcell (see section 3.2.3) provide voltage signals to analog-digital-converters (ADC), which are communicating over the CAN interface with SILAB as

well. Other components like the Hexapod utilize their own specific interface DPUs and communicate directly with SILAB. SILAB allows to run various threads at different update rates. While e.g. the rendering tasks of visualization DPUs are typically updated at 60 Hz (in accordance with the frame rate of modern TV or projection hardware), the vehicle dynamics calculation sets higher demands on its update rate. The BRT-Simulink co-simulation itself is set to an update rate of 1 kHz. However, due to hardware limitations, the SILAB DPU containing the compiled C-code as well as the DPUs running the mockup sensors and actuators runs at 250 Hz. This means, that the co-simulation performs four iterations, where the inputs coming from the SILAB environment stay constant. Every fourth iteration, the co-simulation receives new inputs from SILAB and SILAB reads the current states of the co-simulation.

3.1.3 Vehicle Model

The vehicle model used in this research is not parameterized to represent a specific, real motorcycle. For once, that comes from the lack of available data and the immense effort needed to gather such data and validate the model. For the given research question, it is also not necessary to match dynamic data to any specific, real motorcycle. The newly developed input cue is supposed to work on any kind of single-track vehicle and the motorcycle's system responses to rider motion inputs should not show qualitative changes when using different vehicles. Lastly, the state of the art indicated, that the current aim of development must rather be to design a simulator that behaves and feels like a real motorcycle at all. Physical validity and comparability to a real motorcycle type are noble goals, but insignificant, if riders will refuse to accept the simulator as a motorcycle at all, and if adoptions in motion cueing and force feedback controllers will overshadow any adoptions made in the dynamics model. With that in mind, the parameters of the BRT model implemented in the DESMORI simulator were heuristically chosen to represent any current middleweight road motorcycle. Measured data from available measurement motorcycles (e.g. Honda NC 700 X, KTM 790 Duke) have been used as reference points as well as data provided by the BRT standard model or data that is available in literature. A short list of the most important parameters is found in Table 3.1. A complete list of the vehicle parameters can be found in Appendix A.1.

Table 3.1: Vehicle Parameter Overview

Parameter	Size	Parameter	Size
m_{mcy}	182 kg	Δx_{fork}	36 mm
m_{rid}	75 kg	l_{swing}	666 mm
l	1.46 m	Drivetrain	34 kW, 60 Nm, 6-Gear
τ	24°	Tires	120/70/R17, 180/60/R17

BRT provides an integrated **low speed stabilization** that prevents the simulated model from capsizing, when the (offline) virtual rider model is not capable of stabilizing the motorcycle anymore. When reaching a defined velocity threshold, the virtual motorcycle's roll rate is heavily dampened such that the roll angle is basically kept constant at its current value. The steering rates are strongly dampened as well and a strong virtual spring pulls the steering into a center position. The velocity threshold is chosen by the developer depending on the parametrization of the vehicle and rider model.

The velocity threshold for the online simulations performed here is set to 4.5 m/s (about 16 km/h). At this speed, the vehicle is not able to capsize anymore and only high external torques can affect the roll angle from here on. The sudden activation of the steering spring and damper will pull the handlebars in a center position. From here on, the rider must utilize pure positive steering (i.e. two-track vehicle steering), opposing the steering spring and damper torques applied by BRT. This transition feels rather unnatural, especially, when the roll and steer angles are not close to zero at the time where the stabilization activates. However, it allows trained riders to reduce their velocity close to standstill in a stable way. At velocities close to zero, the slip calculation of tire models becomes a crucial factor, as the velocity is a divisor in its calculation. Therefore, the model cannot reach absolute standstill and the iteration of the model is interrupted as a limit velocity of 0.5 m/s is reached.

The tire model bult into BRT is built according to Pacejka's tire model[102]. It is configured to use a combined force and moment calculation of F_x, F_y, F_z, M_x, M_y, M_z, including the relaxation behavior of the tires. Most of the parameters correspond to the default tire definition provided by BRT. However, slight adjustments have been made to affect the overturning torque $T_x(\varphi, a_y, F_s)$ of the front tire to adjust the vehicle's up-righting tendency.

3.1.4 Steering System

According to the state-of-the-art, the DESMORI steering system is equipped with all necessary hardware to allow for implementing an admittance control (see section 2.4.4 and Figure 3.4, left). As shown on the right side of Figure 3.4, the original fork crown of the mockup motorcycle (highlighted in green) is driven by an HarmonicDrive® actuator (red) with a torque sensor (blue) fitted in between. The steering torque is supported against the mockup by a support frame (orange) that is fixed to the motor housing. According to the datasheet[103], the actuator can generate up to 74 Nm of torque with a maximum rotation velocity of 486°/s and provides a halt torque of 47 Nm, which is important, as the rotation speeds during motorcycle rides may often stay low while having high steer torques at the same time. The actuator has a positioning precision of less than 1 arcmin (0.016°).

---

[102] Pacejka, H. B.: Tyre and vehicle dynamics (2006).

[103] Harmonic Drive AG: LynxDrive (2018).
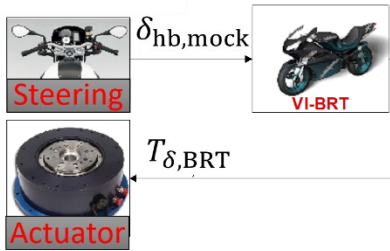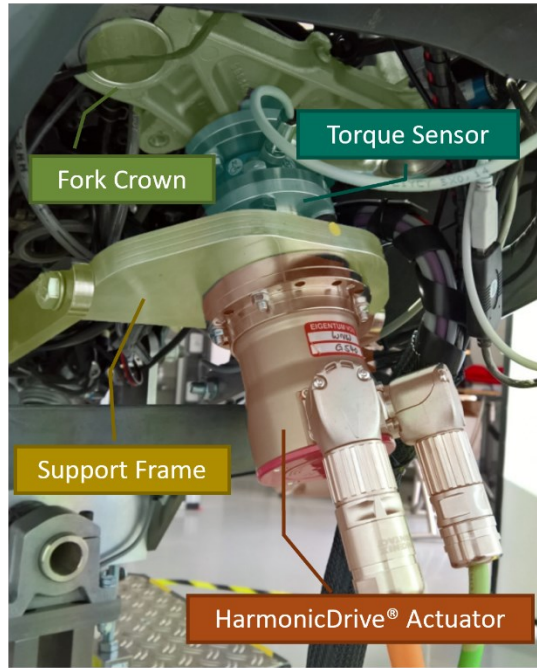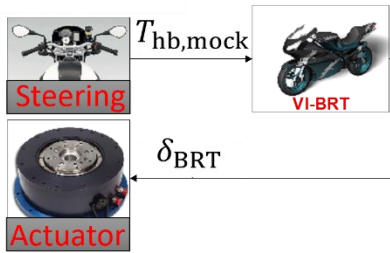
Figure 3.4: Steering Feedback Control Methods and DESMORI Hardware Setup

The motor controller of the HarmonicDrive actuator allows for different input configurations[104]. In *TorqueMode*, the actuator will follow the continuously input setpoint torque. While this mode is generally usable, it generates an inconsistency as the torque is used as both input and output of the steering system. The *ProfilePositionMode* on contrary doesn't allow for continuous setpoints but rather approaches constant setpoints with previously defined acceleration and velocity ramps. This mode will cause high latencies during a simulation and provides the most resistive feeling against exciting handlebar forces. Therefore, the *ProfileVelocityMode* is implemented on the motor controller, allowing for continuous rotation velocity inputs. The data transfer to the controller is implemented via CANopen.
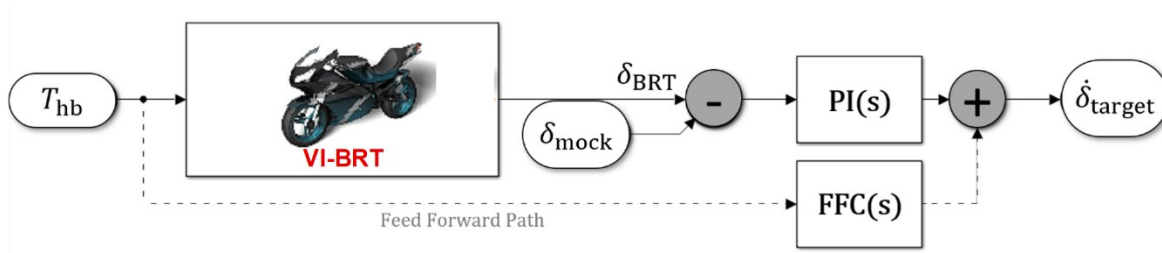
Figure 3.5: PI steer velocity controller and (inactive) feed forward path

As depicted in Figure 3.5, the target steering velocity is controlled by a PI controller that tries to minimize steer angle deviations between the virtual motorcycle and the simulator mockup. To increase the responsiveness of the steering system to rider torque inputs, experiments were performed with a feed forward controller that was reacting directly to the

---

[104] Harmonic Drive AG: YukonDrive (2017).

torques measured by the torque cell. While this approach allows for quick reactions of the handlebars to sudden steer torque inputs, it also generates constant offsets in the steering angle that can be perceived as a wrong cue. For the course of this thesis, the feed forward controller was therefore disabled and only the PI admittance control was utilized.

As stated before, an optimization of the steering control is not part of this thesis. It must however be mentioned again that the steering of a motorcycle (simulator) is still the most effective input to control the lateral dynamics. Revisions of the steering system are a therefore a continuous interest of motorcycle simulator developers.

3.1.5 Multi Cueing

The Mockup provides two main feedback cues to the rider. Firstly, the motion cueing that aims to provide inputs to the rider's vestibular system by means of platform motion, secondly a so-called *g-vest* that aims to stimulate the rider's proprioceptive cues, i.e. activating muscles and body tension to resist wind and accelerations. The implementation of the latter one is straight forward. It uses the vehicle's longitudinal acceleration a_x, velocity v_x and road inclination α_road to calculate the force acting on the rider's upper body mass m_torso according to Equation (3.1) [105]

$$F_{rope} = m_\mathrm{torso} \cdot a_x + k_1 \cdot v_x^2 + k_2 \cdot m_\mathrm{torso} \cdot g \cdot \sin\left(\alpha_\mathrm{road}\right) \qquad (3.1)$$

The two scaling factors $k_{1/2}$ can be used to scale the resulting rope force to the given hardware limitations and interact well with the vestibular cues from the hexapod.

Figure 3.6: Rope Towing Mechanism of the DESMORI Simulator with ① DC Motor, ② Winch, ③ Back Connection to Rider, ④ Front Connection to Rider, ⑤ Manually Inflated Airbag Vest

---

[105] Anton, M.: Bachelor Thesis, Auslegung und Konstruktion eines Seilzugsystems (2014).

The force with a maximum amplitude of 300 N is transmitted to the rider by means of a winch (②in Figure 3.6) that is driven by an DC motor ① and a single rope that is connected to both front and back of the rider via several pulleys ③ & ④. The length of the rope can be adjusted in order to accommodate for different rider sizes. The ends of the rope are connected to a manually inflatable airbag vest ⑤. This allows to provide a well distributed pressure on the whole chest or back respectively, rather than punctual force excitations. An extended system is developed to be used for lateral and vertical accelerations as well. However, it has not yet been installed and tested.[106]

The motion cueing algorithm implemented on the DESMORI simulator generally follows the basic concepts described in section 2.4.3. The motorcycle's vertical and lateral acceleration are neglected. The longitudinal acceleration is scaled and split in a low frequency portion simulated by tilt coordination and a high frequency portion simulated by platform accelerations. This high frequency component is transformed into the hexapod coordinates. The resulting translations are fed into a washout filter to allow the platform to approach a center position during constant riding. An additional lateral and vertical movement of the platform results from the vehicle roll angle and a velocity dependent factor k_v.

$$\begin{bmatrix} \Delta y \\ \Delta z \end{bmatrix} = k_v \cdot \begin{bmatrix} \sin(\varphi) \\ -\cos(\varphi) \end{bmatrix} \tag{3.2}$$

These translational platform offsets allow to simulate different heights of the rotation center of the platform. The empirically parametrized factor k_v allows to adjust the virtual roll axis height such that during low speeds, the roll axis is higher than at high speeds.

The motorcycle's roll, pitch and yaw angle are split into portions that are either simulated by platform motion or rotations of the projection view. High frequency components of the vehicle yaw motion are fed to a washout filter and the platform, while low frequency components are simulated through the visual system. The platform pitch is mainly proportional to the vehicle pitch, but adds the tilt coordination portion of the longitudinal acceleration and a portion of the road pitch angle as well. The tilt coordination portion of the signal is added to the visual pitch, as it is not supposed to be experienced as a tilting motion of the motorcycle.

The roll angle representation is a rather peculiar cue to provide in a motorcycle riding simulator, as described in section 2.4.3. Again, a suitable combination of visual roll angles and platform tilt angles must be found. The platform angles are mechanically limited to 15°. However, not even this amount of roll angle is feasible during online simulations, as a rider will need strong efforts to not fall of the mockup, as centrifugal accelerations are missing. As an empirical limit, 12° of platform tilt angle were found feasible. A soft limitation algorithm ensures, that this limit is only reached at low angular velocities to reduce the jerk, when approaching the limit. The highest possible roll angles of the BRT model are at 60°. If a constant scale for the platform roll angle were to be chosen, the hexapod had to represent

---

[106] Emig, L. et al.: Project Report, Entwurf eines Seilzugsystems zur Querdynamikdarstellung (2018).

20 % of the motorcycle roll angle, while 80% had to be represented visually. This is however not feasible, as high visual roll rates were found to increase sickness effects. As a result, a dynamic scaling is implemented on the DESMORI Simulator. The platform scaling factor varies between 35 % and 30 % from low to high velocities. The visual scaling factor varies between 30 % and 60% from low to high velocities This results in a total roll angle scale (haptic and visual) of 65 % up to 90 %.

A simplified overview of the block diagram representing the motion cueing algorithm is depicted in Figure 3.7. For the ease of reading, it is not showing all scaling factors, saturations or gains respectively.
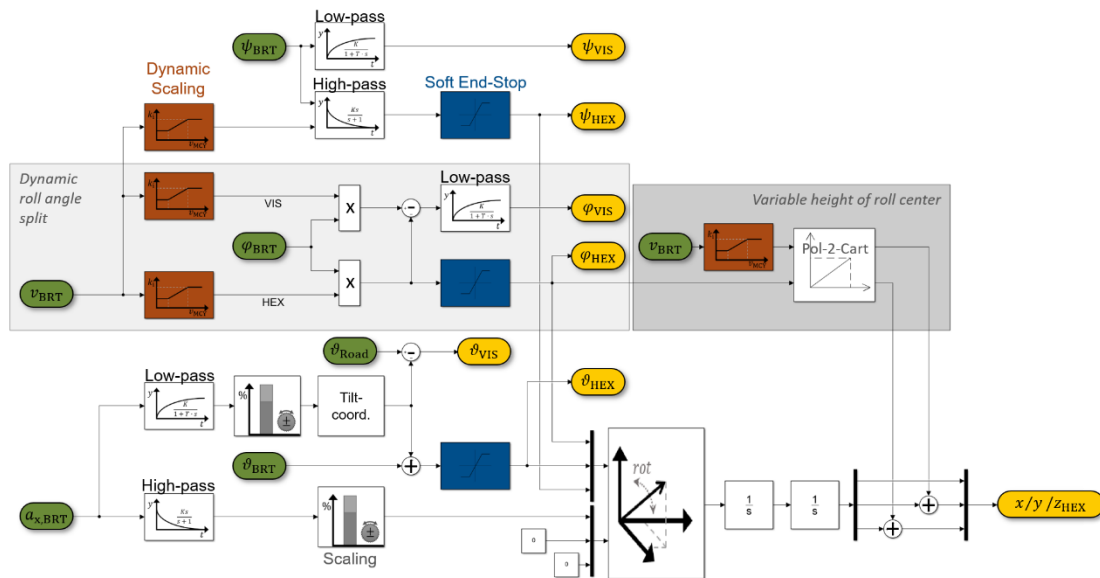
Figure 3.7: Overview of the Motion Cueing Algorithm

The green input signals provide dynamic states from BikeRealTime, while the yellow outputs will eventually communicate with the hexapod and the projection view. The red blocks show velocity dependent scaling factors that are applied to all roll angle related signals, as well as the platform yaw. The blue blocks show the soft end-stops that prevent platform yerk.

As previously stated, the motion cueing of DMRS is not the focus of this thesis and the topic can only be mentioned briefly here. However, a few noteworthy effects were observed during the development of the DESMORI simulator and shall be mentioned here:

- Despite the implausible resulting force, study participants preferred to use the simulator with roll angles (see Guth[107]).
- The reduction of visual roll rates led to decreased sickness symptoms. This became especially relevant at low-speed maneuvering or in slalom maneuvers.
- The yaw representation affects the cornering feeling in terms of e.g. the self-steering gradient. Due to the hardware limitations and the resulting demand for a washout filter however, the yaw angle cannot be used to its full potential.

---

[107] Guth, S. et al.: Motion cueing algorithm to reproduce motorcycle dynamics (2015).

- ▪ The perceived steer torque shows a dependency to the roll angle representation. A small platform roll-scale leads to a "heavier" steering perception, even if the steering controller parameters are kept constant. This indicates that steering FFB algorithms and MCA should not be handled separately in future research.

3.2 Rider Motion Input

With the abovementioned components, it is possible to build a complete simulator that agrees to the state of the art. The projection view exceeds the field of view of all abovementioned simulators, except for those using a head mounted display. Using a hexapod as motion base is the current standard for high fidelity DMRS. The simulation environment provided by SILAB is proven in industry, as is the multi body vehicle simulation BikeRealTime. The *g-vest* provides additional cues for the representation of longitudinal dynamics, comparable to the IFSTTAR simulator[108] The overall setup is therefore usable as any of the other simulators as well. It allows to freely maneuver around a given track based on real riders' inputs to throttle, brake and steering while providing feedback through multiple cues.

From here on, the DLRC capabilities, that are hypothesized to resolve some of the challenges of the state-of-the-art simulators, must be added to the overall system. The following subsection will select a suitable input entity that allows to measure rider inputs on the simulator. In section 3.2.2 a model that allows for a better understanding of the effect of rider motion on the vehicle dynamics is derived. Then, in subsections 3.2.3 to 3.2.5, a measurement concept is presented that allows to sense the rider input on a DMRS. The method depends on a set of individual parameters per rider. Subsection 3.2.6 will discuss, how these can be estimated and checked for plausibility.

3.2.1 Selecting an Input Entity

In general, there are two different approaches that can be used to determine rider motions on the simulator. The first approach coming to mind is to use a camera or other tracking devices to measure the position of a single, or multiple reference points of the rider. This approach is rather simple to implement but shows a few limitations. Firstly, it is always only considering the motion of a finite number of selected reference points. The simplest implementation of this approach would e.g. only track one point on the rider's back by means of a (stereo) camera. The lateral coordinate of the reference point and its second derivative can then be used to simulate inertial effects and the shift of the system CoG in the vehicle model. Such a model won't however be responsive to moving other body parts but the tracked point(s). The precision of the coupling effect thus depends on the number of tracking points.

---

[108] Nehaoua, L. et al.: Design and Modeling of a New Motorcycle Riding Simulator.

Furthermore, it depends on the precision of the locating algorithms (and therefore e.g. the camera resolution and frame rate) and assumptions on the mass and inertia of all body parts considered relevant for the simulation. As mentioned in section 2.5, Westerhof[109][89] sees potential for improvements when using this technology.

The alternative to motion tracking is to follow a force-based approach. If the coupling forces between rider and motorcycle were known, these would not have to be estimated from the measured motions of the rider first. Also, a feasible measurement method could determine coupling effects, no matter if they were induced by leaning to the side, tilting the head or stretching a leg. Also, other modes of action like balancing the vehicle at standstill, that do not affect the rider's posture, could become usable with such an approach. Therefore, the DESMORI simulator was equipped with a force-based measurement technology, as described in the following sub sections. At first, it is shown that a singular torque input suffices as an input to the vehicle model, before the technical solution to the approach is presented.

3.2.2 A Rider-Coupling Model

The simplest model representation of a tilting motorcycle is an inverted pendulum. As previously derived by Cossalter[110], they generally behave likewise: Any angular displacement of the system will generate a gravitational torque T_g that makes the system capsize.

This torque results to:

$$T_g = (\Theta_{xx} + mh_{\mathrm{CG}}^2) \cdot \ddot{\varphi}_{\mathrm{th}} = m \cdot g \cdot h_{\mathrm{CG}} \cdot \sin \varphi_{\mathrm{th}} \tag{3.3}$$

Laplace transformation and linearization of sine around the vertical equilibrium yields the frequency equation $(\Theta_{xx} + mh_{\mathrm{CG}}^2) \cdot s^2 \varphi(s) - mgh_{\mathrm{CG}} \cdot \varphi(s) = 0$ with the real eigenvalue

$$s = \pm \sqrt{\frac{mgh_{\mathrm{CG}}}{\Theta_{xx} + mh_{\mathrm{CG}}^2}} \tag{3.4}$$

This defines a non-oscillating motion. The inverse of the positive solution is the time constant T of the system. It increases slightly if a tire scrub radius $r_{\mathrm{c}} > 0$ is considered:

$$\text{from } T = \sqrt{\frac{h_{\mathrm{CG}}}{g}} \sqrt{1 + \frac{\rho^2}{h_{\mathrm{CG}}^2}} \text{ to } T = \sqrt{\frac{h_{\mathrm{CG}}}{g}} \sqrt{\left(1 + \frac{r_{\mathrm{c}}}{h_{\mathrm{CG}}}\right)^2 + \frac{\rho^2}{h_{\mathrm{CG}}^2}} \tag{3.5}$$

with ρ being the radius of gyration $\rho = \sqrt{\Theta_{xx}/m_\Sigma}$. This increase of the time constant (i.e. a "slower falling") results from the tire-road contact point moving along with the CoG in the direction of the fall. The motorcycle is nevertheless destined to tip over, as the sideways movement of the tire-road contact point is always smaller than the sideways movement of

---

[109] Westerhof, B. E.: Evaluation of the Cruden Motorcycle Simulator (2018).

[110] Cossalter, V.: Motorcycle Dynamics (2006), p. 244.

the CoG, if the tire contour radius r_c is less than the CoG height. To stop the motorcycle from falling, a rider must either bring the gravitational torque to 0 by placing the CoG directly above the tire contact point, or the rider must generate a counter torque that is as large as the gravitational torque, but of opposite sign. This torque can only result from the tire side forces described in section 2.1.3, as the motorcycle has no other contact to the environment, where forces could be supported against.

While the models that consider rider motion can become very complex with increasing number of degrees of freedom, a simple point mass model shall for now suffice to explain the basic dynamics. Therefore, the inverse pendulum analogy is extended to a double inverse pendulum, as depicted in Figure 3.8. Both motorcycle (**M**) and rider (**R**) are considered as point-masses. The rider mass is connected to the motorcycle with a revolute bearing (**S**) at a height h_{mcy} with a lever of $h_{CG,rid}$, while the motorcycle's CoG is at a height of $h_{CG,mcy}$ and rotating around the (infinitesimal thin) wheel's contact point (**W**). Figure 3.8 shows the system in straight configuration ① as well as the process of entering a turn ② and the steady state cornering ③.
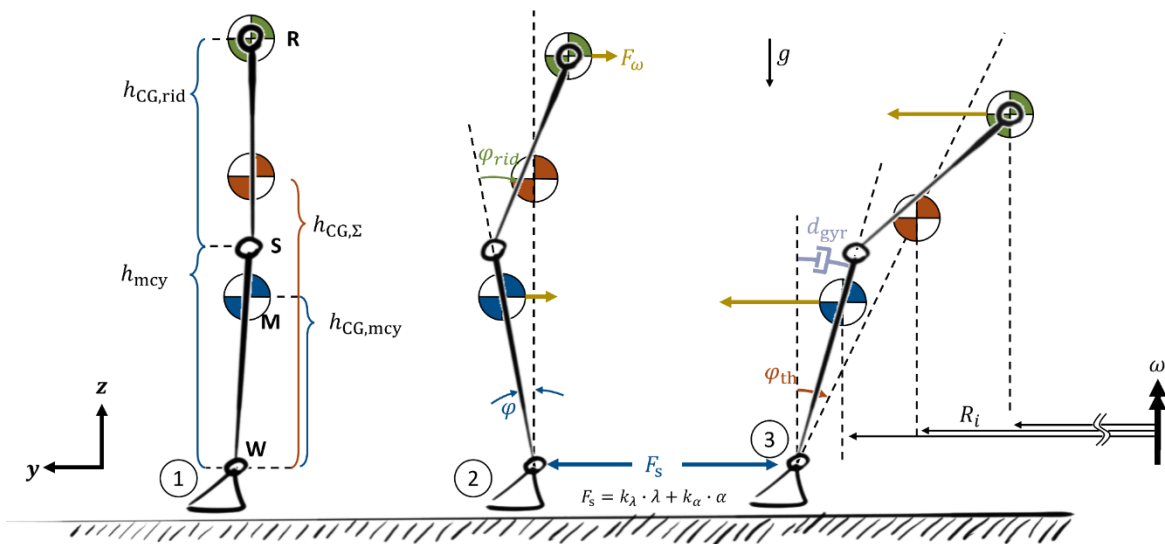
Figure 3.8: Modeling the rider leaning control of a motorcycle by means of a double inverted pendulum. The system CoG (red) is placed between the rider CoG (green) and motorcycle CoG (blue). Numbers indicate: ① straight running, ② initiation of a turn and ③ steady state cornering

To stop the system from capsizing, the contact point (base bearing) must move laterally such that **W** remains underneath the system CoG. This is achieved by utilizing the side forces explained in section 2.1.3. Both steering angles (→ side slip angle) and roll angles (→ camber angle) produce side forces acting horizontally on **W**.

If the rider decides to move his/her body, the resulting inertial forces are only supported against the vehicle's frame (action = reaction). As the rider moves to the right, the motorcycle must move to the left, but the overall system CoG will remain at its initial position. As shown in Figure 3.8 ②, this generates a roll angle of the motorcycle and thus camber side forces, even if no steering angle is applied. These side forces result in a lateral acceleration of **W**

(here: to the left) with associated centrifugal forces acting on motorcycle and rider CoG and a (here: clockwise) rotation of the system. To initiate a turn from straight running, the wheel contact point will thus always move towards the outside of the turn first, before achieving the steady state conditions depicted in ③.

As the velocity increases, the ride becomes more stable e.g. due to the trail and gyroscopic effect. This can be modelled as velocity dependent roll damping of the tilting motion (see Appendix A.4) and is depicted as d_{gyr} in Figure 3.8. With increasing values of this roll damping, the initial movement of the tire contact point towards the outside of the turn becomes very small. Even so small, that this behavior becomes imperceptible for many riders.

In the steady state condition, each mass point i of the motorcycle and rider is subject to centrifugal accelerations $a_{\omega,i} = \omega^2 \cdot R_i$, with the angular velocity ω being equal to the yaw rate of the reference frame $\dot{\psi}$ under no-slip condition. As the roll angle increases, so does the difference in radii R_i between each mass point. This generates an additional overturning moment around the longitudinal axis of the motorcycle frame, as mass points higher above the ground are subject to less lateral acceleration than mass points on ground level. In addition, more mass is concentrated in the lower part of the system (i.e. engine, frame, etc.) than the upper part (i.e. torso, head). However, for typical values of angular velocity, radius, roll angle and mass distribution, the misaligning torque is negligible, as the following example shows.
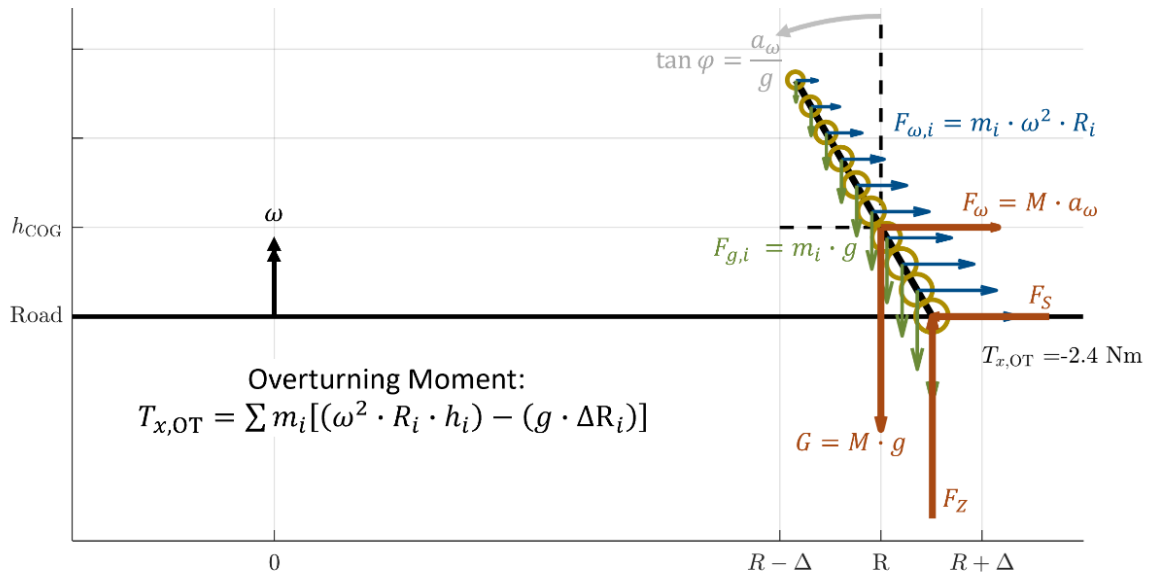
Figure 3.9: Overturning moment due to inhomogeneous centrifugal forces. The yellow circles indicate distributed mass points that are subject to gravity (green) and centrifugal forces (blue) that depend on each points radius around the turn center. While the single point-mass model is in equilibrium (red), the distributed mass point model generates a small overturning moment.

Figure 3.9 shows a hypothetical example, where the total system mass is $m = 250$ kg. For the sake of this example the mass is placed on ten mass points homogeneously distributed along the length of the rod (with $m(h_i) = 40 \text{ kg} - i \cdot 3.3 \text{ kg}, i = 0 \dots 9$) as indicated by

yellow circle's diameter). The radius R at the rod's CoG is 40 m and the rod is tilted at 30° roll angle. Tire width is neglected. This results in a velocity of $v \approx 15 \frac{\text{m}}{\text{s}}$. In this scenario, the overturning moment $T_{x,OT}$ is negative (counterclockwise) and thus it will act increasing the roll angle. However, with $T_{x,OT} = -2.4$ Nm it is small in the abovementioned scenario. A mass of $m_{rid} = 40$ kg that is moving sideways with $y_{rid} = 0.2$ m at 30° roll angle will in contrast generate about 160 Nm. Thus, it is possible to use the following assumptions:

a) The motorcycle and rider are considered as point masses instead of mass continuums for the calculation of steady state equilibrium.

b) All mass points are subject to the same lateral acceleration and thus, the superposition of lateral acceleration and gravitational acceleration always points parallel to the theoretical roll angle for each mass point. (see Figure 3.10)

c) The curved motion around a center with radius R can be represented by a planar model, where all mass points are subject to the same lateral acceleration $\ddot{y}$.
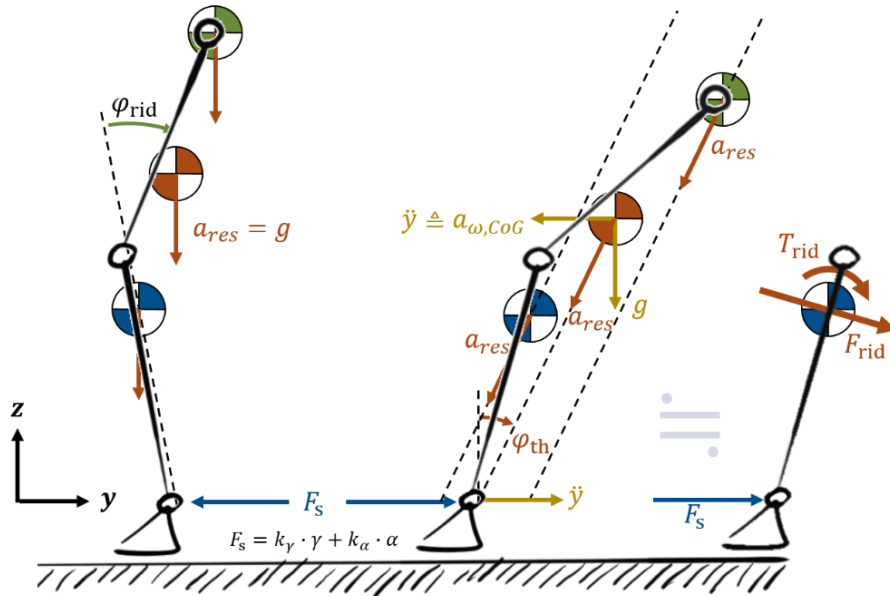
Figure 3.10: Simplified model for resulting accelerations and torques. The centrifugal accelerations for every mass point are assumed equal in size, such that the resultant forces during cornering (middle sketch) become parallel. The Forces and respective levers are substituted by a pair of rider torque and force (right sketch), the latter one being 0 due to the parallel resultant forces.

Let T_{rid} and F_{rid} be a torque/force-pair acting on the motorcycle CoG that can substitute the coupling forces and torques between rider and motorcycle. Assuming that the resultant accelerations from gravity and centrifugal acceleration of each mass point are in parallel and following a Lagrange formalism for the double inverted pendulum model, the substituting torque results to equation (3.6).

$$T_{rid} = h_{\text{CG,rid}} m_{\text{rid}} \begin{pmatrix} \dot{\varphi}^2_{\text{mcy}} h_{\text{mcy}} \sin \varphi_{\text{rid}} \\ + h_{\text{CG,rid}} \ddot{\varphi}_{\text{rid}} + \ddot{\varphi}_{\text{mcy}} \left(h_{\text{CG,rid}} + h_{\text{mcy}} \cos \varphi_{\text{rid}} \right) \\ + \ddot{y} \cdot \cos \left(\varphi_{\text{mcy}} + \varphi_{\text{rid}} \right) - g \cdot \sin \left(\varphi_{\text{mcy}} + \varphi_{\text{rid}} \right) \end{pmatrix} \qquad (3.6)$$

The substitute force F_{rid} is proportional to $\sin \left(\varphi_{\text{th}} - \varphi_{\text{mcy}} \right)$ and can be considered small.

At steady state conditions (i.e. $\ddot{\varphi}_{\text{rid}}$, $\ddot{\varphi}_{\text{mcy}}$, $\dot{\varphi}_{\text{mcy}} = 0$ and $\ddot{y} = const.$) the lateral acceleration can be expressed as a function of the theoretical roll angle:

$$\ddot{y} = g \cdot \tan \varphi_{\text{th}} \qquad (3.7)$$

The theoretical roll angle is geometrically related to the motorcycle roll angle and rider lean angle. The tangent of φ_{th} results to

$$\tan \varphi_{\text{th}} = - \frac{m_{\text{rid}} \left(h_{\text{rid}} \cdot \sin \left(\varphi_{\text{mcy}} + \varphi_{\text{rid}} \right) + h_{\text{mcy}} \sin \varphi_{\text{mcy}} \right) + m_{\text{mcy}} h_{\text{mcy}} \sin \varphi_{\text{mcy}}}{m_{\text{rid}} \left(h_{\text{rid}} \cdot \cos \left(\varphi_{\text{mcy}} + \varphi_{\text{rid}} \right) + h_{\text{mcy}} \cos \varphi_{\text{mcy}} \right) + m_{\text{mcy}} h_{\text{mcy}} \cos \varphi_{\text{mcy}}} \qquad (3.8)$$

The total rider induced roll torque in steady state cornering can thus be rewritten as follows:

$$T_{rid} = - \frac{g h_{\text{rid}} m_{\text{rid}} \sin \varphi_{\text{rid}} \cdot \left(m_{\text{mcy}} h_{\text{mcy}} + m_{\text{rid}} h_{\text{mcy}} \right)}{h_{\text{rid}} m_{\text{rid}} \cos \left(\varphi_{\text{mcy}} + \varphi_{\text{rid}} \right) + h_{\text{mcy}} \cos \varphi_{\text{mcy}} \cdot \left(m_{\text{mcy}} + m_{\text{rid}} \right)} \qquad (3.9)$$

Considering an 85 kg rider mass, the upper body will typically unite about 55 kg[111]. Using this together with other typical values for body weight distribution and motorcycle mass and geometry ($rc \neq 0$), the static rider induced roll torque can be found in Figure 3.11. The curved lines show the equivalent torque T_{rid} that substitutes a rider sitting on the saddle (c.f. Figure 3.10, right). As the rider lean angle φ_{rid} increases (lower lines in the diagram), so does the rider torque T_{rid}. The diagram is point symmetrical around the centre (0|0). The torques become larger, if the rider leans toward the direction of the motorcycle roll angle due to the lateral displacement of the tire contact point and the trigonometric properties of equation (3.9). The diagonal lines show the resulting theoretical roll angle of the combined motorcycle-rider-system. If the motorcycle is vertical (i.e. $\varphi_{\text{mcy}} = 0$), a positive rider lean angle of about $\varphi_{\text{rid}} \approx 40°$ will result in a positive theoretical roll angle of about $\varphi_{\text{th}} \approx 5°$.

---

[111] Richard, H. A.; Kullmer, G.: Biomechanik (2013).
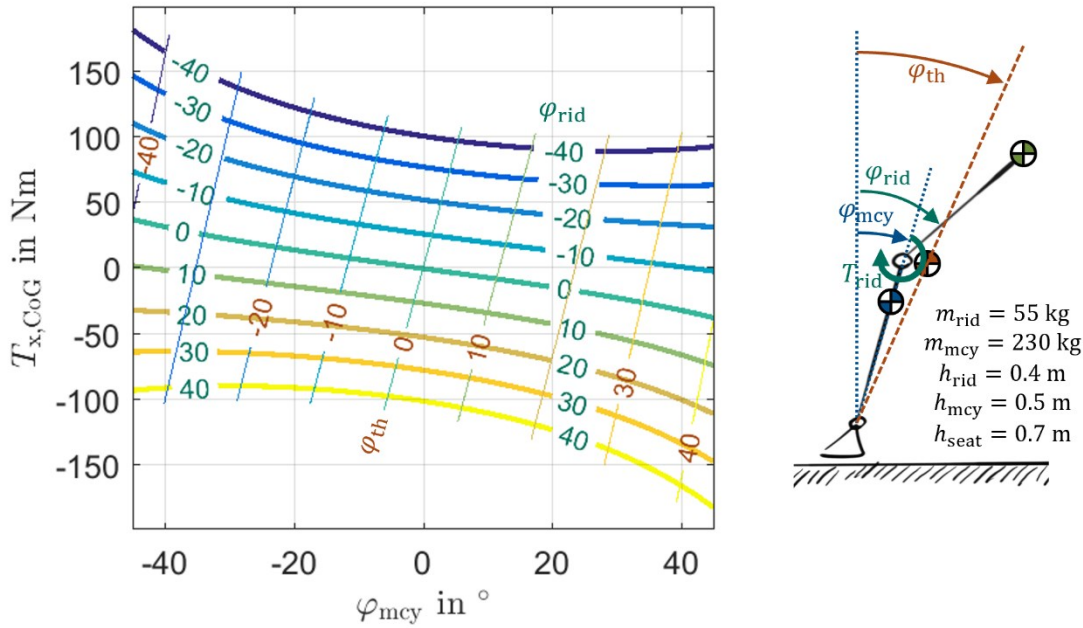
Figure 3.11: Rider induced roll torque in steady state riding conditions for typical values of rider and motorcycle mass and geometry, as stated on the right sketch. The contour lines show the rider lean angle, the diagonal lines the theoretical roll angle. They result in an effective motorcycle roll angle (absicissa value) and a torque around the longitudinal axis at the motorcycle CoG (ordinate).

The model shows, that it is feasible to substitute the rider motion's effect on motorcycle lean by a single torque value acting around the vehicle CoG. This allows for a rather simple measurement setup on the simulator, as described next. The rider induced roll torque reaches values of up to a few hundred Nm, depending on the rider mass and lean angle. This is about one magnitude greater than typical steering torques applied by the rider. However, this must not be interpreted as a higher controlling effort, as it is rather effortless to sit a few centimeters more to the left or right, compared to holding a static load on the handlebars.

3.2.3 Measuring the Roll Torque

The previous sections reason, how a force-based approach to realize a rider motion input is feasible to control a motorcycle. Also, the quality and size of the rider induced roll torque are discussed. To make use of this torque on a motorcycle simulator, a measurement concept is needed, that can determine the rider induced roll torque with high precision.

Two concepts known from literature come to mind, that allow to measure the rider induced roll torque.

- Measuring the contact forces on each contact point between rider and motorcycle
- Modeling the platform dynamics and calculate rider induced differences in control forces of the Stewart platform

The first concept is similar to the solution presented by Cossalter[112], that uses strain gauges on the simulator foot pegs. However, to generate a holistic roll torque value, every contact point would have to be measured that contributes to the rider induced roll torque. This would at least include torques on the handlebar orthogonal to the steer torque, pressure sensitive saddle and kneepads. As this would include vast efforts in terms of mechanical integration and would still only provide some – rather than all – coupling forces, this concept was not selected for development.

The second concept was implemented similarly in the KAIST bicycle simulator[113]. There, the rider's net moment is estimated from each actuator's control force and transformed into the three moments that are used as input to the virtual bicycle model. This concept is rather interesting, as it not only generates roll torque information, but a multi-axial torque signal. However, the estimator shows rather high errors and the hexapod available for the DESMORI simulator doesn't provide the necessary control force signals.

Due to these insufficiencies, a new measuring device is introduced[114]. It consists of a mechanical axis that is fitted on top of the motion platform. The motorcycle frame is mounted on this axis with polymer plain bearings such that the mockup can rotate around the axis. However, a loadcell that is fixed at a lateral distance to the axis will prevent said rotation, as shown in Figure 3.12. This setup can measure the torques that act around the mechanical axis between the mockup and the platform with a resolution of less than 0.2 Nm. As the weight of the mockup (and rider) is carried by the axis, the loadcell must only cope with dynamic loads resulting from inertial effects and the rider induced torque. The axis is mounted as close to the mockup CoG as the packaging allows, to reduce the gravitational torque at platform tilt angles. The height of the mockup is constrained by the position of the foot pegs that must be placed above the moving platform of the hexapod.

By designing the system such that it must not carry the mockup weight and by bringing the axis close to the CoG, the necessary nominal force of the loadcell can be reduced, resulting in an increase of the achievable sensor resolution and precision.

---

[112] Cossalter, V. et al.: Development of a motorcycle riding simulator (2011).

[113] Shin, J.-C.; Lee, C.-W.: Rider's Net Moment Estimation (2004).

[114] Pleß, R. et al.: Manöverumsetzung auf einem dynamischen Motorrad Fahrsimulator (2016).
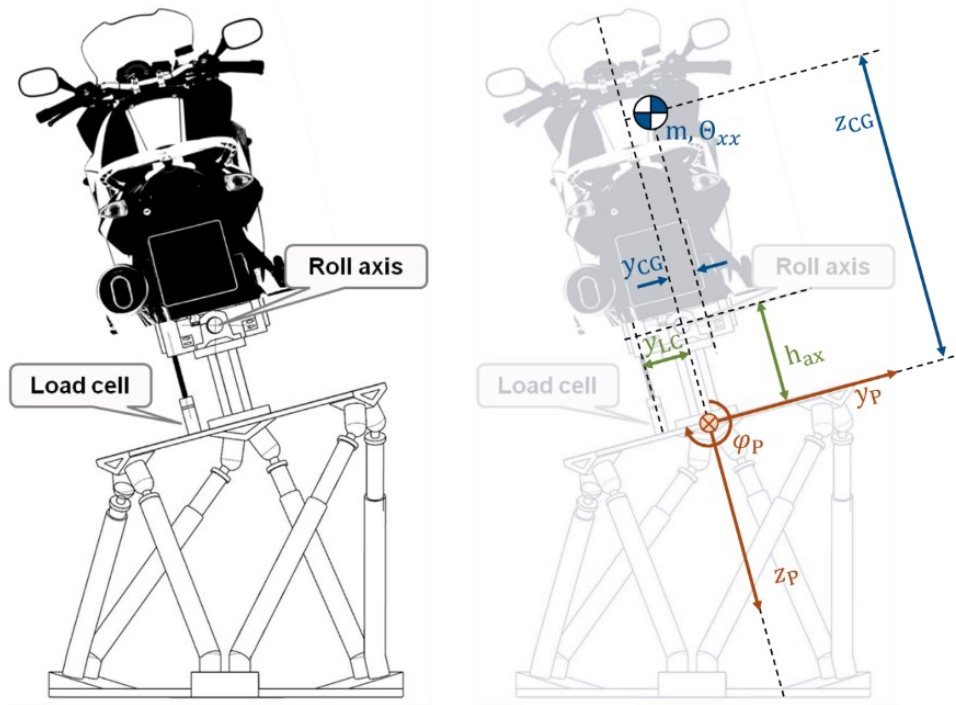
Figure 3.12: Mechanical concept of the DESMORI roll torque determination. Note the red Platform CoSy in the right sketch with z_P pointing downwards. The roll axis is fixed at $h_{\mathrm{ax}} = -0.235$ m above the platform, the load cell is offset at $y_{\mathrm{LC}} = -0.113$ m to the left (depicted green in the right sketch). The mockup (+rider) CoG depicted in blue lies at about $z_{CG} = -0.5$ m (-0.7 m depending on rider stature) and shows negligible lateral offsets.

This measurement approach will react to any change of the roll torque between rider and mockup – independent if it comes from upper body or lower body motion, stretching arms or legs. Furthermore, it enables additional functionalities like balancing the motorcycle at stand still, as the rider's feet pushing on the platform generate measurable torques as well[115].

Two major downsides of the approach arise:

- The currently implemented mechanics are subject to friction from plain bearings. While this causes errors and deviations in the measurement, it is an issue that could in future be easily resolved with revisioning the simulator hardware.
- The platform motion is generating torques around the measuring axis, even without a moving rider. This comes due to the mockup's inertia and eccentricity of the center of gravity w.r.t the roll axis.

In order to determine the purely rider induced roll torque T_{rid} during a simulation, the platform induced roll torque T_{HEX} must therefore be subtracted from the signal derived from the loadcell measurement T_{LC} that contains both rider- and platform induced components.

$$T_{\mathrm{rid}} = T_{\mathrm{LC}} - T_{\mathrm{HEX}} \tag{3.10}$$

This compensation is subject of the following subsection.

---

[115] Albrecht, A.: Master Thesis, Stillstandsimulation auf einem Dynamischen Motorradfahrsimulator (2018).

3.2.4 Compensation of the Platform Induced Torque

The platform motion is known, as it is controlled by the motion cueing algorithm. This allows to calculate an estimation value for the measured torque around the mechanical axis. Therein, it is assumed that

- the mockup (with all possibly attached masses, e.g. the rider) is a rigid body,
- the connection through the loadcell is rigid
- no friction exists around the mechanical roll axis,
- the influence of asymmetric inertial effects (deviation torques) is negligible
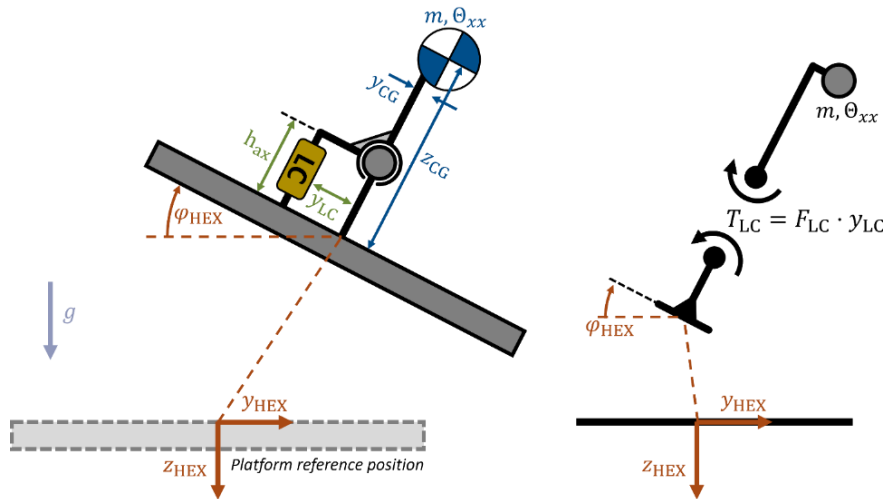
Figure 3.13: Mechanical equivalent representation of the roll torque measurement. Geometric properties with loadcell (left image). Free body diagram with the torque T_{LC} substituting the loadcell (right image). The x and y bearing forces are not depicted. Adjusted representation after[116].

The mechanical equivalent representation of this system is depicted in Figure 3.13. In absence of a rider, the measured torque T_{LC} is purely induced by the mockup and can be estimated according to equation (3.11), applying the abovementioned simplifications:

$$T_{\text{HEX}} = T_{\text{LC,est}} = m \cdot \begin{bmatrix} \rho_{\text{xx}}^2 - h_{\text{ax}}z_{\text{CG}} + y_{\text{CG}}^2 + z_{\text{CG}}^2 \\ (h_{\text{ax}} - z_{\text{CG}}) \cdot \cos(\varphi_{\text{HEX}}) - y_{\text{CG}} \cdot \sin(\varphi_{\text{HEX}}) \\ (h_{\text{ax}} - z_{\text{CG}}) \cdot \sin(\varphi_{\text{HEX}}) + y_{\text{CG}} \cdot \cos(\varphi_{\text{HEX}}) \\ -(h_{\text{ax}} - z_{\text{CG}}) \cdot \sin(\varphi_{\text{HEX}}) - y_{\text{CG}} \cdot \cos(\varphi_{\text{HEX}}) \\ - h_{\text{ax}}y_{\text{CG}} \end{bmatrix}^T \cdot \begin{bmatrix} \ddot{\varphi}_{\text{HEX}} \\ \ddot{y}_{\text{HEX}} \\ \ddot{z}_{\text{HEX}} \\ g \\ \dot{\varphi}_{\text{HEX}}^2 \end{bmatrix} \quad (3.11)$$

This equation contains inertial torques due to the hexapod's rotational, lateral and vertical accelerations $\ddot{\varphi}_{\text{HEX}}, \ddot{y}_{\text{HEX}}, \ddot{z}_{\text{HEX}}$ in the first three rows, as well as the gravitational torques and a centrifugal term in the last two rows. The function is parametrized by the mockup's mass and gyration radius ρ_{xx} as well as the CoG's location relative to the platform y_{CG} and z_{CG}. The height of the mechanical roll axis relative to the platform h_{ax} is a system constant. With

---

[116] Pleß, R.: Approach to a holistic input determination for a motorcycle riding simulator (2016).

the positive z-axis pointing downwards, the mechanical roll axis is placed at $h_{ax} = -0.235$ m above the reference plane of the platform.

It can be seen from equation (3.11), that the torque would only contain the inertial term $m \cdot (\rho_{xx}^2 - h_{ax}^2) \cdot \ddot{\varphi}$ if the mechanical axis were to be placed exactly in the mockup's CoG (i.e. $y_{CG} = 0$ and $h_{ax} = z_{CG}$). This is not the case with the given hardware configuration. However, the exact values of m, ρ_{xx}, y_{CG} and z_{CG} are unknown and must therefore be determined first, to be able to estimate the platform induced torque.

3.2.5 Estimating the Inertial Parameters

In order to simplify the equation's parametrization and application, equation (3.11) can be rearranged and formulated in vector notation such that it consists of one vector $\vec{x}$ containing all motion components and one vector $\vec{\beta}$ containing only the inertial parameters of the mockup (including any part or body connected rigidly to it)

$$T_{LC,est} = \vec{x} \cdot \vec{\beta} \tag{3.12}$$

with the hexapod motion components

$$\vec{x} = \begin{bmatrix} x_1 \\ x_2 \\ x_3 \end{bmatrix}^T = \begin{bmatrix} \ddot{\varphi}_{HEX} \\ \cos(\varphi_{HEX})\,\ddot{z}_{HEX} - h_{ax}\,\dot{\varphi}_{HEX}^2 - \sin(\varphi_{HEX})\,\ddot{y}_{HEX} - g\cos(\varphi_{HEX}) \\ g\sin(\varphi_{HEX}) - \cos(\varphi_{HEX})\,\ddot{y}_{HEX} - \sin(\varphi_{HEX})\,\ddot{z}_{HEX} \end{bmatrix}^T \tag{3.13}$$

and the rigid body parameters

$$\vec{\beta} = \begin{bmatrix} \beta_1 \\ \beta_2 \\ \beta_3 \end{bmatrix} = m \begin{bmatrix} \rho_{xx}^2 + y_{CG}^2 + z_{CG}^2 - h_{ax}z_{CG} \\ y_{CG} \\ z_{CG} - h_{ax} \end{bmatrix} \tag{3.14}$$

The first components x_1 and β_1 of the abovementioned vectors calculate the torque resulting from rotational accelerations of the platform. These however will typically remain small valued, as the platform only simulates about one third of the vehicle's roll angle, depending on the vehicle speed (c.F. section 3.1.5). The second components x_2 and β_2 mainly generate a constant offset in the torque estimation. Dynamic effects are rather small, as lateral accelerations, vertical accelerations, as well as the lateral eccentricity of the mockup CoG y_{COG} are small. The third elements x_3 and β_3 calculate the torque resulting from translational accelerations of the platform as well as gravity when the platform is tilted.

The performance of the torque estimation depends highly on the selection of the β-parameters. Figure 3.14 exemplarily shows the motion components (left column) and the roll torque (right column) during 20 s of an automated (i.e. no rider) riding scenario containing a cornering maneuver and a following double lane change. This scenario combines multiple steady and dynamic states of the platform roll angle that are relevant for the estimator, namely constant 0, steadily in- and decreasing values, constant angles and alternating angles.

The first row of plots shows the motion component x_1 during that scenario and the influence of changing values of β_1 on the estimated torque (color shaded lines). The measured torque $T_{\text{LC,meas}}$ is depicted as a reference (blue dotted line). The second and third row show $x_{2/3}$ and the influence of changing $\beta_{2/3}$ respectively.
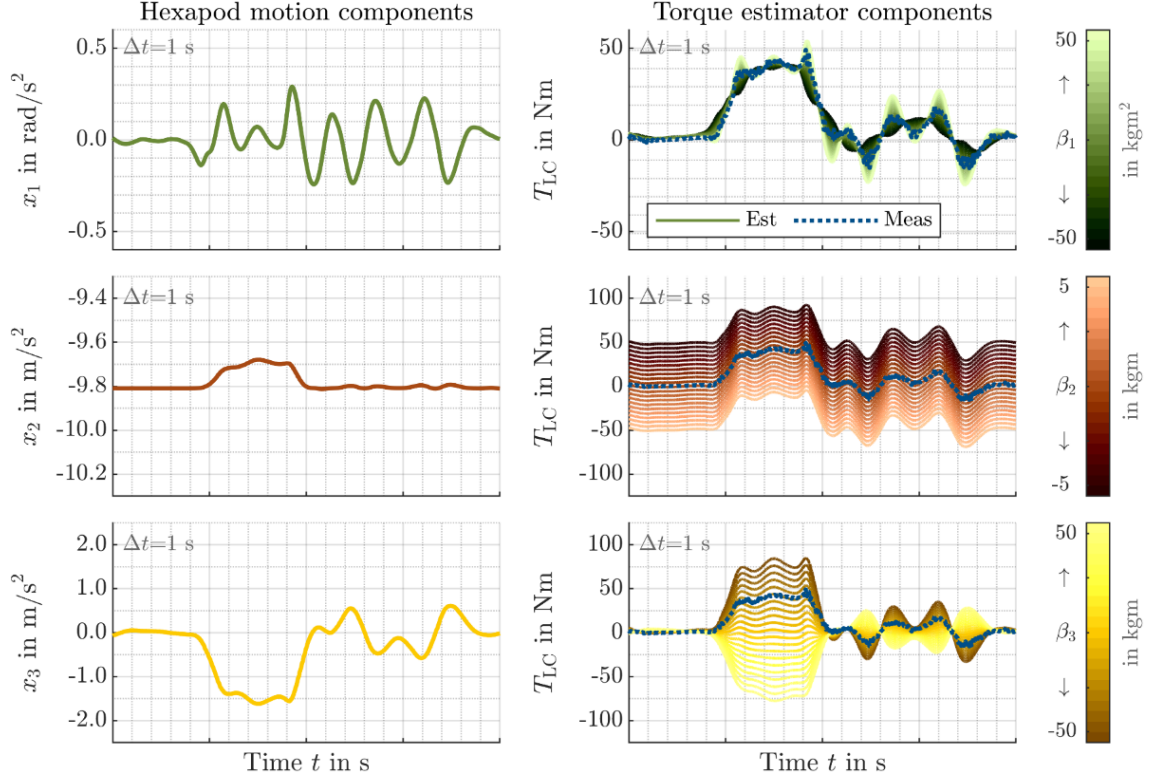
Figure 3.14: Variation of the β-parameters during a curve and double lane change maneuver. The maneuver was performed by a virtual rider controller (i.e. no rider on the mockup). Each ith row of plots shows timeseries of the elements x_i of $\vec{x}$, the second column shows timeseries of $T_{\text{LC,est}} = \vec{x} \cdot \vec{\beta}$ for changing values of β_i, represented by the shade of each colored line. The measured reference torque T_{LC} is depicted as blue dotted lines.

As the top left plot shows, the transients of the maneuver generate roll rates in the range of $\pm 0.3 \ \text{rad/s}^2$. As the top right plot shows, choosing too high (low) values for β_1 affects the torque estimation by means of an overshooting (undershooting) during the transients. Steady states are obviously not impacted, as x_1 only contains the rotational acceleration.

The second component of the motion vector $\vec{x}$ is dominated by $g \cos(\varphi_{\text{HEX}})$, as the translational accelerations and roll rate stay rather small. Consequently, x_2 shows values close to g throughout the whole scenario. Adjustments of $\beta_2 = m \cdot y_{\text{CG}}$ will therefore mainly generate a parallel shift of the estimated torque.

The torque estimation is dominated by the third term of $\vec{x}$ and $\vec{\beta}$, mainly resulting from the gravitational effect $g \sin(\varphi_{\text{HEX}})$ and the lever between the mockup CoG and the mechanical roll axis of the mockup mount.

To determine the correct β-parameters, various methods can be used. One feasible solution is to apply defined motion patterns to the Hexapod. Given, that the resulting torque is measured and the motion is known as well, equation (3.12) can be solved for β using for example a least squares regression for the time-discrete samples i:

$$\sum_{i=1}^{n}\left(\vec{x}_i\vec{\beta} - T_{\text{HEX,i}}\right)^2 = \left\|\vec{f}(\vec{\beta}) - \vec{T}\right\|_2^2 \tag{3.15}$$

The parameters β must be chosen such that the sum of the squared errors is minimized

$$\min_{\beta}\left\|\vec{f}(\vec{\beta}) - \vec{T}\right\|_2^2 \tag{3.16}$$

This regression is easily performed by e.g. applying the *lsqminnorm* function in MATLAB. The hexapod is ideally excited by a dedicated identification signal that contains e.g. sine sweeps along the different hexapod DoF's. For this purpose, the signal depicted in Figure 3.15 was generated and used as set values for the hexapod controller:
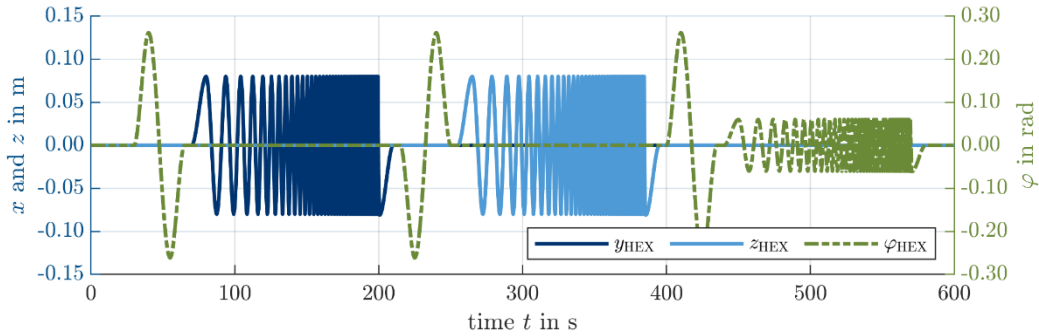
Figure 3.15: Testsignal used for the identification of beta Parameters. The blue lines represent platform translations y_{HEX} and z_{HEX}, the green dash-dotted line represents the platform roll angle φ_{HEX}

Therein, three slow, but large-valued roll oscillations are performed as well as sweeps over the lateral, vertical and roll direction. Therefore, all relevant acceleration terms as well as the gravitational term are well represented in the signal. Applying the regression to the measured torque signal yields to the parameters of the simulator mockup without rider

$$\vec{\beta}_{mock} = \begin{bmatrix} 21.9 \text{ kg m}^2 \\ 1.75 \text{ kg m} \\ -26.2 \text{ kg m} \end{bmatrix}$$

With the known design parameter $h_{\text{ax}} = -0.235$ m (remember positive z pointing downwards) and mockup mass of $m_{\text{mock}} = 102$ kg, the mockup's center of gravity locates at

$$y_{\text{CG,mock}} = -0.017 \text{ m and } z_{\text{CG,mock}} = -0.492 \text{ m}$$

(see Figure 3.12 for reference) with the polar inertia (radius of gyration) of the mockup

$$\Theta_{xx,\text{mock}} = 8.99 \text{ kg m}^2, \left(\rho_{xx,mock} = 0.297 \text{ m}\right).$$

Hofmann[117] shows experiments with various test signals and investigates the repeatability of the estimation. The standard deviation of the estimation results to

$$\sigma_\beta = [0.09 \text{ kgm}^2, 0.04 \text{ kgm}, 0.05 \text{ kgm}]$$

Results of the torque estimation applying these β-values in realistic motion scenarios are depicted in Figure 3.16. The estimation well represents of the overall signal shape, as the top row of plots indicates. The bottom row shows disturbances affecting the estimation.
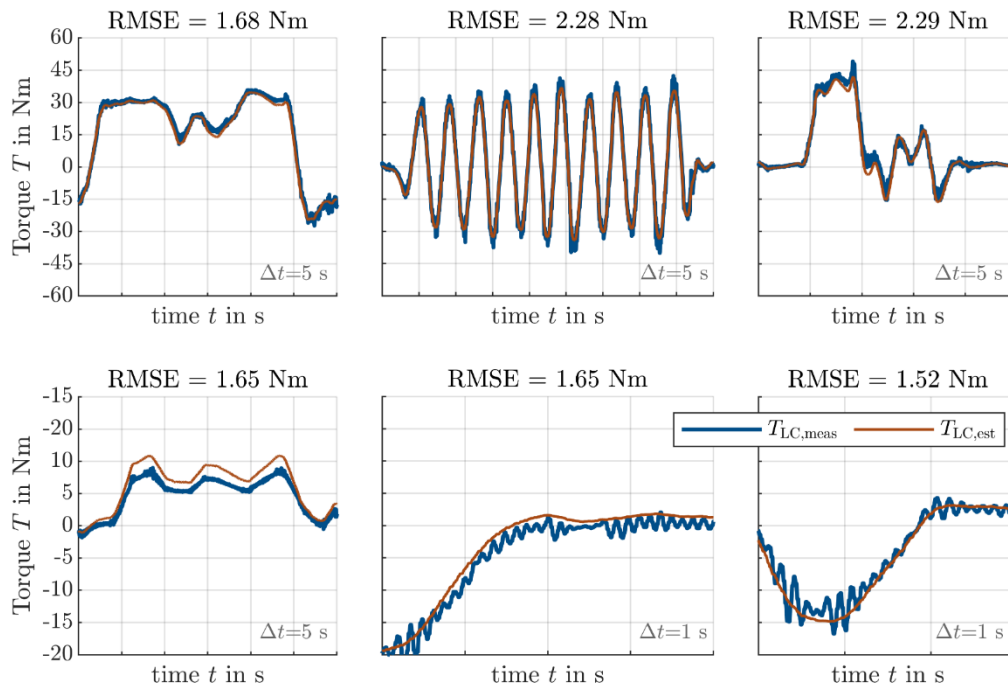
Figure 3.16: Performance of the torque estimator in realistic motion scenarios. The thin red lines show the estimated value, the thick blue lines the measured values. Top row l.t.r.: two consecutive corners; slalom maneuver; corner and double lane change. Bottom row l.t.r.: bearing friction (1); bearing friction (2); high frequency oscillations induced by g-vest.

While the estimation generally matches the measured values rather well, two disturbances can be observed. Firstly, the used plain bearings provide friction, such that during small and slow excitations the measured torques maintain smaller than estimated (bottom left plot in Figure 3.16). As well, when returning from higher platform roll angles to a vertical orientation of the hexapod, small torque values remain (bottom center plot). The bottom right plot shows oscillations of the measured torque value. Hofmann[117] performs an impulse excitation via an impact hammer on the mockup rear frame and identifies an eigenfrequency of 7.8 Hz, which is in accordance with the measurements shown above. The oscillations maintain small in amplitude, especially when a rider body sits on the mockup and acts as a damping mass.

---

[117] Hofmann, M.: Master Thesis, Systemidentifikation am dynamischen Motorrad Fahrsimulator (2016).

The offset due to friction is as well small valued compared against the torque changes resulting from rider motion.

3.2.6 Attaching a Rider to the Simulator

The previous subsections show how it is possible to estimate the dominant components of the torque around the mechanical roll axis that is purely induced by inertial effects and the motion of the platform. When performing an online simulation however, the force measured by the loadcell consists not only of this platform induced torque, but also contains the rider induced torque. The process depicted in Figure 3.17 is used to determine this rider induced roll torque. Firstly, it is assumed that the rider body is a rigid body and is rigidly attached to the mockup. This allows to perform the torque estimation that was presented in subsection 3.2.5: as the left side of Figure 3.17 shows, the vehicle dynamics result in a known platform motion that is then used to estimate the loadcell signal. If the rider is a rigid mass, the difference between the estimation $T_{\text{LC,est}}$ and the measured signal $T_{\text{LC,meas}}$ becomes zero.
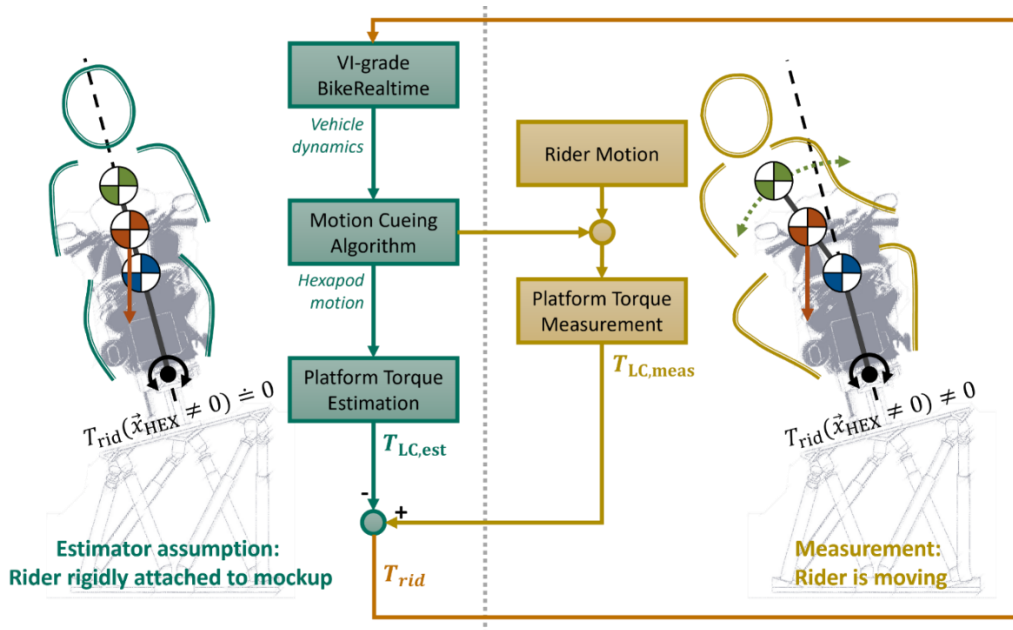
Figure 3.17: Calculating the rider induced torque from measured and estimated torque. The blue (mockup), green (rider) and red (total) CoG correspond to the model presented in Figure 3.8. The rigid rider/mockup-combination on the left generates measurable torques that are ideally equal to the torque estimation. The moving rider on the right will generate ad measurable difference.

The real rider is neither really a rigid body, nor connected rigidly at a fixed position relative to the mockup but moving around. This motion has both active (i.e. riding without hands) or passive components (i.e. reactions to road excitations). Therefore, the difference between

the estimation $T_{\mathrm{LC,est}}$ and the measured signal $T_{\mathrm{LC,meas}}$ will not be zero, but show any effecting torque resulting from the moving, non-rigid rider body[118].

It is obvious, that the torque estimation is depending highly on the inertial properties of the simulator rider. While the β-parameters are constant for the simulator alone, they change individually per rider. The previously derived β-parameters must thus be adjusted for each simulator rider when such precision is relevant in the simulator study. As Hofmann shows that – following the rigid body assumption – the simulator and rider parameters can be added to result in the total parameter set that is relevant during online simulations[119]:

$$\vec{\beta}_{\mathrm{total}} = \vec{\beta}_{\mathrm{rid}} + \vec{\beta}_{\mathrm{mock}} \qquad (3.17)$$

In general, the same identification experiment that was shown in Figure 3.15 could be used to estimate $\vec{\beta}_{\mathrm{total}}$. When firstly introducing a new rider to the simulator, it is however not feasible to ask them to sit on a mockup for 10 minutes and experience sine sweep excitations while maintaining an upright, "rigid" posture. In an everyday study with a newly participating rider, it is much more practical to combine the first simulator contact with the measurement of the body parameters. Therefore, an automated riding scenario is presented to the participants, such that they can get used to experiencing the virtual environment, platform motion and other simulation cues, while possibly reducing curiosity and excitement due to the uncommon testing experience and lab environment. The rider is advised to maintain a centered body posture (i.e. not using lean-in or lean-out). The torque data generated during this scenario can then be used to perform the abovementioned regression.

The platform excitations in such an automated riding scenario do not contain the same amount of signal frequencies that are provided by the previously described test signal. The precision of the β estimation therefore decreases when it is performed with arbitrary riding scenarios rather than using dedicated platform excitations suited for system identification. This is especially true for the estimation of β_1 that could benefit from identification maneuvers that emphasize on a wider range of roll accelerations of the platform.

The effect of this non-ideal identification maneuver to the other two β-parameters is less impactful. For once, the component $x_2 \cdot \beta_2$ can typically be assumed zero, as the lateral offset of the mockup CoG is very small and the rider will intuitively find a balanced seating position, when experiencing that the virtual motorcycle tends to move in one direction without active inputs. A non-zero β_2 would therefore only become necessary, when heavy eccentric components (e.g. measurement devices) are attached to the mockup.

The third component $x_3 \cdot \beta_3$ is dominated by the gravitational effect (see equations (3.13) and (3.14)). This effect is well represented by an automated riding scenario as soon as it contains e.g. a cornering maneuver that slowly brings the hexapod to its maximum roll angle.

---

[118] Pleß, R. et al.: Manöverumsetzung auf einem dynamischen Motorrad Fahrsimulator (2016).

[119] Hofmann, M.: Master Thesis, Systemidentifikation am dynamischen Motorrad Fahrsimulator (2016).

In order to increase the confidence of the estimated values, or as a quick alternative for parametrization, and a second approach can be used to estimate the β-parameters. Therefore, it is necessary to measure or estimate the rider mass, CoG-height and inertia such that equation (3.14) and (3.17) can be used to calculate the total β-parameters:

$$\vec{\beta}_{\text{total}} = \vec{\beta}_{\text{rid}} + \vec{\beta}_{\text{mock}} = m \begin{bmatrix} \rho_{xx}^2 + y_{CG}^2 + z_{CG}^2 - h_{\text{ax}}z_{CG} \\ y_{CG} \\ z_{CG} - h_{\text{ax}} \end{bmatrix} + \begin{bmatrix} 21.9 \text{ kg m}^2 \\ 1.75 \text{ kg m} \\ -26.2 \text{ kg m} \end{bmatrix} \quad (3.18)$$

Yet, this calculation is prone to estimation errors as well, as the inter-individual inertial properties are not easily measured. According to statistical data known from literature, a human's gyration radius ρ_{xx} in a riding posture is assumed to be in the range of $0.3...0.5$ m[120]. The height of the rider's CoG above the motion platform is above the mockup's saddle ($z_{\text{saddle}} = -0.62$ m), in the range of $z_{CG} = -0.7 ... -0.9$ m. With these two sizes as well as the rider's weight, it is possible to use the lookup maps in Figure 3.18 to estimate a rider's β-parameters without needing to perform the abovementioned test routine.
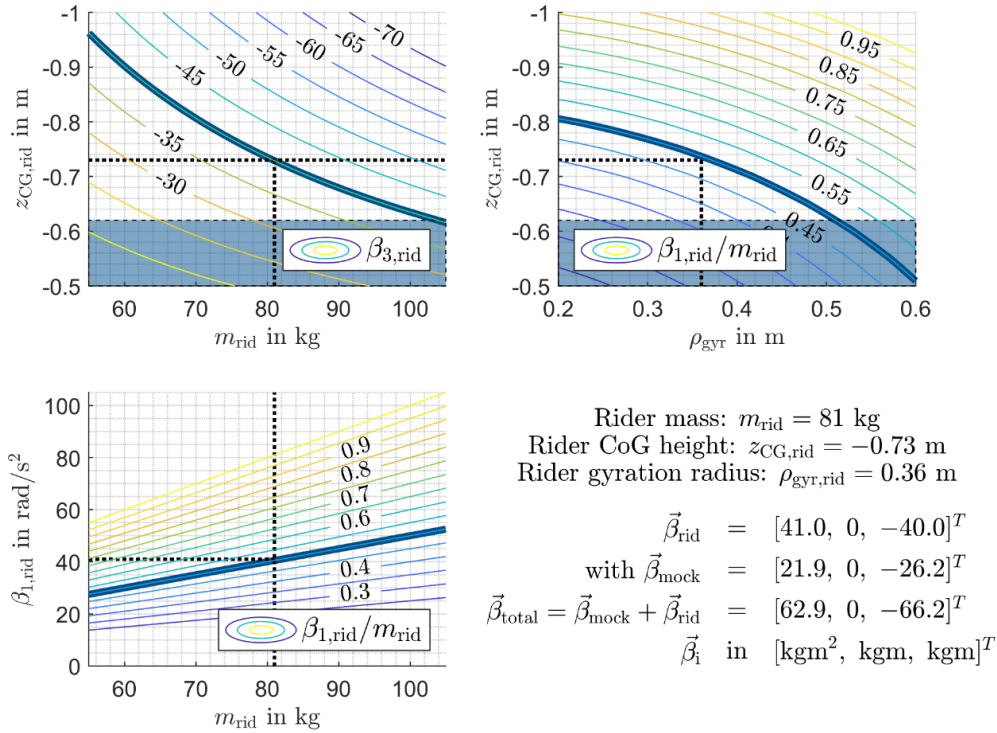
Figure 3.18: Estimation of β-parameters based on body measurements. The blue area indicates the saddle height as a lower boundary for $z_{\text{CG,rid}}$. Knowing the rider's mass and having an educated guess on $z_{\text{CG,rid}}$ and $\rho_{\text{gyr,rid}}$ allows to evaluate the rider's parameters $\beta_{3,\text{rid}}$ (contour line in top left plot) and $\beta_{1,\text{rid}}$ (contour line in top right plot, multiplied by mass in bottom left plot).

It is again assumed, that β_2 is zero. The top left contour plot maps the rider mass and CoG height to β_3 according to the bottom row of equation (3.14). The top right contour plot maps the rider's gyration radius and CoG height to β_1/m. The bottom left contour plot can then

---

[120] Santschi, W. R. et al.: Moments of inertia and centers of gravity of the living human body (1962).

be used to read out β_1. The rider's parameters must be added to the known mockup parameters according to equation (3.18) to determine the final parameters used for the torque estimation in an online simulation. In the given example, the total parameter set results to $\vec{\beta}_{total} = [63 \text{ kgm}^2, 0 \text{ kgm}, -66 \text{ kgm}]^T$. This comes close to the values determined by measuring the torque during an automated riding scenario, as described above, which yields to $\vec{\beta}_{total} = [64.7 \text{ kgm}^2, 0.57 \text{ kgm}, -71.5 \text{ kgm}]^T$. The difference in the values for β_3 can be explained by an estimation error of $z_{\text{CG,rid}}$ of just about 4 cm. Given the highly individual rider size, weight distribution and posture on the motorcycle, there is however no simple way to determine a more precise estimation for $z_{\text{CG,rid}}$. The same holds true for the radius of gyration $\rho_{\text{gyr,rid}}$. Therefore, the lookup method for determining the parameter set may only provide a rough estimate. It is therefore suggested to use the automated ride method for the parametrization of a rider and use the lookup tables to check for plausibility of the determined values.

The list in Table 3.2 shows the weights and sizes of five different riders, as well as the resulting parameter set from both the lookup method and the automated ride method. Whenever possible, the latter method was used during the studies described later.

Table 3.2: List of $\vec{\beta}_{total}$ elements for five riders

		Rider 1	Rider 2	Rider 3	Rider 4	Rider 5	Mockup
Size in cm		184	190	163	170	175	-
m_{rid} in kg		83	78	67	65	83	102
$z_{\text{CG,rid}}$ in m		-0.73	-0.82	-0.70	-0.71	-0.72	-0.47
$\rho_{\text{gyr,rid}}$ in m		0.36	0.42	0.37	0.39	0.32	0.297
Lookup	β_1	63	70	51	51	58	-
	β_2	0	0	0	0	0	-
	β_3	-66	-72	-55	-54	-64	-
Auto-ride	β_1	64,7	55.6	56.8	55.23	85.2	21.9
	β_2	0.57	0.00	0.72	0.61	0.16	1.75
	β_3	-71.5	-70.1	-66.6	-65.2	-73.4	-26.2

The deviations between the two available estimation methods can result from estimation errors on both sides. The lookup method struggles from unprecise information about the radius of gyration and CoG height. The auto-ride method struggles from riders not maintaining a "rigid" upright posture while experiencing the scenario. While these uncertainties are not desirable, other identification methods lack of usability and cannot be suggested for everyday studies. For professional use, the aforementioned platform-excitations can be used, without providing a realistic riding scenario. Furthermore, professional riders may iteratively adjust their individual parameters to reach the desired motorcycle responses to rider leaning.

3.3 Applicability of the Simulator

The DESMORI simulator, as described in the previous sections, has been used throughout multiple studies, proving its applicability for different use cases. Aside from unpublished contract research, it was used e.g. in Merkel[121] to investigate the controllability of autonomous emergency braking (AEB) scenarios under non-ideal riding conditions (i.e. riding with just one hand or without hands) and to investigate the effect of warning elements on the performance of AEB. Further publications from Merkel[122], Sevarin[123] and Will[124] investigate innovative HMI concepts like augmented reality glasses or reaction times of motorcyclists to warning cues presented from cooperative intelligent transport systems (C-ITS). In the project UR:BAN, the simulator was used in a multi-driver simulation[125]. Will[126,127] shows, how the DESMORI simulator is a feasible tool to perform test procedures that are standardized for passenger car simulators but are yet subject to real vehicle studies in the motorcycle domain. While the DESMORI simulator proves to be usable for performing such studies, there is no feasible way to compare it against the other simulators known from literature. To the author's knowledge, there exists no collective study comparing high fidelity motorcycle riding simulators of different research institutes or companies that would allow to rank one simulator against another. Also, validation methods specific for motorcycle riding simulators are rare. Instead of holistic system validations, many studies will concentrate only on specific aspects of the simulation. An absolute validity of a driving simulator for the use in any riding scenario is practically impossible to achieve and is not even necessary in most use cases. Instead, a relative validity is often sufficient in simulator studies. The fidelity of a (D)MRS necessary to perform certain studies is yet unclear. According to Blaauw[128], there is no immanent connection between physical and behavioral validity, while other authors expect the fidelity of a simulator to be critical for a successful study[129,130].

---

[121] Merkel, N. L. et al.: Automatische Notbremssysteme für Motorräder (2022).

[122] Merkel, N. L.: Safety Potential of Data Glasses (2022).

[123] Sevarin, A. et al.: Assessment of Visual and Haptic HMI Concepts (2020).

[124] Will, S.: Motorcycle Rider Reaction Times as Response to Visual Warnings (2022).

[125] Will, S.: Approach to Investigate Powered Two Wheelers' Interactions (2018).

[126] Will, S.; Hammer, T.: Assessing Powered Two Wheelers' display and control concepts (2016).

[127] Will, S.; Schmidt, E. A.: Powered two wheelers' workload assessment (2015).

[128] Blaauw, G. J.: Driving Experience and Task Demands in Simulator (1982).

[129] Leonard, J. J.; Wierwille, W. W.: Human Performance Validation of Simulators (1975).

[130] Zöller, I. M.: Diss., Einfluss ausgewählter Gestaltungsparameter auf die Fahrerverhaltensvalidität (2015).

In in the nationally funded project "*Anwendungsmöglichkeiten von Motorradfahrsimula-toren*" [131](Fields of application for motorcycle riding simulators), the DESMORI simulator was compared against a real vehicle as well as a static motorcycle riding simulator. This comparison aims to show, how different fidelity levels of motorcycle riding simulators affect their usability for various applications, i.e. handling analyses, assistance system development or HMI development. The study shows, how the DESMORI simulator exceeds a reference static motorcycle riding simulator in terms of perceived realism, while demanding higher rider workloads than both the static simulator and the real motorcycle.

---

[131] Hammer, T. et al.: Anwendungsmöglichkeiten von Motorradsimulatoren (2021).

4 Performance Measures

In section 2.2, stability and handling characteristics of motorcycles have been presented, that are known from literature. The associated performance measures can compare various motorcycles or configurations against each other. An investigation of motorcycle handling properties on a DMRS was performed by Massaro and Sadauckas[132]. They come to the result that "testing or at least factor screening in the virtual environment with an (expert) human-in-the-loop can save time and money with better experimental control." However, the research at hand doesn't aim towards rating the handling of two different motorcycles, but towards rating how the performance of a simulator is affected by introducing a rider motion input. To investigate the beneficial effects of the newly designed DLRC system, objective measurements of valid performance measures (PM) must be conducted. Where the abovementioned motorcycle performance measures don't suffice to rate the simulator or DLRC performance, new measures need to be developed. In accordance with the previously defined research questions and working hypotheses, the PM should be capable to

- show a qualitative change in vehicle states by utilizing rider motion in steady state riding conditions
- rate the DLRC's dynamic effects in terms of vehicle response to rider leaning inputs and trajectory following capabilities
- rate the DLRC's potential to lower the achievable speed threshold
- show if the DLRC eases the access to the simulator

Firstly, it must be discussed, in which scenarios an increased performance could even become observable. Therefore, it is feasible to classify riding scenarios into separate categories. From literature, different concepts are known, that are used to segment the motorcycle riding task. Hammer[133] uses so called minimal scenarios as building blocks for any riding maneuver. Magiera [134] uses so called maneuver primitives to segment cornering maneuvers in different states and state transitions. For the research described in this thesis, a similar approach is used. However, a classification is used that is less fragmented than the abovementioned. Therefore, three main riding categories are defined:

Stationary   Transient   Dynamic

Each of these main categories is further separated into sub-categories. A stationary scenario could either be a straight running maneuver or a constant radius cornering maneuver at constant speed. During these maneuvers, all vehicle states ought to maintain constant. A transient scenario on the contrary will contain a change of certain vehicle states, resulting in a transition from one equilibrium condition to another. Again, this can either happen in

---

[132] Massaro, M. et al.: Simulators for Assessment of Handling (2016).

[133] Hammer, T. et al.: Anwendungsmöglichkeiten von Motorradsimulatoren (2021), p. 21.

[134] Magiera, N.: Diss., Identifikation des Fahrfertigkeitsniveaus von Motorradfahrern (2020), p. 39.

straights or curves. For example, in straight running, the motorcycle roll angle can be varied while maintaining a straight trajectory by changing both steering and leaning inputs accordingly. In cornering, a change of either steering or leaning input will result in a changing curvature. The dynamic scenarios can be seen as a (potentially fast) sequence of transients. A coast-down maneuver is technically a transient maneuver but is here considered in close connection with the stationary straight maneuvers. U-turn, (double-)lane change and slalom maneuvers are typically used for dynamic testing[135] and qualify for simulator testing just as well. If DLRC is by any means effective, this should become observable in at least one of the stationary, transient or dynamic sub-categories when activating or deactivating each of the two control loops. With DLRC, four possible control configurations exist. The rider of a simulator may either use the steering input or not, as well as he may either use the leaning input or not. The steering condition is simply varied by taking the hands on (H1) or off (H0) the handlebar. The leaning condition is varied by turning the roll torque determination on (L1) or off (L0). These four control configurations in combination with the aforementioned sub-categories result in the test classification shown in Table 4.1:

Table 4.1: Classification of potential DLRC investigations

Test Categories		*Hand Off Lean Off*	*Hand On Lean Off*	*Hand Off Lean On*	*Hand On Lean On*
Stationary	*Straight*	SS_{L0}^{H0}	SS_{L0}^{H1}	SS_{L1}^{H0}	SS_{L1}^{H1}
	Curve	SC_{L0}^{H0}	SC_{L0}^{H1}	SC_{L1}^{H0}	SC_{L1}^{H1}
	Coast Down	CD_{L0}^{H0}	CD_{L0}^{H1}	CD_{L1}^{H0}	CD_{L1}^{H1}
Transient	*Straight*	TS_{L0}^{H0}	TS_{L0}^{H1}	TS_{L1}^{H0}	TS_{L1}^{H1}
	Curve	TC_{L0}^{H0}	TC_{L0}^{H1}	TC_{L1}^{H0}	TC_{L1}^{H1}
Dynamic	*U-Turn*	DU_{L0}^{H0}	DU_{L0}^{H1}	DU_{L1}^{H0}	DU_{L1}^{H1}
	Lane Change	DL_{L0}^{H0}	DL_{L0}^{H1}	DL_{L1}^{H0}	DL_{L1}^{H1}
	Double-Lane Change	DD_{L0}^{H0}	DD_{L0}^{H1}	DD_{L1}^{H0}	DD_{L1}^{H1}
	Slalom	DS_{L0}^{H0}	DS_{L0}^{H1}	DS_{L1}^{H0}	DS_{L1}^{H1}

This classification provides a structure to find and discuss effects of a rider motion input and define performance measures for each relevant test. The H1/L1 condition obviously resembles real motorcycle riding while the H1/L0 condition resembles state of the art motorcycle simulators. The H0/L0 condition may serve as a reference for the motorcycle's open-loop behavior without any rider input. The H0/L1 condition resembles riding a motorcycle without hands. The following sections derive adequate PM for the abovementioned test categories by firstly reviewing the motorcycle qualities and characteristic values known from literature before developing new measures, where needed. An overview about the final PM selected for testing is given in section 4.6. Afterwards, chapter 5 derives study designs that allow to test for these PM and chapter 6 will show the results of the performed studies.

---

[135] Kooijman, J. D.; Schwab, A. L.: A Review on Handling Aspects in Bicycle and Motorcycle Control (2011).

4.1 Stationary Scenarios

This section derives and discusses potential PM that allow to rate the effect of DLRC during stationary riding conditions. These apply to motorcycling in two different scenarios: straight running at constant velocity as well as constant radius cornering. The main goal in these scenarios is to maintain stability in an equilibrium condition. Any deviation from such must be rated negatively, while the exact location of the equilibrium during cornering is irrelevant.

4.1.1 Straight Running at Constant Velocity

The only relevant quality of a motorcycle (simulator) during straight running at constant speed is its capability to maintain the equilibrium. The only independent variable that can be varied is the chosen vehicle speed. This results in the following questions:

- What (if any) are the expected effects during straight running, when switching between the different control modes SS_{L0}^{H0} to SS_{L1}^{H1}?
- Will these effects vary for different velocities?
- What measurements allow to rate the performance during straight running?

It is obvious, that the vehicle in the SS_{L0}^{H0} condition will show its pure open-loop behavior that only depends on the vehicle configuration. Depending on the stability of the capsize mode at a certain speed, the motorcycle will either go straight[136] or tilt over. With decreasing speeds, the capsize mode will become increasingly instable and the motorcycle will tilt over. In SS_{L0}^{H1} a rider can stabilize the capsize mode by steering (see section 2.1). SS_{L1}^{H0} also allows the rider to generate a stabilizing roll torque to the motorcycle dynamics (see section 3.2). However, this control mode is expected to be less efficient. The combination SS_{L1}^{H1} is presumed allow riders to ride most naturally, as it resembles the real motorcycle control cues.

There exists no comparable study of the rider motion's effect on the straight running stability in real life riding. Obviously, investigations of the L0 conditions may not contain real rider bodies and therefore necessitate autonomous motorcycles that have been successfully implemented only recently by BMW Motorrad[137] and others, as discussed by Assad[138]. Yokomori[139] shows increasing amounts of various rider and vehicle states at straight running with decreasing velocities in both standard riding (i.e. SS_{L1}^{H1}) and riding without hands (i.e. SS_{L1}^{H0}) conditions. Other studies concentrating on the stability of motorcycles in straight

---

[136] Assuming a perfectly symmetrical motorcycle with CoG in the middle plane.

[137] Hans, S. et al.: Why automatization is the future.

[138] Marília Maurel Assad: Diss., control strategies for autonomous scale motorcycles (2018).

[139] Yokomori, M. et al.: Rider's Operation of a Motorcycle Running Straight at Low Speed (1992).

running typically perform modal analyses of the model equations[140]. Such are however not feasible for the investigation at hand.

Any effect of using DLRC should become observable through changing amounts of lateral dynamic quantities like the wheels' lateral displacement, roll rates or steering angles while riding at different, constant speeds. For a quantitative assessment of said phenomena, the cumulative distribution function (CDF) can be applied, that allows for their statistical evaluation throughout a maneuver. An improved stability should become observable by a steeper inclination of the CDF plot, as visualized in the hypothetical plot in Figure 4.1. It is anticipated that a simulator without DLRC will be point symmetrical in $\varphi_{mcy} = 0$, as the used dynamic model doesn't have eccentric masses but is rather built symmetrically. However, introducing the rider body to the system can cause an offset in the CoG's lateral position if he sits with offset to the center by a deviation $y_{rid,0}$ and thus provoke static roll angle offsets as well. These must not be rated negatively but rather verify the static effects of rider posture.
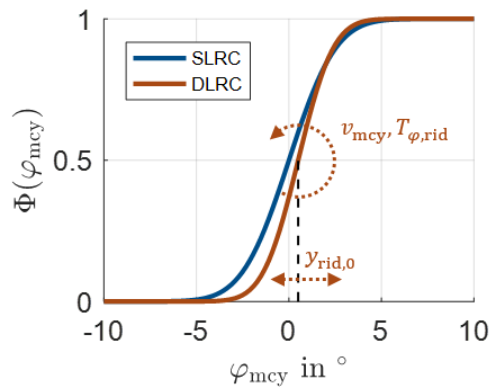
Figure 4.1: Hypothetical CDF plot of the roll angle distribution. Increasing velocities as well as stabilizing rider actions should result in steeper inclinations of the curve.

In addition to the distribution functions of the lateral dynamic quantities, their frequency components can be evaluated. It is anticipated, that by adding a (real) rider body's effect to the (virtual) motorcycle system, the oscillating behavior of the motorcycle states will show significant differences. Around the rider body's eigenfrequency, the rider might for example act as an absorber, thus reducing motorcycle roll amplitudes. To analyze the vehicle oscillations, 1/3-octave bands are used here. The lowest third's center frequency is chosen such that it contains the first harmonic of a track-segment with a duration of 30 s at constant velocity. Therefore, this center frequency results to $f_0 = \frac{1}{30}$ Hz. From there on, every next third's center frequency lies at $f_{i+1} = f_i \cdot \sqrt[3]{2}$. The power spectrum is calculated according to Appendix A.5. The performance during straight running can be rated higher, as the power spectrum reaches lower values, as this indicates a more stable ride.

---

[140] Cossalter, V. et al.: Inertial and Modal Properties of Racing Motorcycles (2002).

4.1.2 Constant Radius Cornering

For steady state cornering, the same reasoning applies as for straight running. As the velocity decreases, the capsize mode becomes more pronounced and demands more stabilization effort from the rider. This is possible in all conditions but $\text{SC}_{\text{L0}}^{\text{H0}}$ with changing effectiveness and efficiency. The deviations from the steady state conditions in terms of lateral track deviations, roll rates and steer angle as described for straight running can serve as performance measure again. Improved performance is again observable by a steeper inclination of the CDF around the equilibrium state. For the course of the research presented here, the SC maneuvers are not presented, but the focus of the cornering evaluation is put on the following transient maneuvers.

4.2 Transient Scenarios

As described previously, in a transient scenario, one or more system inputs are deliberately changed in order to shift from one equilibrium condition to another. The transient may be trajectory-preserving or not. I.e. vehicle states can be varied with or without affecting the current velocity and curvature. To preserve the current trajectory, the sum of camber and sideslip side forces of the tires must remain constant. Thus, an increase of camber side forces must be compensated by corresponding sideslip values. As the roll angle varies, the static steering torque induced by the front tire's vertical load and trail will change as well. Figure 4.2 shows the (infinitesimal thin) front wheel that is slightly tilted by the roll angle φ and able to rotate around the steering axis that is inclined by the steering head angle τ. The steering torque T_δ that must be applied by the rider to maintain equilibrium yields

$$T_\delta = n \sin \tau \cdot \left(F_{z,\text{f}} \sin \varphi_{\text{mcy}} - F_{y,\text{f}} \right), \tag{4.1}$$

with the front wheel normal force $F_{z,\text{f}}$ and the lateral force $F_{y,\text{f}}$

$$F_{z,\text{f}} = m_{\text{mcy}} g l_{\text{r}} / l_{\text{mcy}} \tag{4.2}$$

$$F_{y,\text{f}} = k_\alpha \alpha_{\text{f}} + k_\gamma \gamma_{\text{f}} \tag{4.3}$$
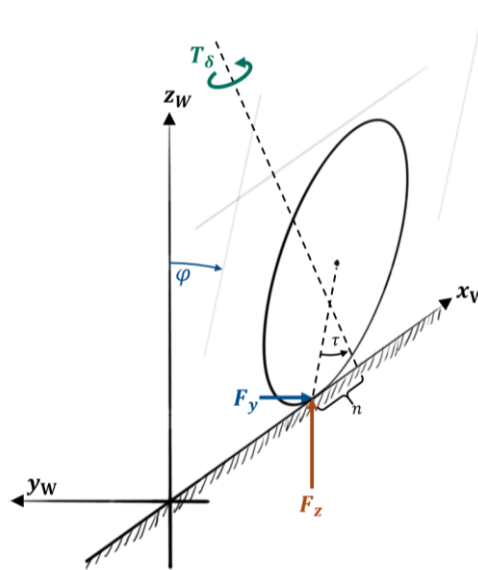
Figure 4.2: Steer torque decomposition at static equilibrium. The trail n acts as a lever between the tire forces and steering axis, resulting in the steering torque T_δ.

If the trajectory's curvature is kept constant (0 for running straight) as well as the velocity, so is the lateral tire force. Increasing roll angles will lead to increasing steering torques by a factor of $\sin \varphi_{\mathrm{mcy}}$ as equation (4.1) implies. If riding in a straight line (i.e. $F_{y,\mathrm{f}} = 0$), but with a positive roll angle (i.e. to the right), this results in a positive steer torque (i.e. pushing the right side of the handlebar, steering left).

Following the classification presented at the beginning of this chapter, the transient scenarios are separated to straight and curved scenarios for the further discussion.

4.2.1 Transients in Straight Running

As derived previously, running straight at constant speed must not necessarily mean riding without a motorcycle roll angle. As the rider applies a roll angle to the motorcycle frame while leaning to the opposite side, the overall system CoG may maintain right above the tire contact line. This change of vehicle states is however only possible by changing both leaning and steering inputs. Therefore, this kind of maneuver is neither possible in the $\mathrm{TS}_{\mathrm{L0}}^{\mathrm{H1}}$ nor $\mathrm{TS}_{\mathrm{L1}}^{\mathrm{H0}}$ condition but only at $\mathrm{TS}_{\mathrm{L1}}^{\mathrm{H1}}$. It is enabled by implementing DLRC and cannot be achieved by DMRS without such DLRC capabilities. An adequate performance measure for transients in straight running is a simple yes/no rating to answer if this kind of maneuver can be performed or not.

4.2.2 Transients in Cornering

The **trajectory-preserving** transients during cornering correspond to the transients in straight running. It is as well only possible to perform in the $\mathrm{TC}_{\mathrm{L1}}^{\mathrm{H1}}$ condition While neither vehicle speed nor path curvature change, several vehicle states do. By leaning into the curve,

both motorcycle roll angle and steer torque are reduced. Depending on the current trajectory and vehicle configuration, the steer torque can also change sign (resulting in a steer torque towards the inside of the curve). This leads to a destabilizing effect, as without the rider's steer input, the motorcycle will eventually capsize. On the contrary, if the rider utilizes lean-out while keeping velocity and curvature constant, the motorcycle roll angle and steer torque will increase. As before, a DMRS without DLRC capabilities will not be able to show this characteristic behavior at all. While the previously discussed straight transient maneuver doesn't have a huge relevance in real riding, transient state adjustments during cornering are commonplace. An adequate performance measure with regard to transients in cornering is again a yes/no rating, if the maneuver can be performed or not.

A quantitative rating is possible by revising the cornering indexes presented in 2.2.3, Table 2.1 on page 19. All indexes that are used for SSC maneuvers describe the ratio of one rider input (either steer torque or lean motion) to some motion state of the vehicle (roll angle, lateral acceleration, steer angle or yaw rate). Except for the steer angle, these motion states are proportional to each other during steady state cornering and it does not provide additional information to look at multiple indexes. Furthermore, the abovementioned indexes that have been used in literature do not contain such two, where leaning and steering inputs are put in context to the same reference vehicle state. Therefore, two new indexes are introduced here that put both the average steer torque input and the roll torque input into relation with the average yaw rate:

$$\delta\Gamma_{\dot\psi} = \frac{T_{\mathrm{hb,avg}}}{\dot\psi_{\mathrm{avg}}} \qquad\qquad \varphi\Gamma_{\dot\psi} = \frac{T_{\mathrm{rid,avg}}}{\dot\psi_{\mathrm{avg}}} \tag{4.4}$$

This allows to also compare the two different input cues with each other while using the same reference size. The yaw rate was selected for this comparison, as it is not directly connected to either of the input torques (as steer or roll angle would be). Furthermore, it is directly linked with following a certain trajectory, while both steer and lean angle might vary depending on the motorcycle configuration and other factors. The two indexes $\delta\Gamma_{\dot\psi}$ and $\varphi\Gamma_{\dot\psi}$ will be referred to as "steer-turn-index" and "lean-turn-index" for the upcoming discussions. For the rating of DLRC, it is thereby not important what exact values are reached, but to test if they show the expected variability.

Secondly, the **non-trajectory-preserving** transients shall be investigated. There, the changes in one input are not compensated by changes in the second input. As the sum of the tire side forces is changing, the lateral force equilibrium and roll equilibrium will inevitably change as well. This leads to a change in roll angle and curvature when the velocity is kept constant. Such transients are possible in TC_{L0}^{H1} (i.e. state-of-the-art DMRS) and – implementing DLRC – in TC_{L1}^{H0} (i.e. riding without hands) as well as their combination TC_{L1}^{H1}.

The first adequate performance measure is therefore again to check if, or if not, it is possible for the rider of the simulator to intentionally vary the curvature with either input cue (while keeping the velocity constant). The steer-turn-index and lean-turn-index cannot provide additional information here, as these indexes are meant to be used with rather constant $\dot\psi$ only.

In order to rate the ease and precision with which the rider can reach a target curvature, a performance measure is needed that can rate deviations from the target trajectory. Therefore, the lane deviation and yaw deviation during cornering can be evaluated. In order to account for the variability in lane selection (on a wide road, a rider may utilize various amounts of corner cutting), the cornering lane can be delimited e.g. by means of cones or road markings. On a track delimited that way, the number of boundary crossings can be used as performance measure as well.

4.3 Dynamic Scenarios

As described at the beginning of this chapter, the dynamic scenarios contain the U-turn, (double-) lane-change and slalom maneuvers. As before, it must be checked, if notable differences in the maneuvers are expected in the conditions Dx_{L0}^{H0} through Dx_{L1}^{H1}. This would indicate potentially beneficial effects by utilizing DLRC. To identify these, performance measures must be derived again that allow to rate the beneficial effect of DLRC.

The motorcycle's and rider's performance in the abovementioned maneuvers is typically measured in terms of the highest velocity at which the rider is able to perform the maneuver, the shortest duration to finish the maneuver, etc. This will eventually end up in a discussion about the handling of the motorcycle. However, the term handling is a quality that is rather difficult to grasp, compared to e.g. stability or maneuverability (see section 2.2), as it typically includes subjective ratings. Multiple approaches exist in literature that try to objectify handling.[141] As the rider of a motorcycle has such a large influence on the composition of any maneuver, comparing different resulting trajectories and dynamics can be problematic.

Following the definition in section 2.2, handling is the quality of a motorcycle that governs the ease and precision with which a rider can perform the correct controls required in support of a certain maneuver. This puts up three demands to achieve good handling:

a) **Perform the correct controls**
A defined maneuver must start and end within specific borders.
b) **Ease**
The rider's physical and mental workload must stay small.
c) **Precision**
During maneuver performance, deviations to the desired trajectory must stay small.

Demand a) is a perquisite, as without a successfully finished maneuver, no further performance evaluation is reasonable. Typically, real riding tests don't fail on this criterion. However, that must not be true for all simulator tests. As e.g. a dynamic maneuver might be too difficult to handle for certain study participants. To describe this basic ability to perform a

---

[141] Kooijman, J. D.; Schwab, A. L.: A Review on Handling Aspects in Bicycle and Motorcycle Control (2011).

certain maneuver, the term *rideability* will be used in this document. Demand b), the ease of performing the maneuver, is often evaluated by subjective ratings. However, experiments are known from literature that can objectify mental workload quantities. The *Surrogate Reference Task* (SuRT), *n-Back Task* or *Peripheral Detection Task* (PDT) are described and used e.g. by Guth[5] to determine the workload needed to perform secondary and tertiary riding tasks like using GPS or radio systems in a board computer of a motorcycle. The focus of this thesis is less on such mental and psychological issues but rather concentrates on the vehicle and simulator dynamics. Thus, the mental workload is not further considered here. Demand c), the precision of the performed maneuver, can be evaluated by a multitude of maneuver specific performance measures that will be discussed below.

The following sections will discuss potential effects of the conditions Dx_{L0}^{H0} through Dx_{L1}^{H1} on performing the maneuvers and derive performance measures concentrating on rideability and precision of the maneuvers.

4.3.1 U-Turn Maneuver

A U-turn – in contrast to riding a 180° curve – describes a 180° turn that is typically performed within tight track boundaries and does not contain a steady state cornering segment. The task is either to turn at a given velocity needing the least space to turn, or to maximize the speed when turning within defined track boundaries. The maneuver combines comparably low velocities with comparably high roll rates and angles. Therefore, the demands on the vehicle model, controllers and rider's skill are very high. Pre-tests on the DESMORI simulator showed a lack of rideability in this maneuver regardless of using DLRC or not. To ensure the rideability, the turning radius had to be increased such that it would contain a constant radius cornering section with less than 35° roll angle and velocities above 30 km/h. Therefore, the U-turn maneuver is not further considered here.

4.3.2 Lane Change Maneuver

A lane change maneuver is defined by the target velocity, the lateral offset that a rider must achieve and the distance that is available for this offset motion. A double lane change consists of two consecutive lane change maneuvers in opposite directions. If the distance between the two is large enough, they can be evaluated as two single lane changes. As the distance becomes shorter however, the maneuver becomes more and more like a single wavelength of a slalom maneuver and loses its lane change character The research at hand will therefore only discuss single lane changes in the following. However, these will be performed in both left and right direction throughout multiple repetitions to account for possible directional effects. The maneuver is rideable in the DL_{L0}^{H1} condition, i.e. the steering input suffices to successfully perform the maneuver. It must therefore be discussed, if and how the leaning input may affect the maneuver in either DL_{L1}^{H0} or DL_{L1}^{H1} condition and what performance ratings can be applied to rate the outcome of the maneuver.

Performing the maneuver in the $\mathrm{DL_{L1}^{H0}}$ condition allows to concentrate purely on the leaning input cue. As before, a yes/no rating over the rideability of this maneuver is the first performance measure. Looking into detail, it is known from the Aström model (section 2.3.2), that a motorcycle will show an opposing motorcycle roll motion as the rider initiates a turn through leaning motions. Thereby, the amplitudes of the counter roll become less prominent with an increase in velocity. The performance of the DLRC system can therefore be rated higher if it can replicate this initial counter motion rather than just showing the quasi-static effect of changing the equilibrium conditions during steady cornering.

The lane-change-roll index (LCRI, section 2.2.3, Table 2.1) is used in literature to rate a real motorcycle's handling characteristics in a lane change maneuver. It relates better handling to needing less steer torque, just as most of the handling indexes known from literature. While this index is designed for rating different vehicle configurations, it may also serve to rate the effect of DLRC. When performing a rather strictly constrained lane change maneuver (i.e. passing through small gates, short transition distance, constant velocity) on a simulator in $\mathrm{DL_{L0}^{H1}}$ condition, it will always necessitate the same steering input, regardless of the rider that is controlling the simulator, if the maneuver is to be performed successfully. As the steering input is the only variable in this scenario, all other vehicle states will be equal through all valid repetitions of the experiment as well and no inter individual rider effects exist. By adding DLRC capabilities, the rider may show different control actions in the $\mathrm{DL_{L1}^{H1}}$ condition, resulting in a variance of the LCRI. Utilizing lean-in would therefore result in smaller values of the LCRI and lean-out would result in higher values compared to the $\mathrm{DL_{L0}^{H1}}$ baseline values.

The changing input cues should become observable in the measured vehicle trajectories as well. To allow for a statistical analysis of the lane change trajectories, the author developed the tanh-fitting method presented in[142]. There, a hyperbolic tangent function is fitted to the measured CoG trajectory by minimizing the loss function

$$E_{\mathrm{tanh}} = RMS\left(\tilde{y}_0 + \frac{\Delta\tilde{y}}{2}\cdot\left(1 + \frac{\tanh(x_{\mathrm{CG}} - \tilde{x}_{\mathrm{mid}})}{\Delta\tilde{y}\big/\left(2\cdot\max\left(\frac{\partial\tilde{y}}{\partial\tilde{x}}\right)\right)}\right) - y_{\mathrm{CG}}\right) \qquad (4.5)$$

Therein, the hyperbolic tangent function is offset longitudinally by $\tilde{x}_{\mathrm{mid}}$ and laterally by $\tilde{y}_0$ and it is scaled longitudinally by the maximum offset rate $\max\left(\frac{\partial\tilde{y}}{\partial\tilde{x}}\right)$ and laterally by $\Delta\tilde{y}$. These four fitting parameters as well as the RMS value allow statements about the precision of the lane change maneuver. The initial offset $\tilde{y}_0$ should ideally be zero, and the amplitude $\Delta\tilde{y}$ should ideally match the width of the lane change maneuver. The maximum offset rate $\max\left(\frac{\partial\tilde{y}}{\partial\tilde{x}}\right)$ shows, how quickly a rider performs the lateral transition and the RMS value rates the quality of the tanh-fitting. Small values will indicate a smooth, undistorted trajectory.

---

[142] Hammer, T. et al.: Anwendungsmöglichkeiten von Motorradsimulatoren (2021).

The location of the turning point of the tanh function $\tilde{x}_{\mathrm{mid}}$ is for now considered less important, but might e.g. provide information about rider reaction times, or the rider's path planning (i.e. if the rider prefers to finish the transition "just in time" or "as early as possible").

In section 2.2.3 the work of Cheli[143] and Bocciolone[144] was presented, indicating that by utilization of rider motion, a delay in the peak steer torques and steer angles can be observed with respect to the peak roll angles. It should therefore be checked, if riding in the $\mathrm{DL}_{\mathrm{L1}}^{\mathrm{H1}}$ condition will similarly delay the appearance of these peaks compared to the $\mathrm{DL}_{\mathrm{L0}}^{\mathrm{H1}}$ condition. However, in the lack of a commonly agreed optimum, apparent changes in the measured delays in the $\mathrm{DL}_{\mathrm{L1}}^{\mathrm{H1}}$ condition may only argue in favor of an increased variability of available riding styles rather than an increased quality.

4.3.3 Slalom Maneuver

A slalom maneuver is defined by the target velocity and cone distance. The maneuver is rideable in the $\mathrm{DS}_{\mathrm{L0}}^{\mathrm{H1}}$ condition, i.e. the steering input suffices to successfully perform the maneuver. It must therefore be discussed, if and how the leaning input may affect the maneuver in either $\mathrm{DS}_{\mathrm{L1}}^{\mathrm{H0}}$ or $\mathrm{DS}_{\mathrm{L1}}^{\mathrm{H1}}$ condition and what performance ratings can be applied to rate the outcome of the maneuver.

The assessment of literature in section 2.2 has shown, that there exist certain characteristic values that describe the performance during a slalom maneuver. At a given slalom frequency and velocity, different peak values, phase delays and amplitude ratios serve to compare different vehicles or vehicle configurations. The investigation of continuous transfer functions is a well-used approach in (offline) simulations. But determining transfer functions from real world experiments (or online simulations) is cumbersome due to the vast number of measurements needed. Every slalom maneuver at constant speed and cone distance will only serve for one datapoint along the abscissa of the transfer function. To allow for sufficient averaging along the ordinate, the number of repetitions must become high as well. Therefore, it is only feasible to check for the alignment of singular datapoints with transfer functions generated by other means of modelling and simulation. The test efficiency can be increased to some extent by using a slalom sweep (i.e. gradually reducing the cone distances). To the author's knowledge, such an experiment has however not been carried out in literature before. This might – among others – result from the long distances needed to build such a maneuver with sufficiently small cone distance change rates. As an example, starting with a slalom frequency of 0.2 Hz and ending at 0.8 Hz with a linear frequency increase rate of 1/12th octave per ten cones necessitates 240 cones and takes five and a half minutes to ride, corresponding to a distance of more than 7 kilometers at 80 km/h. High frequency change rates on the

---

[143] Federico Cheli et al.: *Driver's movements influence on the lateral dynamic of a sport motorbike.*

[144] Bocciolone, M. et al.: *Experimental Identification of Kinematic Coupled Effects* (2007).

contrary will increase the complexity of the riding task and ultimately decrease the signal quality as the signal duration per frequency decreases. The investigation of slalom sweeps is therefore suggested for future research, but only standard slaloms are performed here.

Apart of the analysis of transfer functions and the relative comparison of peak values, Cossalter applied the concept of the so-called Mozzi Axis[145,146] to investigate the rider's influence in slalom maneuvers. This method promises to provide additional information on the rider motion's influence by highlighting the relation of roll and yaw rates during the maneuver (see section 2.2.3). The linearity of the Mozzi trace is used as a measure to quantify the rider's leaning behavior. However, this does not serve as a well-defined performance rating and is therefore not feasible for applications on the motorcycle simulator yet. It is nevertheless suggested to investigate this concept in future research as a potential handling rating possibly for new approaches in motion cueing algorithms for DMRS.

With neither transfer functions nor Mozzi axis being feasible for further investigation, other performance measures are needed that allow to rate a slalom maneuver. Therefore, a new method is suggested here, that can generate baseline values for any motorcycle slalom maneuver and allows to provide an absolute slalom performance rating.

Steady State Slalom Approximation

It is assumed, that the trajectory of a slalom maneuver follows a sinusoidal function. Offline simulations indicate that this is not in general the optimal slalom trajectory when e.g. the maximum slalom speed at a given cone distance is desired. However, this assumption is presumed to suffice for a simple definition of baseline values and is in line with normal (i.e. not dynamic limit) slaloming and is widely used for slalom analyses in literature. The slalom trajectory can therefore generally be described by equation (4.6).

$$y_{\text{target}} = y_0 + \hat{y}_{\text{target}} \cdot \sin\left(2\pi \cdot \frac{1}{2d_{\text{cone}}} \cdot \left(x_{\text{target}} - x_0\right)\right) \qquad (4.6)$$

The rear tire contact point is used as target coordinate $(x_{\text{target}}, y_{\text{target}})$. The longitudinal and lateral offsets x_0 and y_0 are used, if the data shall be fitted to measured coordinates, but they are not of importance for analyzing the amplitude and frequency characteristics. The target slalom amplitude $\hat{y}_{\text{target}}$ is a sensitive factor for all following calculations. It should therefore be well constrained by the experiment design, or the data must be normalized to the amplitude that is individually chosen by the rider.

The explicit formulation of the curvature of a planar curve is given by[147]:

---

[145] Cossalter, V.; Doria, A.: Analysis of Motorcycle Slalom Manoeuvres Using the Mozzi Axis Concept (2004).

[146] Cossalter, V.; Doria, A.: Instantaneous Screw Axis of two-wheeled vehicles (2006).

[147] Merzinger G.; et al.: Formeln + Hilfen Höhere Mathematik, Binomi Verlag, 6. Auflage (2010) p.129

$$\kappa_{target} = \frac{\partial^2 y}{\partial^2 x} \Big/ \sqrt[3]{1 + \left(\frac{\partial y}{\partial x}\right)^2} \tag{4.7}$$

For the trajectory described by equation (4.6), this results to

$$\kappa_{target} = \frac{-\dfrac{\pi^2 \hat{y}_{target}}{d_{cone}^2} \sin\left(\dfrac{\pi}{d_{cone}}(x_{target} - x_0)\right)}{\sqrt[3]{1 + \left[\dfrac{\pi \hat{y}_{target}}{d_{cone}} \cos\left(\dfrac{\pi}{d_{cone}}(x_{target} - x_0)\right)\right]^2}} \tag{4.8}$$

Assuming that $1/\kappa \gg h_{CG} cos\varphi$, and assuming no slip conditions, given the target velocity v_{target}, the target roll angle and yaw rate can be calculated as follows:

$$\varphi_{th,target} = \arctan\left(\kappa_{target} \cdot v_{target}^2 / g\right) \tag{4.9}$$

$$\dot{\psi}_{target} = \kappa_{target} \cdot v_{target} \tag{4.10}$$

The kinematic steering angle δ_{kin} shown in section 2.1.4, equation (2.7) describes the steering angle that is needed to follow a given trajectory under no slip conditions with infinitesimally thin tires. Inserting equation (2.7) in equation (2.8) yields to

$$\kappa_{target} \cdot l = \frac{\sin(\delta_{target}) \cdot \cos(\tau)}{\cos(\varphi_{th,target}) \cdot \cos(\delta_{target}) - \sin(\varphi_{th,target}) \cdot \sin(\delta_{target}) \cdot \sin(\tau)} \tag{4.11}$$

Assuming small steering angles δ_{target}, the equation can be simplified to:

$$\delta_{target} = \frac{\kappa_{target} \cdot l \cdot \cos(\varphi_{th,target})}{\cos(\tau) + \kappa_{target} \cdot l \cdot \sin(\varphi_{th,target}) \cdot \sin(\tau)} \tag{4.12}$$

With the steering head angle τ, and the wheelbase l. Cossalter[148] further simplifies this equation by neglecting the second summand of the denominator. While the assumption of small steering angles is especially true at higher velocities, it may not be used for very slow maneuvers. However, offline simulations of various slalom maneuvers in BRT resulted in steering angles of just less than $\pm 5°$ for velocities down to 40 km/h at cone distances of 14 m. Appendix B.4 shows comparisons between simulator measurements and results from BRT offline simulations during equally parameterized slalom maneuvers in Figure B.16 and Figure B.17. It can be seen that the virtual rider model fails at certain slalom configurations that are rideable for a real rider. Thus, it is not feasible to just use results from offline simulations as a reference to the online simulation.

While the simplified values calculated above may not account for dynamic influences, friction limits, etc. they serve as a simple to use, well-defined baseline for any given slalom configuration that is defined by the cone distance, target velocity and target trajectory width. Except for the steer angle, all kinematic sizes are independent from vehicle parameters. A

---

[148] Cossalter, V.: Motorcycle Dynamics (2006), p. 31.

timeseries comparison of the approximation and corresponding simulator data can be found in Figure B.18 and Figure B.19 of Appendix B.5.

The abovementioned calculations provide well defined reference values of the slalom kinematics, independent of a vehicle parametrization (except for the steering angle). This allows using their amplitudes as reference values and address the measured values as levels. Therefore, the ratio of the measured amplitudes and reference amplitude is calculated and the base 10 logarithm is taken. As the quantities are root-power quantities, a multiplication by 20 provides the respective slalom level in dB. For the roll angle, that exemplarily yields to

$$L_\varphi(t) = 20 \log_{10}\left(\frac{\hat{\varphi}(t)}{\hat{\varphi}_{\text{th},target}}\right) dB \tag{4.13}$$

The phase information ϕ of each quantity can be referenced against the phase of the respective target quantity, or the phase of the target trajectory $\phi_{\text{y,target}}$.

$$\Delta\phi_\varphi(t) = \phi_\varphi(\text{t}) - \phi_{\text{y,target}}(\text{t}) \tag{4.14}$$

The latter allows to maintain the relative phase information of each quantity to the other (e.g. the 90° phase shift between the roll- and yaw rate). The amplitudes and phases of the measured data can be determined from its analytic signal $\tilde{y} = y_r + iy_i$ that consists of the original data $u(t)$ as real part and its Hilbert transformed signal as imaginary part. The Hilbert transform is performed according to equation (4.15):

$$\tilde{h}(t) = \mathcal{H}\{u\}(t) = \frac{1}{\pi} \, p.v. \int_{-\infty}^{\infty} \frac{u(\tau)}{t-\tau} d\tau, \tag{4.15}$$

where p.v. denotes the Cauchy principal value[149]. The absolute of $\tilde{y}$ provides the instantaneous amplitude of the function u at time t and the angle of $\tilde{y}$ provides the instantaneous phase ϕ of the function u at time t. The timely derivative of the instantaneous phase angle is the instantaneous frequency.

$$\hat{A}(t) = |\tilde{y}(t)| \text{ and } \phi(t) = \sphericalangle \tilde{y}(t) \text{ and } f(t) = d\sphericalangle \tilde{y}(t)/dt \tag{4.16}$$

As the abovementioned calculation of reference values does not provide a target value for the steering torque, (and its calculation is much less straight forward than the kinematic sizes) another reference value must be used for calculating the steer torque level. For the use in this thesis, a reference value of $\hat{T}_{\delta,\text{ref}} = 10$ Nm is chosen to bring the measured levels in the same magnitude as the other levels. Figure B.20 in Appendix B.6 exemplarily shows the instantaneous amplitudes and phase delays for several quantities during a slalom maneuver.

The absolute values of the instantaneous amplitudes, phase differences and frequencies can be evaluated as performance measure during slalom. Ideally, they should all remain within reasonably small boundaries. Variances in the values will indicate imperfections during the maneuver. Therefore, it is feasible to analyze the timely distribution of these values.

[149] Kammeyer, K.-D.; Kühn, V.: MATLAB in der Nachrichtentechnik (2001).

Referencing the instantaneous values to the values calculated by the steady state approximation allows to calculate the slalom levels as described above. This might allow absolute ratings of the slalom performance.

4.4 Achievable Low Speed Boundary

The directional stability of a motorcycle decreases with vehicle speed. The rider must compensate for this loss to a certain degree, a coast down maneuver will show smaller oscillations for a longer time (i.e. towards lower velocities), if the rider is capable of perform correct, stabilizing actions. In state-of-the-art DMRS (i.e. H1/L0 condition), this can only be achieved by steering inputs. However, the H0/L1 condition should also be capable to compensate for the loss of stability at lower velocities. Figure 4.3 exemplarily shows the expected behavior of the simulator with and without using DLRC. At a certain time t_0, the vehicle's velocity will reduce below a critical value, where the capsize mode becomes unstable. As the rider tries to stabilize the vehicle, he is forced to use increasing control inputs and will be subject to increasing vehicle oscillations. This is especially true if the rider only uses their leaning motion but no steering input. At a time t_{lim} the rider will abort the maneuver to prevent falling or come to a halt eventually.
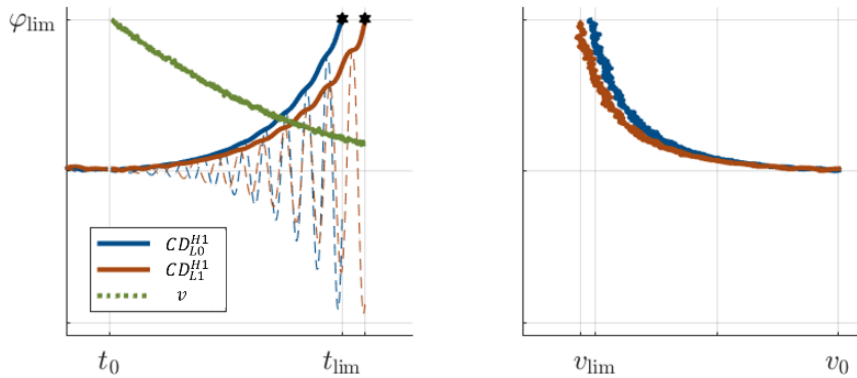
Figure 4.3: Hypothetical increase of roll angle during coast down resulting in a limit velocity.

The instantaneous amplitude (thick lines in Figure 4.3) of the oscillating value (dashed lines) is the analytic representation of the signal and can be determined via a Hilbert transformation as described previously. As it is impractical to achieve the exact same initial velocity and deceleration in every repetition of the given maneuver, the time t_{lim} is not feasible for performance evaluation. Instead, the oscillations are rated against the instantaneous velocity as shown on the right side of Figure 4.3. Both v_{lim} or the integral $\int \hat{\varphi}(v) \, \mathrm{d}v$ may suit as characteristic value to assess the system's performance.

4.5 Mental Model Accordance

Obviously, humans are quick learners and can adapt easily to using new systems. Therefore, a good performance in a simulator experiment might not result from a good system, but from a good performer, who has learned to work well with a possibly faulty system. A well-trained simulator rider might be able to compensate for model errors and might be used to some perception errors and therefore produce rather well test results, when challenged to perform a certain riding task. Thus, the rider's performance in any maneuver or test might not be relatable (solely) to the simulator's fidelity. The *mental model accordance* introduced here shall therefore describe the quality of a simulator to intuitively provoke a rider to behave most naturally when getting in contact with the simulator – just as if riding a real motorcycle.

- ▪ **Mental Model Accordance**
  The quality of a simulator to be recognized as a known, real system and to provoke riders to utilize realistic behavioral patterns common for this known system.

If the implementation of DLRC allows the simulator to behave more like an instable vehicle that can be manipulated by rider motion, this might not necessarily improve the dynamic behavior of the virtual vehicle. But the participant might be more willing to "accept" that they is riding a "real" motorcycle. It is known from own observations and discussions in the motorcycle simulator community that study participants often tend to utilize positive steering (i.e. turning the handlebar far to the right when planning to ride a curve to the right) before being trained on the simulator. Only after an (individual) training duration, the rider will then start behaving "naturally" and utilize counter-steering.

Investigating the mental model accordance that a simulator provides, therefore necessitates to perform studies with participants that encounter the simulator for their very first time and did not get the chance to familiarize with controlling the system in advance. Only then, it is possible to investigate if and how the rider is using the simulator "as a motorcycle" rather than using some computerized tool that might – or might not – behave somewhat alike a motorcycle. A high mental model accordance can only be claimed, when the least amount of training is necessary for the study participant, and they will rapidly accept the simulator as a motorcycle and ride in a natural manner, utilizing natural control actions.

In addition to the immediacy of successful riding, the perceived sickness symptoms can point towards better or worse mental model accordance. However, the evaluation of sickness symptoms cannot be attributed to the simulator fidelity directly. Sickness symptoms could for example result from even small perception errors in an elsewise well performing environment but might as well result from vastly wrong simulation cues. The evaluation of sickness symptoms is possible using e.g. the standardized simulator sickness questionnaire[150].

---

[150] Kennedy, R. S. et al.: Simulator Sickness Questionnaire (1993).

As stated above, a rider's performance in a riding task will quickly increase due to training effects on the simulator. From there on, an investigation of the riding performance will inevitably answer the question "How good is the rider performing on the simulator". In order to prevent study participants from "riding a simulator" and force them to "riding a motorcycle" instead, a study has to be conducted that does not utilize any kind of training on the simulator that allows the participant to train the correct control of the simulator. By such, the rider may only rely on their skills and capabilities of riding a real motorcycle and use only behavioral patterns known from motorcycling rather than patterns learned during a training session on the simulator. Therefore, when a study participant enters a virtual scenario and is experiencing the simulator for the first time, a better riding performance (i.e. stabilization during straight running, lane departures at cornering) should be attributable to higher mental model accordance. Furthermore, an increased difficulty in scenario design (i.e. lower velocities, higher curvatures) should lead to higher failure rates, when only little mental model accordance can be achieved.

To the author's knowledge, there exists no published study, where naïve participants and their performance on the simulator were the subject of the research. And it shall be mentioned again, that this is just as well not recommendable for typical simulator studies, where training effects can cause vast errors in the data evaluation. Anyhow, this is the only way to test for the mental model accordance and user's accessibility of the simulator.

4.6 Selected Performance Measures

In the previous sections, several qualitative and quantitative measures have been discussed that allow to rate the performance in various test categories and how the implementation of DLRC might affect these ratings. Foremost, it was shown, that the implementation of a DLRC should allow to reach vehicle states and system responses that are not possible to reach by purely using the state-of-the-art H1/L0 condition. It is arguable that the rider on a simulator might not necessarily need to reach all these states (i.e. there is probably no need to ride straight with a non-zero roll angle in a study). Nevertheless, every gained mode of control and every newly available riding state must be rated positively, as they benefit the control and sensory modes that contribute to the sense of presence, as described in section 2.4.2. For each of the abovementioned test categories, the selected performance measures are listed in Table 4.2:

Table 4.2: Performance Measures to Rate DLRC Capabilities

Cat.	Scn.	Variation	Evaluation	Meas.	Rating
Stationary	Straight	v	Rideability	-	y/n
			Stability	$\dot{\varphi}_{\mathrm{mcy}}, y_{\mathrm{mcy}}, \ldots$	CDF
			Controls	$\hat{T}_{\mathrm{hb}}, \hat{T}_{\mathrm{rid}}, \ldots$	Power Spectrum
	Curve	v, κ	Rideability	-	y/n
			Stability	$\dot{\varphi}_{\mathrm{mcy}}, \hat{y}_{\mathrm{mcy}}, \ldots$	CDF
			Stability	$\hat{T}_{\mathrm{hb}}, \hat{\dot{\varphi}}_{\mathrm{mcy}}, \ldots$	Power Spectrum
Transient	Straight	$v, \varphi_{\mathrm{rid}}$	Rideability	-	y/n
	Curve (const. trajectory)	$v, \varphi_{\mathrm{rid}}$	Rideability	-	y/n
			Controls	$_{\varphi}\Gamma_{\dot{\psi}}, \ _{\delta}\Gamma_{\dot{\psi}}$	Errorbar
	Curve	v, κ	Rideability	-	y/n
			Precision	$\Delta y, \Delta \psi$, boundary crossings	Errorbar
Dynamic	Lane Change	$v,$ $d_{\mathrm{lon}}, d_{\mathrm{lat}},$ direction	Rideability	-	y/n
			Precision	$tanh$-fitting	Scattering
			Delays	$x(\delta_{\mathrm{max}}, T_{\delta,\mathrm{max}}, \varphi_{\mathrm{max}})$	Errorbar
	Slalom	v, d_{cone}	Rideability	-	y/n
			Precision	Slalom Gains	Errorbar

Cat.	Scn.	Variation	Evaluation	Meas.	Rating
Low-speed Boundary	Coast Down	-	Stability	$v, \varphi_{mcy}, y_{mcy}, \ldots$	Envelope
Mental Model Accordance	Naïve Rider Study	v, κ	Accessibility	See above	See above

With the performance measures and scenarios defined, the next chapter will discuss a study design that allows to collect the relevant data from both professional, trained rider's as well as untrained study participants.

5 Study Design

In the previous chapter, performance measures and test scenarios have been defined that allow to investigate and rate the newly developed DLRC. This chapter describes the virtual tracks and environments, where these investigations can be performed.

5.1 Expert Study

To show the effects that DLRC can have on the dynamics of the virtual motorcycle and simulator, an expert study is conducted, as this allows to deliberately test for specific effects and details in a reproducible way. In this study, the stationary, transient and dynamic effects are tested. To address the mental model accordance and accessibility of the simulator however, a naïve rider panel is needed.

5.1.1 Participant Panel

The experts riding the simulator to collect the data in this part of the study are personnel of the WIVW GmbH that have extensive background knowledge on motorcycle dynamics, rider behavior and simulators and are all active motorcyclists (see Table 5.1). From the list of performance measures in section 4.6, all categories but the mental model accordance can be tested by these experts.

Table 5.1: Participants of the expert study

Expert	**#1**	**#2**	**#3**
Age	32	32	34
Mileage (km/a)	5000	15000	9000

All of the experiments described below can easily be performed by these riders. It is inevitable that they are familiar with the overall setup of the simulator. And – even if not told – they can easily test, which configuration (DLRC on / off) is currently active. Therefore, it is not necessary to withhold them any information about the tested configuration. This is obviously not ideal in terms of generating unbiased results. However, it is at the same time not feasible to build up a highly trained pool of study participants for two separate simulator configurations, without letting them know further details about the technical specifications.

Furthermore, it is assumed, that a participant who is trained on and used to a certain simulator configuration (or motorcycle for that matter) will perform differently, when they is presented with another configuration (or motorcycle) without knowing. Thus, it is only feasible to use riders who are familiar with both configurations and are equally capable of controlling them through various maneuvers to generate the data needed for their black and white comparison.

5.1.2 Stationary and Transient Maneuvers

Two virtual tracks have been implemented as depicted in Figure 5.1.A long straight track used e.g. for the stability analyses in constant straight running as well as the coast down maneuvers. Cones are placed to visually reduce the width of the track and constrain the rider's line choice (left picture) A track of 180° turns in alternating directions with decreasing radii, connected by straights. Signs are placed at the beginning of each corner to indicate e.g. a target speed or a desired rider lean direction. (right picture)
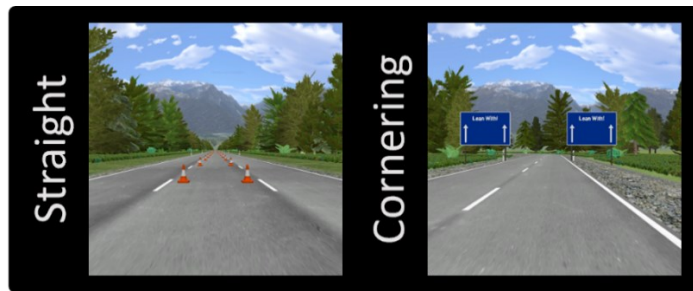
Figure 5.1: SILAB test scenarios for stationary (left) and transient maneuvers (right).

The maps of the two tracks are sketched in Figure 5.2. They consist of multiple intercon-nected segments with individual parameter sets (i.e. changing cone distances, or track radii). All these segments can be chosen as a starting point, when entering the simulation.
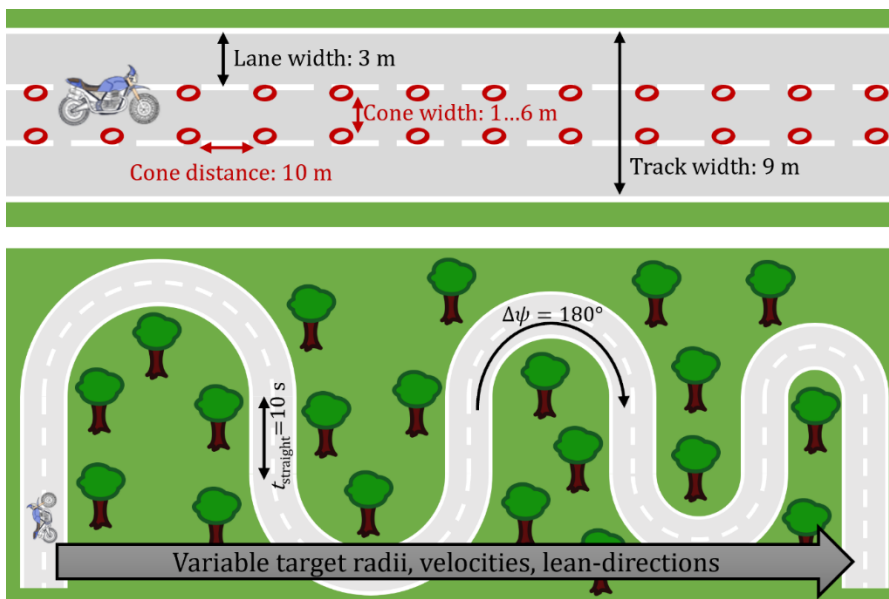
Figure 5.2: Schematic maps of the straight and cornering test tracks. Multiple segments (e.g. straight – curve – straight) are sequentially parameterized (e.g. radius, cone width) and connected.

No traffic environment is simulated in these scenarios. Signs are used to define the stand-ardized maneuver of interest, for example indicating a target speed or leaning instructions. All tracks use autogenerated rural landscapes with trees, bushes and hills blocking the view to the otherwise flat, open area surrounding the tracks. The friction coefficient is constant both on the road as well as offroad. Therefore, a study participant must not fear sliding and skidding, when accidentally exiting the paved road.

A cruise control is set when entering each segment to ensure standardized and constant speeds throughout repetitive testing by the participant panel in the stationary and transient tests. The center track radii of the cornering segments have been chosen such that a certain theoretical roll angle must be applied at a given target velocity according to equation (5.1):

$$R_{\text{track}} = {v_{\text{set}}^2}\Big/{g \cdot \tan \varphi_{\text{th,target}}} \tag{5.1}$$

For the TC_{L1}^{H0} scenarios (riding without hands) a target roll angle of 10° (left corners) and 15° (right corners) is heuristically chosen, as these values resemble normal riding conditions (i.e. no dynamically engaged riding). Set velocities of 100 km/h, 90 km/h, 80 km/h, 70 km/h, 60 km/h and 50 km/h, are chosen, as they relate to typical speeds on rural roads. This results in a total of 12 curves with track radii between 446 m and 73 m. As the rider uses the outer or inner lane in either left or right corners, a deviation $\Delta\varphi_{\text{th,lane}}$ to the target value occurs, that is however below 0.3° for the given scenarios. The sequence of curves is listed in Table 5.2. The alternating curve directions are chosen as the track may not cross itself.

Table 5.2: Cornering sequence for the TC_{L1}^{H0} condition

#	1	2	3	4	5	6	7	8	9	10	11	12
v_{set} in km/h	100	100	90	90	80	80	70	70	60	60	50	50
φ_{target} in °	10	15	10	15	10	15	10	15	10	15	10	15
direction	l	r	l	r	l	r	l	r	l	r	l	r

For the $TC_{L0/1}^{H1}$ scenarios, the set velocity of the cruise control was alternating between 110 km/h and 50 km/h in steps of 20 km/h. Target roll angles between 20° and 35° in steps of 5° were permutated through all curves, as were the instructions to the rider to either use lean-in, lean-with, or lean-out[151]. The sequence of curves is depicted in Table 5.3.

Table 5.3. Cornering sequence for the $TC_{L0/1}^{H1}$ conditions. I/W/O = Lean-In / Lean-With / Lean-Out

$\varphi\backslash v$	110 km/h	90 km/h	70 km/h	50 km/h
20°	I/W/O (right)	W/O/I (left)	O/I/W (right)	I/W/O (left)
25°	W/O/I (left)	I/W/O (right)	O/I/W (left)	W/O/I (right)
30°	O/I/W (right)	I/W/O (left)	W/O/I (right)	O/I/W (left)
35°	I/W/O (left)	O/I/W (right)	W/O/I (left)	I/W/O (right)

---

[151] Lean-in, or "hanging off" describes a rider motion towards the inside of the cuve. Lean-with describes the rider being placed in the middle plane of the motorcycle. During lean-out the upper body remains in a rather vertical position, while the motorcycle builds up a roll angle.

As before, the sequence of curve directions must alternate to allow for a consistent course map. To keep the straights in between the curves reasonably short and reduce acceleration or deceleration distances, the velocity is varied stepwise (i.e. no immediate changes from 110 km/h to 50 km/h). Signs indicate the target leaning motion.

5.1.3 Dynamic Maneuvers

According to section 4.3, two dynamic maneuvers have been selected for testing. The lane change and the slalom maneuver. In both cases, a number of configurations is tested in series, i.e. there are no interruptions through curved segments, restarting the simulator, etc.

5.1.3.1 Lane-Change Maneuver

The lane change track consisting of a three-lane straight road with cones indicating the permitted, respectively prohibited sections of the road. The map of the scenario is depicted in Figure 5.3, with the lower screenshots showing the sequence of events within the SILAB environments. The map is copied and appended ten times using the same parametrization. After ten repetitions, a change in parameters (i.e. target velocity and transition distance) is performed. The vehicle speed is controlled by the rider in the $DL_{L0/1}^{H1}$ conditions, while a cruise control must be active in the DL_{L1}^{H0} condition.
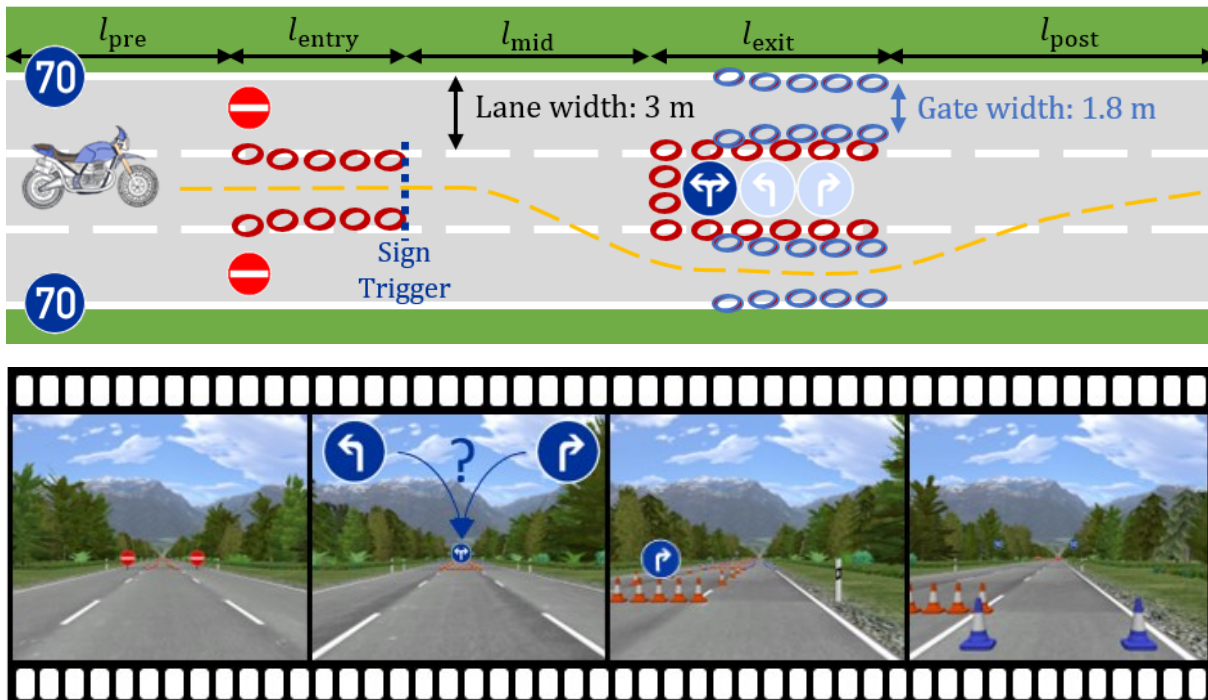
Figure 5.3: Design of the lane-change / avoidance maneuver

The rider starts running straight on the middle lane of the three-lane track. The "pre-" and "post-"section's lengths depend on the parameterized velocity and are chosen such that a rider can relaxedly return to the middle lane after each repetition of the maneuver. The rider

enters the relevant area of the experiment through a 1.8 m wide corridor of cones, that is used to constrain the rider to a well centered position on the track (leftmost picture).

While passing the corridor, the riders will already see the section with the blocked middle lane. A traffic sign that is initially pointing to both neighboring lanes will change to randomly showing only one direction once that the rider reaches the end of the corridor, entering the "mid-"section of the track. The length of this segment l_{mid} is chosen such that the rider has approximately 2.5 s to react and change the lane at the indicated target speed. In the "exit-"section, the lane width is again constrained by a corridor of cones. This urges the rider to come to a straight riding state at a defined lateral offset, instead of "corner cutting" through the outside lane, entering the "post-"section.

Table 5.4 lists the parameters used in this study. The entry and exit lengths have been kept constant for all parametrizations at 50 m, respectively 75 m. The post and pre lengths allow for 7 seconds to return from the outside to the middle lane. In order to allow riding without hands in the DL_{L1}^{H0} condition, the identical lane-change tracks for 110 km/h and 70 km/h in the $DL_{L0/1}^{H1}$ condition are used, but with 80 km/h respectively 70 km/h. This results in a maximum duration of 3.6 s to reach the lateral offset of 3.0 m

Table 5.4: Parametrization of the lane-change track for various velocities and DLRC configurations

$DL_{L0/1}^{H1}$	DL_{L1}^{H0}	l_{pre}	l_{entry}	l_{mid}	Δy_{mid}	$\Delta t\,(DL_{L0/1}^{H1})$	$\Delta t(DL_{L1}^{H0})$	l_{exit}	l_{post}
km/h		m	m	m	m	s	s	m	m
110	80	150	50	80	3	2.6	3.6	75	60
90	X	125	50	65	3	2.6	X	75	50
70	50	100	50	50	3	2.6	3.6	75	40
50	X	70	50	35	3	2.5	X	75	30
30	X	42	50	20	3	2.4	X	75	17

5.1.3.2 Slalom Maneuver

The slalom maneuver is realized on a two-lane road. The cones are parametrically placed to allow for different slalom frequencies. The cones are placed such that they mandate a specific direction. This helps to unify the gathered data by preventing 180° phase shifts between different riders or repetitions. A screenshot of the virtual test track and a map of the

maneuver are depicted in Figure 5.4. In accordance with e.g. the publications of Cossalter[152], the cone distances are increasing from 14 m in multiples of 7 m.
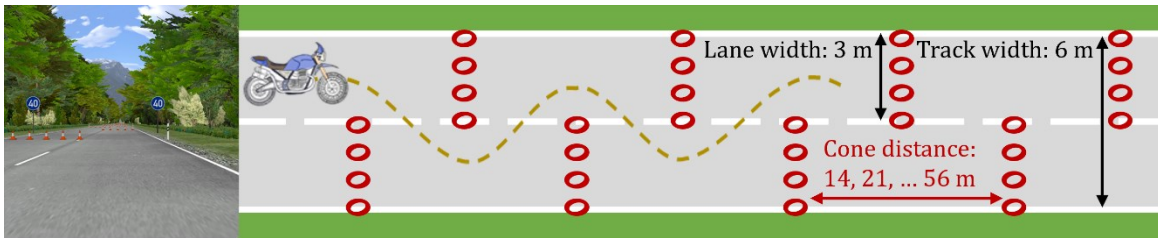
Figure 5.4: Screenshot from the virtual slalom test track (left) and sketch of the scenario map with mandatory phase indicated by cones (right). Two lane track, 20 cones (i.e. 10 full wavelengths).

Table 5.5 highlights the configurations that have been selected for testing such that at least two slaloms were performed per velocity and such that the slalom frequency was varied in three groups at approximately 0.25 Hz, 0.4 Hz and 0.8 Hz as these reach from rather simple to rather demanding, yet controllable values (see section 2.2.3). The slalom amplitude is not constrained by means of track design but can be chosen freely by the rider.

Table 5.5: Slalom frequencies for different velocities and cone distances

Hz	56 m	49 m	42 m	35 m	28 m	21 m	14 m
100 km/h	0.25	0.28	0.33	0.40	0.50	0.66	0.99
80 km/h	0.20	0.23	0.26	0.32	0.40	0.53	0.79
60 km/h	0.15	0.17	0.20	0.24	0.30	0.40	0.60
40 km/h	0.10	0.11	0.13	0.16	0.20	0.26	0.40

5.1.4 Low Speed Boundary

The final expert study according to chapter 4, is to determine the achievable low speed boundary. This performance is only tested in straight running and can simply be performed on the standard straight track depicted at the top of Figure 5.2. While this track is used with a cruise control in the previous experiments, a coast down maneuver is performed here. Therefore, the rider will put the gearbox into neutral after the simulation start with a velocity of 120 km/h and try to keep the motorcycle stable as long as possible. As visual reference, cones are placed along the full length of the track in a width of 2 m.

---

[152] Cossalter, V.; Doria, A.: Analysis of Motorcycle Slalom Manoeuvres Using the Mozzi Axis Concept (2004).

5.2 Naïve Rider Study

The fourth hypotheses H_{Wc} presented in section 1.2 aims towards the accessibility of the simulator for normal motorcyclists. If the simulator equipped with DLRC is capable of increasing the riders' mental model accordance with real motorcycling, it should become visible in better performing naïve riders, as described in section 4.5.

5.2.1 Participant Panel

$N = 6$ riders participated in the naïve rider study. None of the participants had ever before been riding a dynamic motorcycle simulator. Two of the participants had to abort the study after the first three, respectively the first ten levels due to emerging sickness symptoms. The riders are characterized in Table 5.6. The panel size characterizes a pilot study, investigating the above-mentioned hypotheses on easy access or intuitive operation. At this stage, it is not yet meant to suffice for inferential statistics evaluations. Therefore, the results presented in this thesis will focus on descriptive statistics and observations during the study.

Table 5.6:Characterization of the study participants of the naïve rider study

Rider	**#1**	**#2**	**#3**	**#4**	**#5**	**#6**
Type	Novice	Veteran	Daily rider	Daily rider	Expert	Commuter
DLRC	On	Off	On	On	On	Off
Age	32	47	45	36	26	34
Self assessed skill (1-15)	7	11	10	10	11	8
Mileage (km/a)	500	1000	15000	21000	6000	2000

5.2.2 Procedure

The study participants were welcomed and received and signed an informed consent at the beginning of the study. All participants are provided with the same superficial technical information on the simulator and vehicle model. (e.g. simulated motorcycle type and the standard control inputs: throttle, brakes, clutch, gears). The participants are reminded of the "counter-steering" effect to prevent them from experiencing instant failure when firstly turning the handlebar on their own, possibly expecting a computer game rather than a real motorcycle. The participants are then introduced to questionnaires and scales that become relevant during testing (see 5.2.4). Apart from questionnaires before and after the experiment, the riders are supposed to answer three questions repeatedly during riding, to evaluate the subjectively perceived rideability, realism and workload during the various scenarios.

For the familiarization of the participants of the simulator, a new process is suggested here to enable the naïve rider study: To get new participants accustomed to the simulator (e.g. visual presentation, platform motion, mounting the vehicle, etc.) without already enabling them to learn the peculiarities of the vehicle controls, they ride as a passenger on that simulator in an automated scenario. The simulator rider (or in this case: passenger) is confronted with scenarios that they will perform later on their own. This is presumed to decrease the participant's nervosity and curiosity which is natural for most people when getting in contact with a high-fidelity simulator for the first time. It also allows study participants to get used to the projection system, sound simulation and overall experience of sitting on a moving platform, experiencing mixed cues from virtual and real environment. In the special case of the DESMORI simulator, this procedure allows to measure the rider's body parameters that are needed for the evaluation of the rider induced roll torque anyway, as previously described in section 3.2. In addition to the identification via this automated ride, the β-parameters have been estimated using the lookup maps depicted in Figure 3.18.

Finally, the test scenario begins on a wide, straight road at an initial velocity of 120 km/h to guarantee the system's stability. The start of the scenario is initiated by the rider intentionally twisting the throttle grip, rather than forcing a start by the operator pushing a button.

5.2.3 Track Design

The track consists of an initial straight and wide curve as well as three main submodules "Open Ride" (OR), "Reference" (Ref) and "Slalom" (SL) that will be discussed in detail in the following subsections. The total duration of the experiment is aimed at 30 minutes, as experiences from different studies conducted with the DESMORI simulator show, that the level of concentration decreases after approximately that time

A total of 16 modules or – due to the increasing difficulty of the scenarios - "levels" is performed. This number results from the aimed study duration and the desired number of variations (velocity and curvature). The modules difficulty is parameterized by varying the target velocity (slower) and curvature (higher). The levels are combined into groups of four levels per velocity. The velocities have been chosen to be 100 km/h, 80km/h, 60 km/h and 40 km/h. This range covers velocities that provide proper self-stabilization of the motorcycle in a typical rural riding scenario, as well as slow velocities that are expected to put a high workload on the participants, especially considering that this would be their first contact with a DMRS. Within each group, the curvature of the scenarios is increased steadily. The virtual environment shows fields, forests and villages to provide the rider with a typical riding scenery. Only one slalom maneuver per speed is performed, to maintain a most natural rural riding experience without too many artificial maneuvers and to keep the overall study duration reasonably short. Table 5.7 shows the list of scenarios that are performed. Starting at 100 km/h, the track curvature is increased in consecutive maneuvers. After four levels and a slalom maneuver at one target velocity, the next lower target velocity is tested.

Table 5.7: List of scenarios in the naive rider study. The indexes of Openride (OR), Reference (Ref) and Slalom (SL) maneuvers indicate their "level".

km/h							*Increasing Curvature*			
100	OR_1	Ref_1	OR_2	Ref_2	OR_3	Ref_3	SL_1	Ref_4	Ref_4
80	OR_5	Ref_5	OR_6	Ref_6	OR_7	Ref_7	SL_2	OR_8	Ref_8
60	OR_9	Ref_9	OR_{10}	Ref_{10}	OR_{11}	Ref_{11}	SL_3	OR_{12}	Ref_{12}
40	OR_{13}	Ref_{13}	OR_{14}	Ref_{14}	OR_{15}	Ref_{15}	OR_{16}	Ref_{16}	SL_4

5.2.3.1 Initial Straight and Bend

After actively twisting the throttle grip of the simulator for the first time, the rider is provided with a 1.5 km long, straight two-lane road with a lane width of 6 m and no other traffic participants. At this velocity, there is plenty time for the rider to make first small steering actuations and experience the sensitivity of the steering. If the rider tends to use too little throttle, they is advised to accelerate to maintain at stable, easily controllable speed for the beginning. During the first 1.5 km the rider is allowed to familiarize with the simulator controls, steering, throttle, brakes, etc. and must not mandatorily stay on the correct side of the road (or even on the road at all). After this first contact, the rider is instructed to stay within the limits set by the road markings and signage and to ride calmly (i.e. not riding slalom on straights or testing the acceleration behavior etc.). The long straight is followed by a soft bend with a curvature of $\kappa = 1.1e^{-3}$ m and an arclength of 800 m this results in about 30 seconds of riding with 5° of roll angle at around 100 km/h. Provided the track width of 6 m per lane, this gives a lot of room for corrections and adjustments and is far off any troubling experience – at least compared to real life riding.

5.2.3.2 Open Ride Scenario

An open ride scenario serves as a filler track that is not directly relevant for the data evaluation. Instead, it is used to relax the rider and provide them with a normal motorcycle riding scenario on the simulator. It is also used to ask the rider about the three abovementioned ratings for rideability, workload and realism. A duration of 45 seconds at speeds of either 100 km/h or 80 km/h proved feasible for that purpose. During that, the rider is provided with a rural road consisting of a sequence of curves. The track layout is generated randomly during the design phase of the track according to the following process:

- The design velocity v_{design}, track width w_{design}, track duration t_{track}, maximum target roll angle $\hat{\varphi}_{target}$ and maximum arc angle per bend $\Delta\psi_{max}$ are defined.
- The target velocity and track duration result in the total scenario length l_{total}.
- The target velocity and maximum target roll angle result in the maximum allowable curvature $\hat{\kappa}_{design}$.

- The maximum length of a bend l_{max} results from the target velocity and the maximum arc angle defined above.
- Random number generators are used to generate each bend's curvature and length:
  - $\kappa_i = rand(\pm\hat{\kappa}_{design})$
  - $l_i = rand(l_{max})$
- Multiple bends are attached to each other, until the total scenario length is reached.

Similarly, a slight height profile is generated for each open-ride scenario. This process results in rather organic rural roads that are constrained by defined limits and allows to vary the difficulty in a defined way from level to level. The chosen constraints are listed in Table 5.8 and the resulting track segments are depicted below in Figure 5.5.

Table 5.8: Constraints of the random generator of the open-ride scenarios. A total track duration of $t_{track} = 45$ s is chosen for all segments. The maximum arc angle per bend $\Delta\psi_{max}$ is chosen at 80°.

OR_i	1	2	3	4	5	6	7	8	9	10	11	12	13	14	15	16
v_{design}	100 km/h								80 km/h							
w_{design}	5.0 m				4.0 m				3.5 m				3.0 m			
$\hat{\varphi}_{target}$	10°		15°		20°		25°		15°		20°		25°		30°	
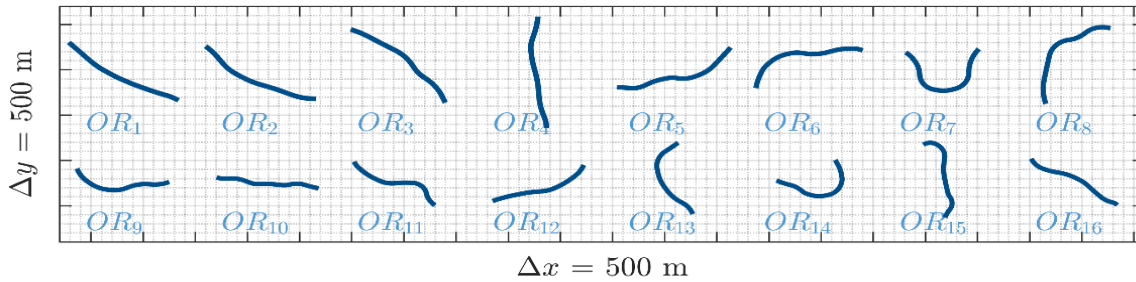
Figure 5.5: Maps of the 16 open ride scenarios with increasing difficulty.

5.2.3.3 Reference Scenario

The reference scenario contains the main experiments for the evaluation of the naïve rider's performance on the simulator. Namely, these are straight running, constant cornering and lane change maneuvers. All three experiments are subtly merged into the rural road environment to keep the rider's behavior as naturalistic as possible. The whole scene is depicted in Figure 5.6. Coming from an open ride scenario with suggested target velocity (leftmost image), the rider will approach a target vehicle (second image), that serves as a visual anchor to control the target velocity. Depending on the open-ride speed the rider chose, it is just as well possible, that the target vehicle is not reached before entering the reference scenario (middle image). The rider is however instructed to always obey the traffic signs that tell the allowed velocity.
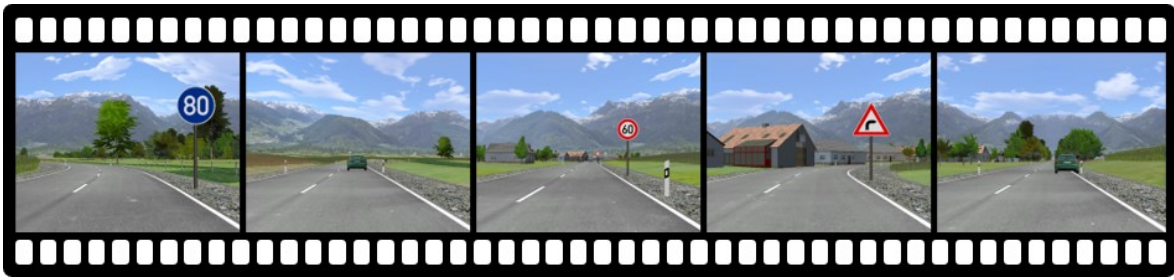
Figure 5.6: Scenes from the reference scenario. L.t.r.: Open-ride; reaching the target vehicle; entering the reference straight; approaching the reference curve; overtaking the target vehicle.

While following the target vehicle over the straight path for a duration of 10 seconds, there is opposing traffic preventing the study participant from overtaking the target vehicle. The continuous flow of opposing traffic ends exactly when the participant enters the curve of the reference maneuver (fourth image). This curve is always righthanded, as this typically reduces the rider's urge to overtake a leading vehicle. As there are no visual obstructions placed on the inside of the corner, it also allows a good sight throughout the whole curve. A variation of the curve direction is not called for, as it might unnecessarily generate additional variations: On the one hand, left or right bends might cause different corner cutting behavior. On the other hand, motorcyclists are often known to prefer one direction over the other.

Table 5.9: Reference curve parameters. Every row states the parameters of the four increasingly difficult curves per velocity. The target roll angle increases in steps of 5°.

v_{target}	w_{design}	φ_{target}	R_{design}	$\Delta\psi_{design}$	φ_{target}	R_{design}	$\Delta\psi_{design}$	φ_{target}	R_{design}	$\Delta\psi_{design}$	φ_{target}	R_{design}	$\Delta\psi_{design}$
km/h	m	°	m	°	°	m	°	°	m	°	°	m	°
100	5.0	10	446	18	15	294	27	20	216	37	25	169	47
80	4.0	10	285	22	15	188	34	20	138	46	25	108	59
60	3.5	15	106	45	20	78	61	25	61	78	30	49	97
40	3.0	15	47	68	20	35	92	25	27	119	30	22	146

The selected parameters for the reference curve are listed in Table 5.9. The curve's arc angle is chosen such that it takes 5 s at target velocity to ride through. The curves begin and end smoothly by using clothoids. Therefore, the constant cornering section is reduced to about 3 s of, depending on the amount of corner-cutting applied by the rider. Lastly, after exiting the curve, another straight follows, that takes 20 s at target velocity to ride through. The target vehicle will set the right indicator 5 s into the straight and – after two more seconds – start decelerating and swerve to the right. This is commonly understood by motorcyclists as the car driver indicating their willingness to be overtaken. The study participants are instructed to perform a "clean" overtaking maneuver, i.e. entering the opposing lane, riding straight and – after checking the own lane – returning back. At this point, the relevant

sections of the reference scenario are over and the study participant will answer the three abovementioned questions while entering the next open ride scenario. The maps of all reference scenarios are depicted to scale in Figure 5.7. They show the decreasing track lengths and increasing curvature per each of the 16 levels.
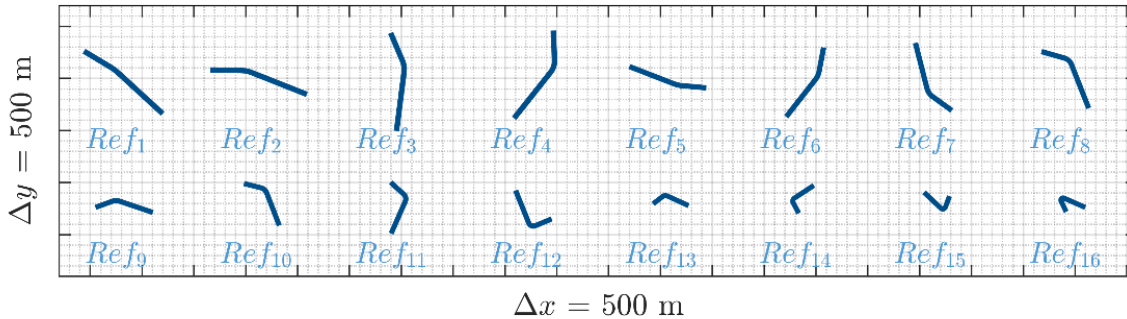
Figure 5.7: Maps of all reference scenarios with increasing difficulty by means of decreasing velocity and increasing curvatures

5.2.3.4 Slalom Maneuver

The slalom maneuver presented to the study participants is designed equally as discussed in section 5.1.3.2. The cruise control is automatically activated when entering the track segment to allow for a better comparability among different study participants. The cone distances and resulting slalom frequencies per velocity are listed in Table 5.10. Only low slalom frequencies have been implemented to reduce the difficulty of the maneuver to a reasonable level for the naïve riders.

Table 5.10: List of the selected slalom velocities and cone distances and resulting slalom frequencies

	S1	**S2**	**S3**	**S4**
v in km/h	100	80	60	40
d_{cone} in m	56	42	28	14
f_{slalom} in Hz	0.25	0.26	0.3	0.4

5.2.4 Questionnaires

The participants of the naïve rider study are provided with a few questionnaires in order to evaluate their subjective ratings over the simulation quality. The questionnaires were formulated in German and the wording is – wherever relevant – added in parentheses. The questions have been developed with a focus on the rider's control modes and the simulator's realism. The scales have been selected in cooperation with human factors experts at the WIVW GmbH, where they have proven their usability in many other studies as well.

5.2.4.1 Simulator Sickness Questionnaire

While the simulator sickness rates on the DESMORI Simulator are well within the typical rates for any simulator study on any simulator, it can be somewhat overwhelming for the study participants to ride the simulator for a longer period of time without any previous experience on such a system. In order to monitor the sickness levels of the study participants, they answered the standardized Simulator Sickness Questionnaire[153] (SSQ) three times throughout the study. Firstly after arriving at the laboratory to generate a baseline. Secondly after the video ride and lastly after the main experiment. The SSQ asks for ratings on several bodily indicators (e.g. dizziness, sweating, headache, blurry view,…) on a four level scale (not | some | middle | strong). During the experiment they are regularly asked about their current feeling and – if the participant shows sickness symptoms or asks to stop – the experiment is aborted.

5.2.4.2 Initial Inquiry

The first questionnaire before the simulator ride is used to investigate the rider's riding style and experience with motorcycles. There exists no standardized questionnaire for this purpose and the questions formulated here have been developed by the author under consultation of human factors experts at WIVW. Aside from questions regarding e.g. their yearly mileage and private vehicles, the participants shall describe how they typically control their motorcycle. Therefore, they answer, how much they utilize the following three control strategies:

I control my motorcycle by steering

Not at all (*gar nicht*)			A little (*wenig*)			Balanced (*ausgewogen*)	A lot (*viel*)			Only (*ausschließlich*)		
-6	-5	-4	-3	-2	-1	0	1	2	3	4	5	6

I control my motorcycle by leaning

Not at all			A little			Balanced	A lot			Only		
-6	-5	-4	-3	-2	-1	0	1	2	3	4	5	6

I control my motorcycle by pressure on the foot pegs

Not at all			A little			Balanced	A lot			Only		
-6	-5	-4	-3	-2	-1	0	1	2	3	4	5	6

---

[153] Kennedy, R. S. et al.: Simulator Sickness Questionnaire (1993).

5.2.4.3 Online Inquiry

As mentioned before, the riders answered three questions after each of the levels during riding to rate the simulator's performance in the previously ridden reference maneuver:

The participants should firstly state the most appropriate verbal anchor and specify their impression by naming a number indicating the more detailed tendency. The first question asked for the rideability of the simulated motorcycle. While any rider might understand different meanings to "rideability", the verbal anchors provide a more specific sense to every rider, such that they can answer accordingly.

How do you rate the rideability (*Fahrbarkeit*) of the simulated motorcycle?

very ponderous (*sehr schwerfällig*)			inert (*träge*)			just right (*genau richtig*)	nervous (*nervös*)			very instable (*sehr instabil*)		
-6	-5	-4	-3	-2	-1	0	1	2	3	4	5	6

The second question aimed towards the rider's effort to maneuver the motorcycle. As discussed by Hammer[154], the effort to ride a simulated vehicle must not correlate with the perceived realism but is a relevant marker to address the ease of access of the simulator.

How much effort did the previous section demand from you (*wie sehr […] beansprucht*)

none	very little			a little			middle			a lot			very much		
0	1	2	3	4	5	6	7	8	9	10	11	12	13	14	15

The last question asked about the perceived realism. This question is somewhat independent to the previous questions, as a motorcycle might be very ponderous to ride and needing a lot of effort to maneuver around a tight curve, yet be perceived as a real(ly large and heavy) vehicle in a realistic environment (compared to a very light and sportive personal motorcycle).

How realistic was the simulator's riding behavior (*[…] hat sich das Fahrverhalten angefühlt*)

not at all	very unrealistic			unrealistic			middle			realistic			very realistic		
0	1	2	3	4	5	6	7	8	9	10	11	12	13	14	15

All three questions were asked in the same order in every repetition to allow for a quick and repeatable answering process with as little distraction as possible. The relevant scales were printed out and placed on the left rear-view mirror, such that the rider must not remember them by heart.

---

[154] Hammer, T. et al.: Anwendungsmöglichkeiten von Motorradsimulatoren (2021).

5.2.4.4 Final inquiry

After performing the experiment, the riders answered a final questionnaire that aimed towards an overall rating of the simulator and investigated whether the rider was able to experience the different control methods, i.e. steering and leaning.

At first, two questions were posed to get an overall rating of the simulation and the vehicle:

How do you rate the overall realism of the simulation? (*Realismus der Simulation insgesamt*)

not at all	very unrealistic		unrealistic			middle			realistic			very realistic		
0	1	2	3	4	5	6	7	8	9	10	11	12	13	14	15

How do you rate the overall rideability (*Fahrbarkeit*) of the virtual motorcycle?

very ponderous (*sehr schwerfällig*)			inert (*träge*)			just right (*genau richtig*)	nervous (*nervös*)		very instable (*sehr instabil*)		
-6	-5	-4	-3	-2	-1	0	1	2	3	4	5	6

This approach distinguishes between the simulation environment, including all possible visual, auditive, etc. cues and the vehicle behavior without considering e.g. the projection and sound quality. Additionally, the study participants were asked if they missed any specific cue that they know from real riding or if they can verbalize which vehicle characteristic was expected that could have potentially improved the given rating.

Lastly, the study participants were asked to provide four ratings that try to gain a deeper understanding of the riding behavior on the simulator, all of which are rated on the same 16-point verbal categorization scale:

How easy could you follow your desired path?

How easy could you affect your path by the use of steering inputs?

How easy could you affect your path by shifting your weight?

How easy was it for you to predict the vehicle behavior?

impossible	very difficult		difficult			middle			easy			very easy		
0	1	2	3	4	5	6	7	8	9	10	11	12	13	14	15

The first question provides additional information on choosing and achieving a certain path on a given road. The second and third question are especially interesting when e.g. a participant in the DLRC-on condition won't experience this possibility or – even more interesting – when a participant in the DLRC-off condition proclaims the applicability of weight shifting on the simulator. The last question provides additional information, as it not only targets successful riding but the rider's understanding or intuition of the provided system.

6 Results

This chapter shows and discusses the measurements and study results gathered in the expert studies as well as the naïve rider study. The stationary maneuvers are discussed at the beginning of this chapter, followed by the transient and dynamic maneuvers. Contrary to the previous chapters, the analysis of the low-speed boundary is included to the stationary maneuver section due to its close relation to the stationary straight maneuvers at different speeds.

6.1 DLRC Performance in Stationary Maneuvers

Following the discussions from 4.1 and 0, the DLRC's performance in stationary maneuvers is rated by analyzing the frequency distribution of lateral dynamic quantities as well as the power spectrum of the control quantities.

6.1.1 Stationary Straight Frequency Distributions

Firstly, the vehicle oscillations during straight running are analyzed. The three-lane straight road described in section 5.1.2 was used. According to section 4.1, different velocities are held constant over a duration of 30 s by means of a cruise control. During the experiment, the velocity decreases from 120 km/h to 20 km/h in steps of 10 km/h. That boundary results from the low-speed stabilization becoming active at about 16 km/h and 20 km/h still being controllable for well-trained riders of the simulator three of such participated in the test.

The plots in Figure 6.1 show the empirical cumulative distribution of the absolute values of the motorcycle CoG's lateral displacement w.r.t. the center line of the track. Each subplot represents the data collected at one velocity by the three riders (color coded) in the three conditions SS_{L0}^{H1} ("state of the art"), SS_{L1}^{H1} (DLRC active) and SS_{L1}^{H0} ("riding without hands"). In the SS_{L1}^{H0} condition, the steering torque was however not necessarily 0, but minor torques could appear due to inertial effects on the handlebar, as the steering angle feedback was active on the mockup. In the lower line of subplots, the abscissa was scaled to a tenth of the upper line of subplots to allow for a better readability.

The data shows, that – expectedly – the SS_{L1}^{H0} condition performs worst in this comparison. Throughout all velocities, the lateral displacement has the largest amounts compared to the other conditions, with growing magnitudes, as velocity decreases. At the lowest velocity of 20 km/h, only rider #2 is barely able to continue the ride but not within the road limits (dotted green line). A comparison of the two other two conditions shows only small differences throughout all velocities. All riders in both $SS_{L0/1}^{H1}$ conditions stay within the middle lane of the road at 30 km/h and above. In general, the lateral displacements in both $SS_{L0/1}^{H1}$ conditions are in the same order of magnitude.

Figure 6.1: Empirical cumulative distribution function of lateral displacement absolutes during straight running. Riders are color coded; the riding condition is coded by line style. Each line contains data from riding 30 s at constant speed that is set by a cruise control.
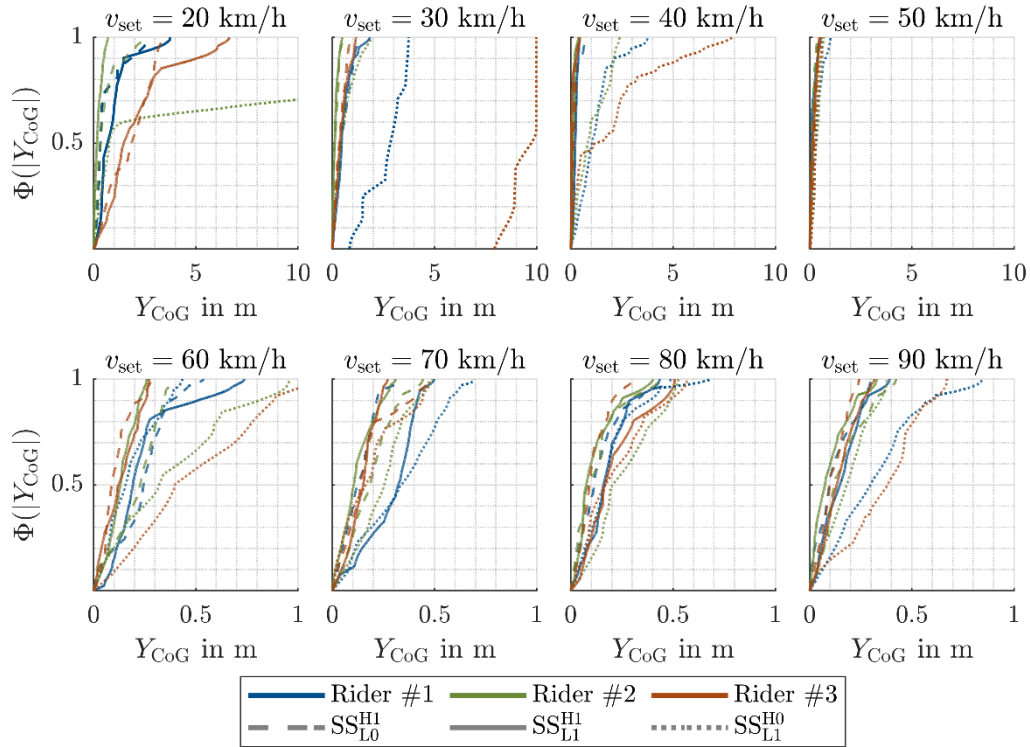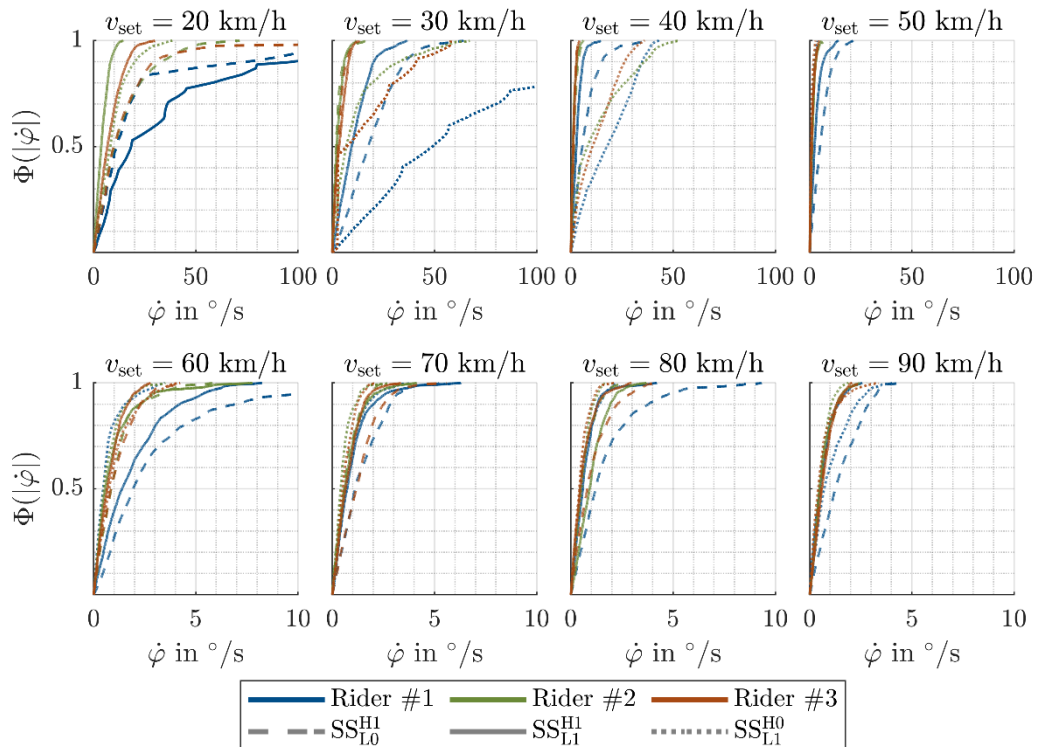

Figure 6.2: Empirical cumulative distribution function of the motorcycle roll rate absolutes during straight running. Riders are color coded; the riding condition is coded by line style. Each line contains data from riding 30 s at constant speed that is set by a cruise control.

At the lowest velocity, rider #2 succeeds in staying within one lane width (± 1.5 m) with activated DLRC. All other lines will eventually overcome this limit. Riders #2 and #3 show their highest lateral displacements at 20 km/h in the SS_{L1}^{H1} condition. However, this value cannot provide the full picture to rate the riding stability, as e.g. the rider might traverse away from the road in a straight and stable manner. For that purpose, the roll rate is a more feasible quantity and is therefore depicted in Figure 6.2. The line colors and styles are chosen as before, as is the change of magnitude in the scales of the lower subplots.

Starting at 120 km/h (not depicted here), the distributions in between the three conditions show little to no differences. However, between 80 km/h and 50 km/h it can be seen, that the SS_{L1}^{H0} condition even shows the lowest observed roll rates per rider. This indicates, that just by gripping the handlebars, a certain lateral excitation appears. The effect becomes stronger, as the rider's body tension increases. This behavior is in line with e.g. the investigations of Cheli[155], Doria[156] and Scherer[157] showing the coupled effect between the vehicle roll motion and steering inputs. On the simulator, roll excitations of the hexapod similarly induce rider body responses that are eventually transferred into the handlebar. As the multi cueing cannot provide (or substitute) centrifugal accelerations, the simulator rider's body tension will typically be greater than on a real motorcycle while the motion platform is tilted, as they has to actively counteract gravitational forces.

As the speed decreases further, from 40 km/h and below, the roll rates of the SS_{L1}^{H0} condition increase rapidly due to the vehicle immanent instability. As the motorcycle enters the capsize mode, it will start oscillating with large roll amplitudes and ultimately tip over, if no intervention by the rider happens. Real road experiments show this behavior at comparable speeds. Pleß[158] shows, that the test rider in that study must perform steering interventions at around 23 km/h to prevent the used motorcycle from capsizing. Until 30 km/h, all test riders on the simulator show equal or smaller roll rates in the SS_{L1}^{H1} condition than in the SS_{L0}^{H1} condition. This is also true at 20 km/h for two of the riders. Rider #1 however cannot maintain a stable ride and shows large amounts of roll rates in both $SS_{L0/1}^{H1}$ conditions – the largest with DLRC being activated (continuous blue line).

The same overall behavior is observable in other quantities, like the yaw rate or steering angle as well. Figure 6.3 shows the 95-percentiles of the motorcycle roll rate (top left plot), rear wheel lateral displacement (top right plot), yaw rate (levelled CoSy, bottom left plot) and steer angle (BRT, bottom right plot) in the same color and line style coding as before. It can clearly be seen how decreasing velocities result in increasing magnitudes. The lateral displacement becomes large in the SS_{L1}^{H0} condition throughout all velocities, as this only

---

[155] Federico Cheli et al.: Driver's movements influence on the lateral dynamic of a sport motorbike.

[156] Doria, A. et al.: The response of the rider's body to roll oscillations (2012).

[157] Scherer, F.: Master Thesis, Koppelkräfte auf Realfahrzeug und Motorradfahrsimulator (2018).

[158] Pleß, R. et al.: The Influence of Rider Motion on Motorcycles and Riding Simulators (2018).

allows for slow and less precise corrections of course angle disturbances. The shown angles and rates will stay small in this condition, at least while riding above the capsizing mode.
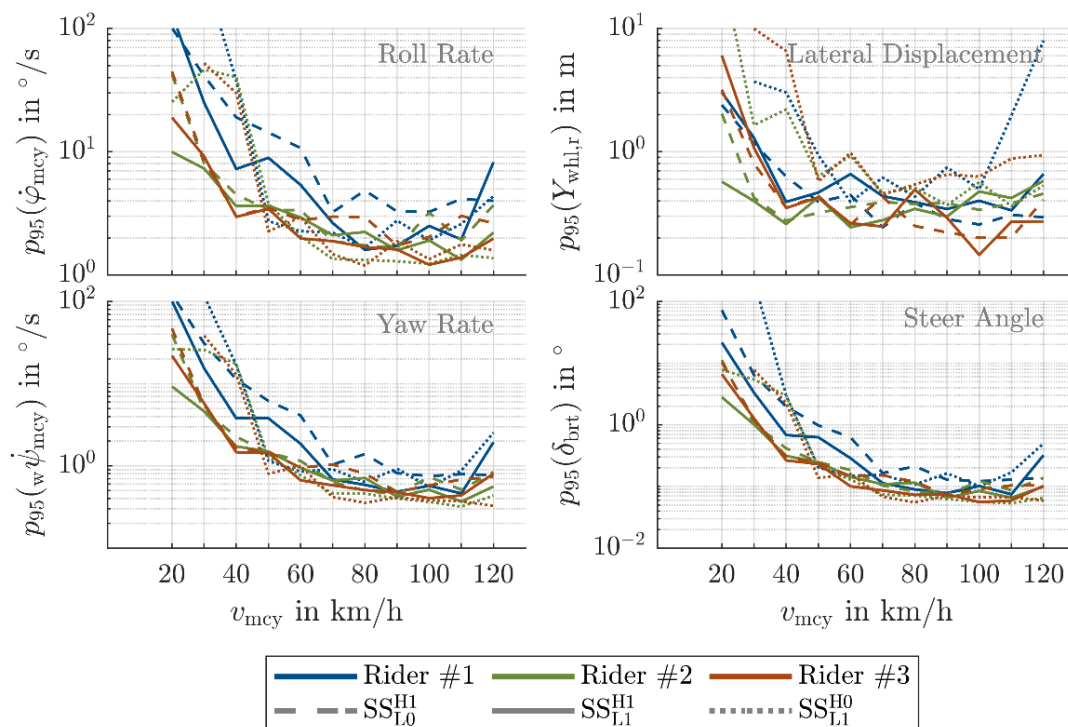
Figure 6.3: 95-percentiles of different lateral dynamic quantities. Riders are color coded; the riding condition is coded by line style. Each datapoint at every 10 km/h shows the 95-percentile of the quantity during 30 s of riding at constant speed. The lines have been drawn for better readability but don't represent measured data.

The data indicates that the use of DLRC can reduce the amplitudes of lateral dynamic quantities while the capsize mode is sufficiently dampened (typically at speeds above 30 km/h). At very low velocities however, the stabilization becomes a bigger challenge and only two of the three riders can benefit from the DLRC being active.

6.1.2 Stationary Straight Power Spectrums

In section 4.1.1 it was argued that the attachment of the (real) rider to the virtual motorcycle should become observable in the power spectrum of the simulated lateral dynamic quantities. The spectral power of the motorcycle roll rate is depicted by means of a 1/3-octave band spectrum in Figure 6.4. The lowest third's center frequency is chosen at 1/30 Hz such that it contains the 1st order wave over the full length of each straight segment at constant speed. Each subplot shows the data of one rider in one condition. The coloration indicates the velocity, starting with green lines at high speeds, ranging to red lines at low speeds. The lines are drawn for better readability, but do not indicate measured values. The grey lines in the SS_{L1}^{H0} condition indicate steering interventions from the rider to prevent the motorcycle from

falling. While the simulator is ridden without hands in that condition, the steer torque sensor maintains activated to allow a rider to intervene and regain control whenever necessary.

Figure 6.4: Power spectrum of the motorcycle roll rate. Levels are calculated with a reference rate of $\dot{\varphi}_{\mathrm{ref}} = 1$ rad/s. Velocities are represented by color (120 km/h green $\rightarrow$ 20 km/h red). Grey lines show data, where the rider gripped the handlebars during the $\mathrm{SS}_{\mathrm{L1}}^{\mathrm{H0}}$ condition to prevent a fall.
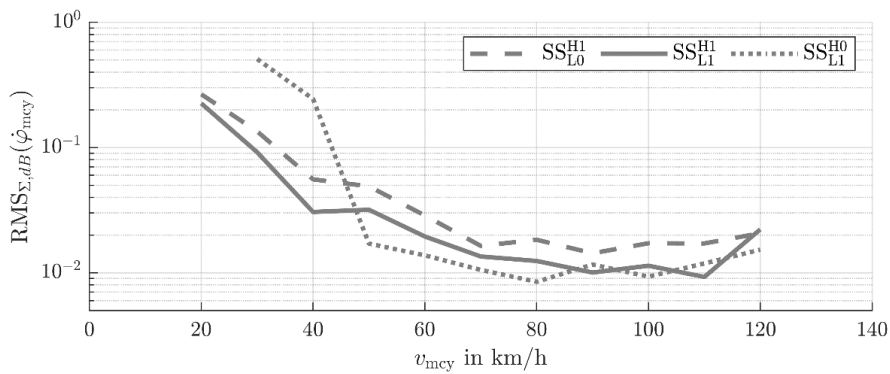
Figure 6.5: Sum RMS of the overall roll rate power spectrum (0.033 Hz - 6.77 Hz) averaged over three riders.

Figure 6.4 shows the power spectrums of the roll rate. As in the previously discussed frequency distributions the signal amplitudes increase with decreasing velocity (from green to red). This increase is most dominant in the frequency range between 0.2 Hz and 3 Hz. The signal power is in all conditions highest at frequencies between 0.4 Hz and 1 Hz and decreases both below and above that frequency range. Furthermore, it can be seen that the power spectrum in the SS_{L1}^{H1} condition overall shows slightly lower values compared to the SS_{L0}^{H1} condition and even less in the SS_{L1}^{H0} condition. This effect is however better observable in Figure 6.5. It shows the sum level over all 1/3-octave bands, averaged over the three riders. The system with activated DLRC shows smaller power levels throughout the whole velocity range. At high velocities, the SS_{L1}^{H0} condition shows the smallest overall power level. However, as the velocity approaches the capsize mode, the power level rapidly increases.
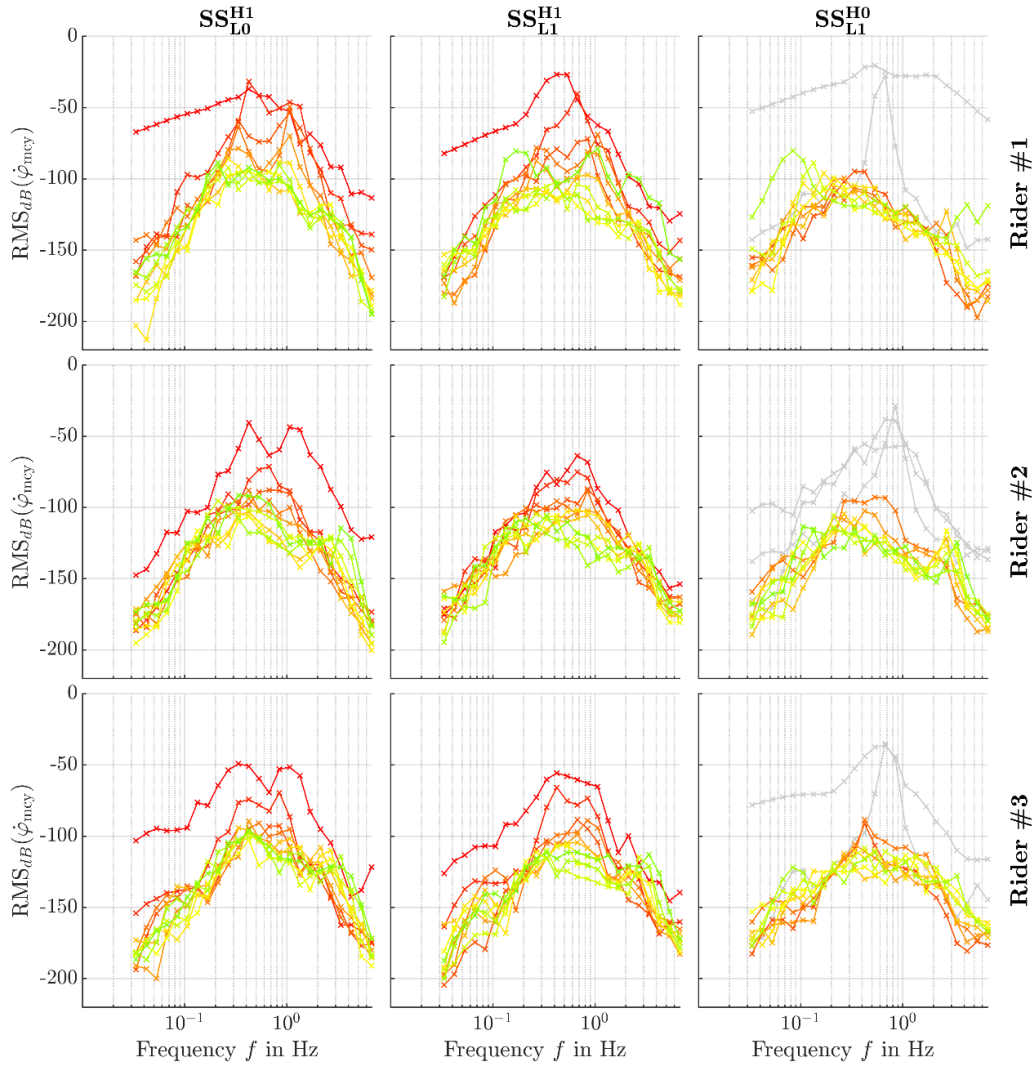

Figure 6.6: Power spectrum of the steer torque. Levels are calculated with a reference rate of $T_{ref} = 1$ Nm. Velocities are represented by color (120 km/h green → 20 km/h red). Grey lines show data, where the rider gripped the handlebars during the SS_{L1}^{H0} condition to prevent a fall.
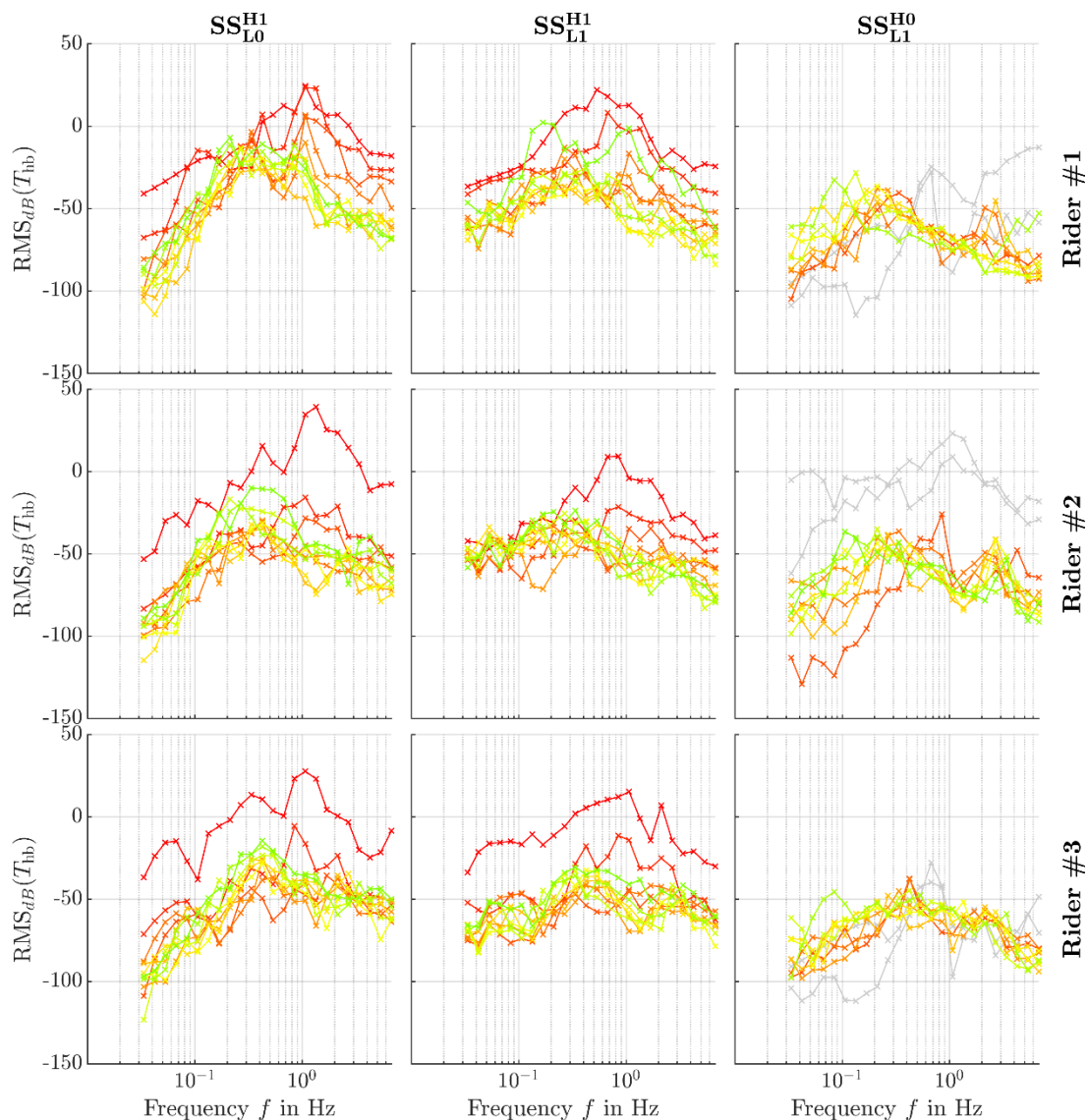
119

Figure 6.6 is layout similarly to Figure 6.4 but shows the steer torque. The rightmost column shows the SS_{L1}^{H0} condition. Therefore, the rider is not controlling the handlebars. As stated previously however, the torque sensor is not disconnected and inertial effects will cause minor steer torques that are seen here in the power spectrum.

Contrarily to the roll rate power spectrum, the hill-shape is less pronounced for the steer torque. In the SS_{L0}^{H1} condition, the signal power decreases towards the very low frequencies, indicating very small steady steer torque components. In the SS_{L1}^{H1} however, this effect less much smaller, so the power level maintains higher towards the low frequencies. One possible explanation for that behavior is, that in the SS_{L0}^{H1} condition, any directional disturbance can only result from steering inputs. Once that the motorcycle is in equilibrium while running straight, it would therefore be beneficial to minimize any steering input at all to maintain in that equilibrium. This is supported by the previously shown power spectrum of the roll rate, where riding without hands causes smaller roll rates at speeds above 40 km/h compared to the SS_{L0}^{H1} condition, where only steering inputs are effective. When activating DLRC, directional disturbances will however result not only from steering inputs, but simply from any rider motion on the mockup. The rider could therefore apply minor steer torques to e.g. balance a slight lateral offset of the rider CoG.

In the range between 0.3 Hz and 0.6 Hz, the SS_{L0}^{H1} condition shows a distinct rise in amplitudes compared to the SS_{L1}^{H1} condition. Especially at very low velocities (outstanding red lines), the torque amplitudes maintain lower in the DLRC-on condition as well. This manifests in an overall decreased subjective torque perception.

6.2 Low Speed Boundary

The results above indicate that the utilization of the leaning control loop in addition to the steering loop provides a small stabilizing effect during straight running at low speeds. This becomes observable e.g. in smaller roll rates (see Figure 6.5) as well as other lateral dynamic quantities (e.g. steer angle) that are however not depicted here.

To further investigate the achievable benefit in terms of low-speed range, a coast down maneuver is performed by the three expert riders. Figure 6.7 shows the roll angle of the virtual motorcycle over its velocity for four conditions: with/without controlling the handlebar and with/without enabled rider motion input. The three riders are color coded in each plot. The data is cut off when the roll angle hits 45° for the first time, as this is assumed to be a limit which if exceeded can already easily result in a fall in an equivalent real riding scenario.

It is clear, that without any control input in the CD_{L0}^{H0} condition (**C**oast **d**own, **h**ands **off**, **l**ean **off**), the motorcycle's trajectory is only subject to its system dynamics and internal disturbances. Due to slight differences at the beginning of the maneuver (starting the simulation and shifting into neutral) the three lines are not identical, but the envelopes of the curves are very similar.
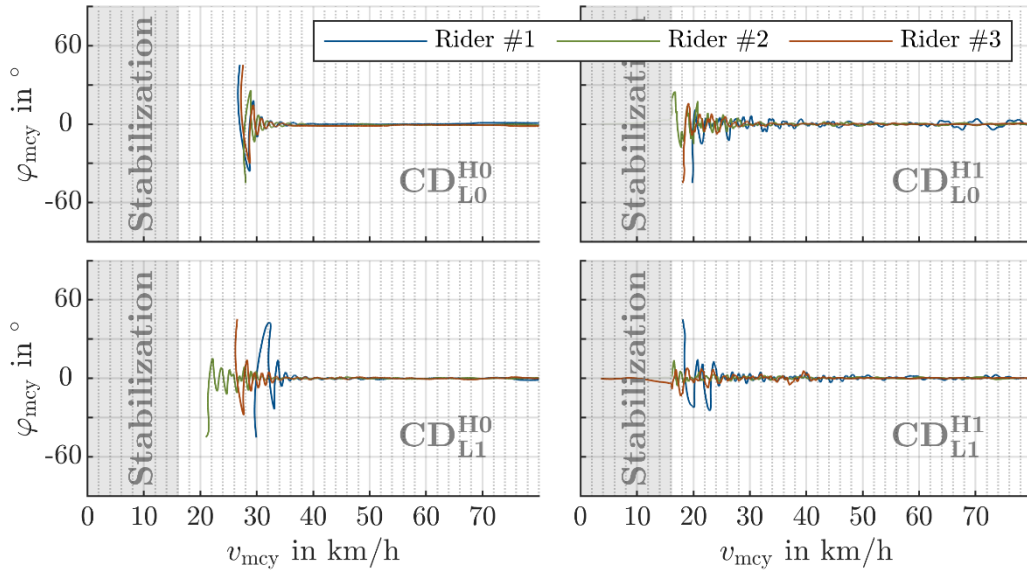
Figure 6.7: Coast down maneuver in four different conditions. Three riders are color coded. The grey area signalizes the velocity range, where BRT's artificial stabilization becomes active.

The trajectory in that condition is quickly diverging from the road (not depicted above) with no possible way of maneuvering back. While the velocity is yet high enough, the roll angle will increase only marginally, but the motorcycle will eventually drive off the road. As the top left plot shows, beginning at around 40 km/h, the roll angle reaches substantial values and soon starts oscillating (so-called "low speed weave"). After only a few wavelengths, the motorcycle will tilt over at around 26 km/h.

By applying a steering torque in the $\mathrm{CD}_{\mathrm{L0}}^{\mathrm{H1}}$ condition, (top right plot) the riders can compensate for minor disturbances and offsets in the system, such that the motorcycle will stay within the lane (again not depicted). The roll angle will – even at high speeds – reach values of a few degree which is reasonable, as now the rider is coupled to the vehicle dynamics and any motion of platform or rider will most likely cause a minor change in the measured steer torque (as discussed with regard to the roll rates in Figure 6.2). Increasing values in this velocity range may therefore not be mistaken as an inferior system behavior. They rather represent a real motorcycle's sensitivity to steering inputs quite well.

The roll amplitudes increase below 40 km/h for all riders, as the motorcycle enters the capsize mode. In contrast to the experiment in the $\mathrm{CD}_{\mathrm{L0}}^{\mathrm{H0}}$ condition, the riders are now able to intervene and balance this mode. Rider #1 shows the largest roll angles throughout the whole maneuver and eventually fails to stabilize the vehicle at around 20 km/h. Riders #2 and #3 show increasing roll angle amplitudes at 30 km/h and below. Only rider #2 succeeds to reach the area of artificial stabilization provided by BikeRealTime.

The bottom right plot shows the coast down maneuver in the $\mathrm{CD}_{\mathrm{L1}}^{\mathrm{H1}}$ condition. As discussed previously, this results in smaller roll oscillations throughout the complete speed range. Rider #1 is again not capable to stabilize the ride sufficiently, but reaches slower velocities as in the $\mathrm{CD}_{\mathrm{L0}}^{\mathrm{H1}}$ condition. Below 20 km/h, riders #2 and #3 also show a sudden increase in roll angle, before BRT will activate the low-speed stabilization at around 16 km/h.

Lastly, the bottom left plot shows the roll angles during a coast down maneuver while riding without hands in the CD_{L1}^{H0} condition. A comparison to the plot above, indicates the rider motion's influence on the capsize mode. Rider #2 reaches velocities down to almost 20 km/h just by utilizing rider motion. This behavior is well in line with observations from real motorcycling as presented in Pleß[159]. Rider #3 delays the tilt over by a few km/h compared to the CD_{L1}^{H0} condition. Rider #1 again struggles with the control. It must however be stated that such maneuvers are just as challenging in real life as well.

The measurements during constant straight running (section 6.1) and coast down both show a clear effect when utilizing DLRC. The additional control loop allows to stabilize the capsize or low-speed weave mode. Well trained riders can make use of this even when riding without hands. When using both control loops, the motorcycle roll rates maintain small, allowing to have better control over the vehicle when riding slow. However, at very low velocities, the leaning control loop – as implemented on the DESMORI simulator – is not capable of simplifying the balancing of the motorcycle. This could however result from many reasons. Beside imperfections of the DLRC (friction, body parametrization, latency), there are also uncertainties regarding e.g. the motion cueing and the steering force-feedback-controller that are active fields of research. To the author's knowledge, a valid simulation that intuitively allows stabilization of the capsize mode during low(est possible) speeds through balancing actions does not exist yet. The DLRC implemented here is on its own not sufficient to cope with the motorcycle's system immanent instability.

6.3 DLRC Performance in Transient Maneuvers

Following the discussions from section 4.2 three kinds of transients – i.e. changing between different steady states – are investigated. Firstly, the transients during straight running are discussed, showing if it is possible to vary the vehicle roll angle while maintaining a straight ride. Secondly, transients during cornering are discussed. These can either preserve the current trajectory (i.e. not change the curvature at constant speed) or change the current trajectory (i.e. changing the curvature).

6.3.1 Roll Angle Variation During Straight Running

As described in section 4.2.1, DLRC capabilities on a motorcycle riding simulator should allow riding modes that are not possible by purely using the state-of-the-art steering control. And the performance of a DLRC (or any other kind of system) can be rated higher when it allows to achieve more vehicle states that are known from real life but aren't possible on

---

[159] Pleß, R. et al.: The Influence of Rider Motion on Motorcycles and Riding Simulators (2018).

state-of-the-art simulators. Therefore, it is tested in the following, if the DLRC implemented here enables riders to ride in a straight line with non-zero roll angles.
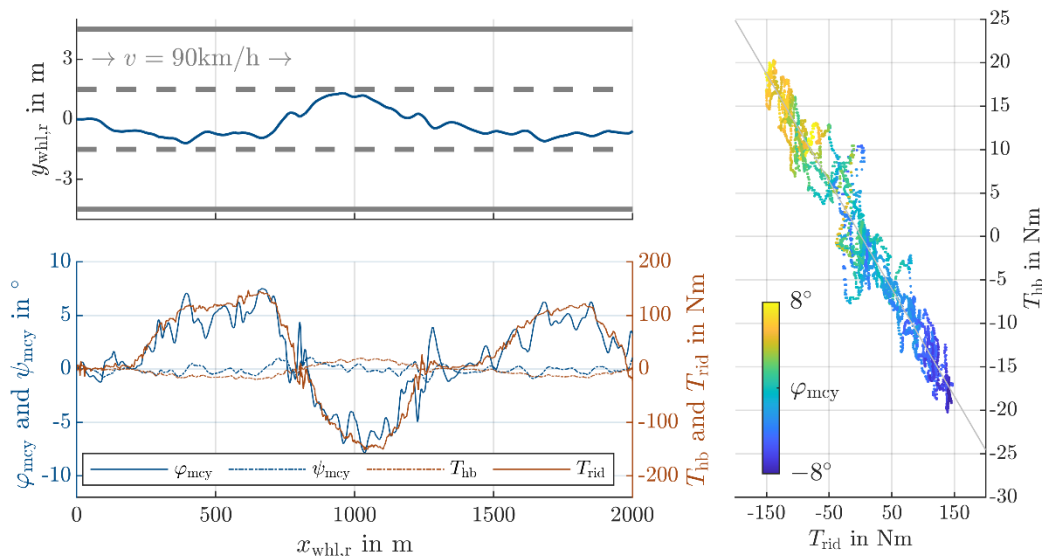

Figure 6.8: Straight transient maneuver $\text{TS}_{\text{L1}}^{\text{H1}}$ at $v_{\text{set}} = 90$ km/h. Top left: motorcycle rear tire trajectory along the three lane road with 2 km lenght. Bottom left: distance series of angles (blue) and torques (red) showing the changing vehicle states under changing rider inputs. Right: Linear combinations of steer and lean torque resulting in roll angles that preserve the straight trajectory. Regression line at $T_{\text{hb}} = -0.124 \cdot T_{\text{rid}} + 0.157$ Nm with $R^2 = 95.7\%$.

The experiment is conducted on a three-lane straight road with the simulator in $\text{TS}_{\text{L1}}^{\text{H1}}$ configuration (**T**ransient **s**traight, **h**ands **on**, **l**ean **on**) as shown in the top left plot in Figure 6.8. A cruise control is set to 90 km/h and the rider must slowly lean sideways while performing the correct steering inputs to maintain a straight trajectory. The top left plot shows that the rider is riding fairly straight (consider the vastly different scaling of the x- and y-axis!). The yaw angle of the levelled CoSy in the depicted segment stays within $\pm 1°$ as shown in the dash-dotted blue line in the bottom left plot. While riding straight, the rider is nevertheless capable to create motorcycle roll angles by leaning towards one direction and applying a steer torque in the other direction. As seen in the bottom left distance series in Figure 6.8, the rider induced roll torque T_{rid} (see section 3.2) reaches values of ± 150 Nm (continuous red line). By adjusting the steer torque T_{hb} to values between ± 20 Nm (dash-dotted red line) the rider achieves motorcycle roll angles φ_{mcy} of $\pm 8°$ with only minimal changes of the heading. These values are well within the magnitude estimated by the model presented in Figure 3.11. There, a motorcycle roll of $\varphi_{\text{mcy}} \sim 8°$ while riding at $\varphi_{\text{th}} = 0$ also results in $T_x \sim 150$ Nm.

The right plot shows the linearity of that effect. The regression line has a coefficient of determination of $R^2 = 95.7\%$ and equates to $T_{\text{hb}} = -0.124 \cdot T_{\text{rid}} + 0.157$ Nm. Torque combinations that lay close to that line allow to continue running straight while the motorcycle is tilted to one side. Remember, that this kind of maneuver is not possible on a simulator without DLRC capabilities. If only one control input (either steering or leaning) is

available, the virtual motorcycle will not run straight, unless that input is zero (considering a precisely symmetric vehicle model). Therefore, being able to perform this maneuver in TS_{L1}^{H1} configuration proves an added performance compared to state-of-the-art simulators.

6.3.2 Roll Angle Variation During Constant Cornering

The previous section has shown, how the rider induced roll torque will affect the roll equilibrium of the virtual motorcycle and how opposing steering inputs can be used to reach another equilibrium condition even without changing the trajectory. The same effect is known from real riding in curves. The steer torque during steady state cornering is reduced, as a rider performs a lean-in motion and vice versa. Also, the motorcycle roll angle is subject to the rider's CoG position, as described in section 2.1.2. A different combination of the rider induced roll torque and the steer torque will allow to ride on the same trajectory (i.e. the same velocity and curvature during steady state cornering).

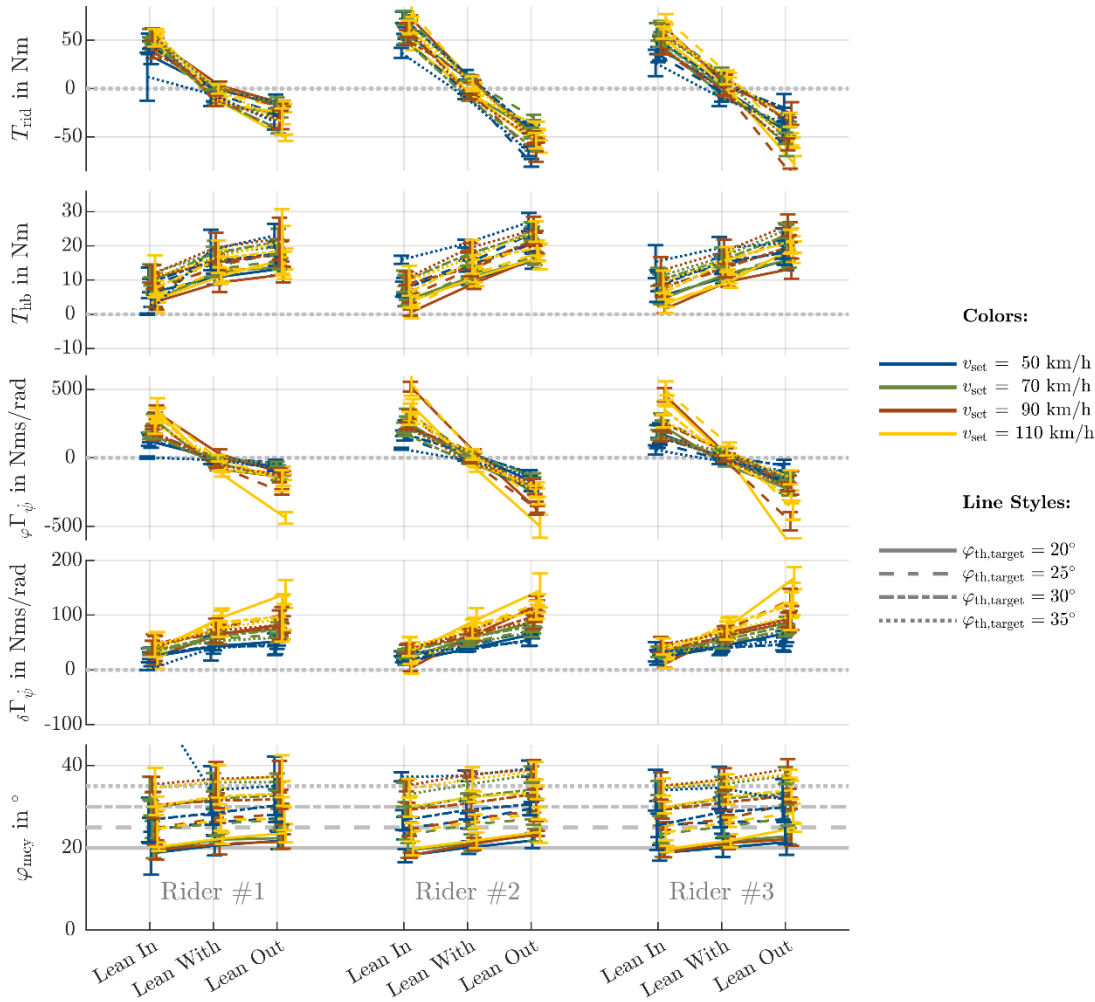Figure 6.9: Change of vehicle states under different leaning conditions. Each column of plots represents one rider. The set speed is color coded; the target theoretical roll angle is coded via line style. The error bars indicate means and standard deviations within a $180°$ constant cornering segment. Top to bottom: Rider induced roll torque, steer torque, lean-turn-index, steer-turn-index and roll angle.

To test for this effect, the constant radius cornering maneuver described in section 5.1.2 is performed in the $\mathrm{TC_{L1}^{H1}}$ condition (**T**ransient **c**ornering, **h**ands **on**, **l**ean **on**) with the velocities and radii parameterized according to Table 5.3. Figure 6.9 shows the data collected by three riders at four different velocities and radii each in three leaning conditions. Subgroups of this data for singular velocities and roll angles are shown in Appendix B.1. The error bars indicate means and standard deviation within a 180° constant cornering segment. The lines have been added for better readability but do not result from measured data (i.e. "leaning halfway out"). The set velocity is color coded and the target theoretical roll angle is coded via line style. The figure contains data of both left-handed and right-handed curves. In order to allow for a better readability and comparability of the data, the sizes have been normalized by the direction of the curve. Positive values indicate an in-turning direction. For example the positive roll torque indicates lean in; increasing steer torques increase the roll angle.

The first two lines of plots in Figure 6.9 show the rider induced roll torque T_{rid} and the steer torque T_{hb}. The rider induced roll torque is close to zero during lean-with and shows opposite signs during lean-in and lean-out. The amplitudes reach smaller values than in the $\mathrm{TS_{L1}^{H1}}$ condition shown in the previous section. They are however again in line with the magnitudes estimated in Figure 3.11.

As the roll torque increases (lean-in), less steer torque is needed to ride through corners with equal curvature at equal velocities. In all tested segments and under all leaning conditions, the steer torque stays greater than zero. This behavior relates to a rather stable vehicle. If the torque were to change signs, the motorcycle would become instable and the rider would have to steer towards the inside of the curve to prevent the motorcycle from tilting over. Parametric changes of e.g. the tire model or vehicle geometry allow to quickly vary the motorcycle's dynamic behavior in that regard. Such variations of the virtual motorcycle are however not in the focus of the work presented here.

The bottom row of plots in Figure 6.9 shows the roll angles of the virtual motorcycle. Rider #1 generates an outlier in the dataset, as the lean-in maneuver at 50 km/h and 35° roll angle resulted in a crash (blue dotted line). According to the motorcycle fundamentals and theoretical models presented in sections 2.1, 2.2, 2.3 and 3.2, it is expected, that the motorcycle will show less roll angle when the rider utilizes lean-in and vice versa. This exact behavior can be seen throughout all experiments and configurations. As the rider generates more roll torque towards the inside of the curve, the motorcycle roll angle decreases accordingly.

The data proves, that the rider's motion affects the virtual motorcycle as known from real motorcycling. Again, it is at this point less important to show an exact numerical baseline from a specific real motorcycle, but to show, that the observed effects represent plausible vehicle behavior. Depending on the kind of simulator study, one might either take efforts to measure and validate the parameters of the real vehicle on the simulator or rather only adjust the simulator's parameters to provide the desired rideability and handling properties.

The third and fourth row of plots show the lean-turn-index $_{\varphi}\Gamma_{\dot{\psi}}$ and steer-turn-index $_{\delta}\Gamma_{\dot{\psi}}$ presented in section 4.2. Generally, they both show the same behavior as the rider induced

roll torque or the steer torque respectively. However, through the division by the yaw rate, the data shows more pronounced velocity clusters. The steer turn index increases with increasing velocities and shows slightly larger gradients, when transitioning from lean-in to lean-with. Such steeper gradients can also be observed for the lean-turn-index at higher velocities. Following the typical reasoning from literature, smaller steer-turn-indexes would relate to better handling. Therefore, both slower velocities and utilizing lean-in would arguably result in the best handling. The same holds true for the lean-turn-index that is as well smaller valued at smaller velocities. As discussed in section 4.2.2, the absolute values of the indexes are irrelevant for rating the DLRC capabilities, as they are rather suited to rating different vehicles or vehicle setups against each other. Therefore, it must be concluded that the handling indexes known from literature don't provide a lot of benefit for the rating of the simulator and DLRC capabilities.

6.3.3 Trajectory Variation Through Leaning

According to section 4.2, it is to be tested, if using the leaning control loop is feasible to willingly affect the motorcycles curvature. As before, the constant radius cornering track is used. As shown in Table 5.2, the radii and velocities are chosen such, that a theoretical roll angle of 10° (left corners) and 15° (right corners) must be applied at set velocities of 100 km/h, 90 km/h, 80 km/h, 70 km/h, 60 km/h and 50 km/h, resulting in a total of 12 curves. The map is shown in the upper plot of Figure 6.10. The lower plot shows measurements of one rider either in the TC_{L1}^{H0} condition (red error bars, riding without hands) or the TC_{L0}^{H1} condition as a reference (green error bars, pure steering control). The error bars indicate the mean values and standard deviation of the CoG's lateral position throughout each 180° corner. The blue dashed line represents this center line, the continuous blue lines represent the outside borders of the road.
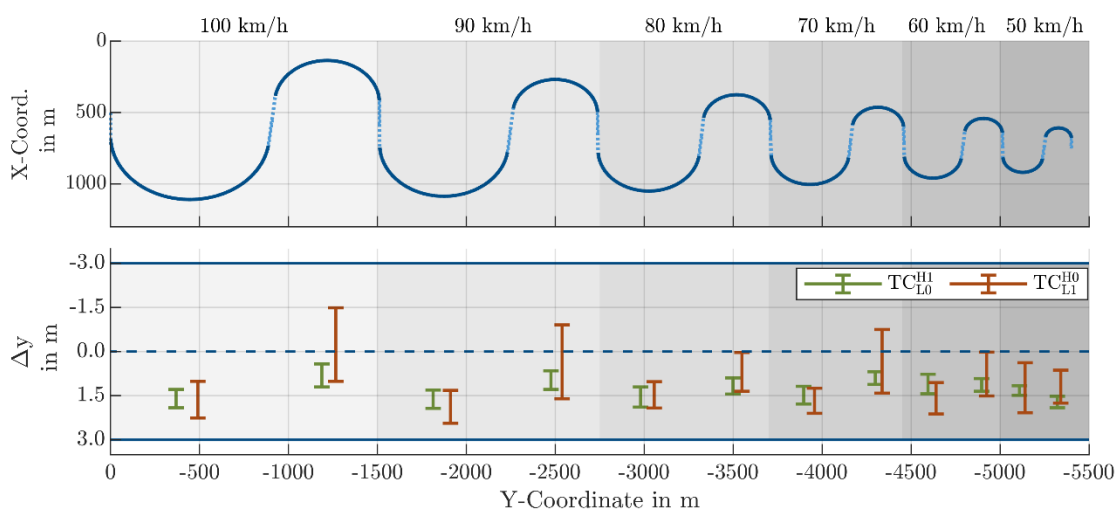

Figure 6.10: Varying the curvature while riding without hands (TC_{L1}^{H0}, red, right bars). The top plot shows the scenario map. The error bars in the lower plot show mean values and standard deviations of the CoG lateral position during the corner. The TC_{L0}^{H1} condition is depicted as a reference (green, left bars). The grey shading indicates the set velocity.

The figure shows, that in all cases the motorcycle is controllable through any given curvature at all given speeds just by using the leaning input. The TC_{L0}^{H1} condition expectedly shows better performance by means of smaller standard deviations than the TC_{L1}^{H0} condition, as it allows for much quicker and more precise controls and corrections than riding without hands. However, it can be seen, that especially in the 10° conditions, riding without hands achieves almost as good values as the baseline at speeds from 100 to 60 km/h. When increasing the target roll angle to 15°, the rider still manages to stay on the road, but the performance decreases drastically and the deviations tend towards the opposing lane, (i.e. to a wider radius). The decreasing performance also becomes observable when looking at the distribution of the roll angle and the yaw angle deviation in Figure 6.11.
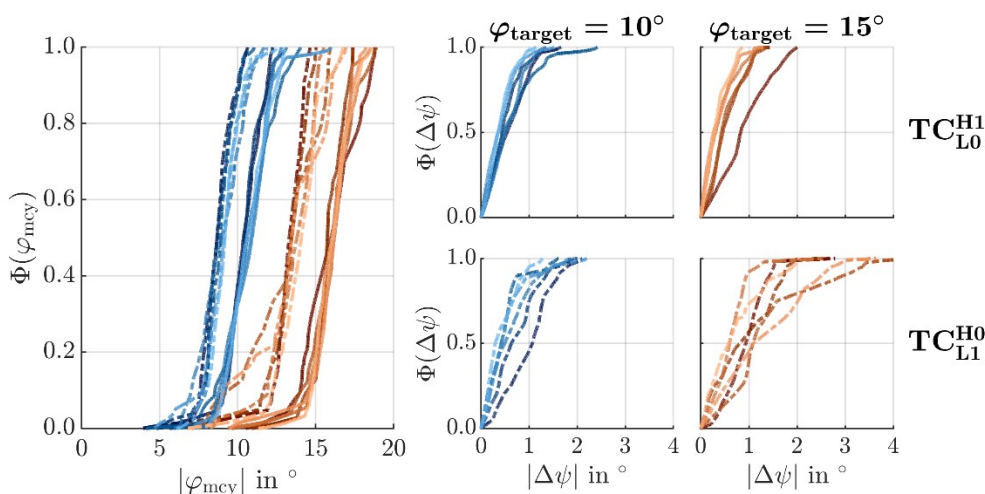

Figure 6.11: Empirical cumulative distribution functions of the roll angle (left) and the yaw angle deviations (four smaller plots). The colors refer to the target roll angles. Darker color shades indicate lower velocities. Riding without hands (TC_{L1}^{H0}) is depicted as dash-dotted line.

The lefthand plot shows the empirical CDF of the vehicle roll angle. As expected, the TC_{L1}^{H0} condition (dash-dotted lines) will require smaller motorcycle roll angles, as the rider leans towards the inside of the curve, generating a significant fraction of the theoretical roll angle by shifting their CoG (see Figure 2.3). The plot also shows a wider spread of roll angles when riding without hands compared to riding with hands (continuous lines). This decreased performance is also observable in the deviation between the yaw angle of the levelled CoSy and the current direction of the road $\Delta\psi$ (four small plots). When using the handlebar to control the motorcycle, the yaw angle deviation stays small, with one exception being the curve at 50 km/h (dark red line, top right plot). When riding without hands (lower plots), these deviations increase, especially in the 15° condition. The values in the 10° condition however stay reasonably small.

The results of this section show, that DLRC allows to deliberately manipulate the virtual motorcycle's states and trajectory through leaning motions on the simulator. The vehicle states respond to leaning inputs as expected from real life, by e.g. changing the vehicle roll angle and steer torque demand. The next step is to investigate the performance of DLRC in dynamic maneuvers.

6.4 DLRC Performance in Dynamic Maneuvers

As discussed in section 4.3, the effect of DLRC in dynamic maneuvers will be investigated in a single lane change maneuver and slalom maneuver. In both cases, it is of interest, if the use of DLRC allows to provoke realistic vehicle responses and if the rideability of the simulator in theses maneuvers increases due to the implementation of DLRC.

6.4.1 DLRC Effects on Lane Change Maneuver

The lane change maneuver tested in this research is described in detail in section 5.1.3.1. A lateral offset of $\Delta y = 3$ m must be achieved within defined distances at defined velocities according to Table 5.4. Per rider, 10 consecutive repetitions at each velocity were performed, before reducing the velocity. In contrast to the previous experiments, the rider controls the throttle by themself here. The following plots in this sub-section contain data from the same rider. The data collected with other riders showed no relevant differences. Figures at different velocities can be found in Appendix B.2.

Figure 6.12 shows the trajectories of the front tire contact point during a lane change maneuver at 90 km/h in the DL_{L0}^{H1} configuration (left) and the DL_{L1}^{H1} configuration (right). The plot depicts the road markings (dashed grey lines) as well as the outside border of the road (green "grass" area). The rider comes from the left through the corridor of cones (red circles). Precisely when exiting the corridor at a distance of 50 m, the traffic sign presents the target direction (see section 5.1.3.1). Therefore, the lateral motion will only appear after some reaction time once exiting the corridor.
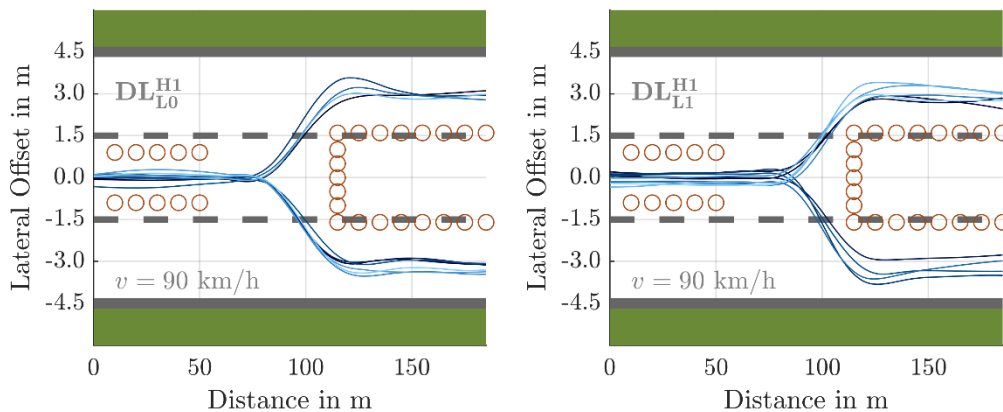
Figure 6.12: Trajectories of the front tire contact point during lane change at 90 km/h. 10 consecutive repetitions of the same rider (different shades of blue). The left plot shows the state-of-the-art configuration. In the right plot, DLRC is activated.

The data shows no directional effects. The correlation coefficients between each measurement in one condition are always greater than 99%. In the following it is therefore assumed, that left- and right-hand lane changes can be evaluated as equal by mirroring the left hand lane change data onto the right hand data.

On the first glance, the DL_{L1}^{H1} trajectories show slightly more lateral scattering, but less amount of overshooting compared to the DL_{L0}^{H1} trajectories. To further investigate the lane change behavior, the curves of different dynamic states of the motorcycle must be discussed. Figure 6.13 shows the lane change maneuver in the baseline condition DL_{L0}^{H1}. Therefore, the rider induced roll torque T_{rid} (red line and area) is zero in this timeseries. The steer torque (yellow) steer angle (green) and roll angle (blue) of the 10 repetitions are depicted by their mean value (line) and standard deviation (shaded area). Angles are referenced on the left ordinate, torques on the right.
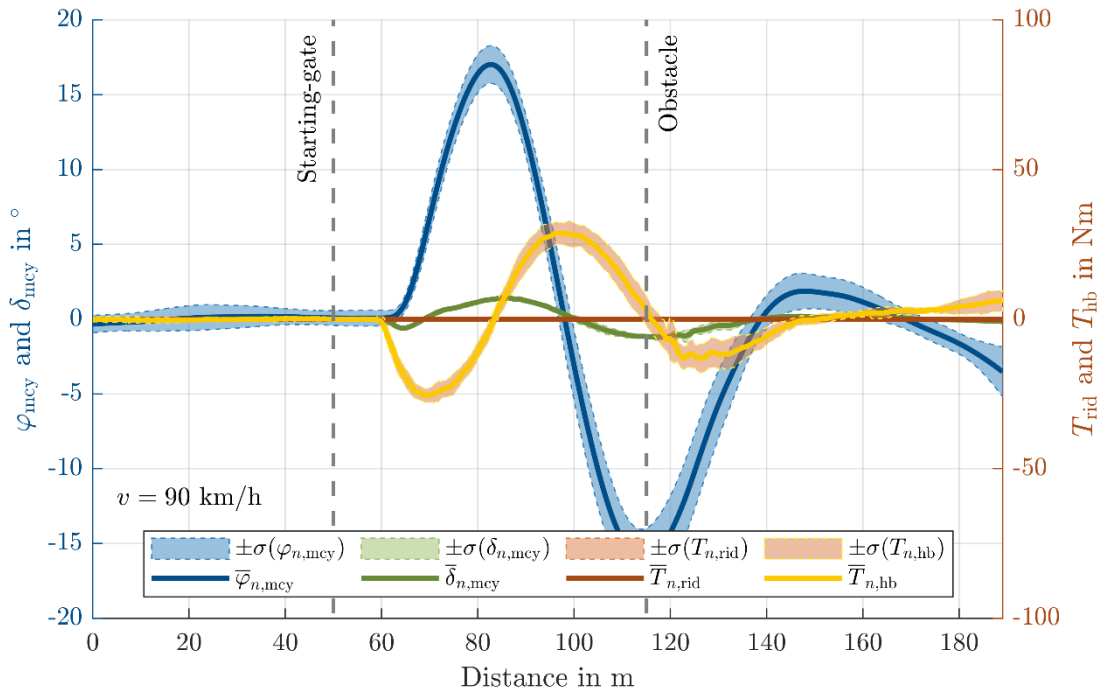

Figure 6.13: Lane change maneuver at 90 km/h in DL_{L0}^{H1} condition. Each line represents the average value of the $n = 1 \ldots 10$ repetitions at that distance (abscissa) The areas indicate the respective standard deviation. After passing the starting gate (dashed line) the rider traverses laterally in order to avoid the obstacle (second dashed line). Data of left-hand lane changes has been mirrored.

The plot shows the typical behavior of a motorcycle during an avoidance maneuver. Firstly, a rapidly applied steer torque (at 60 m) causes the counter steer impulse (green line, initially negative). While continuing to apply this torque, the roll angle builds up and the steering system rotates towards the direction of the lane change as well. The rider applies an opposite steer torque in an effort to return to straight running on the outside lane aside of the obstacle. At the end of the plot, the increasing roll angles show, how the rider smoothly initiates the return to the center lane for the experiment's next repetition. As the speed is easily kept constant, and the target trajectory is rather constrained, there is not really any room for choosing alternative lines. Furthermore, any variation can only result from steering inputs. Therefore, the data shows rather small standard deviations. In contrast to that, larger standard deviations appear in Figure 6.14 that shows the same experiment in the DL_{L1}^{H1} configuration. This again indicates the responsiveness of the virtual motorcycle to the rider's leaning input.

This second control input will cause offsets or disturbances as a reaction to any small rider motion, no matter if it is a moving head, arm or upper body (see section 3.2). Any such disturbance will cause slight changes in the vehicle's trajectory approaching the avoidance maneuver and will therefore cause scattering in the data.
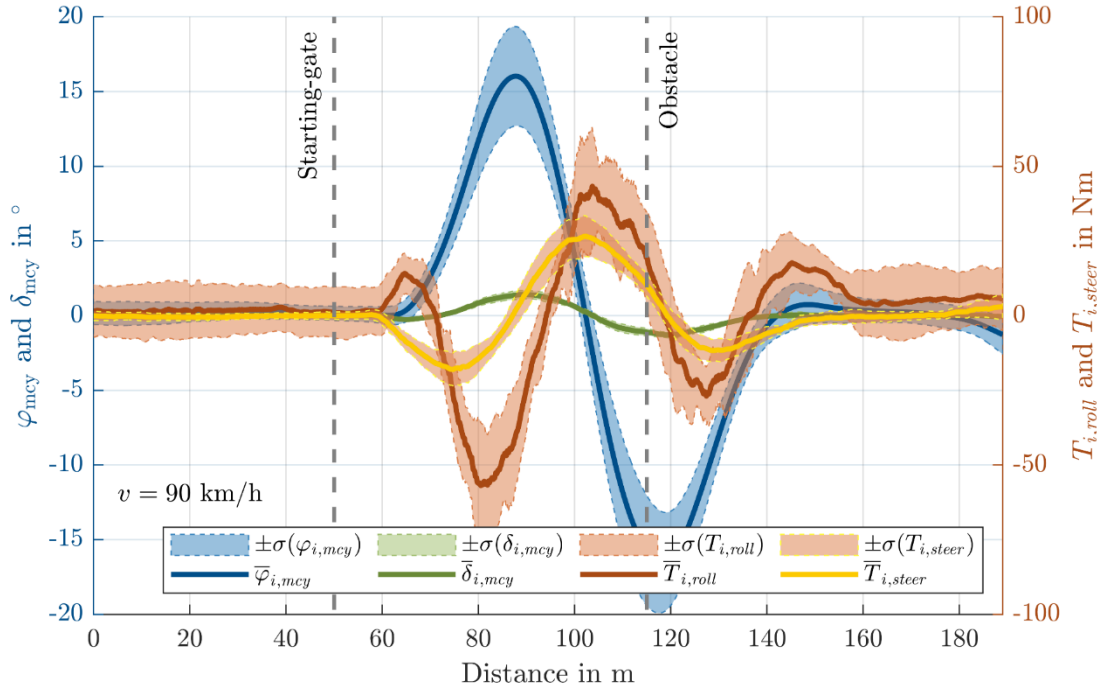

Figure 6.14: Lane change maneuver at 90 km/h in DL_{L1}^{H1} condition. Each line represents the average value of the $n = 1 \ldots 10$ repetitions at that distance (abscissa). The areas indicate the respective standard deviation. After passing the starting gate (dashed line) the rider traverses laterally in order to avoid the obstacle (second dashed line). Data of left-hand lane changes has been mirrored.

Nevertheless, the overall characteristic of the plot stays the same as with the DL_{L0}^{H1} baseline. As the rider leans to one side, their inertial force is supported against the motorcycle frame, resulting in a small roll torque impulse (red) at the beginning of the maneuver. This rider induced roll torque impulse is built up at instance with the steering torque. This highlights, that both inputs often come together automatically: A rider moving to the right will most likely push against the right handlebar, introducing a supporting counter steering input. The steer angle therefore results in much smaller values, however. As a fraction of the turning is now performed by the rider's lean input, there is less steering effort needed, to follow the target trajectory, as described in the previous section. Therefore, also the steer torque amplitudes remain smaller than before. The rider initiates the lane change maneuver just as before at a distance of 60 m. However, the maximum amplitudes of the dynamic states are delayed by about 5 m compared to the previous experiment in the DL_{L0}^{H1} condition. One explanation for this might be the added inertia that is virtually connected to the motorcycle through the roll torque determination.

To rate the handling of a motorcycle in lane-change maneuvers, the Lane-Change-Roll Index was described in section 2.2.3 and is calculated here for every repetition using the average

velocity during the transition phase, as well as the peak-to-peak values of the steering torque and roll rate. The two-dimensional error bars in Figure 6.15 take the standard deviation of the mean vehicle speed for every repetition into account in the horizontal direction. The vertical direction shows the mean and standard deviation of the Lane-Change-Roll Index.
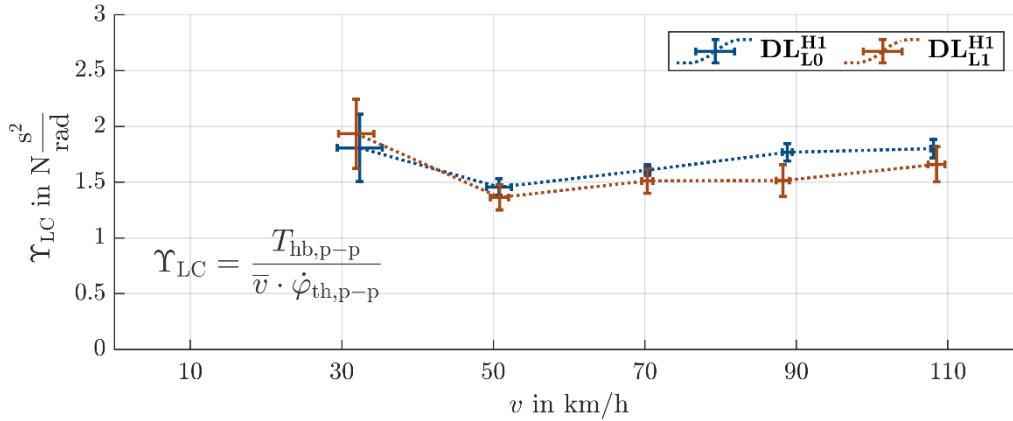

Figure 6.15: Lane Change Roll Index in lane-change maneuvers at different velocities. Each error bar of the DL_{L0}^{H1} (blue) and DL_{L1}^{H1} condition (red) contains data from one rider in 10 repetitions

For all velocities above 30 km/h, the index becomes larger with speed and is in general larger in the DL_{L0}^{H1} condition. This shows again, how lean in will reduce the steer torque demand. This holds true not only during the transient maneuvers shown previously, but also in highly dynamic maneuvers.

It must however be noted, that as the velocity reaches the region of the capsize mode (starting around 40 km/h for the given virtual motorcycle, as it is shown in Figure 6.7) the motorcycle becomes more difficult to control and the rider will put more effort into stabilizing the motorcycle. Despite the challenging system dynamics, the simulator and virtual motorcycle is in general controllable through the given maneuver at 30 km/h but shows rather high oscillations in both steer and roll angles as depicted in Figure 6.16. The rider continuously tries to stabilize the motorcycle before eventually providing the slightly pronounced initial steer impulse (55 m) that starts the lateral motion. In contrast to the measurements shown before, the small steer torque will instantly cause the motorcycle tilting towards the outside lane of the road. Due to the small amount of self-stabilization, the roll angle increases rapidly, as does the steer angle. The previously well observable roll torque excitation is rather small and seems to show an opposite phase as before, indicating a lean-out behavior that is also typical at low speeds in real motorcycle riding. The maximum of the up-righting steer torque (shortly after the obstacle line) happens shortly after the roll angle maximum. This shows that the up-righting motion of the motorcycle rather results from its own dynamics (i.e. low speed weave) rather than the rider's steering input.
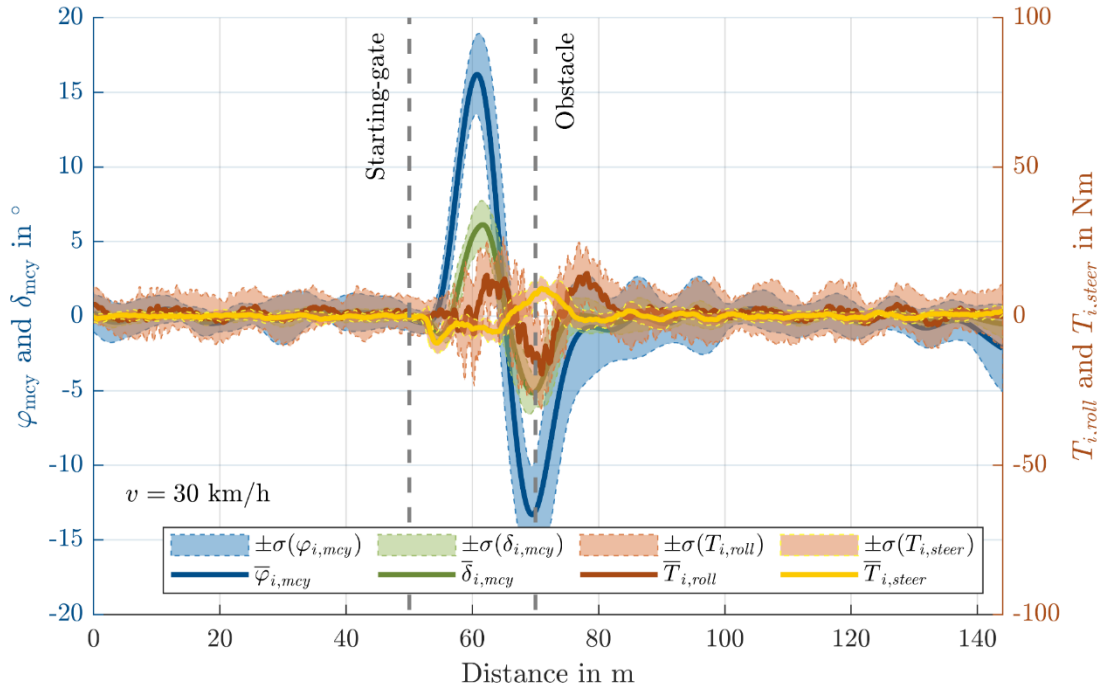
Figure 6.16: Lane change maneuver at 30 km/h in DL_{L1}^{H1} condition. Each line represents the average value of the $n = 1 \ldots 10$ repetitions at that distance (abscissa) The areas indicate the respective standard deviation. After passing the starting gate (dashed line) the rider traverses laterally in order to avoid the obstacle (second dashed line). Data of left-hand lane changes has been mirrored.

Lastly, the dynamic trajectory following capabilities when utilizing only the leaning control loop are investigated in the lane change maneuver in DL_{L1}^{H0} condition. More than the transient cornering maneuvers from section 6.3, the lane change maneuver highlights the dynamic aspects of the leaning control loop, as it necessitates rather strong leaning excitations, an instant change from one direction to the other, as well as a stabilizing action at the end of the maneuver. Figure 6.17 shows the trajectories at the two different speed conditions selected in section 4.3. Again, one expert rider performed $N = 10$ repetitions at the same velocity before changing to the next velocity. The speed is set by a cruise control.
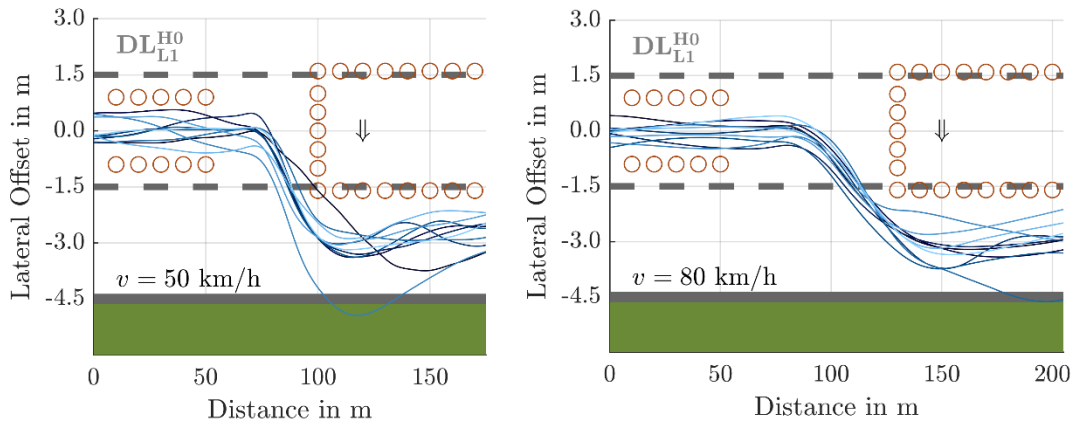

Figure 6.17: Trajectories of the front tire contact point during lane change without hands. 10 consecutive repetitions of the same rider (different shades of blue). The left plot shows the maneuver at 50 km/h, the right plot at 80 km/h.

In both speed conditions, there is one repetition, where the rider failed to stay within the boundaries given by the road geometry, while all other repetitions were successfully performed. On the first glance, the data of the experiment at 50 km/h shows greater instability and oscillations compared to the experiment at 80 km/h, which is expected, due to the lesser amount of self-stabilization. As before, Figure 6.18 and Figure 6.19 provide a detailed insight into the dynamic properties of the scenario. As the $\text{DL}_{\text{L1}}^{\text{H0}}$ condition utilizes only leaning inputs, the steer torque is not depicted. The figure shows, how the rider's initial leaning motion to the right will again generate a roll torque to the left that causes the motorcycle to roll left as well (small negative bump in the blue signal at 64 m). This comes from the inertial effect, as the rider mass acceleration is only supported against the motorcycle frame. The behavior is in line with the Aström model that was presented in section 2.3.2, that is also showing the opposing motorcycle roll motion as a reaction to the rider lean angle.

Due to the gyroscopic effect, the steering will turn left as well, as the negative bump in the zoomed area in the top right corner of the figure depicts. This leads to the tire contact points moving to the left, while the motorcycle inertia maintains its direction of travel, therefore building up a roll angle to the right. This is when the motorcycle traverses towards the right lane. As the rider initiates the counter motion, the inertia is again only supported by the motorcycle frame. This is, where the rider induced roll torque reaches its maximum value as does the roll rate and steering rate. Shortly after the roll angle maximum is reached, so is the maximum of the left turning roll torque, as the rider accelerates towards the middle plane of the motorcycle again.

Figure 6.18: Lane change maneuver at 50 km/h in $\text{DL}_{\text{L1}}^{\text{H0}}$ condition. Each line represents the average value of the $n = 1 \ldots 10$ repetitions at that distance (abscissa). The areas indicate the respective standard deviation. Data of left-hand lane changes has been mirrored. The top right plot shows a zoomed fraction of the steer angle, highlighting the gyroscopic effect when initiating the lane change.

133

When the maneuver is performed at higher velocity (Figure 6.19), it can be seen, that the rider builds up much more momentum at the beginning of the maneuver. While the rider induced roll torque reaches much higher values than before, the motorcycle's roll rate will stay significantly lower, which is reasonable due to the gyroscopically induced damping effect discussed in section 3.2.2. Therefore, the maximum roll angle towards the left is only reached after passing the obstacle. The steer angle will stay within much smaller amplitudes as previously at 50 km/h, which is also an effect of the increased self-stabilization and greater effort needed, to turn at higher velocities.
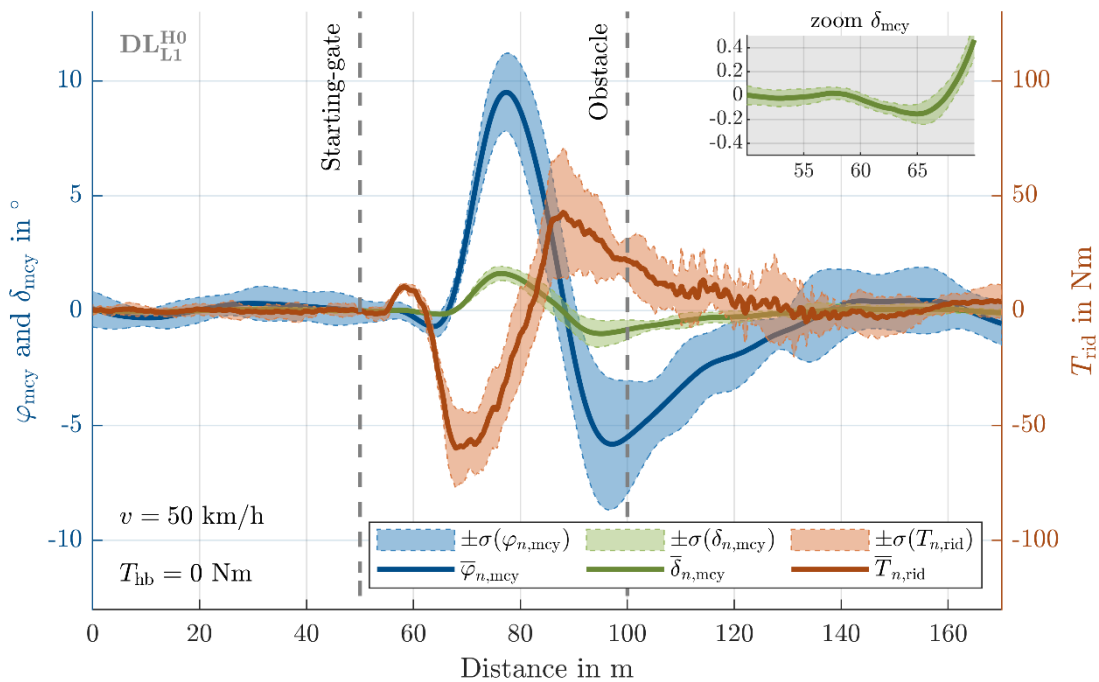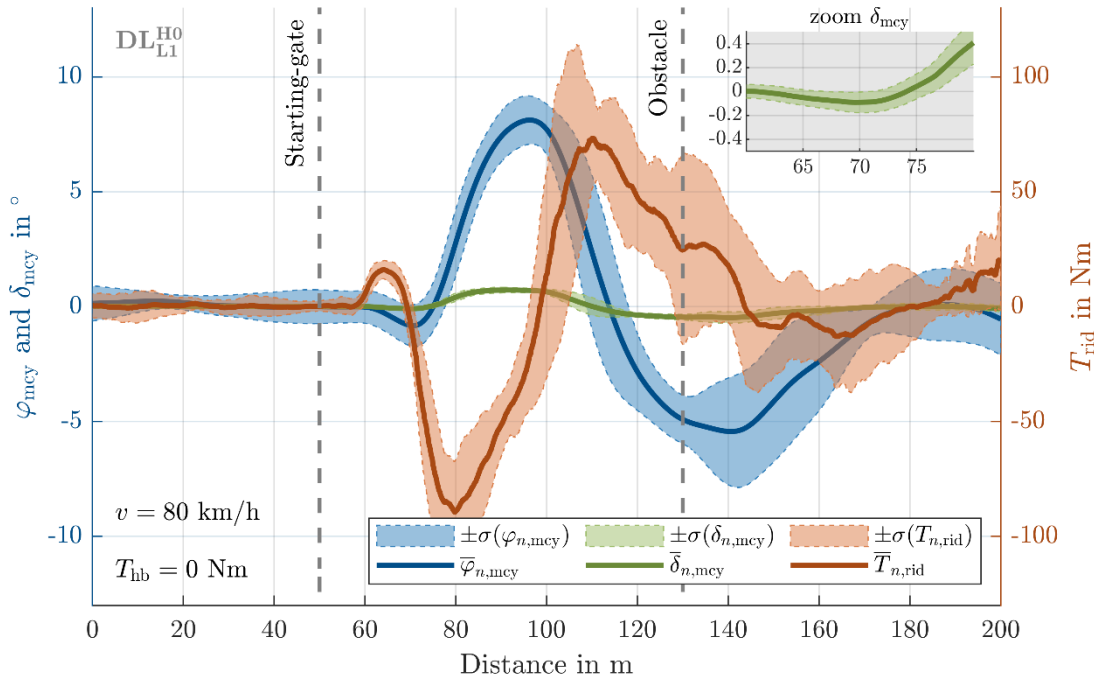

Figure 6.19: Lane change maneuver at 80 km/h in DL_{L1}^{H0} condition. Each line represents the average value of the $n = 1 \ldots 10$ repetitions at that distance (abscissa). The areas indicate the respective standard deviation. Data of left-hand lane changes has been mirrored. The top right plot shows a zoomed fraction of the steer angle, highlighting the gyroscopic effect when initiating the lane change.

6.4.2 Characteristic Values of the Lane Change Maneuver

The previous analysis of signals in the distance domain proved that the implementation of DLRC causes plausible vehicle responses during lane change maneuvers. When riding without hands in the DL_{L1}^{H0} condition, the effect of the rider mass being supported against the motorcycle frame can be observed. Both steer and roll angles build up small values in the opposing direction of the lane change, before turning in the same direction. During the maneuver in DL_{L1}^{H1} condition, the steer torque will reach smaller values compared to the DL_{L0}^{H1} condition, as the rider utilizes leaning motions. Also, an effect of DLRC on the relative position of the peak values of the lateral dynamic quantities can be observed. As discussed in section 4.3.2, these delays supposedly change depending on the rider leaning motion.

Cheli[160] indicates that by utilization of rider motion, a delay in the peak steer torques and steer angles can be observed with respect to the peak roll angles. This behavior could not be observed in the available data (see Appendix B.3). Furthermore, to the author's knowledge, there exists no definition of an ideal behavior in that regard. Therefore, the delays have not been further investigated.

As another approach to rate the performance during a lane change maneuver, the tanh-fitting method was presented in section 4.3.2, that was firstly developed by the author in [161]. There, it allowed to compare a real motorcycle, static simulator and dynamic simulator against each other. The same method is applied here for the comparison of the DLRC-configurations. The left plot in Figure 6.20 shows the trajectory of the motorcycle's CoG (blue) and the hyperbolic tangent that is fitted on this trajectory (green). This results in five characteristic values per maneuver: both longitudinal and lateral offset and scale of the hyperbolic tangent as well as the RMS error that describes the quality of the fit. The bubbles in the right plot of Figure 6.20 show the lateral displacement at the end of the lane change that is calculated from the lateral scale and offset of the hyperbolic tangent (ordinate) and the maximum lateral change rate that is calculated from the scales of the hyperbolic tangent function (abscissa) and the RMS error value (bubble size).
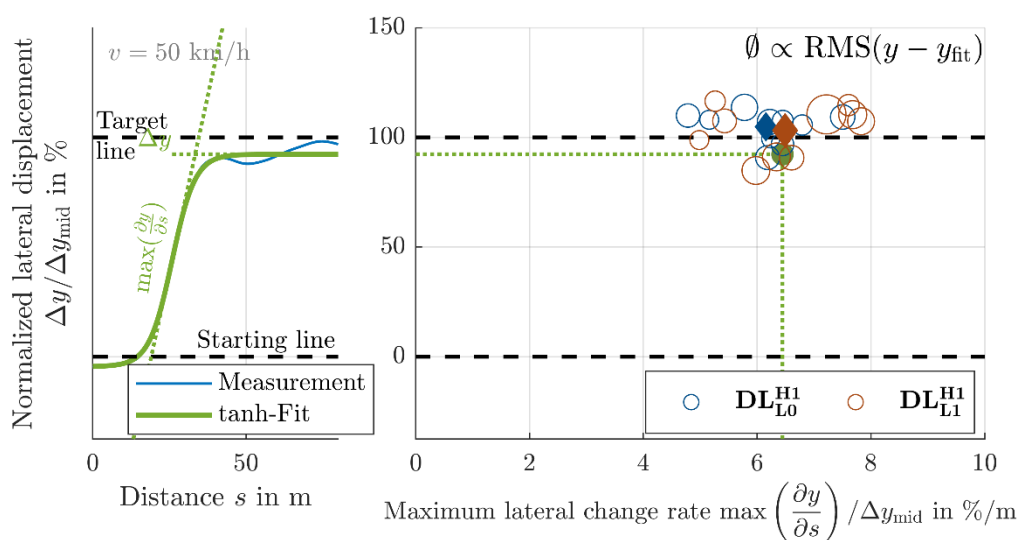
Figure 6.20: Tanh-fitting of motorcycle trajectories in a lane-change maneuver. The left plot shows one example fit (green). The right plot shows the fitting parameters in DL_{L0}^{H1} (blue) and DL_{L1}^{H1} condition (red). The abscissa and ordinate values have been normalized by the target lateral offset.

It can be seen, that in both conditions, the data is spread between 80% and 120% lateral displacement with maximum lateral change rates between 4 %/m and 8 %/m. The filled

---

[160] Federico Cheli et al.: Driver's movements influence on the lateral dynamic of a sport motorbike.

[161] Hammer, T. et al.: Anwendungsmöglichkeiten von Motorradsimulatoren (2021), p. 66.

diamonds show the mean values of each cluster. The performance during a lane change maneuver is rated higher, when the clusters and RMS error stay small.

The data in Figure 6.20 indicates, that the rider performs slightly worse in the DL_{L1}^{H1} condition than in the DL_{L0}^{H1} condition as the bubbles are slightly larger and wider spread in the figure. The evaluation is repeated at all tested velocities. As the length of the middle segment l_{mid} varies (see Table 5.4), it is feasible to normalize the maximum lateral change rate by this length. Figure 6.21 shows the bubble clusters that are constructed analogous to the right plot in Figure 6.20, but with the normalized abscissa. The ordinate is limited to the relevant value range around 100% lateral displacement and does not show 0.
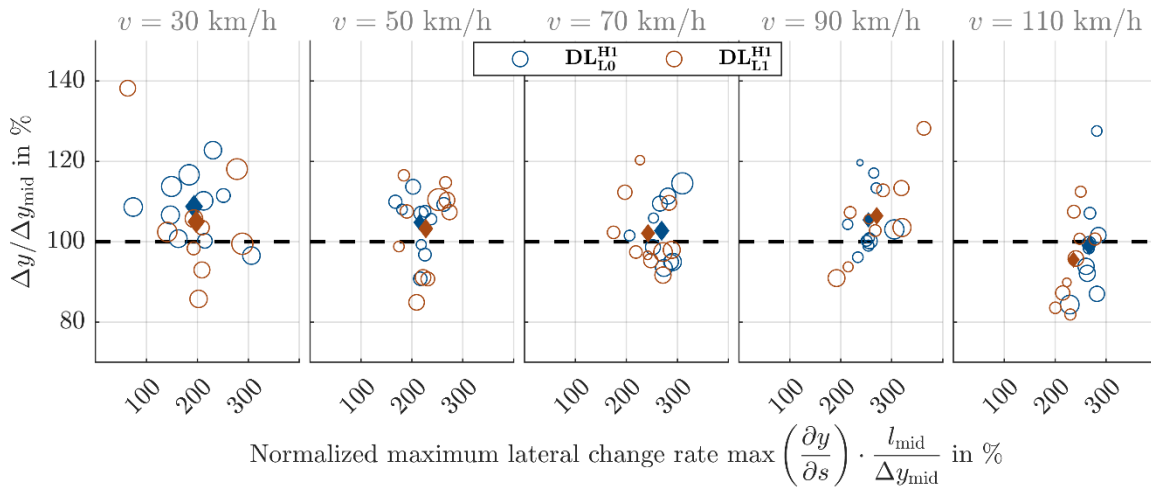

Figure 6.21: Bubble clusters of the tanh-fitting for different lane change test configurations. The Bubble diameters are proportional to the RMS error of the tanh-fitting of the motorcycle's CoG trajectory. The diamonds show the average position and size of the bubble clusters. Both axes are normalized by the target lateral offset Δy_{mid} and target length Δl_{mid} of the lane change maneuver.

The data shows only minor differences between the the DL_{L1}^{H1} (red) and DL_{L0}^{H1} condition (blue). The normalized maximum lateral change rate is rather similar for all maneuvers. At the highest velocity, the two clusters are rather clearly separated with the DL_{L1}^{H1} showing smaller change rates and RMS error values. However, the other plots don't show such clear clustering. At the lowest velocity, both test conditions show a significant increase in the RMS errors compared to the higher velocities. Furthermore, the bubbles show the biggest scattering throughout the whole data set. Clearly, this is the most demanding maneuver (see Figure 6.16.) and shows the lowest performance ratings, as the rider struggles to stabilize the capsize mode on the simulator.

It was previously discussed, that the evaluation of timely delays is not feasible for the performance evaluation during lane change maneuvers. The presented tanh-fitting method is superior to this approach, as it allows to rate the performance during a maneuver in terms of the RMS error and scattering of the bubble clusters. However, the comparison of the DL_{L1}^{H1} and DL_{L0}^{H1} condition didn't show big differences, indicating the small effect that DLRC has on the performance in a lane change maneuver.

6.4.3 DLRC Effects on Slalom Maneuver

In section 4.3, it was shown that several characteristic values known from literature are not feasible to be applied to rating the simulator performance. Alternatively, the evaluation of instantaneous amplitudes and frequencies is suggested. Referencing these values to a steady state approximation leads to the newly introduced slalom levels. In the following two sections, firstly the evaluation of the instantaneous amplitudes and frequencies is presented, before discussing the slalom level analysis.

6.4.3.1 Instantaneous Amplitudes and Frequencies

Table 5.5 in section 5.1.3 lists 11 slalom maneuvers that are used for the evaluation. They range from 100 km/h to 40 km/h (set by a cruise control) and request slalom frequencies between 0.25 Hz and 0.97 Hz. Through calculation of the analytical function, the instantaneous amplitudes and frequencies of the lateral dynamic quantities are calculated. Figure 6.22 shows this on the example of the motorcycle roll angle.
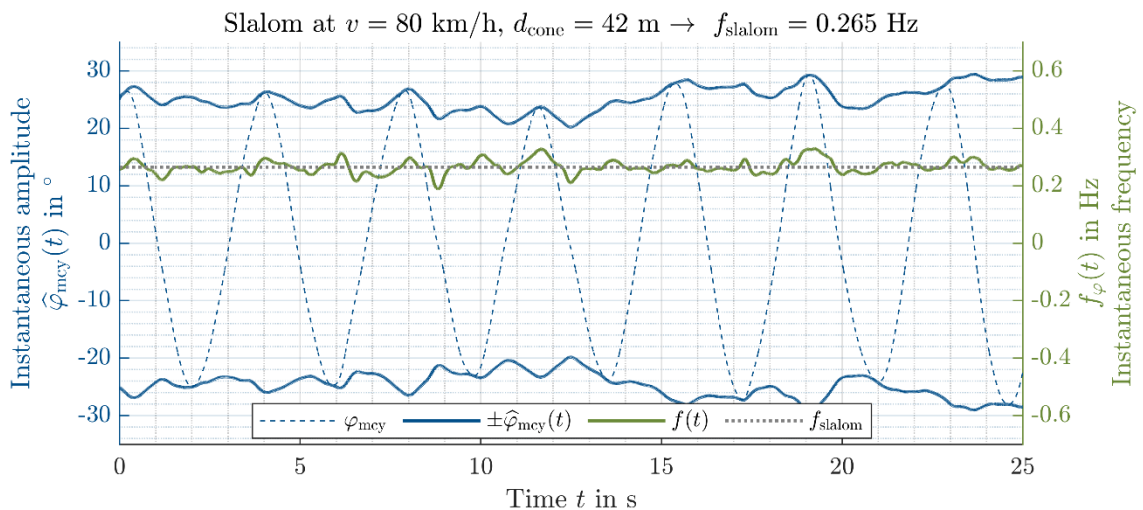
Figure 6.22: Instantaneous amplitude and frequency of the motorcycle roll angle φ_{mcy}. The instantaneous frequency (continuous green line) is close to the target slalom frequency (dotted green line). The instantaneous amplitude (continuous blue line) builds the envelope of the measured signal (dashed blue line). The example shows a slalom at 80 km/h with a cone distance of 42 m.

It can be seen from the figure, that the amplitudes are not constant throughout the maneuver, but rise and fall (here: between 20° and 30° roll angle). The performed slalom maneuver can be rated higher, when such deviations stay smaller.

As before, the identical maneuvers have been performed in both $\mathrm{DS_{L0}^{H1}}$ and $\mathrm{DS_{L1}^{H1}}$ condition to potentially find differences in the performance when implementing DLRC. Figure 6.23 shows the distribution of the motorcycle roll angle (left) and rear tire's lateral offset (right) with DLRC turned either off ($\mathrm{DS_{L0}^{H1}}$, blue) or on off ($\mathrm{DS_{L1}^{H1}}$, green) by means of errorbars. These indicate the p_{10} and p_{90} percentiles as well as mean values.

Figure 6.23: Distribution of instantaneous frequencies (top) and amplitudes (bottom) during various slalom maneuvers. Left: Motorcycle roll angle, right: Lateral offset of the rear tire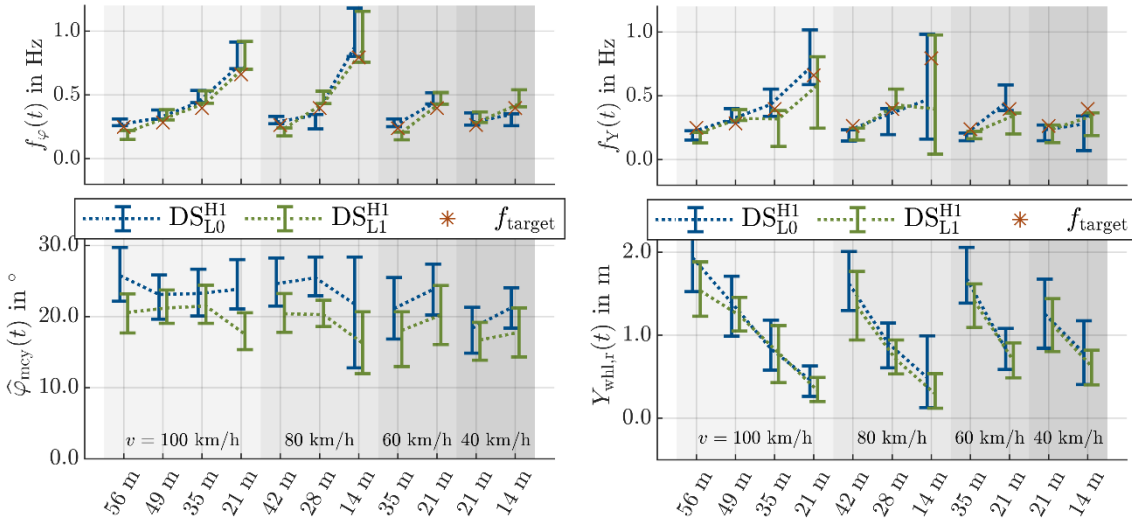. The error bars show the mean values (dotted lines) and range from the p_{10}-percentile to the p_{90}-percentile. The red asterisks indicate the slalom target frequency.

From both plots it can be seen that the mean instantaneous frequencies are rather close to the target frequencies, which is a prerequisite to even perform a successful slalom maneuver. However, the data also shows large deviations, especially when the target frequency is high, indicating that the rider struggles with performing this maneuver. The two slaloms at 100 km/h (80 km/h) and a cone distance of 21 m (14 m) are barely controllable for the rider. Throughout all measurements, the instantaneous amplitudes of both quantities are smaller in the DS_{L1}^{H1} condition. A smaller width of the motorcycle trajectory will obviously cause smaller amplitudes in all other lateral dynamic quantities as well. However, the scenario design did not constrain the target width of the slalom (see section 5.1.3.2). Therefore, the reduced amplitudes might not be attributable to the use of DLRC, but just to a differently chosen slalom width of the rider. As this effect is however observable throughout all slalom configurations, it is nevertheless assumed that the smaller amplitudes are caused from using DLRC rather than from arbitrarily chosen slalom widths. Aside from decreasing the amplitudes, it can also be seen, that the amplitude deviations decrease compared to the DS_{L0}^{H1} condition. As stated above, this is attributed to a better performance, as it implies that the rider can follow the slalom easier.

It is obvious, that the evaluations depend vastly on the slalom width. In order to generate values that relate to a defined baseline value instead, the slalom levels have been derived in section 4.3.3. They are based on a steady state slalom approximation that calculates baseline values of the kinematic motorcycle quantities as a function of speed, cone distance and slalom width and are discussed in the next subsection.

6.4.3.2 Evaluation of the Slalom Levels

The steady state slalom approximation presented in section 4.3.3 allows to calculate reference values for the curvature, yaw angle (levelled CoSy) and -rate, roll angle and -rate as well as the steering angle. By using the simplified approximation values (instead of e.g. more precise multi body simulation estimations), the calculations are independent of vehicle specific parameters – except for the steer angle approximation that depends on the wheelbase and steering head angle.

$$\left[\kappa, \psi, \dot{\psi}, \varphi, \dot{\varphi}, \delta\right]^{T} = f(v, d_{\text{cone}}, \hat{y}_{\text{slalom}}, l, \tau) \tag{6.1}$$

The harmonic sizes provide both amplitude and phase information. The amplitudes are used to calculate the levels according to equation (4.13). The phase difference between the measured and the approximated signal provide additional information on the timely behavior. Figure 6.24 shows exemplarily, how the levels and phases are evaluated in the following. After performing the maneuver, the magnitude of the first order oscillation of the rear tire trajectory is evaluated and used as $\hat{y}_{\text{slalom}}$ in equation (6.1). This results e.g. in the approximated roll angle φ_{ref} and its (constant) instantaneous amplitude $\hat{\varphi}_{ref}(t)$ that are depicted in grey in the top plots of Figure 6.24 as well as the (linearly increasing) signal phase that is depicted in the bottom left plot. With these reference sizes, the slalom level L_{sl} and phase difference $\Delta\Phi$ of the continuous measured signals are calculated. Their deviation throughout a slalom maneuver with 10 full wavelengths is depicted in the error bars of the bottom right plot that show the mean value as well as the p_{10} and p_{90} percentile.
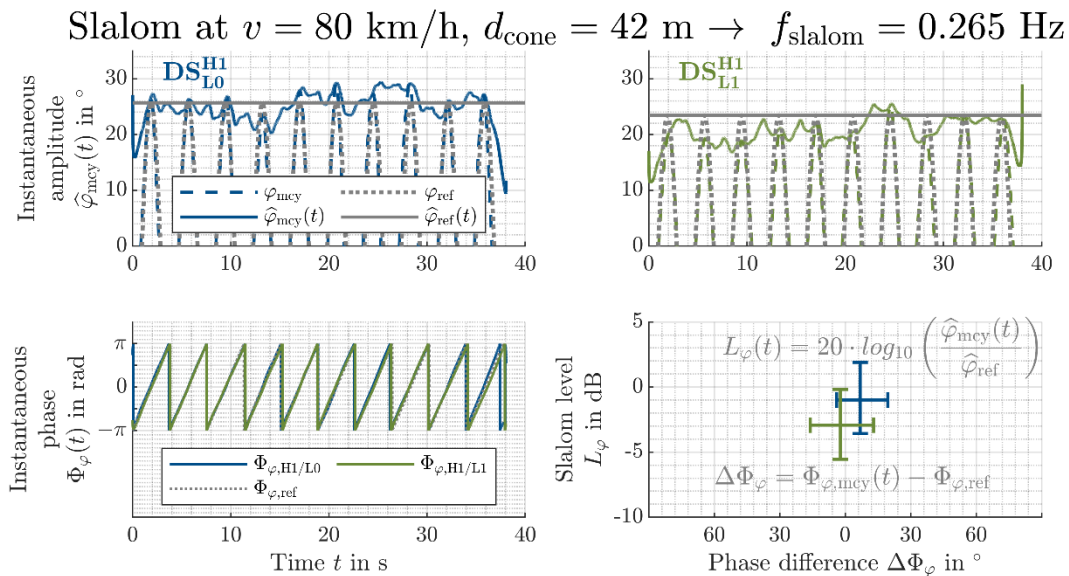
Figure 6.24: Example calculation of slalom level and phase difference. The top plots show the measured roll angle (colored) and the reference value of the steady state approximation (grey). They are used to calculate the slalom roll level (ordinate, bottom right plot). Similarly, the reference roll angle phase is subtracted from the measured phase. The error bars of both level and phase difference range from the p_{10} to the p_{90} percentile during a slalom with 10 wavelengths.

In total, 11 different slalom configurations have been tested according to Table 5.5. They can be grouped in four velocities and three frequencies. The slaloms were performed in DS_{L0}^{H1} and DS_{L1}^{H1} condition. Applying the previously shown method, this results in 22 of the 2-dimensional error bars (bottom right in Figure 6.24) per quantity that is investigated. Figure 6.25 provides an overview about the motorcycle roll angle under all slalom configurations and both DLRC conditions. Upwards pointing triangle markers indicate the DS_{L0}^{H1} condition and downwards facing triangle markers indicate DS_{L1}^{H1} condition. The colors indicate the different set velocities. The slalom frequencies that result from the specific cone distances are proportional to the diameter of the circles of each marker. This allows to identify each specific performed slalom maneuver.
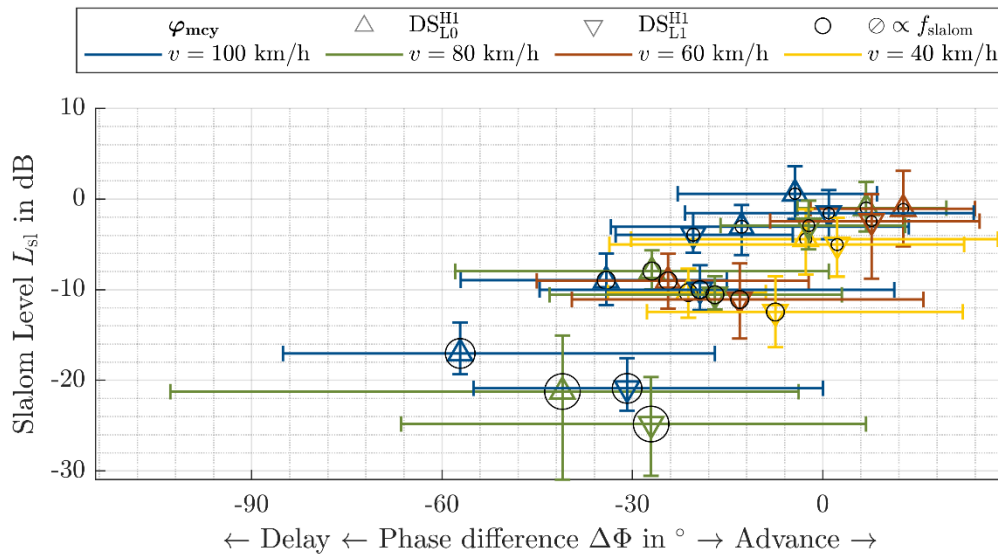

Figure 6.25: Slalom level and phase difference plot of the motorcycle roll angle. DLRC conditions are indicated by the triangle direction. The set velocities are color-coded. Larger circles indicate higher slalom frequencies. The levels and phase differences relate to the reference amplitudes and phases derived from the steady state slalom approximation. The error bars show the mean, p_{10} and p_{90} percentiles of one rider over a slalom maneuver with 10 full wavelengths.

Figure 6.25 shows a pronounced clustering of the data over the slalom frequency. As the frequency increases, the slalom level decreases and the delays with respect to the reference roll angle increase. Obviously, the measurements will come closer to the reference values from the steady state approximation (i.e. $L_{sl} = 0$) when the maneuver becomes less dynamic. The lower slalom levels of the roll angle at higher dynamics are reasonable, as it is beneficial (at least from an energetical standpoint) to reduce the roll angle amplitudes when needing to turn quickly. The slalom levels of the roll angle are always smaller in DS_{L1}^{H1} condition than in the DS_{L0}^{H1} condition. This could – as before – be relatable to needing less motorcycle lean angle, when performing a lean-in motion.

The same effect can be observed, when looking at the slalom levels of the steer angle. Figure 6.26 shows the mockup steer angle levels in all slalom configurations. The layout of the plot is identical with the previous one. As before, the levels of corresponding maneuvers are

lower in the $\text{DS}_{\text{L0}}^{\text{H1}}$ condition. Contrary to the motorcycle roll angle, the steer angle plot shows a pronounced velocity dependent clustering. As the velocity increases, so does the slalom level. The slalom frequency rather affects the phase delay but has a smaller influence on the observed slalom level.
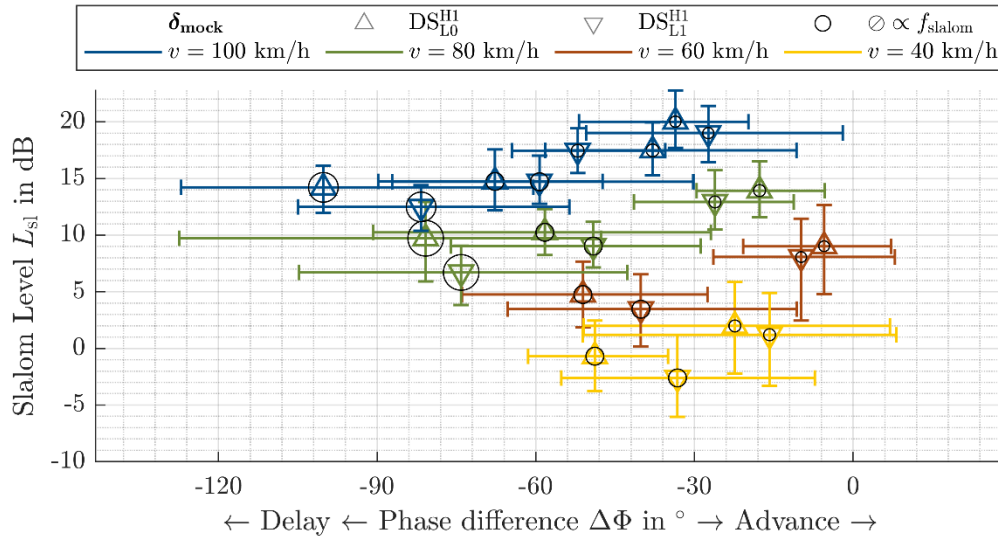

Figure 6.26: Slalom level and phase difference plot of the motorcycle steer angle. DLRC conditions are indicated by the triangle direction. The set velocities are color-coded. Larger circles indicate higher slalom frequencies. The levels and phase differences relate to the reference amplitudes and phases derived from the steady state slalom approximation. The error bars show the mean, p_{10} and p_{90} percentiles of one rider over a slalom maneuver with 10 full wavelengths.

In order to relate the different quantities to each other, it is feasible to show the data in a polar diagram and refer all phase delays to the reference phase of the slalom trajectory, such that the relative phases between the signals can be observed. However, this analysis does not provide additional information for the discussions of this thesis and is therefore only exemplarily shown in Appendix B.9.

6.4.4 Dynamic Maneuver Conclusion

It was previously discussed, that the performance measures known from literature do not suffice to rate the performance during dynamic maneuvers such that they were usable for the evaluation of DLRC capabilities. The tanh-fit method for the evaluation of lane changes and the slalom levels have been used to overcome these shortcomings. Both methods concentrate on rating deviations during the maneuver and it was shown, that the implementation of DLRC led to lesser deviations throughout most of the maneuvers. Still, there remains an uncertainty when using these methods, as they still have to prove themselves in more studies in both real-life testing and on the simulator. Apart of these newly developed evaluation tools, it was shown, that the leaning control loop allows maneuvering through dynamic maneuvers while riding without hands and provokes dynamic vehicle responses that are expected from real riding.

6.5 Naïve Rider Study

The previous sections showed the functionality of DLRC when used by professional riders. Dynamical effects of real motorcycling can be replicated and vehicle states like the steer torque and roll angle are correctly affected. As hypothesized in section 1.2, this improved performance should have a beneficial effect on the accessibility of the simulator to new participants, as it enables participants to apply intuitive control strategies, with the simulator reacting expectedly. This property is referred to as "mental model accordance" in section 4.5 and is tested in the experiment described in section 5.2.

6.5.1 Estimating the Rider Parameters

As described in section 5.2., the study participants firstly experience the simulator by means of a video ride. The torque measurements during that maneuver provide the rider's body parameter estimate, that is double checked against an estimation via the lookup map presented in section 3.2. The participants estimation values are listed in Table 6.1.

Table 6.1: Estimations of rider body parameters via video ride (vid) and look-up method (lu)

Rider	**#1**	**#2**	**#3**	**#4**	**#5**	**#6**
$\beta_{1,vid}$	55,2	88,8	121,5	85,2	52,0	60,8
$\beta_{1,lu}$	45	80	100	68	53	68
$\beta_{2,vid}$	0,61	0,34	0,64	0,16	0,39	0,0
$\beta_{2,lu}$	0	0	0	0	0	0
$\beta_{3,vid}$	-65,2	-75,2	-76,8	-73,4	-61,3	-71,3
$\beta_{3,lu}$	-56	-72	-76	-70	-58	-66

Overall, both estimation methods show comparable results for the estimation of the β_3-parameter, that mainly compensates the gravitational torque, when the hexapod is tilted. The estimation of the β_1-parameter, that mainly compensates the inertial torque due to roll accelerations, shows larger deviations between the two estimation methods. For the following part of the study, the values resulting from the video ride have been implemented.

6.5.2 First Contact

At the beginning of the study, the participants are informed about the motorcycle controls (steering, throttle, brakes, etc.), but not about the possibility to use rider motion as an input to the vehicle dynamics. After the video ride, the participants will start their own ride without any further training. The simulation starts at an initial velocity of 120 km/h as the participant

firstly actuates the throttle (as did the previous video ride). Figure 6.27 shows this moment for two study participants per DLRC condition.
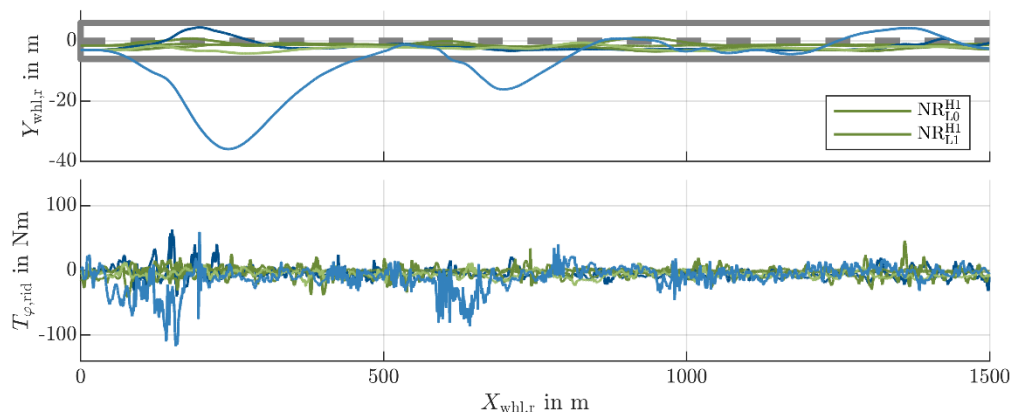

Figure 6.27: First contact to the simulator for four riders with (green) and two riders without (blue) using DLRC. The grey lines in the top plot indicate the road markings. The color shading is used to differ between each two riders per condition. The bright blue rider received help by the experimenter at 250 m and 600 m, before managing to stay on the road on their own.

The top plot shows the vehicle's trajectories on the sketched road. The bottom plot shows the rider induced roll torque of each maneuver. However, only in the maneuvers with activated DLRC (green) these torques are used as input to the vehicle model. The data shows, how the participants in the $\text{NR}_{\text{L0}}^{\text{H1}}$ condition (**N**aïve **r**ider, hands **on**, lean **off**) try to react to the increasing trajectory deviation by actively leaning towards the desired direction of travel, without success. As the vehicle doesn't react to this input, they increase their leaning such that the rider induced roll torques become considerably high compared to the values reached in the $\text{NR}_{\text{L1}}^{\text{H1}}$ condition. There, only small torque inputs can be observed and the trajectories maintain well within the road limits. The participant that was constantly departing from the road received help from the experimenter to return to the road. After handing the controls over to the rider again, the same behavior is observed again at around 600 m. Only at the end of the initial straight, the rider succeeds to stay on the road and continued the study without interventions by the experimenter until the second to last level of the study.
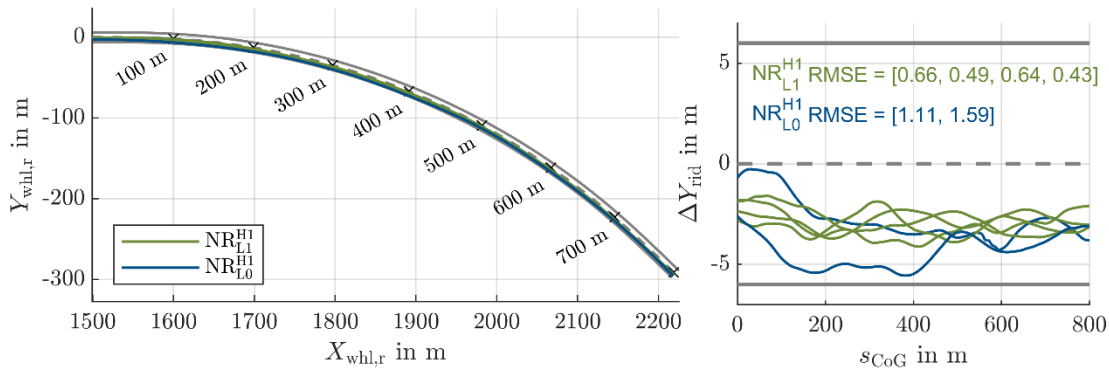
Figure 6.28: First contact of the participants to a wide curve ($\varphi_{\text{th,target}} = 5°$ at 100 km/h). The left plot shows the map of the segment. The right plot shows the lane position of each rider. The DLRC condition is color coded. The RMSE of the lane deviation is stated for each of the six riders.

Figure 6.28 shows the first cornering maneuver of three participants per DLRC condition. The riders in the $\text{NR}_{\text{L1}}^{\text{H1}}$ condition struggle less to follow the road and stay well within the middle of the lane, while in the $\text{NR}_{\text{L0}}^{\text{H1}}$ condition, higher deviations are observed. This manifests in higher RMSE values of the rear tire's lateral lane position (right plot).

After this initial phase of the study, the actual testing with consecutive open ride maneuvers, reference maneuvers and slalom maneuvers started, as described in section 5.2.3.

6.5.3 Reference Maneuver Straight

At the start of every reference maneuver, the participants were going in a straight line before entering the reference curve. Figure 6.29 shows the empirical cumulative distribution function (eCDF) of the roll rates during that passage. Each line contains the data of all participants in that condition over all straights that were performed at equal velocities.

For the $\text{NR}_{\text{L0}}^{\text{H1}}$ condition, this results in only one rider after level 3, as the other participant ended the study there. The singular eCDF plots for each level of the track with single lines per rider are depicted in Appendix C.1.
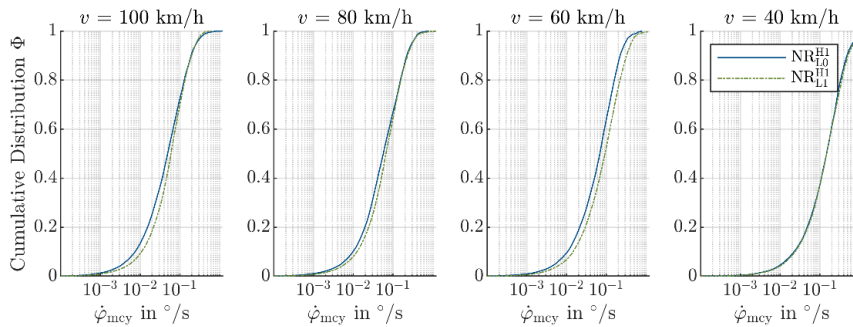

Figure 6.29: eCDF of the roll rates during straight running segments of the reference meanuever. Each line contains the measurements of all riders at the specific DLRC condition and speed.

The eCDF was also evaluated from professional riders during straight running in section 6.1.1. The p_{95} percentiles of the roll rates are depicted in Figure 6.3. The values observed here reach higher values than the reference data both with and without the use of DLRC.

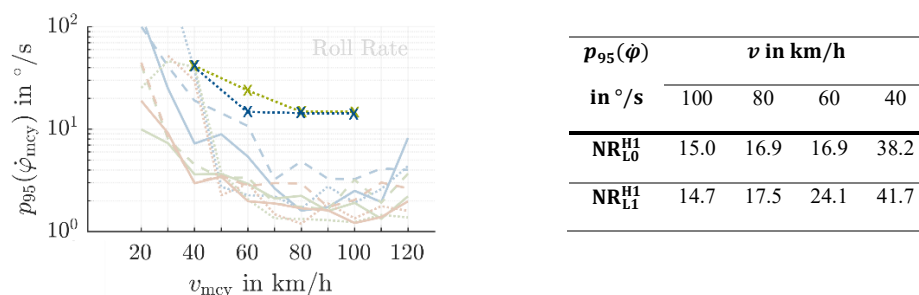| $p_{95}(\dot{\varphi})$	v in km/h			
in °/s	100	80	60	40
NR_{L0}^{H1}	15.0	16.9	16.9	38.2
NR_{L1}^{H1}	14.7	17.5	24.1	41.7

Figure 6.30: Referencing the observed roll rates to the data from professional riders. The faded plot in the background corresponds to the top left plot in Figure 6.3. The crosses mark the p_{95} percentiles of the roll rates in the naïve rider study in the NR_{L0}^{H1} condition (blue) and NR_{L0}^{H1} condition (green).

The slightly increasing roll rates also manifest in increasing values of lane deviations, as Figure 6.31 exemplarily shows. The exact lane position was not constrained except for the lane markings and the participants were free to choose their line on their own. Thus, offsets of the mean values may not be rated negatively. Especially at the lowest tested velocity of 40 km/h, the riders struggle to maintain on the lane in the NR_{L1}^{H1} condition.
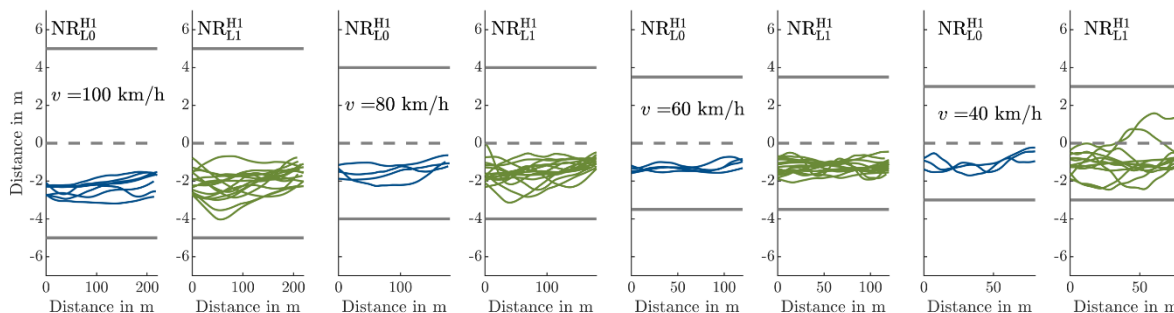
Figure 6.31: Lane deviations during straight running segments in the reference maneuver.

6.5.4 Reference Maneuver Curves

A similar behavior is observable in the reference curve and overtaking maneuver that followed on the previously discussed straight segment. While the study participants that didn't struggle with sickness symptoms were capable of maneuvering through all 60 km/h levels, they eventually failed in one of the 40 km/h reference curves or latest in the 40 km/h slalom that ended the track. Figure 6.32 shows a few exemplary roll angle timeseries of different levels. Therein, the track length is normalized to the length of the curve segment. The roll angle oscillations increase heavily with decreasing velocities. Due to the vast scattering of the data and the missing representation of the NR_{L0}^{H1} condition (only one dataset is available in the later levels), a comparison of performance measures is at this point not possible by evaluating the simulator measurements.

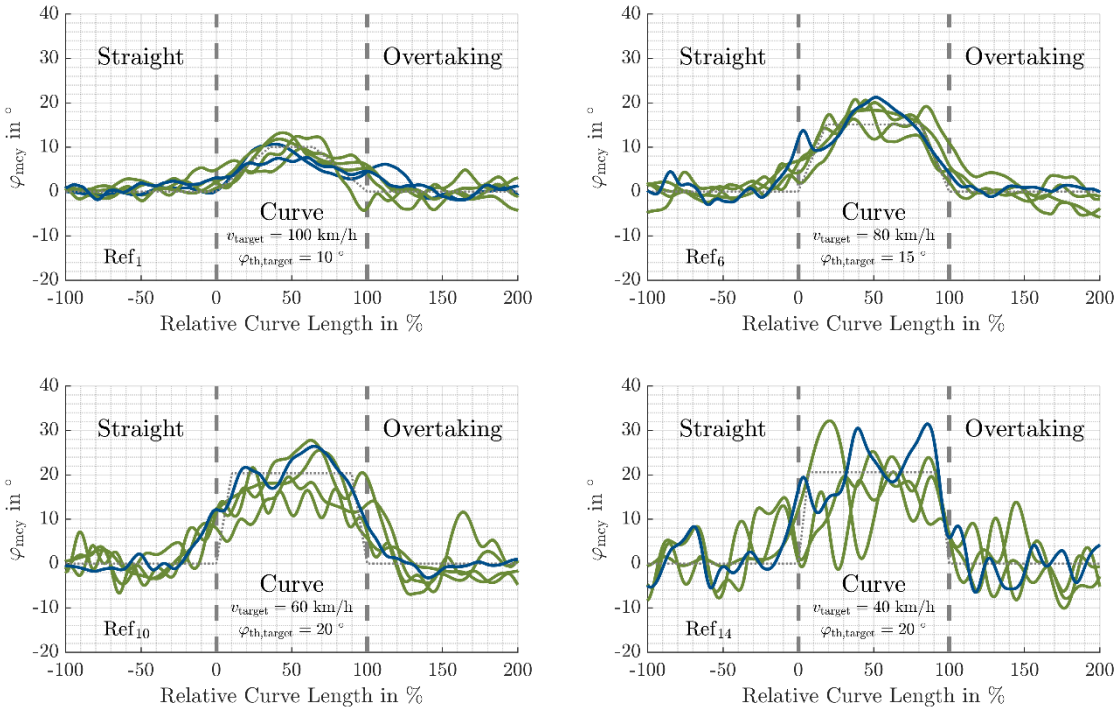Figure 6.32: Roll angle timeseries of the reference scenario in different levels of the study. The NR_{L0}^{H1} condition (blue) is only tested by one rider at velocities below 100 km/h. The simulator shows high amounts of oscillations for riders in both NR_{L1}^{H1} condition (green) and NR_{L0}^{H1} condition (blue).
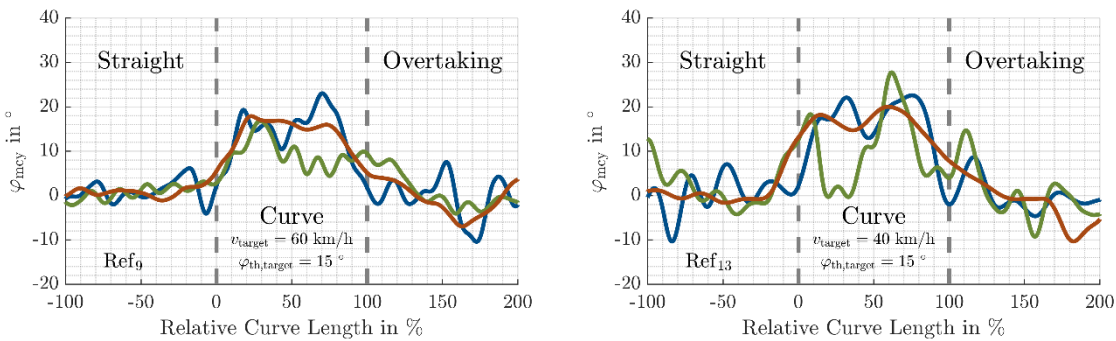
Figure 6.33: Roll angle timeseries of the three riders (color-coded) in NR_{L1}^{H1} condition only.

There exist however large interindividual differences among the riders. Figure 6.33 shows the roll angle timeseries for just the three participants in the NR_{L1}^{H1} condition. Participant #4 (green) shows large, valued roll angle oscillations throughout almost all maneuvers, while participant #5 (red) shows the least amount of oscillations among all participants.

6.5.5 Reference Lane Change and Slalom Maneuvers

The reference segments ended with an overtaking maneuver that was supposed to provoke a lane-change maneuver in a natural manner. However, due to the vast amount of oscillations some of the riders experienced through the reference curves, they often opted for a less demanding trajectory by e.g. exiting the curve on the outside lane, or they performed harsh

maneuvers to quickly get past the car rather than performing clean and distinct lane changes. Therefore, no further evaluation of the lane change maneuvers is performed in this pilot study. The same is true for the slalom maneuvers. These have been aborted by some of the riders, as they suffered from dizziness.

6.5.6 Subjective Evaluation

In section 5.2.4, questionnaires were presented that the study participants had to answer during the study. After every performance of a reference maneuver, the riders were supposed to answer three questions about the rideability of the previous section (rated from -6 "very ponderous" to +6 "very instable"), about the workload in the previous section (rated from 0 "none" to 15 "very much") and about the perceived realism (rated from 0 "not at all" to 15 "very realistic"). The ratings are listed in Table 6.2, but for now cannot provide a reliable picture to rate the effect of DLRC, as participant 6 is the only one finishing the study without the use of DLRC.

The empty fields in Table 6.2 result from the riders ending the study after experiencing sickness symptoms (rider #2 from level 3 on, rider #3 from level 11 on) or from the inability to formulate answers to the questionnaire, as e.g. the rider was expressing their experiences and perceptions rather than just providing a number rating (rider #3 and #6 in a few of the first levels). Overall, the ratings tend towards the vehicle being nervous or even unstable (positive values in the rideability rating) and the workload being rather high (values above 9 in the workload rating). Expectedly, the realism rating depended highly on the perceived oscillations. Therefore, rider #4 shows very low ratings, while rider #5 rates the realism higher.

Table 6.2: Subjective ratings during the naive rider study. Each column contains the ratings from one rider. The bottom row contains the overall rating that was provided after the study.

Rating		Rideability (-6…6)						Workload (0…15)						Realism (0… 15)					
Rider		1	2	3	4	5	6	1	2	3	4	5	6	1	2	3	4	5	6
DLRC		1	0	1	1	1	0	1	0	1	1	1	0	1	0	1	1	1	0
Level																			
Reference Maneuver	1	2	2	4	5	-2	4	10	8	3	14	9	12	13	8	7	2	7	2
	2	0	2	2	2	1		5	8	2	10	8		13	10	8	5	9	
	3	0			2	1		4			5	9		13			5	7	
	4	0		3	4	0	0	6		10	8	6	6	12		2	4	10	7
	5	5			4	1	2	13			9	9	6	2			3	9	6
	6	2		4	5	1	0	7		10	10	8	6	5		6	3	9	6
	7	2		3	4	2	0	7		11	10	8	6	8		6	3	9	7
	8	0		5	3	0	0	6		13	11	8	4	12		2	3	9	8
	9	4		5	5	0	3	11		13	12	7	8	3		3	2	10	5
	10	2		6	5	0	0	9		15	11	7	8	8		2	2	10	6
	11	-2			6	0	0	12			15	7	7	4			1	9	7
	12	-1			5	0	0	7			13	7	6	10			3	10	7
	13	4			6	1	2	12			15	9	9	3			1	7	6
	14	5			6	2	2	14			15	9	10	1			1	7	6
	15	5			6	3		14			14	10		1			2	6	
	16				2							10						6	
Slalom	1	-2		5		-2	0	12		15		10	7	14		1		9	7
	2	1		4	5	3	0	10		11	13	10	10	9		4	3	7	7
	3	0			5	0	0	6			14	10	6	14			2	8	8
	4																		
Overall		3			4	1	1							11			2	10	7

148

7 Conclusion and Outlook

In this thesis, the effects of a Dual Loop Rider Control Mechanism was investigated. The DLRC was realized by means of a mechatronical system that measures the rider induced roll torque and uses this as an input on the DESMORI dynamic motorcycle riding simulator.

7.1 DLRC Design Review

In Chapter 3, the design of the DESMORI simulator and its DLRC system were presented. The simulator proved to be applicable in multiple studies and the DLRC proved to affect the vehicle dynamics as expected from real life in many scenarios. However, it is shown that the developed system depends on a set of rider parameters that are cumbersome to estimate (section 3.2), which is especially disadvantageous when the study does not allow for iteratively tuning these parameters for the participant, as it is for example the case in the naïve rider study presented above. While the force based measurement is in the end preferred against optical rider motion measurements, the issue remains that there is no feasible method to generate baseline values from real road testing with regard to the rider induced roll torque.

7.2 Performance Measure Review

In Chapter 4, performance measures were derived that allow rating the performance of the simulator with and without DLRC in various scenarios. It was shown, that several measures known from literature do not suffice for that purpose. Especially for the discussion of dynamic maneuvers, no sufficient ratings were available. Two approaches have been presented, to overcome this issue. The tanh-fitting method for the evaluation of lane change maneuvers was applicable for this use case and allows to rate the precision and repeatability of the maneuver by a small set of characteristic values. The newly developed slalom levels are based on a steady state slalom approximation that allow to generate an absolute baseline for a specific slalom maneuver. Both methods however must still be validated in a larger number of studies on the simulator as well as in real life testing.

7.3 Study Design Review

In Chapter 5, the studies performed in this research have been presented. The expert study allowed to show the dynamic effects that DLRC has on the virtual motorcycle. However, the naïve rider study showed, that such effects are not necessarily transferrable to normal riders. Specific remarks to single experiments are provided in the following.

7.4 Study Results

The following sections review the main outcomes of the performed studies and discuss the hypotheses that were presented in section 2.6.

7.4.1 Expert Rider Study Review

In the expert study, multiple effects of using DLRC were observed. Firstly, the stationary straight maneuvers showed decreasing amounts of lateral dynamic quantities in the SS_{L1}^{H1} condition. The scenario was rideable in the SS_{L1}^{H0} condition, where it showed the least amount of e.g. vehicle roll rates at high velocities. This indicates, that the steering input provokes a substantial fraction of the vehicle oscillations, just by a rider being attached to the handlebar. The coast down maneuver showed a reduced velocity boundary for both CD_{L1}^{H1} condition compared to the CD_{L0}^{H1} condition and the CD_{L1}^{H0} condition compared to the CD_{L0}^{H0} condition.

In the transient maneuvers it was proved that DLRC allows to achieve changes in vehicle states that are not possible in the state-of-the-art condition with only using a steering input. The TS_{L1}^{H1} condition allowed to vary the motorcycle roll angle while continuing to run in a straight line. The TC_{L1}^{H1} condition also showed realistic effects, as the adjusted vehicle roll angles and steer torques, resulting from the rider's leaning motion while riding on an equal trajectory at equal velocity. Furthermore, the TC_{L1}^{H0} condition allowed to maneuver through various curvatures without hands. Thereby, the limitations of that control cue at high velocities were observable, as expected from real life riding.

The dynamic maneuvers have shown only small effects of DLRC. Both lane-change and slalom maneuver signals were dominated by the overall vehicle dynamics and only minor changes were observed, when activating DLRC. The DL_{L1}^{H1} condition showed a reduced amount of steer torque compared to the DL_{L0}^{H1} condition and therefore a reduction of the Lane-Change-Roll index, which is expected when the rider performs lean-in. A slight reduction of the RMS error in the tanh-fitting method was observed, indicating smoother lane transitions. The DL_{L1}^{H0} condition prove to be rideable and showed realistic dynamic effects, like the motorcycle roll angle response to rider lean excitations when initiating the lane-change. The newly introduced slalom levels are designed to overcome limitations of other slalom ratings known from literature that only allow for a relative assessment between different vehicles or configurations. However, only minor effects were observed when changing from the DS_{L0}^{H1} condition to the DS_{L1}^{H1} condition. The observed level reductions and changes in phase offsets are small. The variance of the levels and phase offset within 10 wavelengths of the slalom reduces for high velocities, but the overall effect is insignificant. This indicates, that the dominant input in the dynamic maneuvers – as expected – is the steering input and improvements in the simulator performance in dynamic maneuvers will most likely be achieved by improvements in steering controllers.

7.4.2 Naïve Rider Study Review

The data collected in the naïve rider study cannot provide a deep insight to rate the performance of the simulator with activated DLRC against the simulator with deactivated DLRC. The only outstanding effect can be observed at the very instance of the test ride, where the two riders in the $\mathrm{NR_{L0}^{H1}}$ condition made high efforts to return to their desired lane by applying high rider induced roll torques which were, however, inactive in that condition. All other riders that participated in the $\mathrm{NR_{L1}^{H1}}$ condition were immediately able to stay on their lane without any support from the experimenter.

Apart from that, the study participants showed large amounts of vehicle oscillations and struggled to control the simulator especially as the velocities decreased. The beneficial effect of DLRC reducing the amount of vehicle roll rates known from the $\mathrm{SS_{L1}^{H1}}$ test was not observable here. One reason for that might be the imperfection of the rider parameter estimation presented in section 3.2. Unfortunately, the quality of the parameter estimation cannot be quantified here and given the nature of the naïve rider study, it is not possible to e.g. iterate towards better fitting parameters, as it is possible in professional use of the simulator or after a longer simulator familiarization.

It was argued in section 4.5 and 5.2 that rating the mental model accordance is only applicable when testing with naïve riders. However, this necessitates that the DLRC configurations must be tested from separate groups of participants (i.e. a between-subject study design). Given the large interindividual differences, this results in a large number of study participants that are needed to find statistically relevant results between the two groups. For a follow-up study, it is therefore suggested to switch from this between-subject-design to a within-subject-design of the study coping for potential sequence effects (i.e. learning) by means of permuted conditions with randomized assignment of participants to the groups. This might give the benefit of a relative subjective rating of the simulator with and without DLRC from each rider.

Furthermore, a more reliable method for the identification of rider parameters is needed or tuning of these parameters must become a specific aspect of that study. The performance of the DLRC presented here is highly depending on estimating the platform induced roll torques. Errors in that estimation result in implausible roll torque inputs to the vehicle dynamics model and could result in the observed oscillations.

Two of the participants suffered from sickness symptoms and willingly ended their study when performing a slalom maneuver. These have also been reported from the other participants to provoke the highest discomfort. This might result from the continuously high visual roll rates presented to the rider, or from misperceptions caused by the motion cueing. For a future study design, it is suggested to reduce the duration of the experiments and perform maneuvers that are less prone to causing sickness symptoms.

7.5 Checking The Hypotheses

In section 2.6, it was hypothesized that a DMRS will benefit from the implementation of DLRC in different aspects:

- *H_{Wa}: It will provide an additional controllable input allowing simulator riders to intentionally changing vehicle states.*

Firstly, DLRC was supposed to provide an additional controllable input capable of intentionally changing equilibrium in steady state conditions. The results from sections 6.1 and 6.3 proved, that this really is the case. The system is capable of affecting the motorcycle trajectory in an intuitive matter. The curvature of the virtual motorcycle's trajectory can be purposely changed just by means of leaning motion. Thereby, the motorcycle shows realistic reactions, like a variation in motorcycle roll angle, changes in the steady state steer torque, or limitations of this control cue at higher velocities.

- *H_{Wb}: It will show more realistic vehicle responses in lateral dynamic maneuvers.*

Secondly, DLRC was supposed to increase the fidelity in lateral dynamic maneuvers. For this thesis, a lane change and slalom maneuver have been selected to test this hypothesis. In these, a reduction of steering efforts was observable, when a rider made use of lean in. When riding without hands, realistic effects, like the counter-leaning motion of the motorcycle frame due to the support of rider inertial forces were observed. Two new methods have been applied to rate the maneuver performance. The tanh-fitting for evaluating the lane change maneuver, and the steady state slalom approximation that resulted in so called slalom levels for various kinematic quantities. However, the experiments showed overall only small effects when adding DLRC to the system. A slight reduction of steer torques, roll angles and other quantities was observed, while the overall quality of the maneuvers did not change much. This indicates, that with increasing dynamics, the importance of the rider induced roll torque shrinks compared to the steering inputs. The steering is obviously still the most effective input to the motorcycle's lateral dynamics. Nevertheless, DLRC was able to add realistic action-effect patterns that were not present in state-of-the-art DMRS.

- *H_{Wc}: It will ease access to the simulator to naïve riders.*

Thirdly, DLRC was supposed to ease access to the simulator for naïve riders. In a participant study with motorcyclists, who have never been using a dynamic motorcycle riding simulator before, it was found, that the use of DLRC was helping at the very first moments of riding the virtual motorcycle. The participants that did not use DLRC on the contrary struggled with maneuvering over the first few hundred meters until getting used to the steering behavior of the simulator. The further maneuvers and subjective evaluations could however not show a significant effect of DLRC due to the small number of participants and overall workload and struggle of riding.

▪ *H_{Wd}: It will reduce the simulator's achievable low speed boundary through stabilizing effects induced by rider impedance and motion.*

Lastly, DLRC was supposed to reduce the simulator's achievable low speed boundary through stabilizing effects induced by rider impedance and balancing motion. The results have shown, that the realized DLRC is in fact capable of reducing vehicle oscillations at low speeds. However, "low" in terms of motorcycle riding simulators is still high compared to real motorcycling. The troublesome dynamic area of the motorcycle simulator will begin at around 40 km/h. From there on, a trained rider will be able to control and stabilize the motorcycle until about 30 km/h, but at less than 20 km/h there is still a need for artificial stabilization that typically does not allow for realistic single-track vehicle behavior anymore.

▪ *H_1:DLRC capabilities increase the fidelity of lateral dynamic behavior on motorcycle simulators, as they enable riders to employ control strategies known from real riding.*

It is therefore concluded that the use of DLRC is in general beneficial for dynamic motorcycle riding simulators. It allows to utilize behavioral patterns and control modes, that are known from real riding but are ineffective on simulators without DLRC. It also allows to provoke vehicle states that are impossible to achieve when only one rider control loop is available. However, adding DLRC capabilities to a DMRS is not sufficient to overcome the challenges that still exist in the domain of dynamic motorcycle riding simulators, like the steering force feedback controllers and motion cueing.

7.6 Outlook

The DLRC realized in this thesis works properly and provides good controllability and can help at stabilizing the virtual motorcycle while impacting the handling only a little. The additional control cue allows riders to utilize realistic control behavior and they will experience a realistic response. However, it is still a highly demanding task to control the simulator for several riders. As mentioned above, this likely results from the steering force feedback controller, which has the largest effect on the motorcycle lateral dynamics. Future research and development should therefore concentrate on the steering simulation in order to improve the overall riding behavior. There, a promising concept lies within hybrid impedance-admittance controllers. These could improve the steering behavior such that at lower speeds it rather accepts steer angles as input to the vehicle dynamics and providing a torque feedback, while at high speeds the handlebar becomes more stiff, measuring torques and feeding back the handlebar position. However, this will not only effort improvements in control theory but also necessitate changes in the vehicle model to allow for such kind of hybrid control.

The DLRC realized in this thesis relies on an estimation of rider body parameters, that are used to estimate the platform induced roll torque. For this parameter estimation the rider is assumed to be a rigid point mass located in the center plane of the motorcycle. This

estimation is prone to errors and these are tedious to investigate, as a non-professional study participant will not be able to formalize any issues they might have with the system and the experimenter can hardly correct any false estimations without "feeling" on the motorcycle what's wrong. For future work it is suggested to look into sensor data fusion of both force-based measurements and position-based measurements.

The DLRC realized in this thesis allows to affect the virtual motorcycle in the lateral direction. This is fair and at least one step further as other comparable simulators go. However, one substance of this thesis is the statement, that the rider body's influence must not be neglected on motorcycle riding simulators. In consequence, it is suggested to also track the riders longitudinal and vertical motion such that e.g. a change in wheel loads due to rider front/back movement or a vehicle suspension response to rider vertical motion can be simulated. A promising concept to measure both the rider induced roll- and pitch-torques while being less sensitive to the placement of the mechanical roll axis on the simulator platform has been developed by Delgado[162], but was not yet realized. All such cues might result in higher subversive acceptance, meaning that a rider might not consciously perceive this effect and consider it plausible, but that they unconsciously accepts the presented system as a real motorcycle rather than a simulator, even without being able to formulate why.

The measurements and effects described in this thesis relate to general motorcycle behavior and effects known from literature and personal riding, as it was not yet the goal to simulate one specific type of motorcycle and represent its dynamics. Current, yet unpublished work however indicates, that professional simulator riders can identify different vehicle types in a blind test. The next step in the quality rating of DLRC should therefore be testing it with validated models against real vehicles. This however poses the difficulty, that for the torque determination used in this thesis, there exists no simple way to measure baseline values in real motorcycling. There, only camera-based measurements of the rider lean angles have successfully been used in research. Therefore, either a measurement method must be developed to determine the rider induced roll torque on a real motorcycle, or position-based measurements must be implemented on the simulator. Such a position-based measurement could be used to validate the existing system, or to further improve the quality of the DLRC through sensor data fusion.

---

[162] Delgado, R.: Master Thesis, Integrierte Roll- und Nickmomentenmessung auf einem Simulator (2018).

A Appendix

A.1 Vehicle Model Parameters

Parameter	Size
Total mass (Mcy + Rid)	182 kg + 75 kg
Wheelbase	1.46 m
Steering head angle	24°
Steering offset	36 mm
Swingarm length	666 mm
Engine & Transmission	34 kW, 60 Nm, 6-Gear
Tires	120/70/R17, 180/60/R17

A.2 Simulation Parameters

Parameter	Size	
Loadcell lever	0.131 m	
Loadcell precision	2 mV/V	
HarmonicDrive ratio	80	
Maximum Steer Angle	±18 °	
Maximum Steer Rate	5 rad/s (287 °/s)	
Steer Controller P	27	
Steer Controller I	0.16	
Steer Controller N	100 (filter constant)	
Steer Controller T	0.1	Lowpass of BRT Steer angle

A.3 Aström K-Factors
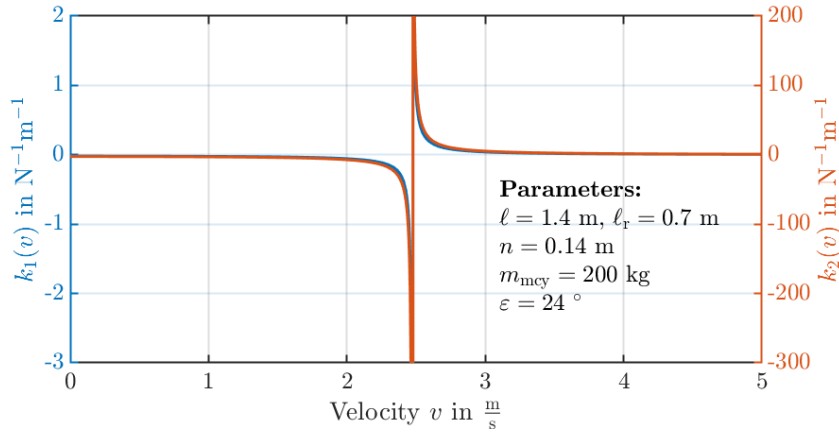
Figure A.1: k-factors according to Aström. Own representation based on Aström's[50] equations.

A.4 Gyroscopic Effect Induced Damping

Consider the front assembly of a motorcycle containing of a wheel and fork being aligned vertically.

The gyroscopic moment of the front wheel results to

$$\begin{bmatrix} M_x \\ M_y \\ M_z \end{bmatrix} = \begin{bmatrix} \Theta_x \cdot \omega_x \\ \Theta_y \cdot \omega_y \\ \Theta_z \cdot \omega_z \end{bmatrix} \times \begin{bmatrix} \omega_x \\ \omega_y \\ \omega_z \end{bmatrix} \tag{A.1}$$

Assuming that

$$\begin{bmatrix} \omega_x \\ \omega_y \\ \omega_z \end{bmatrix} = \begin{bmatrix} \dot{\varphi} \\ v/r_{\text{dyn}} \\ \dot{\psi} + \dot{\delta} \end{bmatrix} \tag{A.2}$$

And that the simplified yaw rate at steady state cornering is calculated as

$$\dot{\psi} = g \tan(\varphi)/v \tag{A.3}$$

The two relevant moments around the assembly's vertical ("steering") and longitudinal ("roll") axis result to

$$M_x = \Theta_y \cdot \left(g \tan(\varphi)/v + \dot{\delta} \right) \cdot v/r_{\text{dyn}} \tag{A.4}$$

$$M_z = -\Theta_y \cdot \dot{\varphi} \cdot v/r_{\text{dyn}} \tag{A.5}$$

The teering rotation can be expressed by the sum of the gyroscopic moment and all other torques acting around the steering axis (rider steer torque, tire-road-interaction) as $T_{\text{s,ax}}$

$$\Theta_{\text{steer}} \ddot{\delta} = M_z + T_{\text{s,ax}} \tag{A.6}$$

Laplace transformation of each differential equation above yields to

$$M_x(s) = \Theta_y \cdot \left(\frac{g}{v}\varphi(s) + \frac{\delta(s)}{s}\right) \cdot v/r_{\text{dyn}} \tag{A.7}$$

$$M_z(s) = -\Theta_y \cdot \frac{\varphi(s)}{s} \cdot v/r_{\text{dyn}} \tag{A.8}$$

$$\Theta_{\text{steer}} \frac{\delta(s)}{s^2} = M_z(s) + T_{\text{s,ax}}(s) \tag{A.9}$$

Combining and rearranging the second and third formula yields to

$$\frac{\delta(s)}{s} = -\frac{\Theta_y}{\Theta_{\text{steer}}} \cdot \frac{v \cdot \varphi(s)}{r_{\text{dyn}}} + \frac{T_{\text{s,ax}}(s)}{\Theta_{\text{steer}}} \cdot s \tag{A.10}$$

Combining and rearranging this equation with the longitudinal torque M_x equation yields

$$M_x(s) = \Theta_y \cdot \left(\frac{g}{v}\varphi(s) - \frac{\Theta_y}{\Theta_{\text{steer}}} \cdot \frac{v \cdot \varphi(s)}{r_{\text{dyn}}} + \frac{T_{\text{s,ax}}(s)}{\Theta_{\text{steer}}} \cdot s\right) \cdot \frac{v}{r_{\text{dyn}}} \tag{A.11}$$

With

$$\varphi(s) = s \cdot \dot{\varphi}(s) \tag{A.12}$$

this expression can be simplified as

$$M_x(s) = \left(\frac{\Theta_y g}{r_{\text{dyn}}} - \frac{\Theta_y^2 v^2}{\Theta_{\text{steer}} r_{\text{dyn}}^2}\right) s\dot{\varphi}(s) + \left(\frac{\Theta_y v}{\Theta_{\text{steer}} r_{\text{dyn}}}\right) sT_{\text{s,ax}}(s) \tag{A.13}$$

This equation contains the gyroscopic effect on the motorcycle roll torque due to roll rates (left part) and steer torques (right part)

The function shows a damping behavior of the gyroscopic effect (i.e. the moment $M_x(s)$ acts in the opposite direction of $\dot{\varphi}(s)$), if the expression in the first bracket is negative:

$$\frac{\Theta_y}{\Theta_{\text{steer}} r_{\text{dyn}}} v^2 > g \tag{A.14}$$

Therefore, the gyroscopic effect causes a damping of the roll motion that increases with velocity and the inertia of the rotating wheel Θ_y, and decreases with the inertia of the steering assembly Θ_{steer} and wheel radius.

The right term of the equation shows the "counter-steering" effect, as positive torques around the steering axis (i.e. turning left) generate positive roll torques (i.e. rolling right).

A.5 Power Spectrum Evaluation

To analyze the stochastic lateral dynamic signals during straight running, the power spectrum is calculated according to the following process:

Firstly, the signal measured during straight running is cut such that it has a length of $2^n, n \in \mathbb{N} > 0$ samples. This signal is then windowed with a Tukey-Window and a fast Fourier transformation is performed, resulting in the amplitude spectrum $\hat{A}(f)$.

According to Kammeyer[163] the power spectral density (PSD) results from normalizing the product of the FFT and its complex conjugate $\hat{A}^*(f)$ by the spectral resolution Δf

$$PSD_{f\pm} = \frac{\hat{A}(f) \cdot \hat{A}^*(f)}{\Delta f} \tag{A.15}$$

Adding the power from positive and negative frequencies yields to

$$PSD_{f>0} = 2 \cdot PSD_{f\pm}(f > 0) \tag{A.16}$$

Each of the n_t 1/3-octave bands is divided into n_f frequency samples at

$$f_i = f_0 \cdot \left(2^{\frac{1}{3}}\right)^{\frac{i-n_f}{n_f}} \quad i = 0,1,2,\dots,(n_f \cdot n_t + 1) \tag{A.17}$$

Of band width

$$\Delta f_i = f_i \cdot \left(2^{\frac{1}{3}}\right)^{\frac{0.5}{n_f}} - \left(2^{\frac{1}{3}}\right)^{\frac{-0.5}{n_f}} \tag{A.18}$$

The equidistant PSD is interpolated onto this new frequency grid by using Piecewise Cubic Hermite Interpolating Polynomials with the *interp1* function in MATLAB.

A Hanning window with 50% overlap around each 1/3-octave's center frequency is used when calculating the RMS value

$$RMS_{\text{third}} = \sqrt{\sum_{2/3 \, oct.} \text{hann}_i \cdot PSD_i \cdot \Delta f_i} \tag{A.19}$$

---

[163] Kammeyer, K.-D.; Kühn, V.: MATLAB in der Nachrichtentechnik (2001).

B Simulator Measurements

B.1 Constant Radius Cornering Subgroups

The following figures show the change of vehicle states under different leaning conditions, as discussed in subsection 6.3.2 and shown in Figure 6.9. Each column of plots represents one rider. The set speed is color coded; the target theoretical roll angle is coded via line style. The error bars indicate means and standard deviations within a 180° constant cornering segment. Top to bottom: Rider induced roll torque, steer torque, lean-turn-index, steer-turn-index and roll angle. Each figure shows a subgroup of the data, concentrating on either just one velocity or one roll angle.
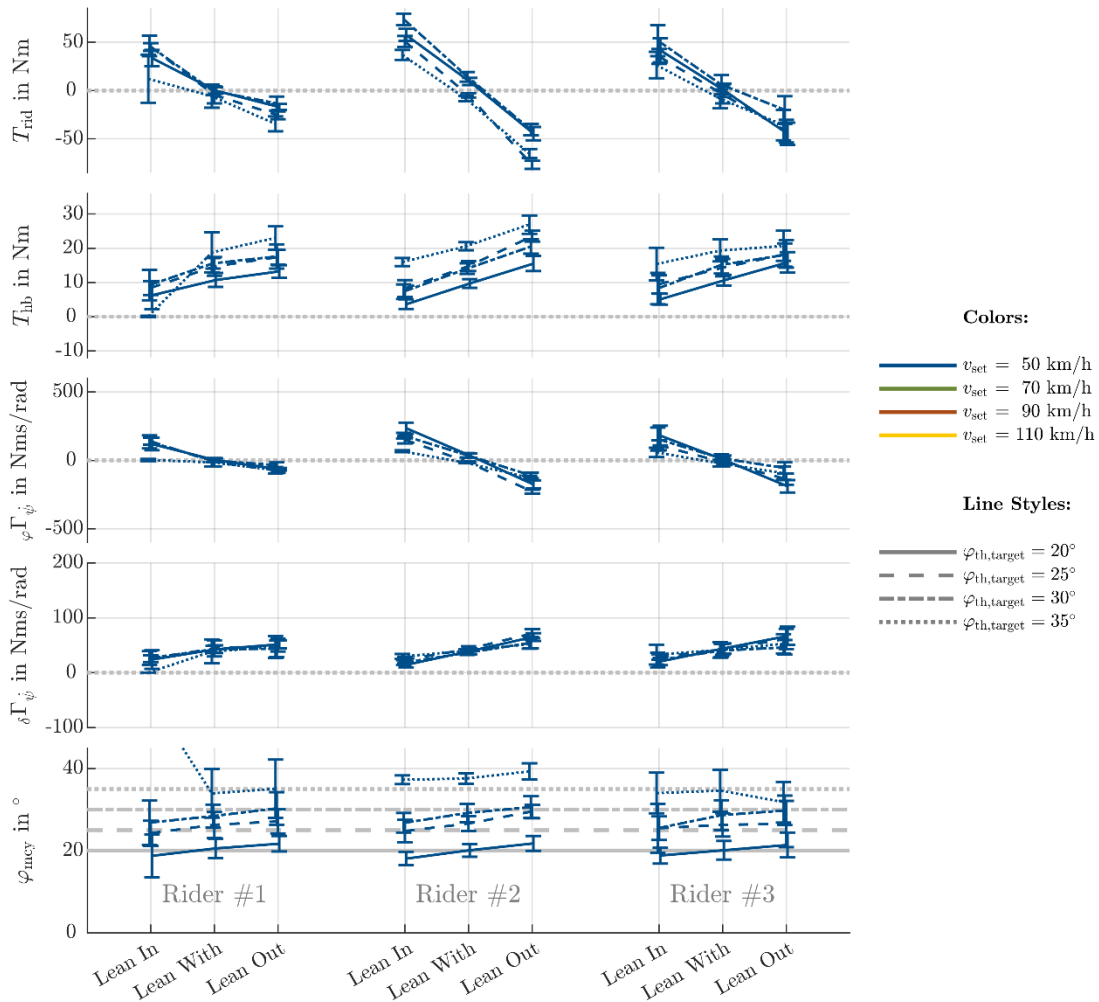
Figure B.2: Vehicle states under different leaning conditions (1) during constant cornering at 50 km/h. Rider 1 fails in the lean in condition at 35° target roll angle.
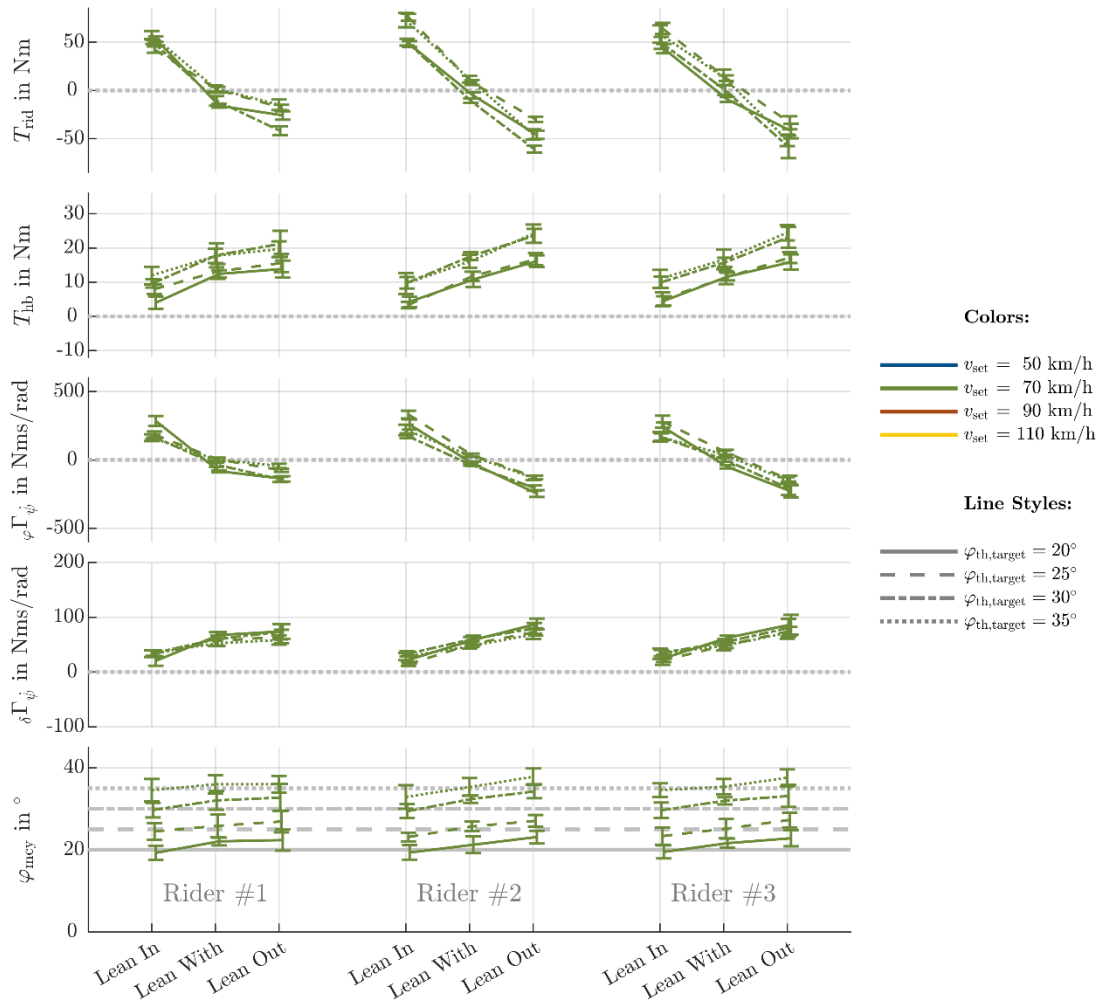
Figure B.3: Vehicle states under different leaning conditions (2) during constant cornering at 70 km/h.
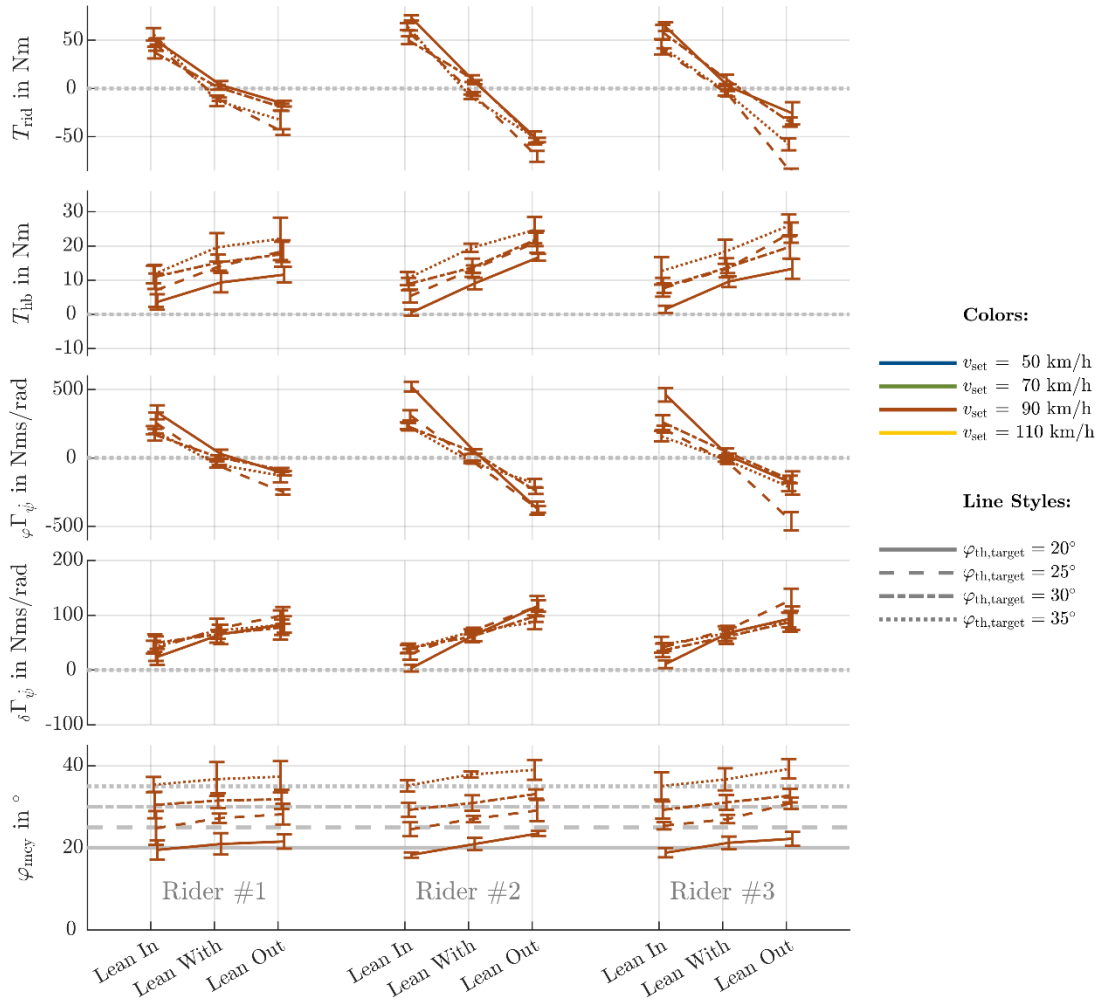
Figure B.4: Vehicle states under different leaning conditions (3) during constant cornering at 90 km/h.
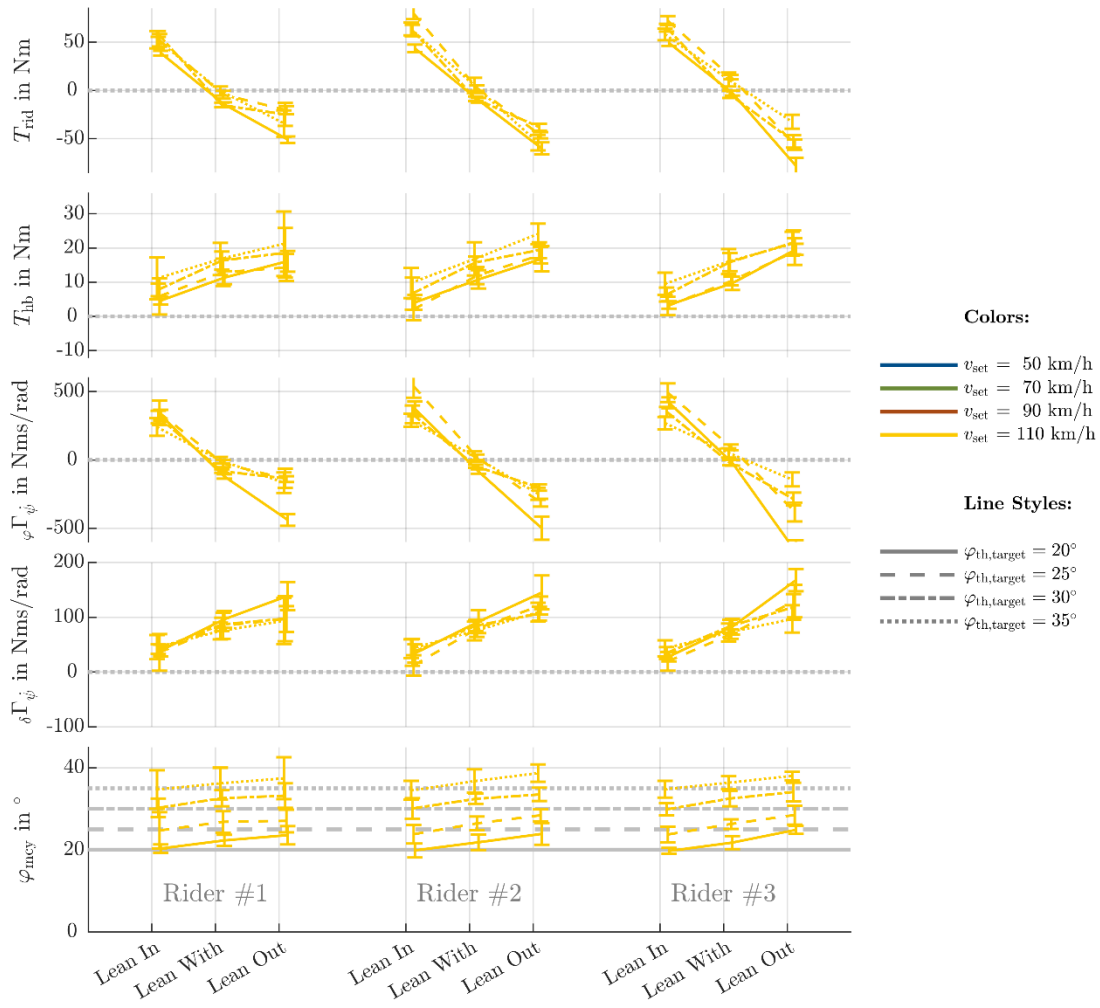
Figure B.5: Vehicle states under different leaning conditions (4) during constant cornering at 110 km/h.
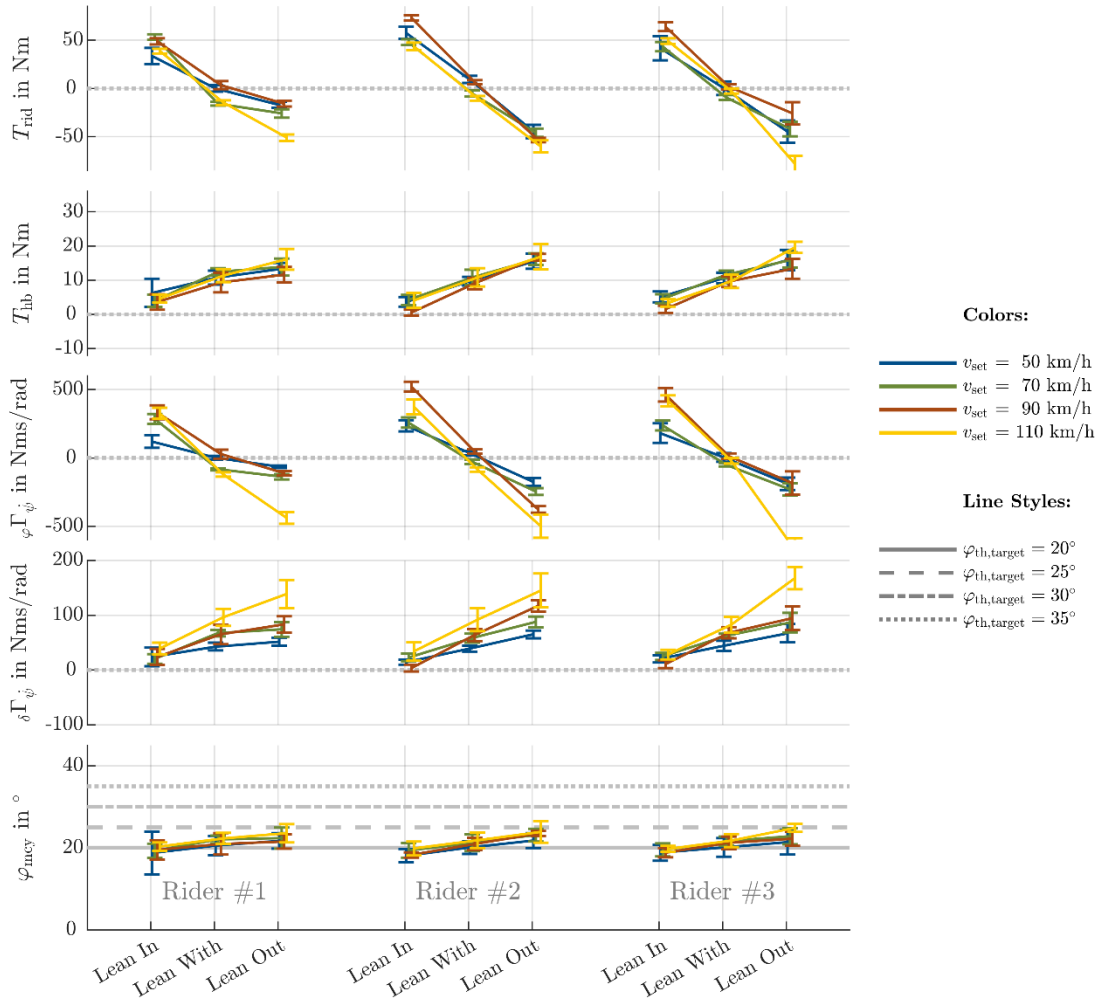
Figure B.6: Vehicle states under different leaning conditions (5) during constant cornering at 20 ° target theoretical roll angle.
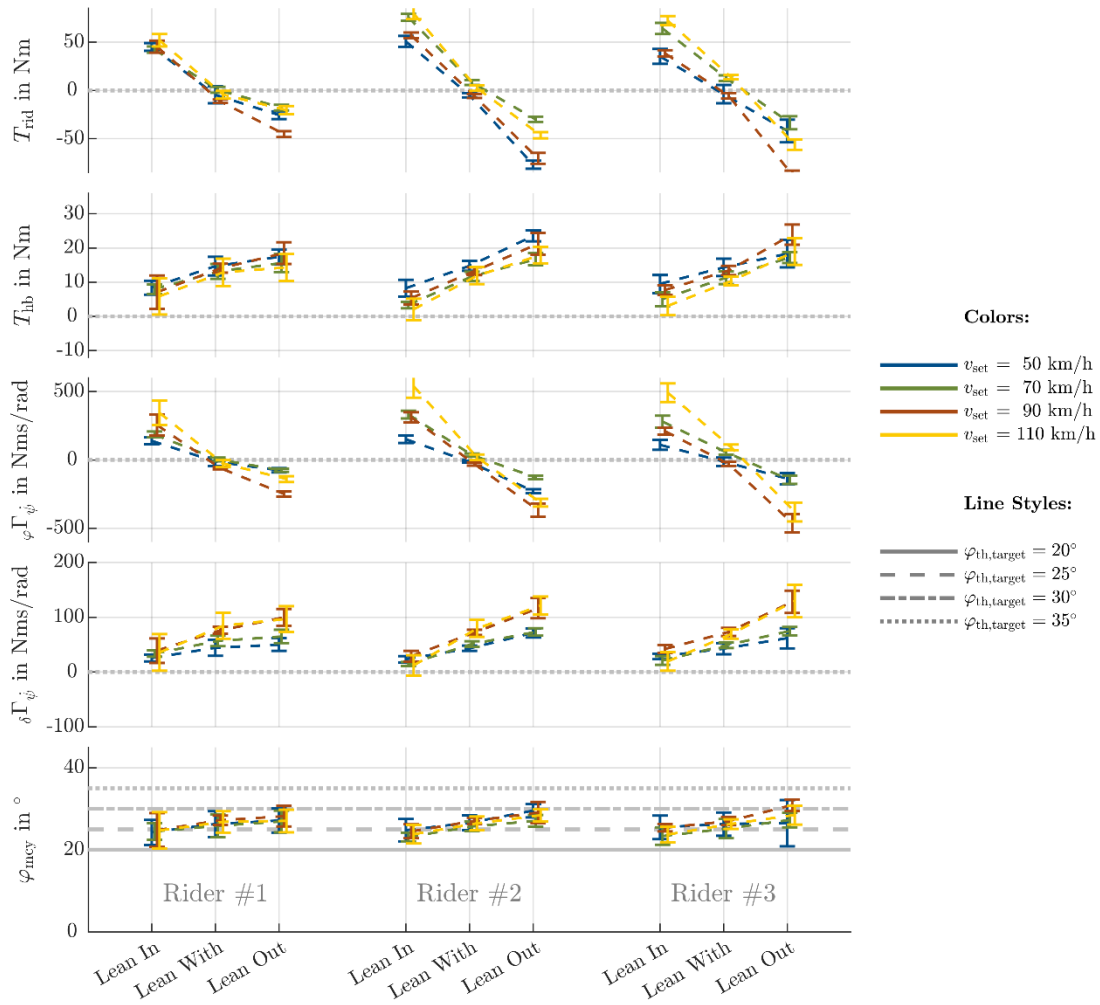
Figure B.7: Vehicle states under different leaning conditions (6) during constant cornering at 25 ° target theoretical roll angle.
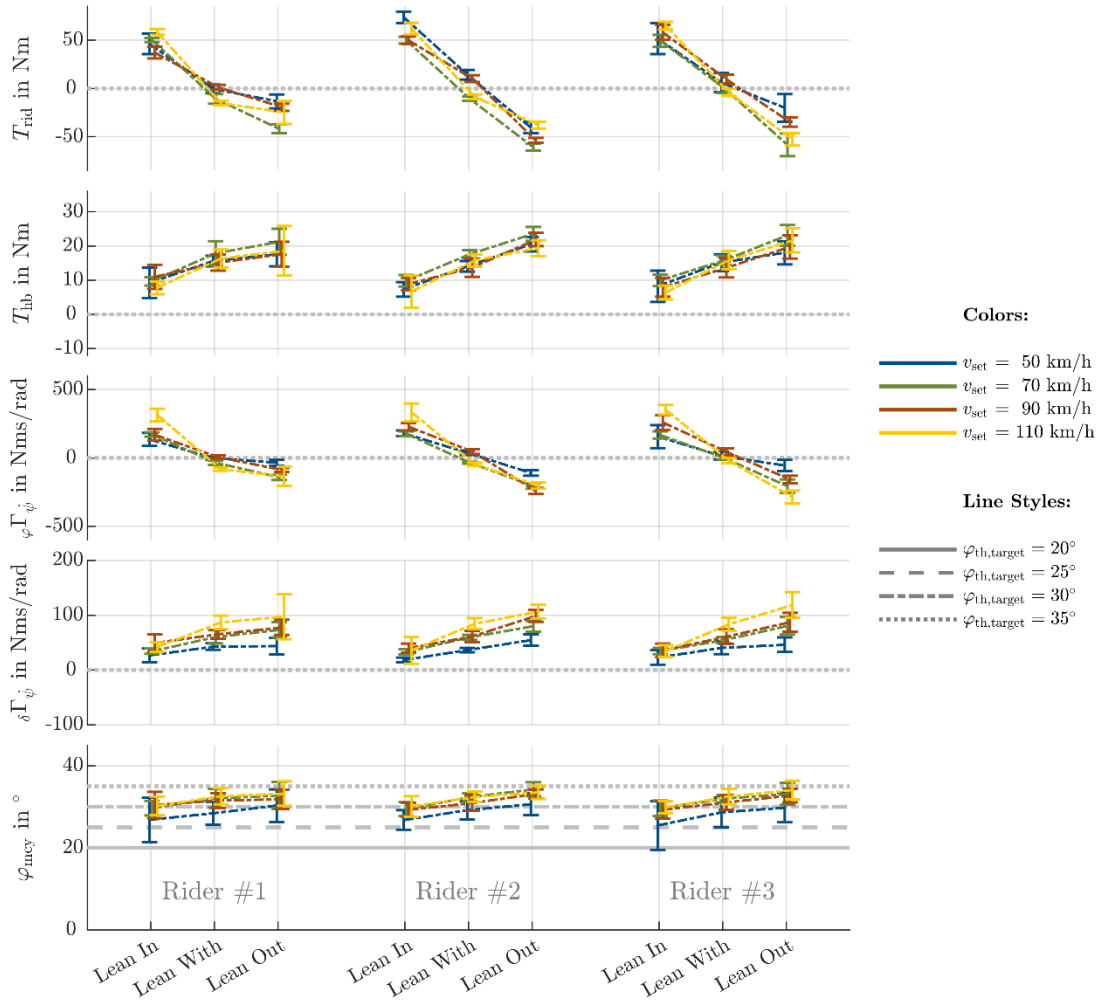
Figure B.8: Vehicle states under different leaning conditions (7) during constant cornering at 30 ° target theoretical roll angle.
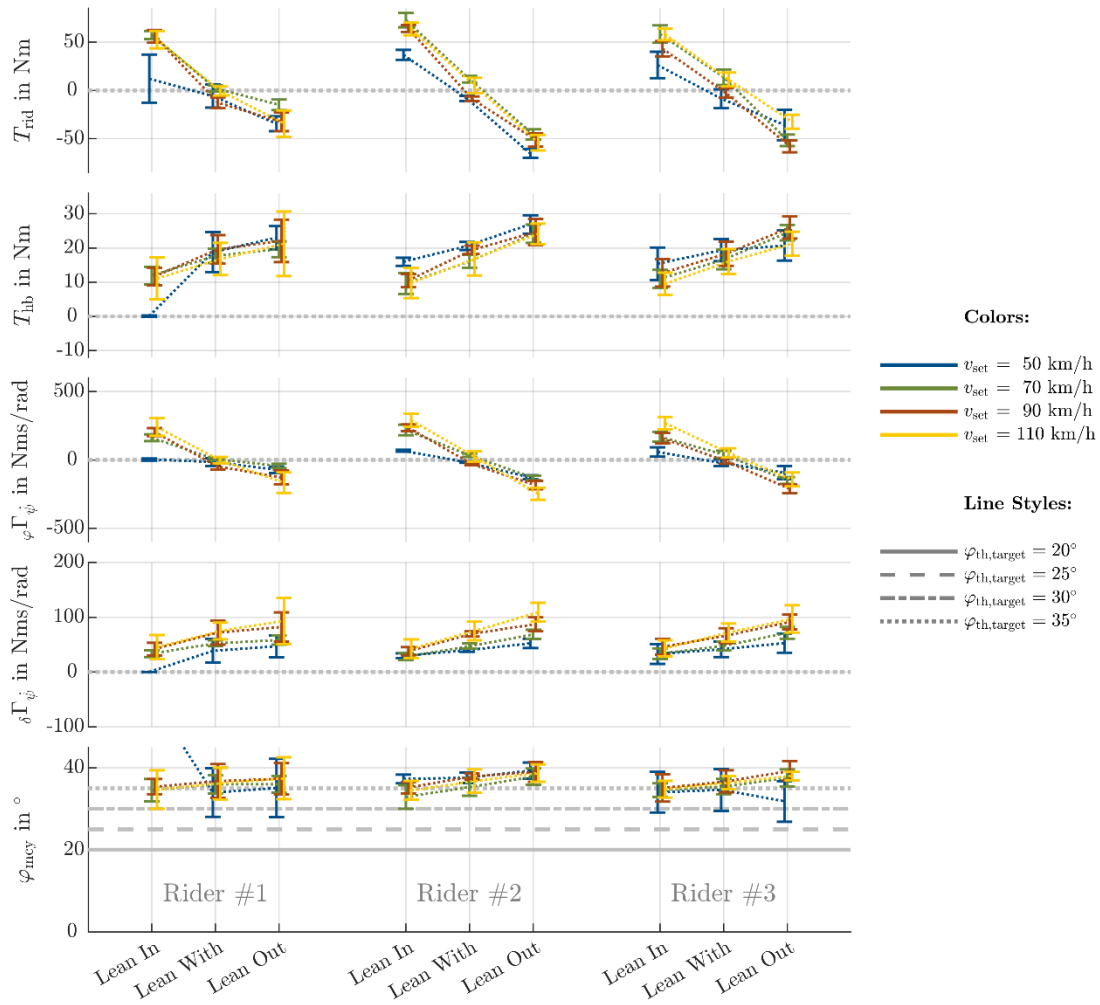
Figure B.9: Vehicle states under different leaning conditions (8) during constant cornering at 35 ° target theoretical roll angle.

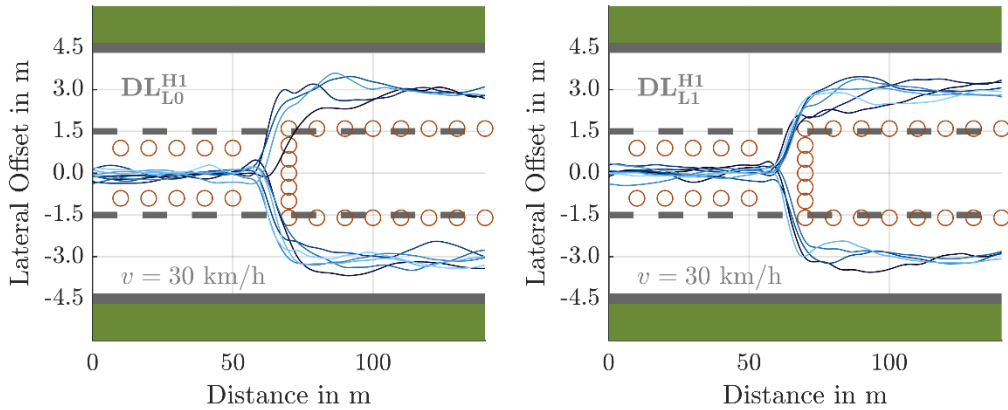# B.2 Trajectories of LC_{L0}^{H1} and LC_{L1}^{H1} maneuvers

Figure B.10: Lane change maneuver at 30 km/h in DL_{L0}^{H1} condition (left) and DL_{L1}^{H1} condition (right)
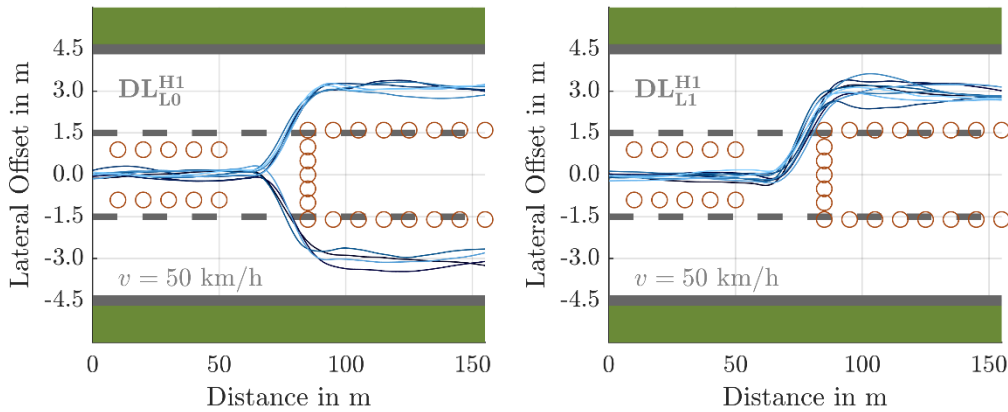

Figure B.11: Lane change maneuver at 50 km/h in DL_{L0}^{H1} condition (left) and DL_{L1}^{H1} condition (right)
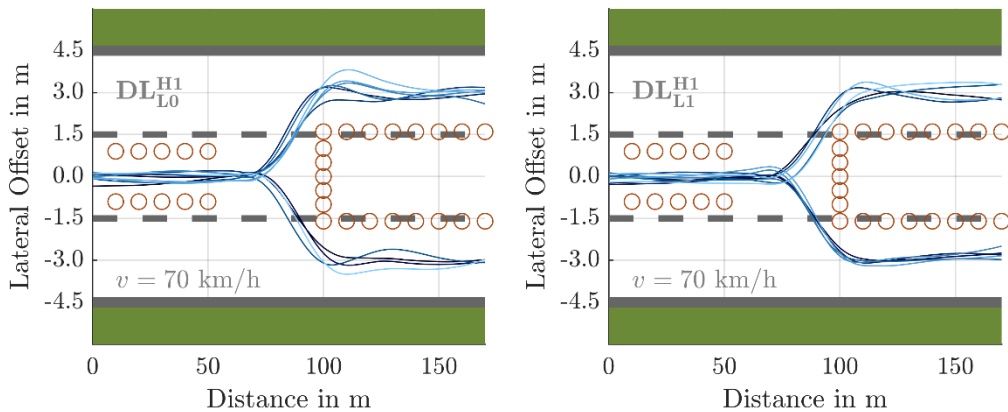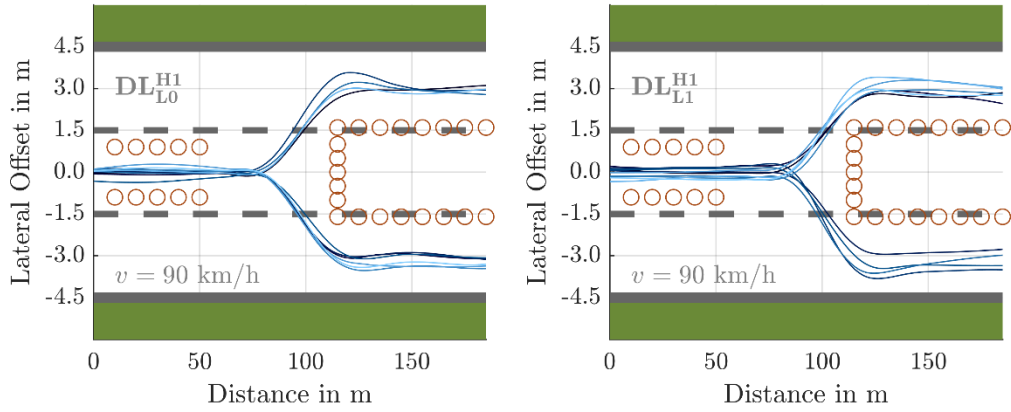

Figure B.12 Lane change maneuver at 70 km/h in DL_{L0}^{H1} condition (left) and DL_{L1}^{H1} condition (right)

Figure B.13 Lane change maneuver at 50 km/h in DL_{L0}^{H1} condition (left) and DL_{L1}^{H1} condition (right)
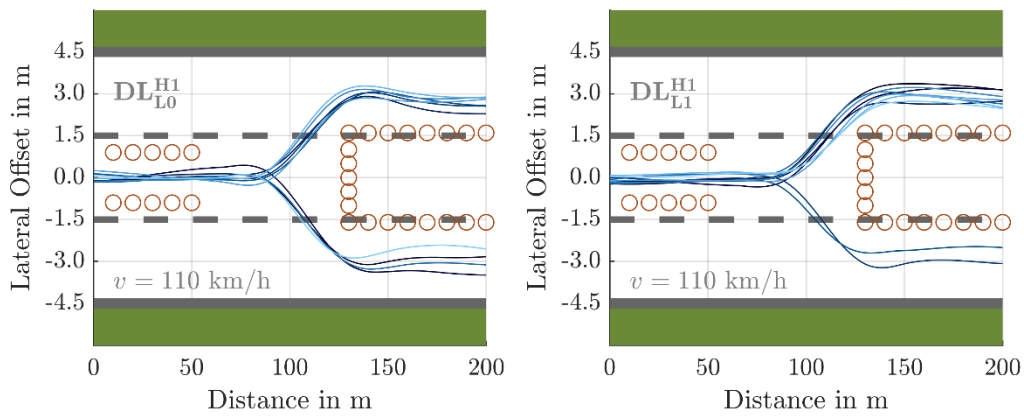

Figure B.14 Lane change maneuver at 50 km/h in DL_{L0}^{H1} condition (left) and DL_{L1}^{H1} condition (right)
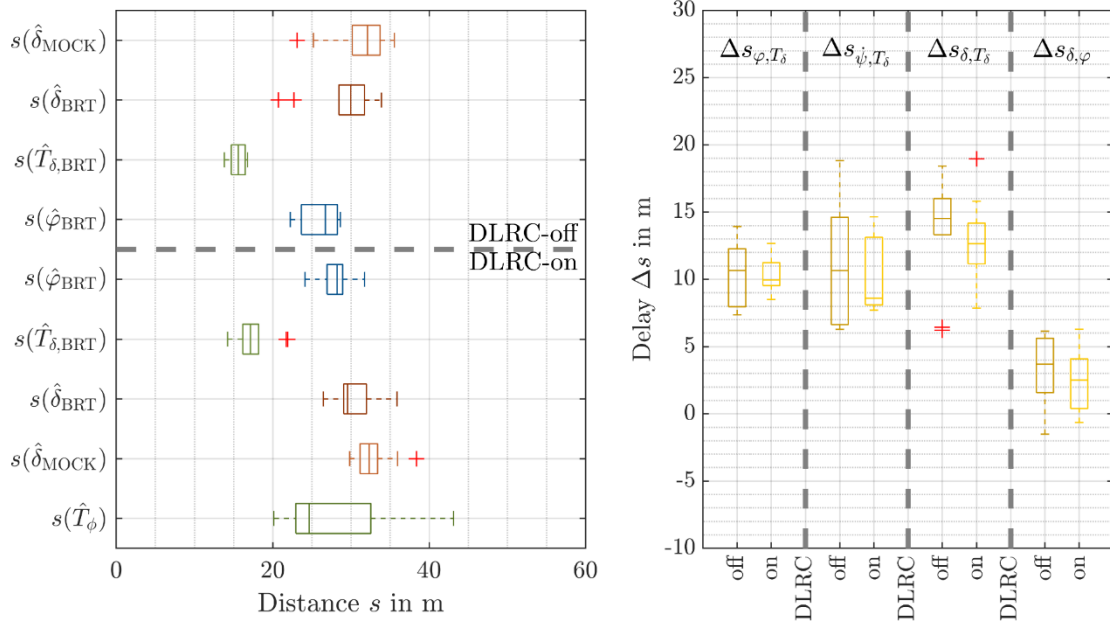
B.3 Lane Change Delays

Figure B.15: Locations of the Extremal Values (left) and Delay Indexes (right) at 70 km/h

The left plot shows the good correlation of the datasets measured with or without DLRC. The rather strictly constrained maneuver doesn't allow for large deviations and therefore, differences in the measured values are rather subtle. The first extreme value in all configurations and through all velocities is always the steer torque. Its occurrence depends almost solely on the rider reaction time to the sign showing the avoidance direction. The steer torque peak is followed by the roll angle peak (blue). Then, the virtual motorcycle's steer angle follows shortly after. This behavior is in accordance with the expected behavior that was already predicted in section 2.2.3. The steering maximum is a result of an intended steering motion towards the inside of the turn, which – analogous to the counter steering impulse in straight running – helps to initiate the uprighting roll motion. Furthermore, the advance of the steer torque peak to the roll angle peak (leftmost index in the right plot) increases with velocity and tends to be smaller, when the rider utilizes lean-in, which is assumed here and only possible in the DLRC-on configuration. This – again – is in accordance with the expectations and literature review from section 2.2.3.

B.4 Bike Real Time Offline Slalom

Using the available multi-body-simulation as reference for slalom maneuvers is generally possible. However, the virtual rider model must be parameterized accordingly. The standard model is not capable of performing some maneuvers, that are possible for a simulator rider, as shown below. Therefore, another method to generate a slalom reference is preferred.

Figure B.16: Four repetitions of the slalom maneuver (colored) against the BRT offline simulation reference (grey) at 40 km/h and 14 m cone distance
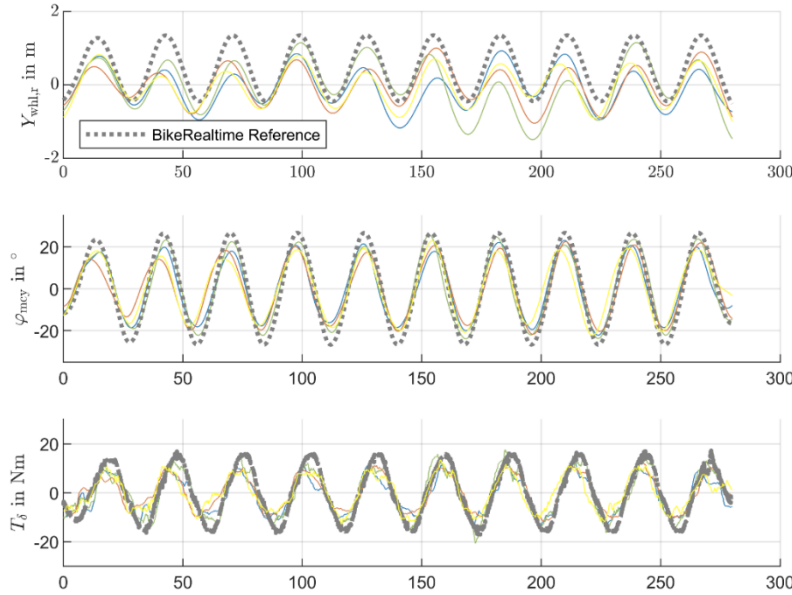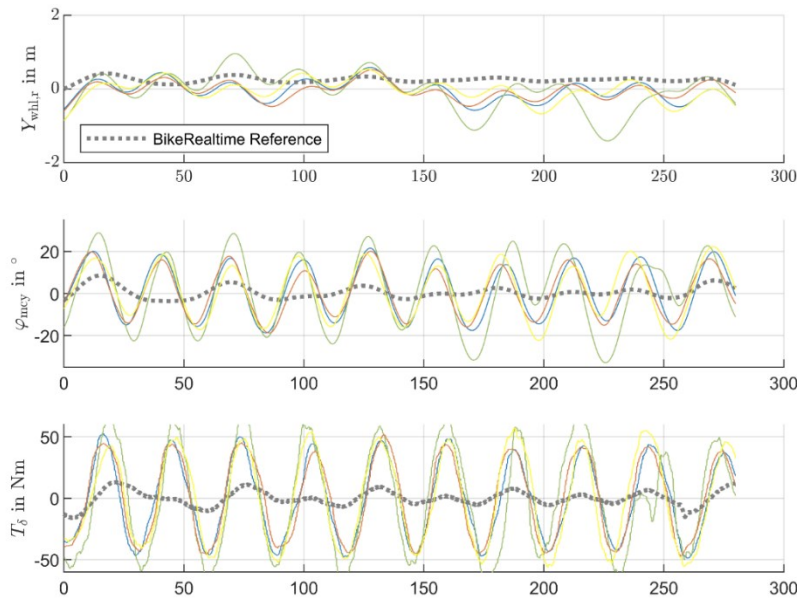

Figure B.17: Four repetitions of the slalom maneuver (colored) against the BRT offline simulation reference (grey) at 80 km/h and 14 m cone distance. The BRT virtual rider model is not capable of this maneuver. One reason, why offline simulations don't suffice as reference.

B.5 Steady State Slalom Approximation

The figures below depict the steady state slalom approximation (right) for the simulator measurement (right). For the approximation, the amplitude of the 1st order slalom oscillation of the measured trajectory is used as an input. The following quantities result from the trajectory as described in section 4.3.3.

Figure B.18: Slalom quantities of a simulator measurement (left) and the steady state approximation (right) at 80 km/h and 42 m cone distance
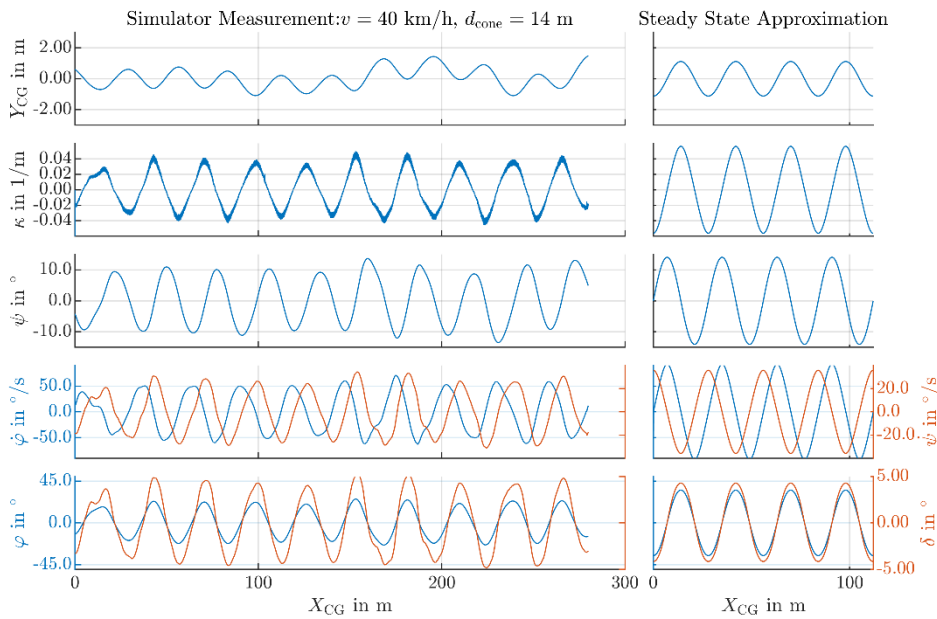
Figure B.19: Slalom quantities of a simulator measurement (left) and the steady state approximation (right) at 40 km/h and 14 m cone distance

B.6 Instantaneous Frequencies and Amplitudes
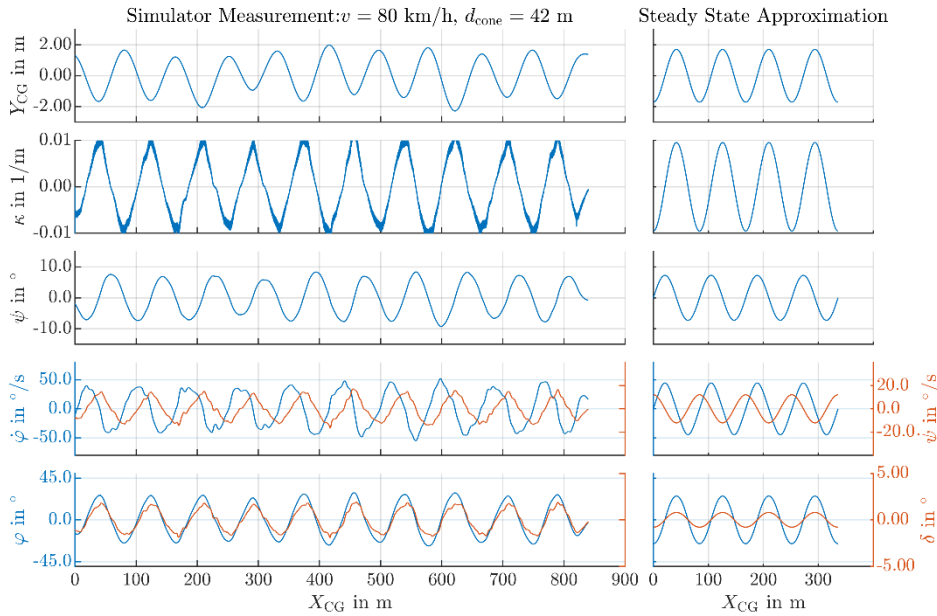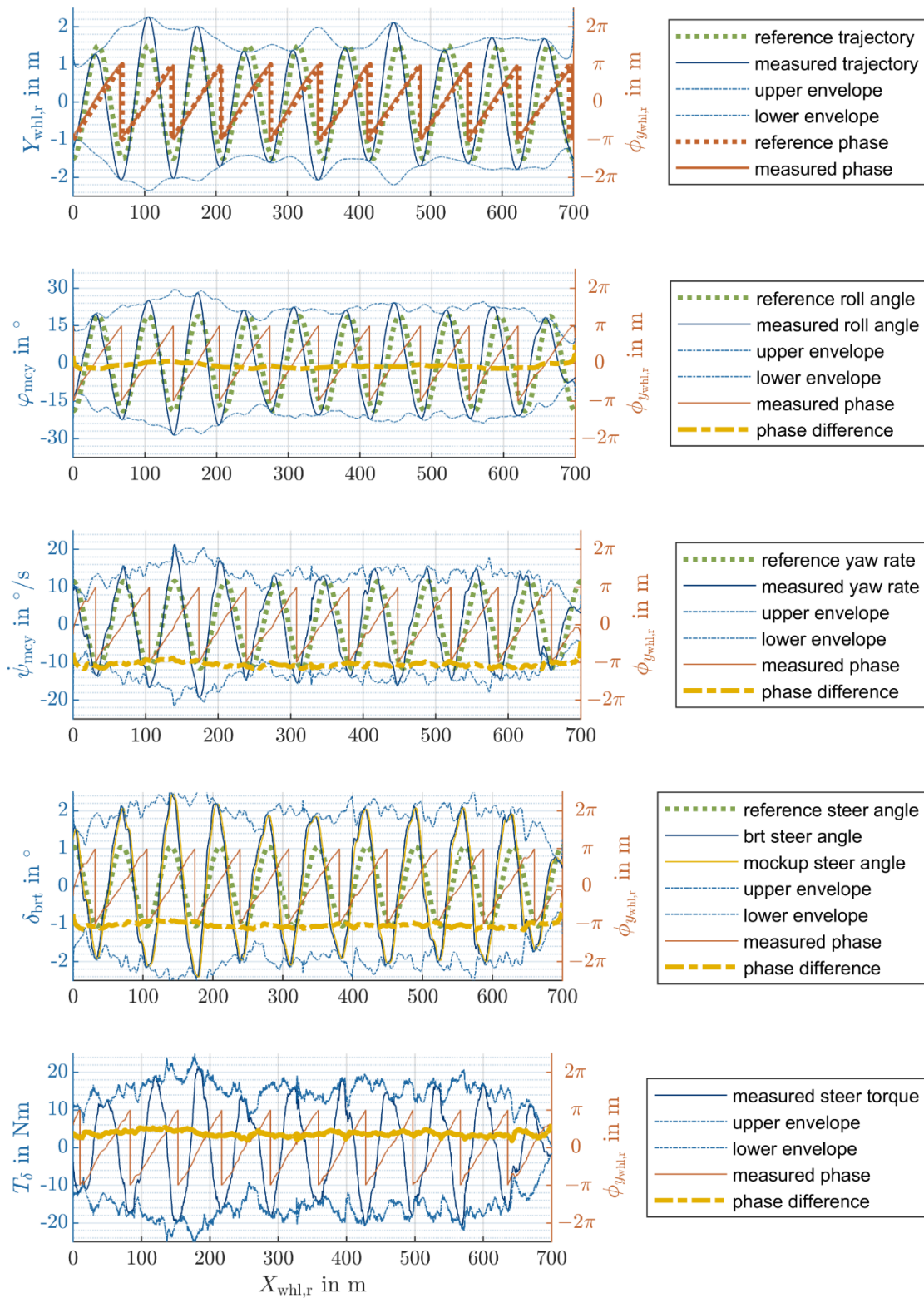

Figure B.20: Instantaneous Amplitudes, Phases and Reference Signals during Slalom 40/ km/h 14m

B.7 Variance of Frequencies and Amplitudes

In section 6.4.3 the variances of the instantaneous frequency and amplitudes of the motorcycle roll angle and lateral position of the rear tire contact point are shown. The following plots relate to the steer angle, CoG poaition and steer torque and show comparable results, i.e. reduced levels and less deviations within the maneuver.
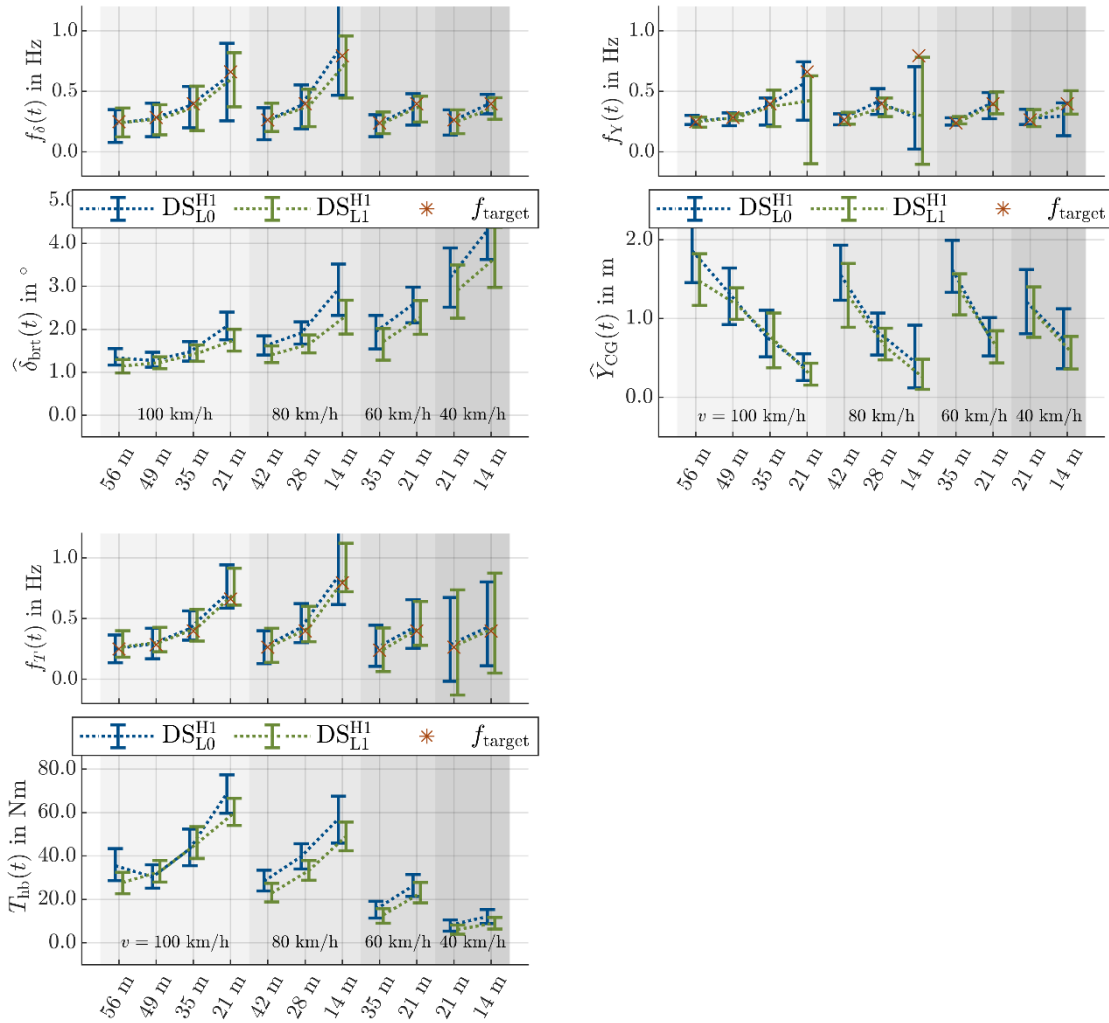
Figure B.21: Distribution of instantaneous frequencies (top) and amplitudes (bottom) during various slalom maneuvers. Top left: Motorcycle steer angle, right: Lateral offset of the motorcycle CoG, bottom: steer torque. The error bars show the mean values (dotted lines) and range from the p_{10}-percentile to the p_{90}-percentile. The red asterisks indicate the slalom target frequency

B.8 Level Phase Plots

The data below shows the slalom level and phase plots of a different rider, compared to section 6.4.3 . The measurements are of the same order of magnitude and show the identical clustering as for the other rider. The reduction of levels and the phase delay for the DS_{H1}^{L1} are existent, but less prominent as before.
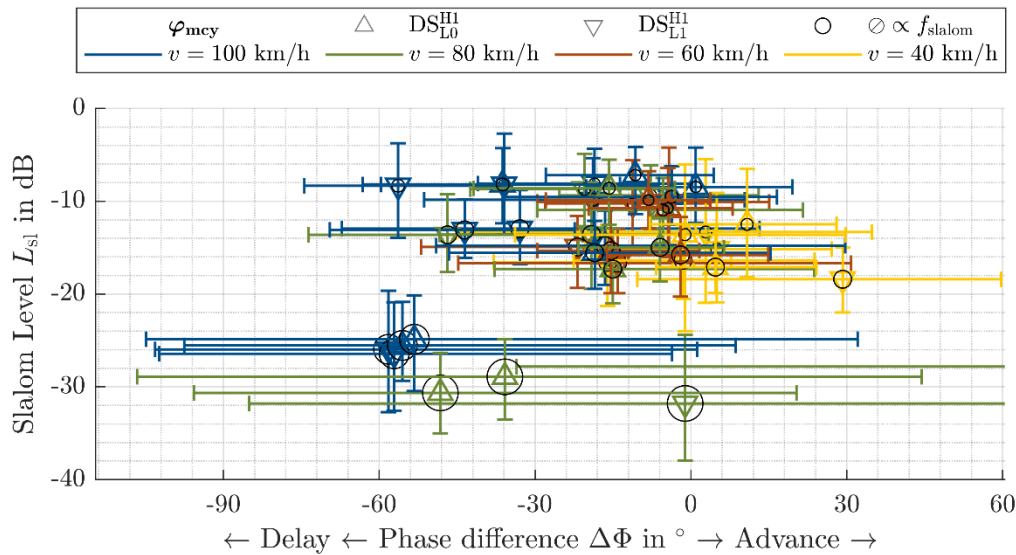
Figure B.22: Slalom level and phase plot of the motorcycle roll angle for one rider in two repetitions per DLRC condition.
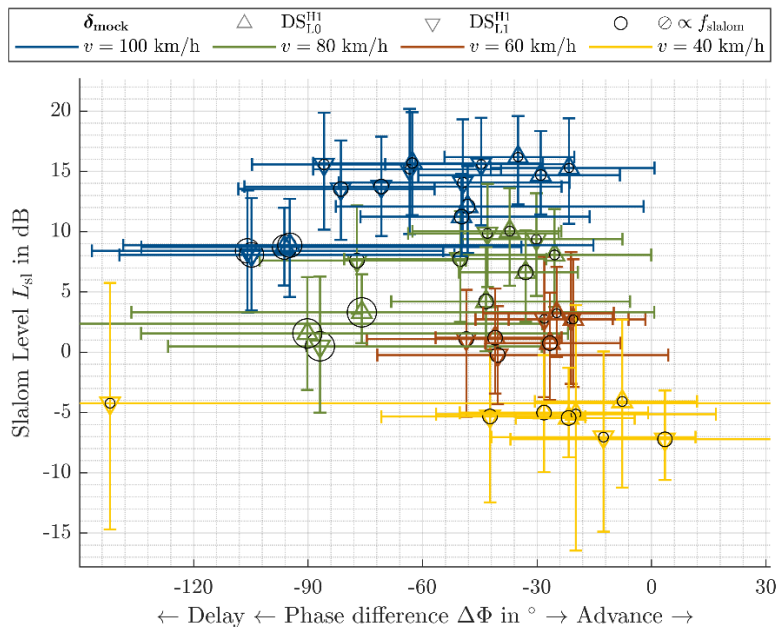
Figure B.23: Slalom level and phase plot of the motorcycle roll angle for one rider in two repetitions per DLRC condition.

B.9 Polar Plots of Slalom Levels

Figure B.24: Polar plots of the slalom levels and phase delays of multiple quantities (identified by the marker symbol). The DLRC condition is color coded. The slalom level is read on the radial axis. The dashed line highlights the 0dB level.

Each polar plot in Figure B.24 shows the data of the two different DLRC conditions. Six different quantities are plotted. They are distinguishable by the used marker in the center of each cluster. The radial positi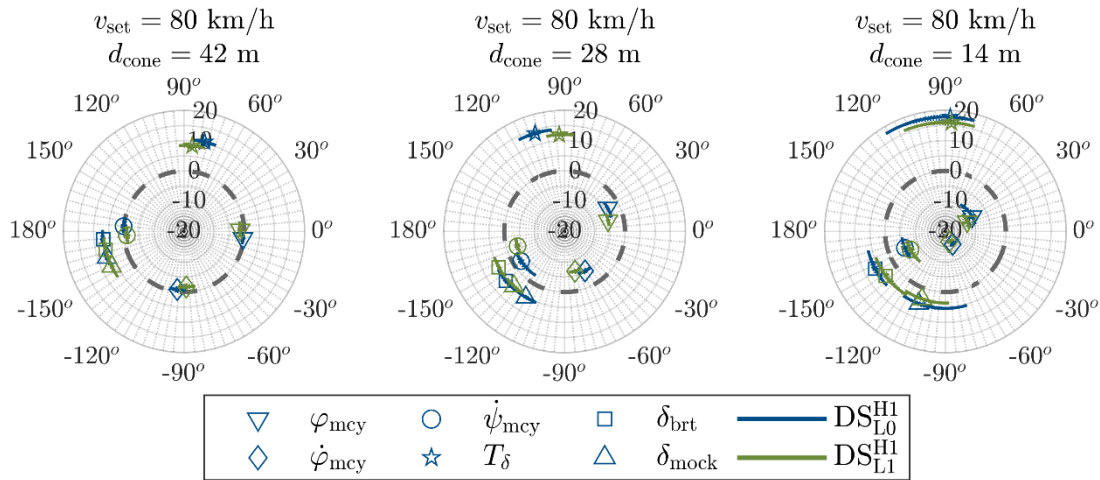on of any datapoint indicates the slalom level of the respective value in dB, as derived in the previous section. If a datapoint lies on the 0 dB level (dashed line), this means that the amplitude of that value is equal to the reference value. The Angle of each datapoint represents the phase delay with respect to the reference slalom trajectory. The clusters indicate the interquartile range of both level and phase delay of each entity. As the clusters increase in size, the slalom is therefore less homogeneously ridden. This is especially the case in the 14 m slalom in the rightmost plot.

The left plot shows a rather well performed slalom maneuver throughout both DLRC conditions. The levels of roll angle (about -0° phase) roll rate (about -90° phase) and yaw rate (levelled CoSy, about 180° phase) are all close to 0 dB and therefore close to the steady state approximation. The level of the steer torque (about 75° phase) in contrary is not attributable to a steady state equivalent, as the reference value for all maneuvers was simply chosen to be 10 Nm due to the lack of a simple torque reference calculation. The level of the steer angle of the virtual motorcycle (about 180° phase) is rather large, between 10 dB and 15 dB. This is expected, as the steer angles in a dynamic maneuver will always need an "overshooting" amplitude whenever the rider intends to change from one steady state to another.

As the maneuver becomes more demanding, the deviations within the maneuver increase, resulting in larger clusters. For increasing slalom frequencies, the slalom levels of roll and yaw sizes tend to decrease, while the steer torque levels increase. The steer angle levels on contrary grow with vehicle speed and are rather not affected by cone distance.

C Naïve Rider Study

C.1 eCDF in Reference Straights

The following images show the distribution of roll rates during each straight of a reference scenario in the naïve rider study. As not all riders finished all levels, the number of lines is varying from level 1 to 16.
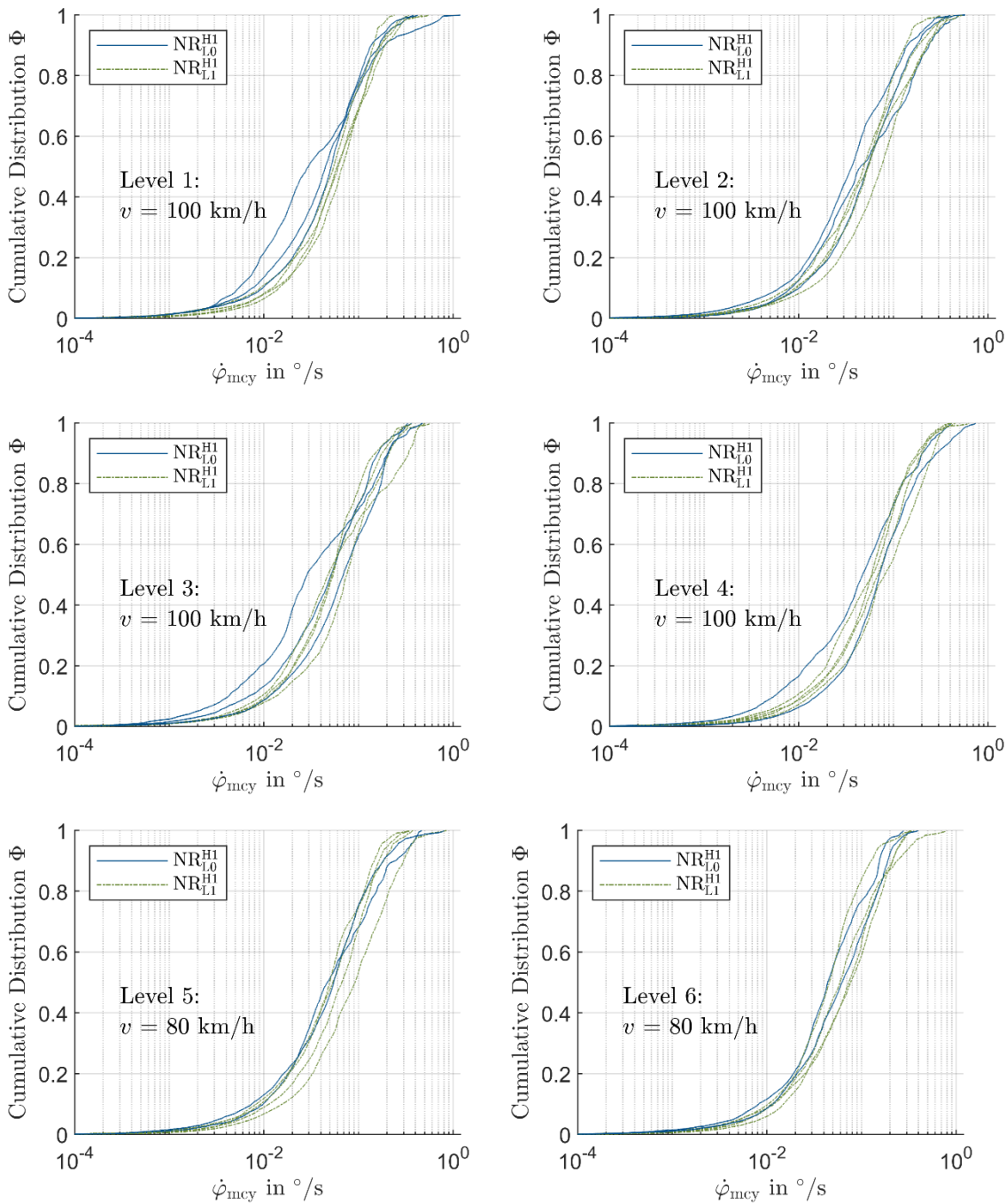

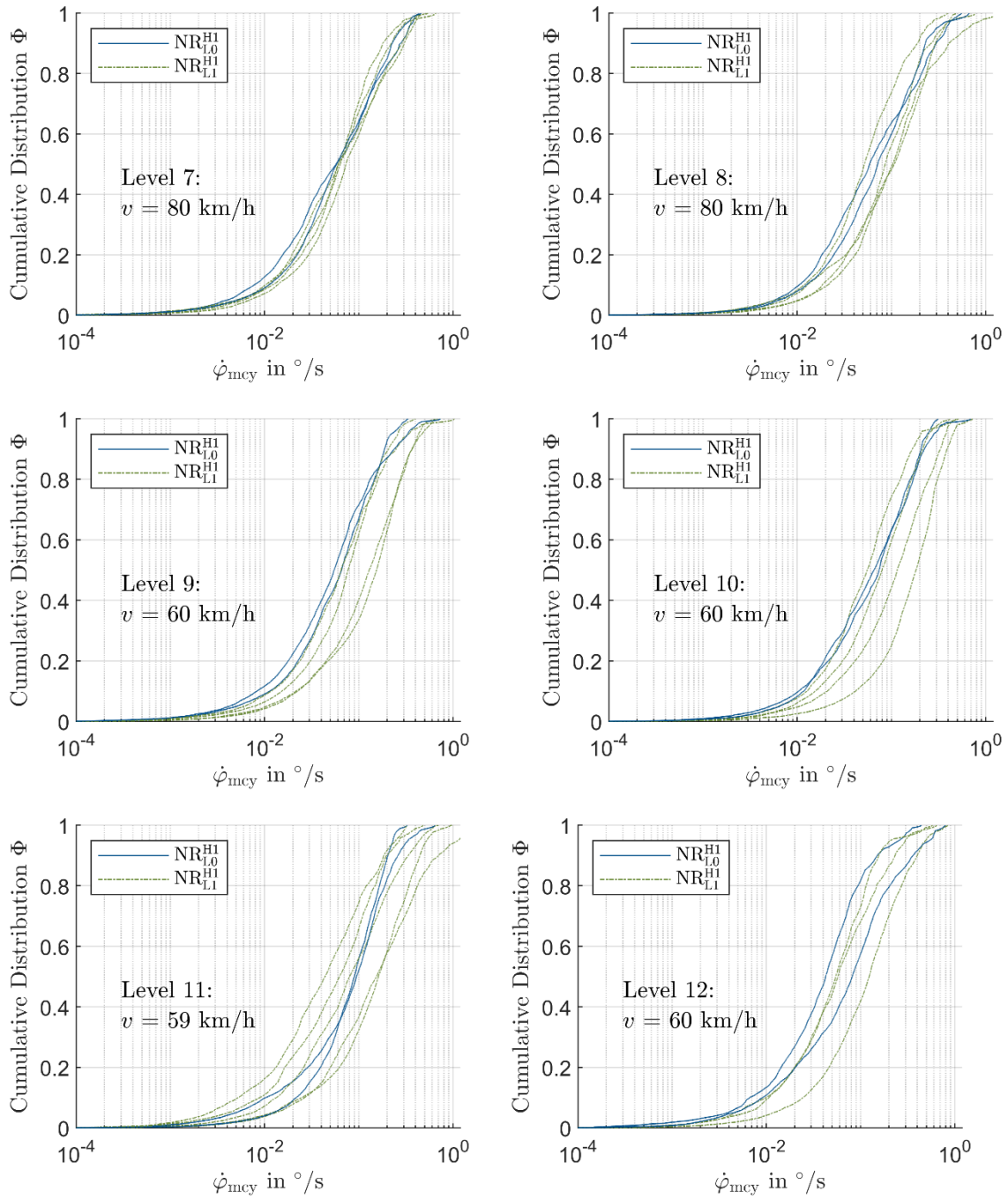Figure C.25: eCDF of roll rates in straight running for level 1 to 6

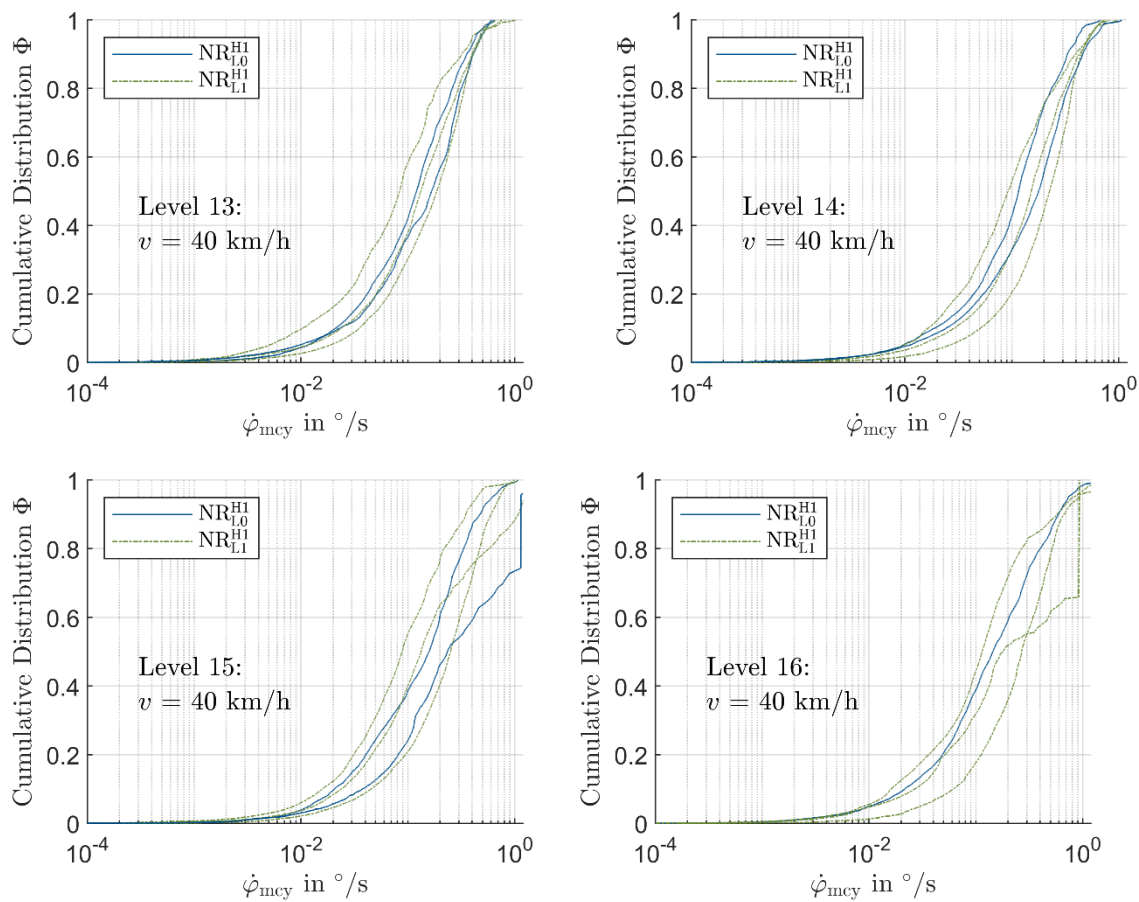Figure C.26: eCDF of roll rates in straight running for level 7 to 12

Figure C.27: eCDF of roll rates in straight running for level 13 to 16

List of References

Adams, B.: Pressuring the Pegs (2014)
Adams, B.: Pressuring the Pegs, Riding Skills Series; https://www.cycleworld.com/sport-rider/sportbike-riding/pressuring-pegs-motorcycle-riding-tip/, 2014

Albrecht, A.: Master Thesis, Stillstandsimulation auf einem Dynamischen Motorradfahrsimulator (2018)
Albrecht, Alexander: Stillstandsimulation auf einem Dynamischen Motorradfahrsimulator, Master Thesis
TU Darmstadt, 2018

Allen, R. et al.: A Short History of Driving Simulation (2011)
Allen, R.; Rosenthal, T. J.; Cook, M. L.: A Short History of Driving Simulation, in: Fisher, D. L.; Rizzo, M.; Caird, J. K., Lee, J.D. (Eds.): Handbook of Driving Simulation for Engineering, Medicine, and Psychology, Taylor & Francis Group, FL, USA, 2011

Anton, M.: Bachelor Thesis, Auslegung und Konstruktion eines Seilzugsystems (2014)
Anton, Marc: Auslegung und Konstruktion eines Seilzugsystems zur Darstellung von Horizontalkräften an einem Motorradfahrsimulator, Bachelor Thesis
TU Darmstadt, 2014

Arioui, H. et al.: Mechatronics of a Motorcycle Simulator (2010)
Arioui, H.; Nehaoua, L.; Hima, S.; Séguy, N.; Espié, S.: Mechatronics, Design, and Modeling of a Motorcycle Riding Simulator, in: IEEE/ASME Transactions on Mechatronics (5), Issues 15, pp. 805–818, 2010

Aström, K. et al.: Bicycle Dynamics And Control (2005)
Aström, K.; Klein, R.; Lennartsson, A.: Bicycle Dynamics And Control, in: IEEE Control Systems Magazinne, 2005

Bandow, F. et al.: Bestimmung der Fahrersitzposition im Fahrversuch (2004)
Bandow, F.; Helbig, K.; Vogt, N.: Bestimmung der Fahrersitzposition im Fahrversuch, in: Automobiltechnische ZeitschriftVol.106, Nr.10, 2004

Barbagli, F. et al.: Washout filter design for a motorcycle simulator (2001)
Barbagli, F.; Ferrazzin, D.; Avizzano, C. A.; Bergamasco, M.: Washout filter design for a motorcycle simulator, in: IEEE Virtual Reality 2001, Yokohama, Japan, 13-17 March 2001

Bartolozzi, M. et al.: Similarities in steering control between cars and motorcycles (2022)
Bartolozzi, Mirco; Berzi, Lorenzo; Meli, Enrico; Savino, Giovanni: Similarities in steering control between cars and motorcycles: application to a low-complexity riding simulator, in: Meccanica (11), Issues 57, pp. 2863–2883, 2022

Betz, A.: Diss., Feasibility Analysis of Wheeled Mobile Driving Simulators (2013)
Betz, Alexander: Feasibility Analysis and Design of Wheeled Mobile Driving Simulators for Urban Traffic Simulation, Dissertation TU Darmstadt, 2013

Biral, F. et al.: Experimental Study of Motorcycle Transfer Functions for Evaluating Handling (2003)
Biral, F.; Bortoluzzi, D.; Cossalter, V.; Lio, M.: Experimental Study of Motorcycle Transfer Functions for Evaluating Handling, in: Vehicle System Dynamics (1), Issues 39, pp. 1–25, 2003

Blaauw, G. J.: Driving Experience and Task Demands in Simulator (1982)
Blaauw, Gerard J.: Driving Experience and Task Demands in Simulator and Instrumented Car: A Validation Study, in: Human factors (4), Issues 24, pp. 473–486, 1982

Bocciolone, M. et al.: Experimental Identification of Kinematic Coupled Effects (2007)
Bocciolone, M.; Cheli, F.; Leo, E.; Pezzola, M.: Experimental Identification of Kinematic Coupled Effects Between Driver – Motorcycle, 2007

BOSCH: Motorcycle Stability Control
BOSCH: Motorcycle Stability Control; https://www.bosch-presse.de/pressportal/de/de/motorrad-stabilitaetskontrolle-msc-von-bosch-157825.html, Access 15.02.2019

BOSCH: Sliding Mitigation
BOSCH: Sliding Mitigation; https://www.bosch-presse.de/pressportal/de/de/rutschverhinderung-157832.html, Access 15.02.2019

Celiberti, F. et al.: MOTORIST Simulator (2016)
Celiberti, F.; Grottoli, M.; Di Gesu, M.: MOTORIST Simulator, 2016

Chiyoda, S. et al.: Development of a Motorcycle Simulator Using Parallel Manipulator (2000)
Chiyoda, Shingo; Yoshimoto, Kenichi; Kawasaki, Daisuke; Murakami, Yoshifumi; Sugimoto, Takayuki: Development of a Motorcycle Simulator Using Parallel Manipulator and Head Mounted Display, 2000

Cooper, G.; Harper, R.: The Use of Pilot Rating in the Evaluation of Aircraft Handling Qualities (1969)
Cooper, G.; Harper, R.: The Use of Pilot Rating in the Evaluation of Aircraft Handling Qualities, Washington D.C., 1969

Cossalter, V. et al.: Inertial and Modal Properties of Racing Motorcycles (2002)
Cossalter, V.; Doria, A.; Mitolo, L.: Inertial and Modal Properties of Racing Motorcycles, in: Motorsports Engineering Conference & Exhibition, SAE Technical Paper Series, SAE International400 Commonwealth Drive, Warrendale, PA, United States, 2002

Cossalter, V.: Motorcycle Dynamics (2006)
Cossalter, Vittore: Motorcycle Dynamics, lulu, Raleigh, NC, 2006

Cossalter, V. et al.: Steady turning of motorcycles (2007)
Cossalter, V.; Lot, R.; Peretto, M.: Steady turning of motorcycles, in: Proceedings of the Institution of Mechanical Engineers, Part D: Journal of Automobile Engineering (11), Issues 221, pp. 1343–1356, 2007

Cossalter, V. et al.: Objective and subjective evaluation of an advanced motorcycle riding simulator (2010)
Cossalter, Vittore; Lot, Roberto; Rota, Stefano: Objective and subjective evaluation of an advanced motorcycle riding simulator, in: European Transport Research Review (4), Issues 2, pp. 223–233, 2010

Cossalter, V. et al.: Development of a motorcycle riding simulator (2011)
Cossalter, V.; Lot, R.; Massaro, M.; Sartori, R.: Development and validation of an advanced motorcycle riding simulator, in: Proceedings of the Institution of Mechanical Engineers, Part D: Journal of Automobile Engineering (6), Issues 225, pp. 705–720, 2011

Cossalter, V.; Doria, A.: Analysis of Motorcycle Slalom Manoeuvres Using the Mozzi Axis Concept (2004)
Cossalter, Vittore; Doria, Alberto: Analysis of Motorcycle Slalom Manoeuvres Using the Mozzi Axis Concept, in: Vehicle System Dynamics (3), Issues 42, pp. 175–194, 2004

Cossalter, V.; Doria, A.: Instantaneous Screw Axis of two-wheeled vehicles (2006)
Cossalter, Vittore; Doria, Alberto: Instantaneous screw sxis of two-wheeled vehicles in typical manoeuvres, in: Vehicle System Dynamics sup1, Issues 44, pp. 669–678, 2006

Cossalter, V.; Lot, R.: A Motorcycle Multi-Body Model for real time simulations (2002)
Cossalter, Vittore; Lot, Roberto: A Motorcycle Multi-Body Model for real time simulations, in: Vehicle System DynamicsVol. 37, No. 6, pp. 423–447, 2002

Cossalter, V.; Sadauckas, J.: Elaboration and quantitative assessment of manoeuvrability (2006)
Cossalter, Vittore; Sadauckas, James: Elaboration and quantitative assessment of manoeuvrability for motorcycle lane change, in: Vehicle System Dynamics (12), Issues 44, pp. 903–920, 2006

Delgado, R.: Master Thesis, Integrierte Roll- und Nickmomentenmessung auf einem Simulator (2018)
Delgado, Ricardo: Entwurf einer Montagevorrichtung für Motorräder mit integrierter Roll- und Nickmomentenmessung auf einem Motorradsimulator, Master Thesis TU Darmstadt, 2018

Donges, E.: Driver Behavior Models (2016)
Donges, Edmund: Driver Behavior Models, in: Winner, Hermann et al. (Eds.): Handbook of Driver Assistance Systems, Springer International Publishing, Cham, 2016

Doria, A. et al.: The response of the rider's body to roll oscillations (2012)
Doria, Alberto; Tognazzo, Mauro; Cossalter, Vittore: The response of the rider's body to roll oscillations of two wheeled vehicles; experimental tests and biomechanical models, in: Proceedings of the Institution of Mechanical Engineers, Part D: Journal of Automobile Engineering (4), Issues 227, pp. 561–576, 2012

Embrey David: Understanding Human Behavior and Error (2005)
Embrey David: Understanding Human Behavior and Error, 2005

Emig, L. et al.: Project Report, Entwurf eines Seilzugsystems zur Querdynamikdarstellung (2018)
Emig, Lars; Fischer, Yannick; Kloas, Kevin; Knoedl, Felix; Zinßer, Lukas: Entwurf eines Seilzugsystems zur Längs- und Querdynamikdarstellung auf einem dynamischen Motorradfahrsimulator, Project Report
TU Darmstadt, 2018

Evertse, M.: Master Thesis, Rider Analysis using a fully instrumented motorcycle (2010)
Evertse, M.: Rider Analysis using a fully instrumented motorcycle, Master Thesis
Delft University of Technology, 2010

Federico Cheli et al.: Driver's movements influence on the lateral dynamic of a sport motorbike
Federico Cheli; Marco Pezzola; Niccola Taroni; Paolo Mazzoleni; Emanuele Zappa: Driver's movements influence on the lateral dynamic of a sport motorbike, in: 19th Mediterranean Conference on Control and Automation

Ferrazzin, D. et al.: THE MORIS MOTORCYCLE SIMULATOR: AN OVERVIEW (2001)
Ferrazzin, D.; Salsedo, F.; Barbagli, F.; Avizzano, C. A.; Di Pietro, G.; Brogni, A.; Vignoni, M.; Bergamasco, M.; Arnone, L.; Marcacci, M.; Masut, L.; Benedetti, A.: THE MORIS MOTORCYCLE SIMULATOR: AN OVERVIEW, in: SAE Technical Paper Series, SAE Technical Paper Series, SAE International400 Commonwealth Drive, Warrendale, PA, United States, 2001

Foerst, R.: Foerst Fahrsimulatoren Firmenhistorie (2011)
Foerst, Reiner: Foerst Fahrsimulatoren Firmenhistorie, Wiehl, 2011

Fu et al.: Stability Analysis of Uncontrolled Motion Single-track vehicles (1978)
Fu; Shibashi; Kikuchi: Stability Analysis of Uncontrolled Motion Single-track vehicles, in: Transactionsn of JSAE No.15, 1978

Grottoli, M.: Development and evaluation of a motorcycle riding simulator (2021)
Grottoli, M.: Development and evaluation of a motorcycle riding simulator for low speed maneuvering
Delft University of Technology, 2021

Guth, S.: Diss., Absicherungsmethode von Anzeigekonzepten mittels Motorradfahrsimulator

Guth, Sebastian: Absicherungsmethode von Anzeigekonzepten zur Darstellung fahrfremder Informationen mittels eines Motorrad-Fahrsimulators, Dissertation TU Darmstadt

Guth, S. et al.: Motion cueing algorithm to reproduce motorcycle dynamics (2015)

Guth, Sebastian; Geiger, Michael; Will, Sebastian; Pleß, Raphael; Winner, Hermann: Motion cueing algorithm to reproduce motorcycle specific lateral dynamics in riding simulators, in: Proceedings of the Driving Simulation Conference and Exhibition, 2015

Hammer, T. et al.: Anwendungsmöglichkeiten von Motorradsimulatoren (2021)

Hammer, Thomas; Pleß, Raphael; Will, Sebastian, et al. (Eds.) Anwendungsmöglichkeiten von Motorradsimulatoren, Berichte der Bundesanstalt für Straßenwesen M, Mensch und SicherheitHeft 323, Fachverlag NW in der Carl Schünemann Verlag GmbH, Bremen, 2021

Hans, S. et al.: Why automatization is the future

Hans, Stefan; Köbe, Markus; Prokop, Günther: Why automatization is the future of rider assistance systems - Intervene before a critical situation, in: Proceedings of the 13th International Motorcycle Conference

Harmonic Drive AG: Harmonic Drive Mechatronik

Harmonic Drive AG: Harmonic Drive Mechatronik; https://harmonicdrive.de/fileadmin/user_upload/Harmonic_Drive_Mechatronik_DE_10535 23_09_2022.pdf, Access 28.11.2022

Harmonic Drive AG: YukonDrive (2017)

Harmonic Drive AG: Anwendungshandbuch AC Servoregler YukonDrive (r), Limburg/Lahn, 2017

Harmonic Drive AG: LynxDrive (2018)

Harmonic Drive AG: Projektirungsanleitung AC Servoantriebe LynxDrive (r), Limburg/Lahn, 2018

Hebb, D. O.: Organization of Behavior (1949)

Hebb, Donald O.: The Organization of Behavior, John Wiley & Sons, Inc., New York, 1949

HME: Honda Riding Trainer (2005)

Honda Motor Europe (North) GmbH: Honda Riding Trainer, 2005

Hofmann, M.: Master Thesis, Systemidentifikation am dynamischen Motorrad Fahrsimulator (2016)

Hofmann, Marius: Systemidentifikation am dynamischen Motorrad Fahrsimulator, Master Thesis, TU Darmstadt, 2016

Huth, V. et al.: Comparison of Warning Concepts (2012)
Huth, Véronique; Biral, Francesco; Martín, Oscar; Lot, Roberto: Comparison of two warning concepts of an intelligent Curve Warning system for motorcyclists in a simulator study, in: Accident; analysis and prevention (1), Issues 44, pp. 118–125, 2012

Kammeyer, K.-D.; Kühn, V.: MATLAB in der Nachrichtentechnik (2001)
Kammeyer, Karl-Dirk; Kühn, Volker: MATLAB in der Nachrichtentechnik, Schlembach, Weil der Stadt, 2001

Katayama, T. et al.: Control Behaviour of Motorcycle Riders (1988)
Katayama, T.; Aoki, A.; Nishimi, T.: Control Behaviour of Motorcycle Riders, in: Vehicle System Dynamics (4), Issues 17, pp. 211–229, 1988

Kennedy, R. S. et al.: Simulator Sickness Questionnaire (1993)
Kennedy, Robert S.; Lane, Norman E.; Berbaum, Kevin S.; Lilienthal, Michael G.: Simulator Sickness Questionnaire: An Enhanced Method for Quantifying Simulator Sickness, in: The International Journal of Aviation Psychology (3), Issues 3, pp. 203–220, 1993

Klews, M. et al.: Preventing lateral sliding in curves (2018)
Klews, Matthias; Wahl, Anja; Georgi, Andreas: Preventing lateral sliding in curves, in: Institut für Zweiradsicherheit e.V. (IFZ) (Ed.): Forschungsheft Nr. 18, Cologne, 2018

Kooijman, J. D.; Schwab, A. L.: A Review on Handling Aspects in Bicycle and Motorcycle Control (2011)
Kooijman, J. D. G.; Schwab, A. L.: A Review on Handling Aspects in Bicycle and Motorcycle Control, in: ASME 2011 International Design Engineering Technical Conferences and Computers and Information in Engineering Conference, Washington, DC, USA, August 28–31, 2011

Leonard, J. J.; Wierwille, W. W.: Human Performance Validation of Simulators (1975)
Leonard, James J.; Wierwille, Walter W.: Human Performance Validation of Simulators: Theory and Experimental Verification, in: Proceedings of the Human Factors Society Annual Meeting (4), Issues 19, pp. 446–456, 1975

Magiera, N.: Diss., Identifikation des Fahrfertigkeitsniveaus von Motorradfahrern (2020)
Magiera, Nils: Identifikation des Fahrfertigkeitsniveaus von Motorradfahrern in Kurvenfahrt im Realverkehr, Dissertation TU Darmstadt, 2020

Marília Maurel Assad: Diss., control strategies for autonomous scale motorcycles (2018)
Marília Maurel Assad: Analysis of control strategies for autonomous scale motorcycles stabilization and trajectory tracking, Dissertation Pontifica Universidade Católica Do Rio De Janeiro, 2018

Massaro, M. et al.: Simulators for Assessment of Handling (2016)
Massaro, Matteo; Cossalter, Vittore; Sadauckas, James; Lot, Roberto: Using Simulators for the Assessment of Handling of Motorcycles, in: Proceedings of the Bicycle and Motorcycle Dynamics, Milwaukee, (WI) USA, 2016

Matschl, G. et al.: Motorcycle Stability Control (2014)
Matschl, Gerald; Mörbe, Matthias; Gröger, Christian: Motorcycle Stability Control - MSC, in: Institut für Zweiradsicherheit e.V. (IFZ) (Ed.): Forschungsheft Nr. 16, Cologne, 2014

Merkel, N. L.: Safety Potential of Data Glasses (2022)
Merkel, Nora L.: Safety Potential of Data Glasses, in: Proceedings of the 14th International Motorcycle Conference, 2022

Merkel, N. L. et al.: Automatische Notbremssysteme für Motorräder (2022)
Merkel, Nora L.; Pleß, Raphael; Winner, Hermann, et al. (Eds.) Automatische Notbremssysteme für Motorräder, Berichte der Bundesanstalt für Straßenwesen F, FahrzeugtechnikHeft 147, Fachverlag NW in Carl Ed. Schünemann KG, Bremen, 2022

Mortimer, R. G. et al.: The relationship of bicycle manoeuvrability to handlebar configuration (1976)
Mortimer, R. G.; Domas, Patricia A.; Dewar, R. E.: The relationship of bicycle manoeuvrability to handlebar configuration, in: Applied ergonomics (4), Issues 7, pp. 213–219, 1976

Nehaoua, L. et al.: Design and Modeling of a New Motorcycle Riding Simulator
Nehaoua, L.; Hima, S.; Arioui, H.; Seguy, N.; Espie, S.: Design and Modeling of a New Motorcycle Riding Simulator, in: 2007 American Control Conference, New York, NY, USA

Nehaoua, L. et al.: Review on Motorcycle Simulators
Nehaoua, L.; Arioui, H.; Mammar, S.: Review on single track vehicle and motorcycle simulators, in: Automation (MED 2011), Corfu, Greece

Nehaoua, L. et al.: Rider Steer Torque Estimation for Motorcycle Riding Simulator (2010)
Nehaoua, Lamri; Khettat, Amine; Arioui, Hichem; Imine, Hocine; Espié, Stéphane: Rider Steer Torque Estimation for Motorcycle Riding Simulator, in: 5th IFAC Symposium on Mechatronics, Boston, MA, pp. 25–31, 2010

Nehaoua, L. et al.: How to Estimate Robustly the Rider's Action (2013)
Nehaoua, Lamri; Arioui, Hichem; Mammar, Saïd: Motorcycle Riding Simulator, in: IEEE Transactions on Vehicular Technology (1), Issues 62, pp. 80–88, 2013

Norman, D. A.: Design rules based on analyses of human error (1983)
Norman, Donald A.: Design rules based on analyses of human error, in: Communications of the ACM (4), Issues 26, pp. 254–258, 1983

Pacejka, H. B.: Tyre and vehicle dynamics (2006)
Pacejka, Hans B.: Tyre and vehicle dynamics, 2. Edition, Elsevier, Amsterdam, 2006

Pleß, R.: Approach to a holistic input determination for a motorcycle riding simulator (2016)
Pleß, Raphael: Approach to a holistic input determination for a motorcycle riding simulator, in: Proceedings of the Bicycle & Motorcycle Dynamics Symposium - Milwaukee, 2016

Pleß, R. et al.: Manöverumsetzung auf einem dynamischen Motorrad Fahrsimulator (2016)
Pleß, Raphael; Will, Sebastian; Hofmann, Marius; Winner, Hermann: Manöverumsetzung auf einem dynamischen Motorrad Fahrsimulator - Lenken, Lehnen und Kopplungseffekte in der virtuellen Umgebung, in: Proceedings of the 11th International Motorcycle Conference, 2016

Pleß, R. et al.: The Influence of Rider Motion on Motorcycles and Riding Simulators (2018)
Pleß, Raphael; Büttner, Alex; Merkel, Leona N.; Winner, Hermann: The Influence of Rider Motion on Motorcycles and Riding Simulators, in: Proceedings of the 12th International Motorcycle Conference, 2018

Reid, L.; Nahon, M.: Flight simulation motion-base drive algorithms (1985)
Reid, Lloyd; Nahon, M.: Flight simulation motion-base drive algorithms: part 1. Developing and testing equations, in: , 1985

Richard, H. A.; Kullmer, G.: Biomechanik (2013)
Richard, Hans A.; Kullmer, Gunter (Eds.) Biomechanik, Springer Fachmedien Wiesbaden, Wiesbaden, 2013

Sandlin, D.: Beckwards Brain Bicycle (2015)
Sandlin, Destin: The Backwards Brain Bicycle - Smarter Every Day 133, Smarter Every Day, YouTube, https://youtu.be/MFzDaBzBlL0, 2015

Santschi, W. R. et al.: Moments of inertia and centers of gravity of the living human body (1962)
Santschi, W. R.; DuBois, J.; Omoto, C.: Moments of inertia and centers of gravity of the living human body, 1962

Scherer, F.: Master Thesis, Koppelkräfte auf Realfahrzeug und Motorradfahrsimulator (2018)
Scherer, Florian: Identifikation von Fahrer-Fahrzeug Koppelkräften auf Realfahrzeug und Motorradfahrsimulator, Master Thesis, TU Darmstadt, 2018

Scherer, F. et al.: Schräglagenangst (2021)
Scherer, Florian; Winner, Hermann; Pleß, Raphael, et al. (Eds.) Schräglagenangst, Berichte der Bundesanstalt für Straßenwesen F, FahrzeugtechnikHeft 142, Fachverlag NW in Carl Ed. Schünemann KG, Bremen, 2021

Sevarin, A. et al.: Assessment of Visual and Haptic HMI Concepts (2020)
Sevarin, Alessio; Will, Sebastian; Rößer, J.; Mikschofsky, N.; Mentaro, L.; Hammer, Thomas; Schneider, Norbert; Mark, Christian: Assessment of Visual and Haptic HMI Concepts for Hazard Warning of Powered Two-Wheeler Riders, in: Proceedings of the 13th International Motorcycle Conference, 2020

Shin, J.-C.; Lee, C.-W.: Rider's Net Moment Estimation (2004)
Shin, Jae-Cheol; Lee, Chong-Won: Rider's net moment estimation using control force of motion system for bicycle simulator, in: Journal of Robotic Systems (11), Issues 21, pp. 597–607, 2004

Slater, M.; Steed, A.: A Virtual Presence Counter (2000)
Slater, Mel; Steed, Anthony: A Virtual Presence Counter, in: Presence: Teleoperators and Virtual Environments (5), Issues 9, pp. 413–434, 2000

Staffetius, T.; Beitelschmidt, M.: Fahrstilerkennung durch Detektion der Sitzposition
Staffetius, Tino; Beitelschmidt, Michael: Fahrstilerkennung und Ableitung der Fahrerfahrung durch Detektion der Sitzposition und Fahrerbewegung auf dem Motorrad, in:

Stedmon, A. W. et al.: MotorcycleSim (2011)
Stedmon, A. W.; Hasseldine, B.; Rice, D.; Young, M.; Markham, S.; Hancox, M.; Brickell, E.; Noble, J.: MotorcycleSim, in: The Computer Journal (7), Issues 54, pp. 1010–1025, 2011

Stedmon, A. W. et al.: Motorcycle Simulator Solutions for Rider Research (2017)
Stedmon, A. W.; Crundall, David; Moore, Dave: Motorcycle Simulator Solutions for Rider Research, in: Young, Mark S.; Lenné, Michael G. (Eds.): Simulators for Transportation Human Factors, CRC Press, Boca Raton : Taylor & Francis, CRC Press, 2017. | Series: The Human factors of simulation and assessment, 2017

Stoffregen, J.: Motorradtechnik (2012)
Stoffregen, Jürgen: Motorradtechnik, Vieweg+Teubner Verlag, Wiesbaden, 2012

Tanelli, M. et al.: Modelling, Simulation and Control of Two-Wheeled Vehicles (2014)
Tanelli, Mara; Corno, Matteo; Savaresi, Sergio M.: Modelling, Simulation and Control of Two-Wheeled Vehicles, John Wiley & Sons, Ltd, Chichester, UK, 2014

Ueberle, M.: Diss., Design, Control, and Evaluation of Kinesthetic Haptic Interfaces (2006)
Ueberle, Marc: Design, Control, and Evaluation of a Family of Kinesthetic Haptic Interfaces, Dissertation TU München, 2006

Vidotto, G. et al.: Improve Hazard Perception (2008)
Vidotto, Giulio; Bastianelli, Alessia; Spoto, Andrea; Torrem E.; Sergys, F.: Using a riding trainer as a tool to improve hazard perception and awareness in teenagers, in: Advances in Transportation Studies, 2008

VI-grade: Compact Simulator
VI-grade: Compact Simulator; https://www.vi-grade.com/en/products/compact_simulator/, Access 28.11.2022

VI-grade: VI-BikeRealTime
VI-grade: VI-BikeRealTime; https://www.vi-grade.com/en/products/vi-bikerealtime, Access 27.11.2022

Walter, J. R. et al.: A control architecture for synthesising biological movement (2021)
Walter, Johannes R.; Günther, Michael; Haeufle, Daniel F. B.; Schmitt, Syn: A geometry- and muscle-based control architecture for synthesising biological movement, in: Biological cybernetics (1), Issues 115, pp. 7–37, 2021

Weller, L. et al.: Was it me? (2017)
Weller, Lisa; Schwarz, Katharina A.; Kunde, Wilfried; Pfister, Roland: Was it me? - Filling the interval between action and effects increases agency but not sensory attenuation, in: Biological psychology, Issues 123, pp. 241–249, 2017

Westerhof, B. E.: Evaluation of the Cruden Motorcycle Simulator (2018)
Westerhof, B. E.: Evaluation of the Cruden Motorcycle Simulator, in: , 2018

Will, S.: Diss., Presence Model for Driving Simulators
Will, Sebastian: Development of a presence model for driving simulators based on speed perception in a motorcycle riding simulator, Dissertation Julius-Maximilians-Universität Würzburg

Will, S.: Approach to Investigate Powered Two Wheelers' Interactions (2018)
Will, Sebastian: A New Approach to Investigate Powered Two Wheelers' Interactions with Passenger Car Drivers: the Motorcycle – Car Multi-Driver Simulation, in: Bengler, Klaus et al. (Eds.): UR:BAN Human Factors in Traffic, Springer Fachmedien Wiesbaden, Wiesbaden, 2018

Will, S.: Motorcycle Rider Reaction Times as Response to Visual Warnings (2022)
Will, Sebastian: Motorcycle Rider Reaction Times as Response to Visual Warnings, in: Proceedings of the 14th International Motorcycle Conference, 2022

Will, S.; Hammer, T.: Assessing Powered Two Wheelers' display and control concepts (2016)
Will, Sebastian; Hammer, Thomas: Assessing Powered Two Wheelers' display and control concepts - results from a pilot study, in: Proceedings of the 11th International Motorcycle Conference, 2016

Will, S.; Schmidt, E. A.: Powered two wheelers' workload assessment (2015)
Will, Sebastian; Schmidt, Eike A.: Powered two wheelers' workload assessment with various methods using a motorcycle simulator, in: IET Intelligent Transport Systems (7), Issues 9, pp. 702–709, 2015

Witmer, B. G.; Singer, M. J.: Measuring Presence in Virtual Environments (1998)

Witmer, Bob G.; Singer, Michael J.: Measuring Presence in Virtual Environments, in: Presence Vol. 7, No.3, pp. 225–240, 1998

Yokomori, M. et al.: Rider's Operation of a Motorcycle Running Straight at Low Speed (1992)

Yokomori, Motomu; Higuchi, Kenji; Ooya, Takio: Rider's Operation of a Motorcycle Running Straight at Low Speed, in: JSME International JournalSeries III, Vol. 35, No.4, 1992

Yokomori, M.; Yamaguchi, S.: The Rider's Motion Control of Stability (1999)

Yokomori, Motomu; Yamaguchi, Shigeki: The Rider's Motion Control of Stability of Motorcycle and Rider System on Low Speed, in: Proceedings of the 1999 SAE Small Engine Technology Confefrence, 1999

Zöller, I. M.: Diss., Einfluss ausgewählter Gestaltungsparameter auf die Fahrerverhaltensvalidität (2015)

Zöller, Ilka M.: Analyse des Einflusses ausgewählter Gestaltungsparameter einer Fahrsimulation auf die Fahrerverhaltensvalidität, Dissertation TU Darmstadt, 2015

Own Publications

Schröter, K.; Wallisch, M.; Vasylyev, O. Schleiffer, J.-E-; Pleß, R.; Winner, H.; Tani, K.; Fuchs, O.: Update on Brake Steer Torque Optimized Corner Braking of Motorcycles. In: Proceedings of the 9th International Motorcycle Conference 2012, pp. 2-46, Institute for Motorcycle Safety e.V., Essen, 2012

Pleß, R.; Schröter, K.; Kranz, I.; Deforth, J.;Hummel, N.; Winner, H.: Quo Vadis, Darmstadt Method for Abrasive Testing. In: Proceedings of the 10th International Motorcycle Conference 2014, pp. 485-505, Institute for Motorcycle Safety e.V., Essen, 2014

Schröter, K.; Seiniger, P.; Pleß, R.: Fahrdynamikregelsysteme für Motorräder. In: Winner, H.; Hakuli, S.; Lotz, F.; Singer, C. (Ed.): Handbuch Fahrerassistenzsysteme, ATZ/MTZ-Fachbuch, Springer Wiesbaden, 2015, DOI: 10.1007/978-3-658-05734-3_42

Pleß, R.; Guth, S.; Will, S.; Winner, H.: Determining the Rider Induced Roll Torque on a Dynamic Motorcycle Riding Simulator. In: Proceedings of the Driving Simulator Conference 2014, Max Planck Institute for Biological Cybernetics, Tübingen, 2015

Guth, S.; Geiger, M.; Will, S.; Pleß, R.: Winner, H.: Motion Cueing Algorithm to Reproduce Motorcycle Specific Lateral Dynamics on Riding Simulators. In: Proceedings of the Driving Simulator Conference 2014, Max Planck Institute for Biological Cybernetics, Tübingen, 2015

Guth, S.; Pleß, R.; Will, S.: Dynamic Motorcycle Riding Simulator Using VI-BikeRealtime. VI-Grade Users Conference 2015, Triest, 2015

Schröter, K.; Seiniger, P.; Pleß, R.: Vehicle Dynamics Control Systems for Motorcycles. In: Winner, H.; Hakuli, S.; Lotz, F.; Singer, C. (Ed.): Handbook of Driver Assistance Systems, Springer International Publishing, 2016, ISBN 978-3-319-12351-6

Pleß, R.; Klonecki, K.: Advancing the Darmstadt Method for Abrasive Testing. Workshop on Traffic Environment, Primary and Secondary Safety of Powered Two-wheeled Vehicles, COST TU1407 Safe2Wheelers, Linz, 2016.

Pleß, R.: Maneuvering the DESMORI motorcycle simulators. Workshop on Accidentology and Motorcycle Simulators, COST TU1407 Safe2Wheelers, Würzburg, 2016.

Will, S.; Pleß, R.; Hammer, T.; Guth, S.; Winner, H.: Bringing Motorcycle Dynamics to the Rider – Technical Solutions and their Contribution to Speed Perception in a Motorcycle Riding Simulator. VI-Grade Users Conference 2016, Wiesbaden, 2016

Will, S.; Pleß, R.; Guth, S.: Bringing single track vehicle dynamics to motorcycle riding simulators – results of a pilot study. In: Proceedings of the Bicycle and Motorcycle Dynamics 2016 Symposium on the Dynamics and Control of Single Track Vehicles, 21 – 23 September 2016, Milwaukee, Wisconsin USA

Pleß, R.; Will, S.; Guth, S.; Hofmann, M.; Winner, H.: Approach to a Holistic Rider Input Determination for a Dynamic Motorcycle Riding Simulator. In: Proceedings of the Bicycle and Motorcycle Dynamics 2016 Symposium on the Dynamics and Control of Single Track Vehicles, 21 – 23 September 2016, Milwaukee, Wisconsin USA

Pleß, R.; Will, S.; Hofmann, M.; Winner, H.: Manöverumsetzung auf einem dynamischen Motorrad Fahrsimulator – Lenken, Lehnen und Kopplungseffekte in der Virtuellen Umgebung. In: Proceedings of the 11th International Motorcycle Conference 2016, pp. 38-60, Institute for Motorcycle Safety e.V., Essen, 2016

Will, S.; Hammer, T.; Pleß, R.; Guth, S.: Assessing Powered Two Wheelers' Display and Conrol Concepts – Results From a Pilot Study. In: Proceedings of the 11th International Motorcycle Conference 2016, pp. 228-243, Institute for Motorcycle Safety e.V., Essen, 2016

Will, S.; Hammer, T.; Pleß, R.; Guth, S.: The use of Proprioceptive Cues in Order to Enhance Presence in a Dynamic Motorcycle Riding Simulator. In: Proceedings of the Driving Simulator Conference 2017, University, Stuttgart, 2017

Pleß, R.: Evolving Motorcycle Simulators. VI-Grade Users Conference 2018, Lainate, 2018

Merkel, N.; Pleß, R.; Scheid, K.; Winner, H.: Einsatzgrenzen Automatischer Notbremssysteme für Motorisierte Zweiräder – eine Expertenstudie. In: Proceedings of the 12th International Motorcycle Conference 2018, pp. 122-144, Institute for Motorcycle Safety e.V., Essen, 2018

Pleß, R.; Büttner, A.; Merkel, N.; Winner, H.: Einfluss der Fahrerbewegung auf Realfahrzeug und Motorradsimulator. In: Proceedings of the 12th International Motorcycle Conference 2018, pp. 144-171, Institute for Motorcycle Safety e.V., Essen, 2018

Will, S.; Hammer, T.; Köbe, M.; Liebick, T.; Maruyama, K.; Onoue, T.; Strack, M.; Mamiya, M.; Matsuda, T.; Pleß, R.; Purschwitz, A.: Powered Two-Wheeler HMI Design For Cooperative Intelligent Transport Systems (C-ITS). In: Proceedings of the 12th International Motorcycle Conference 2018, pp. 258-270, Institute for Motorcycle Safety e.V., Essen, 2018

Merkel, N.; Pleß, R.; Winner, H.: Tolerability of Unexpected Autonomous Emergency Braking Maneuvers on Motorcycles - a Methodology for Experimental Investigation. In: Proceedings of the 26th ESV Conference 2018

Will, S. Pleß, R.: Increasing the Fields of Application for Motorcycle Riding Simulators. VI-Grade Users Conference 2019, Hanau, 2019

Supervised Theses

Hellmann, Adrian: Untersuchung zur Reproduzierbarkeit und Vergleichbarkeit von Motorrad-Messfahrten im Realverkehr, Master-Thesis Nr. 543/14, 2014

Kranz, Isabell: Überarbeitung der Rutschsimulationsmaschine hinsichtlich Funktionserweiterung und Kleinserienfertigung, Master-Thesis Nr. 549/14, 2014

Lichtenthäler, Jonas: Erfassung und Rückführung des Fahrerinduzierten Rollmomentes auf einem Dynamischen Motorradfahrsimulator, Bachelor-Thesis 1187/14, 2014

Hummel, Nicolas: Entwicklung einer Auswerteroutine für die Rutschsimulationsmaschine und Analyse kontinuierlicher Messschriebe, Bachelor-Thesis 1188/14, 2014

Deforth, Jan: Untersuchung der Zeitlichen Varianz von Messergebnissen am Rutschsimulationsprüfstand, Bachelor-Thesis 1195/14, 2014

Hanselka, Sven: Entwicklung technischer Konzepte zur Immersionssteigerung an einem Motorradfahrsimulator, Bachelor-Thesis 1182/14, 2014

Riede, Sascha: Modellierung des Schutzkleidungsprüfstandes in Matlab/Simulink, Bachelor-Thesis 1208/14, 2014

Anton, Marc: Auslegung und Konstruktion eines Seilzugsystems zur Darstellung von Horizontalkräften an einem Motorradfahrsimulator, Bachelor-Thesis 1209/14, 2014

Schmidt, Lisa: Anforderungen an die Homologation eines Zertifizierungswerkzeugs am Beispiel des Schutzkleidungsprüfstands, Master-Thesis 570/15, 2015

Huss, Moritz: Mehrkörpermodellbildung von Motorradsimulator-Bewegungsplattformen, Bachelor-Thesis 1226/15, 2015

Jetses, Bernhardt: Modularisierung des Schutzkleidungsprüfstands 2.x, Bachelor-Thesis 1224/15, 2015

Berger, Jan Nikolas: Entwicklung und Implementierung eines Beobachters zur Rollmomentvorgabe an einem dynamischen Motorradfahrsimulator, Bachelor-Thesis 1240/15, 2015

Böhm, Justus: Modellierung des Lenksystems an einem dynamischen Motorradfahrsimulator, Bachelor-Thesis 1246/15, 2015

Seubert, Christopher: Untersuchung der Sensitivität von Messergebnissen auf die Variation von Prüfparametern am Schutzkleidungsprüfstand, Bachelor-Thesis 1252/15, 2015

Pietsch, Tobias: Erstellung eines Businessplans zur Kleinserienfertigung einer Prüfmaschine, Studien-Arbeit 1236/15, 2015

Hofmann, Marius: Systemidentifikation am dynamischen Motorrad Fahrsimulator, Master-Thesis 613a/16, 2016

Buchen, Florian: Ermittlung funktionaler Anforderung an adaptive Geschwindigkeitsregelsysteme für Einspurfahrzeuge, Master-Thesis 623/16, 2016

Kraft, Michael: Entwicklung eines Herstellungsprozesses von Prüffahrbahnen des Abriebsprüfstandes nach dem Darmstädter Verfahren für Schutzkleidungsprüfung, Master-Thesis 635/16, 2016

Dietz, Christopher: Entwurf eines Werkzeugs zur Herstellung von Probestücken zur Verwendung am Schutzkleidungsprüfstand, Bachelor-Thesis 1271/16, 2016

Vonrath, David: Konzeption eines Motion Cueing Algorithmus für einen Hexapod gebundenen Motorrad Fahrsimulator, Bachelor-Thesis 1286/16, 2016

Berghäuser, Tobias: Erweiterung der Messtechnik am Advanced Abrasion Resistance Tester, Master-Thesis 654/18, 2018

Schön, Oliver: Entwicklung eines Lenkungsreglers für einen dynamischen Motorradfahrsimulator, Master-Thesis 663/18, 2018

Büttner, Alex: Analyse der Fahrerbewegung im Niedriggeschwindigkeitsbereich auf einem Einspurfahrzeug, Master-Thesis 672/18, 2018

Delgado, Ricardo: Entwurf einer Montagevorrichtung für Motorräder mit integrierter Roll- und Nickmomentenmessung auf einem Motorradsimulator, Master-Thesis 712/18, 2018

Walther, Lukas: Entwurf Pseudokritischer Testmanöver für den Motorradfahrversuch, Master-Thesis 717/18, 2018

Scherer, Florian: Identifikation von Fahrer-Fahrzeug Koppelkräften auf Realfahrzeug und Motorradfahrsimulator, Master-Thesis 718/18, 2018

Gimbel, Jonas: Entwurf einer Motorradatrappe mit variabler Ergonomie für einen dynamischen Motorradfahrsimulator, Master-Thesis 722/18, 2018

Albrecht, Alexander: Stillstandsimulation auf einem Dynamischen Motorradfahrsimulator, Master-Thesis 729/18, 2018

Häffner, Nicolas: Entwurf einer stationären Messtechnik zur Bewertung des Kurvenfahrverhaltens von Motorradfahrern im Realverkehr, Master-Thesis 730/18, 2018

Winter, René: Ermittlung von Darstellungsfehlern und Entwurf möglicher Lösungsansätze auf einem dynamischen Motorradfahrsimulator, Bachelor-Thesis 1331/18, 2018

Beck, Daniel: Open-Loop Simulation von Realfahrten auf einem dynamischen Motorradfahrsimulator, Bachelor-Thesis 1332/18, 2018

Bauer, Esra: Entwicklung eines echtzeitfähigen Reifenmodells, Master-Thesis, Institut für Festkörperphysik, 2020